Novel Ruthenium Dihydrogen Complexes and their Application in Catalysis

Von der Fakultät für Mathematik, Informatik und Naturwissenschaften
der Rheinisch-Westfälischen Technischen Hochschule Aachen zur Erlangung
des akademischen Grades eines Doktors der Naturwissenschaften genehmigte Dissertation

vorgelegt von

Diplom-Chemiker
Martin H. G. Prechtl

aus Offenbach am Main

Berichter: Univ.-Prof. Dr. rer. nat. Walter Leitner
Prof. Dr. David Milstein
Tag der mündlichen Prüfung: 28. Juni 2007

Diese Dissertation ist auf den Internetseiten der Hochschulbibliothek online verfügbar.

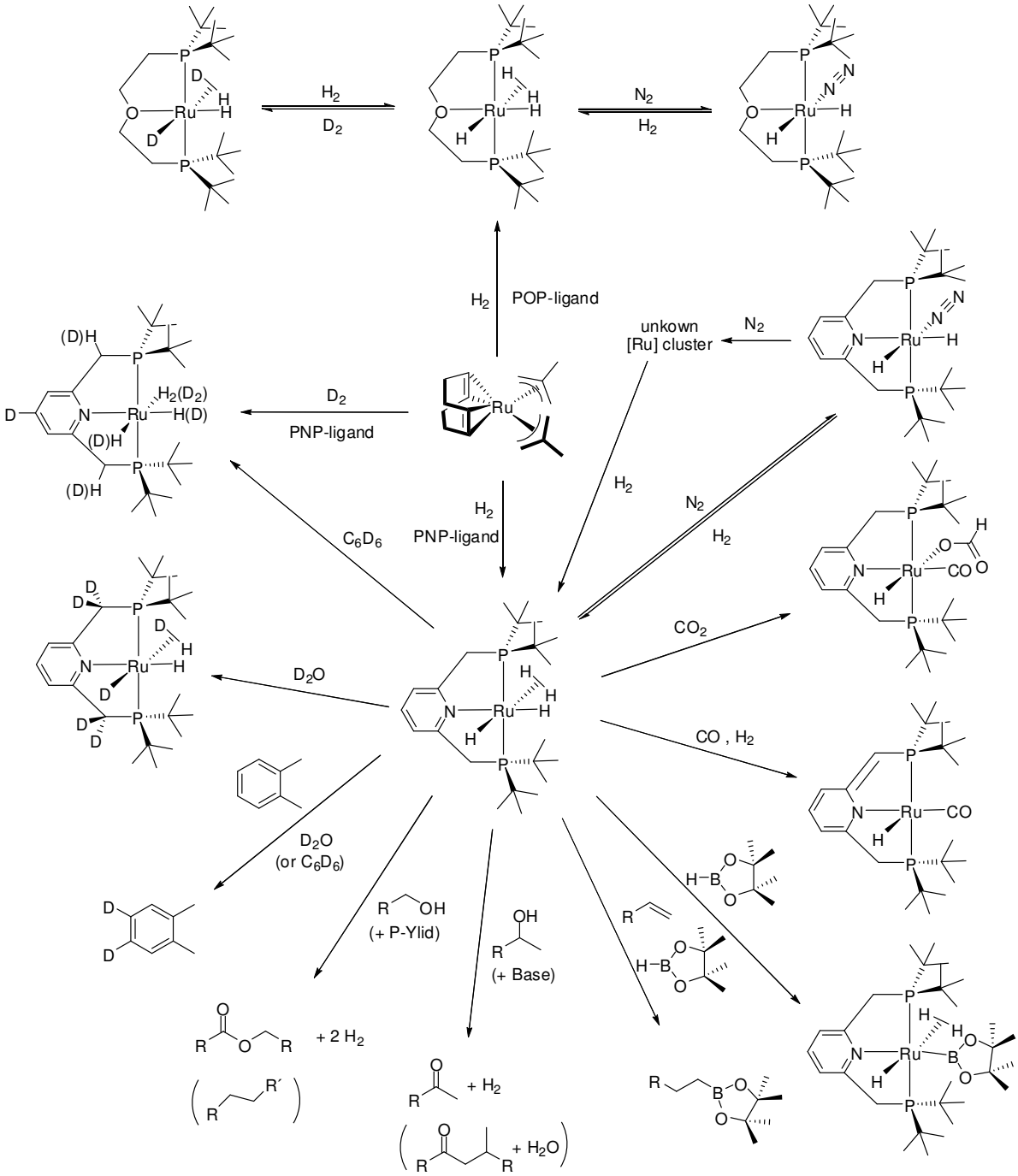
H2
D2
N2
H2
H2
POP-ligand
unkown
[Ru] cluster
N2
D2
PNP-ligand
H2
PNP-ligand
C6D6
H2
N2
H2
CO2
D2O
CO , H2
D2O
(or C6D6)
(+ P-Ylid)
(+ Base)
+ 2 H2
+ H2
+ H2O

Parts of this work are already published:

"H/D-Exchange at Aromatic and Heteroaromatic Hydrocarbons Using D_2O as Deuterium Source and Ruthenium Dihydrogen Complexes as Catalyst" M. H. G. Prechtl, M. Hölscher, Y. Ben-David, N. Theyssen, R. Loschen, D. Milstein, W. Leitner,* *Angew. Chem.* **2007**, *119*, 2319-2322. *Angew. Chem. Int. Ed.* **2007**, *46*, 2269-2272.

"Synthesis and Characterisation of Nonclassical Ruthenium Hydride Complexes Containing Chelating Bidentate and Tridentate Phosphine Ligands" M. H. G. Prechtl, Y. Ben-David, D. Giunta, S. Busch, Y. Taniguchi, W. Wisniewski, H. Görls, R. J. Mynott, N. Theyssen, D. Milstein, W. Leitner,* *Chem. Eur. J.* **2007**, *13*, 1539-1546.

"[Can (PXP)M$(H)_2(H_2)$]-pincer complexes (M = Fe, Ru, Os; X = N, O, S) serve as catalyst lead structures for NH_3 synthesis from N_2 and H_2?" M. Hölscher, M. H. G. Prechtl, W. Leitner*, *Chem. Eur. J.* **2007**, DOI: 10.1002/chem.200700289.

„Neue nicht-klassische Rutheniumhydridkomplexe und die Anwendung in der Katalyse für H/D-Austausch und die Umsetzung von Alkohol und Alkoholderivaten." M. H. G. Prechtl, C. Minnich, M. Hölscher, N. Theyssen, Y. Ben-David, D. Milstein, und W. Leitner,* *oral presentation* at the *40. Jahrestreffen Deutscher Katalytiker* **2007**, 14-16 March 2007, Weimar, Germany. Book of Abstracts, p. 61-62.

"A Novel Ruthenium Dihydrogen Complex Bearing a Bulky Pincer-Backbone and the Application in Catalysis for H/D-Exchange and Dehydrogenation." M. H. G. Prechtl, M. Hölscher, Y. Ben-David, N. Theyssen, D. Milstein, W. Leitner,* *oral presentation* at the *ICOMC XXII* **2006**, *International Conference on Organometallic Chemistry*, 23-28 July 2006, Zaragoza, Spain. Book of Abstracts Vol. 1, p. 151, O91.

The research studies for the PhD-thesis were prepared at the *Max-Planck-Institut für Kohlenforschung* (MPI) in Mülheim an der Ruhr, Germany, and at the *Institut für Technische und Makromolekulare Chemie*, *RWTH Aachen University* (IR-Online experiments) between September 2004 and March 2006 in the research group of Prof. Dr. Walter Leitner.

My acknowledgement goes to:

My Ph. D. supervisor (Doktorvater) **Prof. Dr. Walter Leitner** (RWTH Aachen / MPI Mülheim) is gratefully acknowledged for the interesting subject, for my freedom of practice, his interest in the subject and the excellent work conditions.

For the second review (Korreferat) **Prof. Dr. David Milstein** (Weizmann Institute of Science, Rehovot, Israel) is gratefully acknowledged.

Prof. Dr. Albrecht Salzer (RWTH Aachen) is acknowledged for the participation as the third examiner in my oral defense of the thesis.

Prof. Dr. Carsten Bolm (RWTH Aachen) is acknowledged for the participation as the supervisor for the defense of my thesis.

The former executive director of the Max-Planck-Institut für Kohlenforschung **Prof. Dr. Ferdi Schüth** is acknowledged to give me the possibility to work in this excellent institute.

Dr. N. Theyssen is acknowledged for the supervision, helpful discussions and corrections of my manuscripts during my research at the MPI for Coal Research.

Prof. Dr. D. Milstein and Mr. Y. Ben-David (Weizmann Institute of Science, Rehovot, Israel) are acknowledged for their collaboration within the *German-Israeli-Projectcooperation* (Project DIP-G 7.1 *Directed Catalytic Functionalization of Unreactive Molecules*), helpful discussions and the generous gift of pincer-ligands.

Dr. M. Hölscher (RWTH Aachen) is acknowledged for the DFT-calculations of the ruthenium dihydrogen complexes and the calculations for H/D-exchange reactions. Furthermore, I thank him for helpful discussions and the revisions of our manuscripts.

All analytic departments of the MPI are acknowledged. Especially Dr. R. Mynott´s spectroscopic team is gratefully acknowledged for NMR- and IR-measurements. I thank Mr. W. Wisniewski for T_1-measurements and ^{1}H-NMR spectra-series, Mrs. C. Wirtz for ^{2}H-NMR, Mr. R. Ettl and Mr. M. Stachelhaus for all-time intensive routine NMR-support. Mr. Stoffels and Mr. Reissig are acknowledged for preparative gas chromatography.

Dr. R. Goddard and Mrs. A. Dreier (MPI) are acknowledged for X-ray analysis.

Mr. C. Minnich (RWTH Aachen) is acknowledged for IR-online monitoring in dehydrogenation reactions.

Dr. Oliver Trapp, Mr. S. Vukojevic and Mr. M. Comotti from the MPI are acknowledged for helpful discussions and gas-analyses.

All fine mechanics and glass blowers at the MPI are acknowledged for special equipment.

The staff-members of the Theyssen-group at the MPI are acknowledged for their lab-support: Mr. L. Winkel, Mr. A. Brinkmann, and my (former) apprentices Mr. H. Bruns, Ms. D. Stelmaszyk, Mr. P. Walkamp and Ms. K. Wobser.

Thanks a lot to all my (former) colleagues of the *Leitner* group in Mülheim and at the RWTH Aachen and my colleagues of the *Schüth* group in Mülheim for a nice time.

Furthermore, thanks to my collaboration partners in Aachen (Bolm), Wuppertal (Scherf), Marburg (Glorius), and Sao Paulo (Comasseto, dos Santos, El Seoud).

E muito obrigado para Dr^a. E. Tada por discussões úteis, muita energia e paciência.

Last but not least my parents for their support before and during my PhD-studies.

This work is dedicated to my family and friends for their support, discussions, happiness, fun and patience.

1. Introduction 1
1.1. Background and Motivation 1
1.2. State of the Art and Objectives 2
1.2.1. Ruthenium Dihydrogen Complexes 2
1.2.2. Characterisation of Nonclassical Hydride Complexes 6
1.2.3. Catalysis 9
1.2.3.1. CH-Activation and H/D-Exchange Reactions 9
1.2.3.2. Ruthenium Hydrides in Hydrogen Transfer Processes 11
2. Results and Discussion 15
2.1. The Ruthenium Dihydrogen Complex [Ru(dtbpmp)(H_2)H_2] 15
2.1.1. Synthesis 15
2.1.2. Characterisation 17
2.1.3 Reactivity 23
2.1.3.1. H_2 / N_2 Exchange 23
2.1.3.2. H / D Exchange 26
2.1.3.3. Treatment with carbon monoxide 31
2.1.3.4. Reaction with pinacolborane 34
2.1.3.5. Reaction with CO_2 36
2.1.4. Other PNP pincer ligands for ruthenium hydride complexes 40
2.2. The Ruthenium Dihydrogen Complex [Ru(dtbpoet)(H_2)H_2] 42
2.2.1. Synthesis 42
2.2.2. Characterisation 43
2.2.3. Reactivity 49
2.3. Catalysis 50
2.3.1. Catalytic *H/D*-Exchange between Aromatic Hydrocarbons and Deuterated Solvents 50
2.3.1.1. D_2O as Deuterium Source 50
2.3.1.2. C_6D_6 as Deuterium Source 58
2.3.2. Catalytic Dehydrogenation of Alcohol and Tandem Reactions 67
2.3.2.1. Dehydrogenative Coupling of Primary Alcohols 67
2.3.2.2. Dehydrogenation of Secondary Alcohols 77
3. Summary 82
3.1. Ruthenium Dihydrogen Complexes 82

3.2. Catalysis 84
4 Experimental Section 86
4.1. General 86
4.2. Analytic Methods 86
4.2.1. Nuclear Magnetic Resonance Spectroscopy (NMR) 86
4.2.2. Infrared Spectroscopy (IR) 88
4.2.3. Mass Spectrometry 88
4.2.4. X-Ray 88
4.2.5. Microanalysis 88
4.2.6. Autoclaves for High-Pressure Experiments 89
4.2.6.1. Typ I (glass autoclave, 50 mL) 89
4.2.6.2. Typ II (autoclave, 36 mL) 89
4.3. Synthetic Procedures 90
4.3.1. Literature Compounds 90
4.3.2. Chelating Diphosphine Nitrogen Ligands (PNP-pincer) 91
4.3.3. Ruthenium Dihydrogen Complexes 92
4.3.3.1. Preparation of [Ru(*dtbpmp*)H_2(H_2)] 4 92
4.3.3.2. Preparation of the complex [D_x]-[Ru(*dtbpmp*)H_2(H_2)] [D_x]-4 94
4.3.3.3. Reaction of [Ru(*dtbpmp*)H_2(H_2)] 4 with C_6D_6 to highly deuterated [D_x]-4 95
4.3.3.4. Reaction of [Ru(*dtbpmp*)H_2(H_2)] 4 with D_2O in C_6D_{12} to [D_6]-4 / 26 95
4.3.3.5. Reaction of [Ru(*dtbpmp*)H_2(H_2)] 4 with N_2 to [Ru(*dtbpmp*)H_2(N_2)] 20 96
4.3.3.6. Reaction of [Ru(*dtbpmp*)H_2(H_2)] 4 with carbon monoxide and hydrogen gas to [Ru(*dtbpmp*)(CO)H] 28 97
4.3.3.7. Reaction of [Ru(*dtbpmp*)H_2(H_2)] 4 with pinacolborane 97
4.3.3.8. Solid State Structure: Reaction with CO_2 99
4.3.3.9. Preparation of [Ru(*dtbpoet*)H_2(H_2)] 5 104
4.3.3.10. Reaction of [Ru(*dtbpoet*)H_2(H_2)] 5 with N_2 to [Ru(*dtbpoet*)H_2(N_2)] 52 106
4.3.3.11. Reaction of [Ru(*dtbpoet*)H_2(H_2)] 5 with D_2 to [D_x]-[Ru(*dtbpoet*)H_2(H_2)] [D_x]-5 106
4.3.4. Catalysis 107
4.3.4.1. Catalytic *H/D*-exchange with D_2O as Deuterium Source 107
4.3.4.2. Catalytic *H/D*-exchange with [D_6]benzene as Deuterium Source 113
4.3.4.3. Catalytic Dehydrogenation of Alcohols 119

5 Figure Index 126
6 Scheme Index 129
7 Table Index 132
8 Abbreviation Index 133
9 Compound Name Index 135
10 Compound Structure Index 138
11 Literature 146

1. Introduction

1.1. Background and Motivation

This research study expatiate upon the synthesis and characterisation of new nonclassical ruthenium hydride complexes bearing pincer ligands and their application in catalysis for CH-activation (H/D-exchange), hydrogen transfer processes and fixation of small molecules like N_2 and CO_2.

Two decades ago, *Chaudret* synthesised the first ruthenium dihydrogen complex.[1] Quite recently, a neutral ruthenium dihydrogen complex bearing an aliphatic *POP*-pincer was presented by *Gusev* and co-workers.[2] Furthermore, *Milstein* presented ruthenium hydride complexes with pincer ligands.[3] In the field of catalysis the investigations of *Leitner* and co-workers on ruthenium dihydrogen complexes have shown an impressive potential for CH-bond activation under mild conditions, as well as for hydrogen transfer processes.[4] Established catalysts for CH-bond activation usually need much higher process temperatures.[4a, 5, 6] In contrast, *Leitner* and co-workers presented the application of ruthenium dihydrogen complexes for H/D-exchange between hydrocarbons at room temperature.[4b] H/D-exchange processes are a powerful tool to evaluate the potential of a catalyst for CH bond cleavage and formation. [7, 8] The isotopic exchange reactions can be also of synthetic value, as deuterated and tritiated compounds are used for NMR-spectroscopy, for medicinal research and for drug discovery processes. [9, 10, 11] Furthermore, deuterated polymers are evaluated for OLEDs and are used in optical communication systems. [12] Therefore, there is an increasing interest in mild and selective catalytic H/D-exchange processes from a fundamental and application oriented view. Other potential fields of application for these catalyst class are the selective alkylation of arenes (*Murai-reaction*),[5, 13] the hydrogenation of nitriles towards the synthesis of ε-caprolactam for nylon production[14, 15] and the dehydrogenation of alcohols and hydrogenation of ketones and esters.[3] Another application might be N_2-activation[16] indicated by N_2-fixation in known ruthenium dinitrogen complexes bearing pincer backbones.[2, 3c] These encouraging facts are the reasons for the ongoing investigations in this research area.

1.2. State of the Art and Objectives

1.2.1. Ruthenium Dihydrogen Complexes

The discovery of the first stable transition metal complex, a molybdenum dihydrogen complex, comprising molecular dihydrogen as a side-on bound ligand by *G. J. Kubas* in 1983 was a breakthrough in the historical development of coordination chemistry.[17] Since then, dihydrogen complexes of transition metals have been the subject of considerable interest because they present models for the metal induced activation of the hydrogen molecule,[7, 18] either through oxidative addition or heterolytic cleavage.[7, 18, 19, 20, 21, 22a, 23] In general, it is possible to obtain *nonclassical* metal hydride complexes by direct reaction with hydrogen or by protonation of hydride complexes.[18b] The stable coordination between the molecular dihydrogen and a metal centre is based on two contributions: the donation from the filled H_2 σ-orbital to the empty *d*-orbitals at the metal, and the back bonding of the *d*-electrons to the antibonding σ∗-orbital of the hydrogen ligand (Figure 1). Thus, several factors such as the capability of the metal to donate electrons and the nature of the ligand in *trans* position influence the stability and the reactivity of the *M-H₂* unit.[18, 24] As recently highlighted by *van Leeuwen* et al., the structural demands of an ancillary chelating ligand can also play an important role in defining the properties of the η^2-*H₂* ligand.[25]

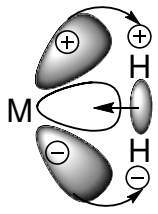

Figure 1: Schematic bonding model between molecular hydrogen and a metal.

In the present work, we report on the synthesis and characterisation of new nonclassical ruthenium hydride complexes with constrained ligand geometries, which substantiate the importance of well defined structural features for the H_2-binding mode and reactivity.[4c, 26]

The chemistry of ruthenium complexes containing *nonclassical* hydride ligands was pioneered by *Chaudret* et al. in 1984 with the synthesis of the hexahydride complex of formula $[Ru(\eta^2\text{-}H_2)_2(H)_2(PCy_3)_2]$ **1a** (Cy = cyclohexyl, Figure 2).[1] From this point on, numerous nonclassical transition metal hydrides were synthesized and investigated.[7, 8, 14, 27, 28, 29] The species **1a** was proven to possess a unique structure with two classical hydrides and two molecular dihydrogen ligands in mutual *cis* position,[1c] as confirmed most recently also by neutron diffraction for $[Ru(\eta^2\text{-}H_2)_2(H)_2(PCyp_3)_2]$ **1b** (Cyp = cyclopentyl).[1d] Meanwhile several ruthenium complexes containing *nonclassical* hydride ligands have been synthesised thus allowing a better understanding of stability, reactivity and binding mode of the $\eta^2\text{-}H_2$ moiety.[29c, 30] Complex **1** has found application as starting material for a variety of ruthenium dihydrogen complexes.[29c, 30, 31] Moreover, it has been used as a catalyst precursor for hydrogenation, [14, 29c] silylation,[32] C-C-coupling reactions (*Murai* reaction)[5, 13b, 31, 33] and metathesis.[34]

Recently, the *Leitner* group reported the synthesis of new complexes **2** and **3** where one or both PCy_3 ligands of **1** are replaced with strongly basic and sterically encumbered heterocyclic carbene ligands (Figure 2).[4b] X-ray crystal structure analysis revealed that the arrangement of the central RuH_6 core is largely retained in these species. The carbene complexes show, however, a distinct reactivity as compared to **1** including an interesting potential in catalytic H/D exchange processes, resulting from the specific ligand environment. [4b, 6]

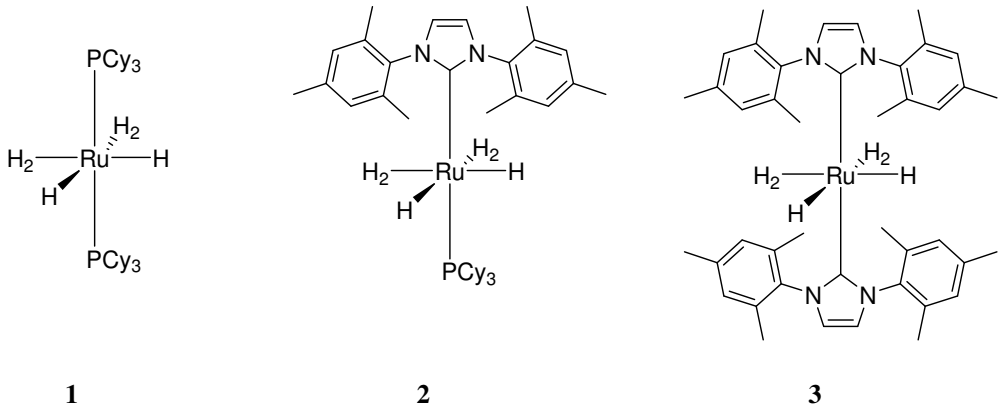

1 **2** **3**

Figure 2: $Ru(H_2)_2(H)_2(PCy_3)_2$ **1a**, $Ru(H_2)_2(H)_2(PCy_3)(IMes)$ **2**, $Ru(H_2)_2(H)_2(IMes)_2$ **3**.

An alternative possibility to expand the structural variety of *nonclassical* ruthenium hydride complexes is to incorporate the donor sites into chelating frameworks of constraint geometries.[25] In the present work, we have therefore set out to investigate more systematically tridentate chelating ligand frameworks (*pincer* ligands) for the stabilization of the mononuclear ruthenium dihydrogen complexes (Figure 3). Preliminary studies from *Leitner´s* team,[4a, 35] and industrial laboratories[14] indicate that binuclear complexes of general formula $[Ru_2H_6(P_2)_2]$ are obtained with chelating ligands P_2 of type $R_2P(CH_2)_nPR_2$. The trans-arrangement of the two P-donor groups together with the occupation of a third coordination site is expected to lead to monomeric complexes with the pincer framework. Further advantage of *pincer* ligands lies in the enhanced stability of their metal complexes due to the enforced *chelate effect*.

Thanks to their interesting catalytic behaviour, transition metal complexes containing tridentate pincer ligands have been extensively studied during the past decade.[36] The fields of application in catalysis varies from e.g. C-C bond formation, CH-, CC-, CN-, CO- bond activation, amination, hydrogenation, elimination, CO_2-activation to dinitrogen and dihydrogen coordination.[36, 37, 38] In recent years the popularity of pincer ligands in catalysis and coordination chemistry was enforced by the groups of *Milstein*,[3, 36, 37, 39] and *Crabtree*[38, 40] and others.[41, 42, 43, 44] However, not before 2005 such pincer ligated ruthenium dihydrogen complexes have been reported.[2, 4c] In contrast rhodium, platinum and osmium complexes are known for some more time.[3b, 36, 41]

The mentioned facts encouraged our study on the development of new nonclassical ruthenium hydride complexes bearing these kinds of ligands for their application in catalysis.

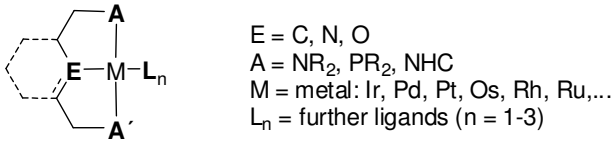

Figure 3: Complexes with pincer ligands.

For the synthesis of complexes similar to **1** it is possible to use the readily available ruthenium precursor [Ru(cod)(2-methylallyl)$_2$] (cod = cyclooctadiene) **6**, in the presence of bulky alkylphosphine ligands, like tricyclohexylphoshine 7 (PCy_3), under hydrogen pressure (Scheme 1).[35] Alternative pathways are also known.[1, 45]

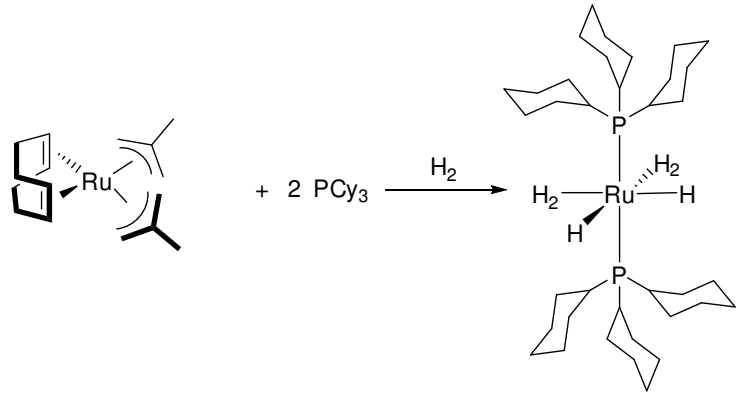

6 **7** **1**

Scheme 1: Synthesis of the *Chaudret*-complex **1** according to *Leitner* and co-workers.

Therefore the first part of this thesis will focus on the synthesis and characterisation of novel (water-stable) ruthenium dihydrogen complexes bearing bulky pincer ligands using the approach depicted in Scheme 2.[35]

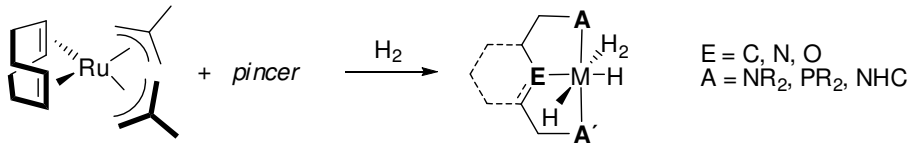

Scheme 2: Synthesis of ruthenium dihydrogen complexes. [35]

To obtain mononuclear structures, we have applied PNP and POP pincer ligands in complexes **4** and **5** (Figure 4), respectively, to adjust a meridional tridentate coordination mode as described in the chapters 2.1.1. and 2.2.1.

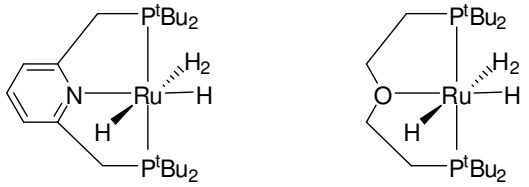

4 **5**

Figure 4: New pincer-type mononuclear complexes [Ru(*dtbpmp*)(H_2)H_2] **4** (*dtbpmp* = 1,3-bis(di-*tert.*-butylphosphinomethyl)pyridine) and [Ru(*dtbpoet*)(H_2)H_2] **5** (*dtbpoet* = 2,2'-oxybis(ethane-2,1-diyl)bis(di-tert-butylphosphine).

1.2.2. Characterisation of Nonclassical Hydride Complexes

This chapter summarises some practical characterisation techniques and information for nonclassical hydride complexes. In general, an enhanced complex stability for nonclassical hydride complexes is observed for central metals with a d^6-configuration and octahedral coordination. Almost all nonclassical hydride complexes are in agreement with this rule.[7] Bulky ligands could lead to a distorted octahedron or even to other coordination types, while smaller ligands direct to higher coordination, binuclear complexes or a conversion of a nonclassical hydride to a classical hydride. The H-H distance in dihydrogen complexes usually ranges from 0.8 to 1.0 Å. In comparison to the H_2 gas (0.74 Å) it is in agreement with an activation of the H-H bond. For the classical polyhydrides complexes the H-H distance is often 1.8-2.5 Å.[7] A strict barrier between these metal hydrides is difficult to estimate because isomerisation could occur easily and a transient area (1.1 to 1.5 Å)[22b] is considered for elongated dihydrogen complexes (also described as “stretched” dihydrogen complexes or compressed dihydrides)[46, 47] (Figure 5).[7, 22b]

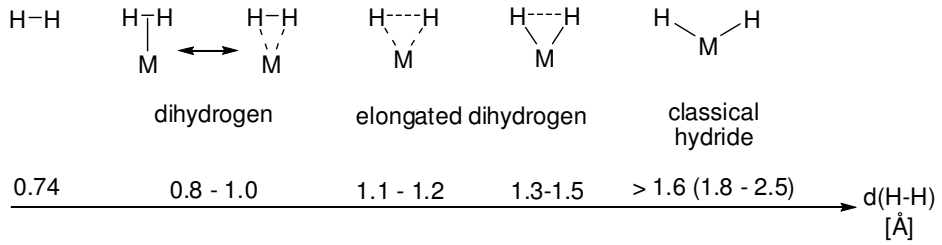

Figure 5: Different metal hydride forms.

An indirect evidence for the presence of a dihydrogen moiety is provided by the generation of the dinitrogen complex via the reversible substitution of the dihydrogen ligand under nitrogen atmosphere. This equilibrium can be monitored by NMR spectroscopy. Nevertheless, this is not a unique indicator since also some classical hydrides, e. g. $[Co(H)_2(PPh_3)]BPh_4$, react to their nitrogen analogues.[48] More detailed information can be obtained by spectroscopic analyses with IR and NMR. As a consequence of the metal coordination the normally IR-inactive stretching oscillation of the free dihydrogen $\nu(H_2)$ becomes asymmetric and thereby IR active. The $\nu(H_2)$ bond of H_2-gas is shifted from about 4300 cm^{-1} to an area between 3100 and 1900 cm^{-1}, ν(M-H) lies between 2200 and 1500 cm^{-1} and the ν_a(M-H_2) between 950 and 850 cm^{-1}.[7, 49] Notably, this energy level does not correlate to the H-H distance because the oscillation frequency depends also on the bond-nature between the metal and hydride moiety, hence an isolated oscillation can not be observed.[50] However, due to the dependence of the oscillation energy from the masses, isotopic substitution leads to a shift of specific bonds which can be assigned according to the *Teller-Redlich-Rule*: A bond shift with the factor $\sqrt{2}$ cm^{-1} can be expected.[51]

The ^{1}H-NMR spectrum of a nonclassical hydride complex shows signals usually in the high field between –5 and –20 ppm at room temperature. $^2J_{PH}$-couplings of nonclassical hydrides are significantly smaller than those of analogous classical hydrides. For this reason the coupling of nonclassical hydrides to other NMR-active nucleus are hardly detectable. More detailed information about the structure can be obtained by analyses of partial *HD*-substituted samples because only intact *HD*-bonds shows the $^1J_{HD}$ (>20Hz) while a classical dihydride shows weak $^2J_{HD}$ (2-3 Hz) and free HD gives $^1J_{HD}$ = 43 Hz.[52] The comparison of the coupling constants *J* with the *HD*- bond length of different dihydrogen complexes leads to a reciprocal behaviour: with enhanced hydrogen distance, the coupling drops.[22] Furthermore, the dihydrogen signal can be analysed with the measurement of the spin lattice relaxation time

(T_1) at various temperatures.[22, 53,] The effectivity of dipole-dipole interaction during the excited-state deactivation in a ^{1}H-NMR experiment between the atom spins is strongly dependent on the distance of the hydrogens. Based on this phenomenon, 1988 *Hamilton* and *Crabtree* recommended this method for the differentiation between nonclassical and classical hydrides if the exchange rate is too high for the detection of *HD*-coupling.[53] Additional, this method makes it possible to calculate H-H bond length.[54] The T_1-relaxation time is determined with inversion-recovery-puls sequencies (180°-t-90°). Due to the relaxation mechanism T_1 passes a minimum at a substance specific temperature (θ_{min}). To determine the H-H bond length, T_1 is measured for the hydride signal at θ_{min}. T_1(min) values for classical hydrides and molecules are >>180 ms (often around 1 s) and between 10-180 ms at 400 MHz for (elongated) dihydrogen complexes.[7] The H-H distance for the two borderlines are calculated as:[55]

$$r_{H-H} = 5.815\ (T_{1min}/\nu)^{1/6} \quad \text{for no rotation} \quad \text{Equation 1}$$

$$r_{H-H} = 4.611\ (T_{1min}/\nu)^{1/6} \quad \text{for fast rotation of the } H_2\text{-ligand} \quad \text{Equation 2}$$

with: r_{H-H} = HH-distance [Å],
T_1 = relaxation time [s],
ν = magnetic frequency [MHz]

It should be mentioned that this detection method does not work for all kind of nonclassical hydrides, e.g. the low T_1(min) value of cobalt hydrides does not change significantly after protonation of the complex.[56] It is assumed that this effect is due to the influence of the metal-hydrogen-dipole-dipole interaction to the relaxation.[57] Finally, *Halpern et al.* pointed out that all possible relaxations pathways are at least important and not only the dipole-dipole interaction (e.g. metals with a high gyromagnetic proportion (Co, Re, Mn), ^{31}P-nucleus, protons of further coordinated ligands and hydride-hydride interaction in polyhydrides).[58] Thus, the determination of the *H-H* distance with T_1(min) values leads to good results for dihydrogen complexes bearing one H_2-ligand but needs to be interpretated carfully for polyhydrides.

More characterisation methods for the determination of the ruthenium dihydrogen moiety can be found with X-ray diffraction and neutron diffraction. These methods are limited due to the requirement of well formed (and large) single crystals, especially for the neutron diffraction.[22b] The *Solid-State*-NMR is another tool for analysing the H-H bond length in the metal dihydrogen complex and the results stay in good agreement with the neutron diffraction but one disadvantage is the interference of the H_2-signal with proton signals of co-ligands which complicates the determination and analysis of the H_2-signal.[17, 59, 60] As an adequate method for structure refinement of the metal dihydrogen moiety, computational methods are also a very powerful tool to verify the experimental data.[26, 61]

1.2.3. Catalysis

1.2.3.1. CH-Activation and H/D-Exchange Reactions

The potential of **1** to catalyse CH-activation is shown in the *Murai*-Reaction as depicted in Scheme 3.[31, 33] The high activity was shown by *Leitner* and *Chaudret* and their co-workers independently by the comparison of conventional reaction conditions ($T \geq 110$ °C)[33] with the present system because the conversion of acetophenone **8** with ethene **9** to the ortho-alkylated products **10** and **11** works already at room temperature.[5, 13a]

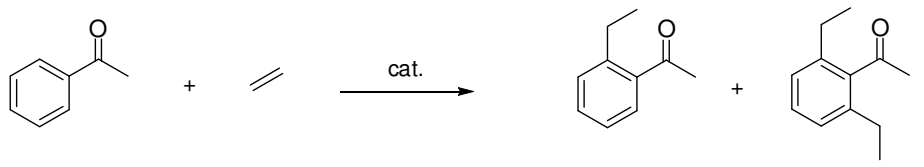

8 **9** **10** **11**

Scheme 3: *Murai-reaction*

Based on these findings, *Leitner´s* group focused in recent years on the investigation of nonclassical ruthenium hydride complexes as potential catalysts.[4, 5, 6] Yields over 90% were reached in the *Murai*-Reaction.[5] These investigations have also shown that the activity of $Ru(H_2)_2(H)_2(PCy_3)(IMes)$ **2** for H/D-exchange between arenes and C_6D_6 is significantly

higher than for **1** (Scheme 4).[4b, 6b] However, although complex **2** has a higher potential for CH-activation, indicated by H/D-exchange, it shows lower conversions in the *Murai*-Reaction.[6]

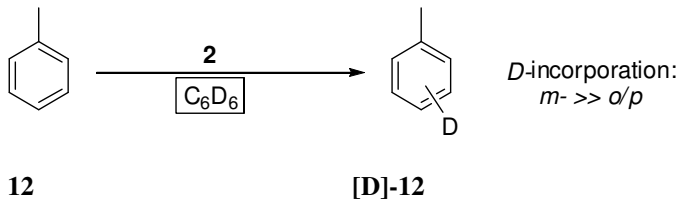

Scheme 4: Deuteration of toluene **12** using **2** as catalyst and C_6D_6 as deuterium source.

As specified above there is still a need for further improvement of the precatalyst structure **2** and optimisation of the reaction conditions for satisfactory CH- bond activation. For this reason, the catalytic H/D-exchange should be more investigated in detail.[4] Catalytic H/D-exchanges under mild conditions are usually performed with D_2 or in deuterated organic solvents like [D_6]benzene or [D_6]acetone and only in very few cases deuterium oxide or [D_4]methanol were used.[9, 62, 63, 64] In recent years, iridium, rhodium and ruthenium complexes showed a promising potential, but reaction temperatures are still well above 100°C for systems utilizing D_2O as deuterium source (Scheme 5).[4b, 9, 63a,b, 64c,d] An efficient system might use deuterium oxide as the cheapest, low-toxic and environmental benign deuterium source, therefore, water-stable catalysts have to be developed.[65, 66] To enhance the stability of appropriate catalysts for H/D-exchange reactions, we extended the structural motifs of nonclassical ruthenium hydrides to complexes with pincer-type ligands, represented with the new complexes [Ru(*dtbpmp*)(H_2)H_2] **4** and [Ru(*dtbpoet*)(H_2)H_2] **5** as here described in the chapters 2.1.1. and 2.2.1. In chapter 2.3.1.1. we report on the efficient and selective H/D-exchange between arenes and D_2O at low temperatures using the new nonclassical hydride complex **4**.[26]

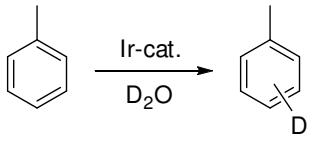

Scheme 5: Iridium catalyzed deuteration of toluene **12** with deuterium oxide as deuterium source.

1.2.3.2. Ruthenium Hydrides in Hydrogen Transfer Processes

Catalytic hydrogenation and dehydrogenation reactions play a major role in industrial processes as well as in the academic research. Metal dihydrogen complexes are most likely intermediates in all of these processes. Vice versa, this implies that dihydrogen complexes are potential hydrogenation catalysts. One reason for this is the reactivity of the dihydrogen ligand and resulting hydrides in the coordination sphere of the catalyst core.[7]

Most ruthenium hydride complexes known in literature can be used for hydrogenation of ketones, aldehydes, alkynes and alkenes under hydrogen gas[27] or under transfer hydrogenation conditions.[67] An interesting example is the the hydrogenation of nitriles according to *Beatty* (*DuPont*), where ruthenium dihydrogen complexes are actually one of the most active catalysts known in literature.[8, 14] *Lau* and co-workers used this catalyst class for hydration of nitriles to amides and for the reduction of ketones, aldehydes and alkynes in a water/organic biphasic systems.[68] Investigations with pincer ligands have not been done yet which shows that there is still a great need of research in the area of nonclassical ruthenium hydride complexes for hydrogen transfer processes.

Garrou reported in 1982 the use of ruthenium dihydrides for the conversion of primary alcohols into the aldehydes.[69] Likewise *Morton* used the ruthenium dinitrogen complex $[Ru(N_2)H_2(PPh_3)_3]$ **13** which is rapidly converted under reaction conditions into the *elongated* ruthenium dihydrogen complex $[Ru(H_2)H_2(PPh_3)_3]$ **14**,[70] under dehydrogenative conditions in primary alcohols (150°C, NaOH) for the transformation into their corresponding aldehydes.[7, 71] The same group reported also in the 80s a rhodium catalysed hydrogen production from alcohols.[72] Recently, *Beller* also presented a hydrogen generation process from alcohols but using different ruthenium catalyst precursors.[73] The dehydrogenation of primary alcohols resulting in homoester formation by intermolecular coupling using ruthenium catalysts was pioneered by the groups of *Shvo*[74] and *Murahashi*.[75] Quite recently *Milstein* published an efficient method for the transformation of primary alcohols into the homesters with abdication of both a sacrificial hydrogen acceptor as well as a base or an acid (like the former standard protocols): 1-hexanol is converted to hexyl hexanoate with 99%

yield in between 6 h and toluene as a solvent under reflux conditions using only 0.1 mol-% of a ruthenium hydride catalyst.[3a, 76] Additionally, the investigation of *Hartwig* and co-workers reflects the catalytic activity of other ruthenium dihydride complexes for the dehydrogenative cyclysation of diols (1,4-butanediol) leading to lactones (γ-butyrolactone) at elevated temperatures (205°C).[77] In the early 1990s also *Lin* and co-workers presented lactonisation with iridium and ruthenium polyhydrides catalysts at remarkable low reaction temperatures (40-75°C).[78] *Milstein* pointed out that the most plausible way for the conversion of primary alcohols into esters, is the formation of the corresponding aldehyde followed by acetalisation which results in a hemi-acetal and this is dehydrogenated into the ester (Scheme 6).[3a] In the present work a nonclassical ruthenium hydride complex showed also remarkable activity in conversion of primary alcohols into their corresponding esters, in fact again under neutral conditions and without the presence of a hydrogen acceptor as discussed in chapter 2.3.2.1.

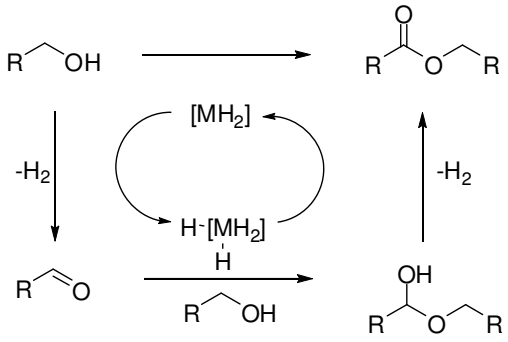

Scheme 6: Ruthenium hydride catalyzed conversion of primary alcohols into esters.

In the last five years, the groups of *Williams* and *Whittlesey* reported a series of new catalytic *tandem-reactions*.[79] In 2002, *Williams* reported the *indirect Wittig-Reaction* of primary alcohols with phosphorylenes in presence of a iridium-catalyst under basic conditions at 150°C.[80a-c] Furthermore, they presented the iridium-catalysed *indirect aza-Wittig-Reaction*, between alcohols and iminophosphorane at 110°C yielding secondary amines,[80d] and other indirect *domino reactions*,[79] e.g.: *(Horner)-Wadsworth-Emmons*,[80a, e] nitroaldol,[80e] and *Knoevenagel Reactions*.[80e] The ongoing research of *Williams* and *Whittlesey* in tandem-catalysis of primary alcohols towards C-C bond formation and transfer-hydrogenation included ruthenium dihydride complexes such as ([$RuH_2(NHC)(PR_3)_2(CO)$]) as catalysts.[67, 80b, 81] Noteworthy, *Lin* showed already in 1993 the potential of transition metal polyhydrides

for catalysed *Knoevenagel-Reactions*.[82] In chapter 2.3.2.1 the application of the new ruthenium dihydrogen complex **4** in an *indirect-Wittig Reaction* with primary alcohols is presented (Scheme 7).

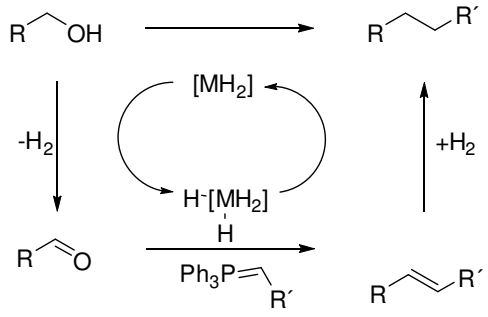

Scheme 7: Ruthenium hydride catalyzed conversion of primary alcohols with phosphorylenes in an *indirect Wittig Reaction*.

In contrast to primary alcohols where an isolable aldehyde is not preferred as product by our catalyst, secondary alcohols can be dehydrogenated to the corresponding ketones under neutral conditions which is discussed in chapter 2.3.2.2. Pioneering work was published by Robinson already in 1975.[83] In the 1980s, *Lin* and co-workers presented efficient acceptorless dehydrogenation catalysis of secondary alcohols by iridium polyhydrides.[84] It was again *Milstein* who reported one of the most active catalysts for this reaction: TON > 900 at a conversion level of 27% or a TON of around 230 at 96% conversion were observed for 2-propanol as a substrate, whereby no hydrogen acceptor but 1.6 mol-% of sodium isopropoxide as a basic co-catalyst was used.[3c] Recently, the group of *Hulshof* published the most efficient system for acidic conditions.[85] We also observed that the chosen pH-value plays a tremendous role but – in contrast to other studies – in terms of selectivity: When we switched from neutral to slightly basic environment by addition of catalytic amounts of base, we obtained a coupling reaction of two molecules of alcohols giving branched ketones (Ct. 2.3.2.2, Scheme 8). Such reactions where secondary alcohols are condensed to higher molecular weight alcohols or ketones under basic conditions are so-called *Guerbet* reactions[86] which have been recently studied extensively by the group of *Carlini*[87] and also by *Williams* and co-workers.[88]

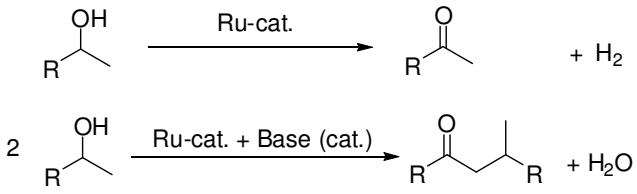

Scheme 8: Catalysis test reactions for dehydrogenation of secondary alcohols and Guerbet-type coupling.

2. Results and Discussion

Chapter 2 discuss the following aspects: The synthesis and characterization of the novel nonclassical ruthenium hydride complexes [Ru(*dtbpmp*)(H_2)H_2] **4**, bearing a PNP pincer, and [Ru(*dtbpoet*)(H_2)H_2] **5**, bearing a POP pincer and reactivity aspects are described. Furthermore, we present here the application in catalysis of [Ru(*dtbpmp*)(H_2)H_2] **4** for H/D-exchange reaction, dehydrogenation reactions involving alcohols and some further test reactions.

2.1. The Ruthenium Dihydrogen Complex [Ru(*dtbpmp*)(H_2)H_2]

2.1.1. Synthesis

In an attempt to generate monomeric nonclassical ruthenium hydride complexes with a chelating ligand framework, we turned the attention toward pincer type ligands which allow a *trans* arrangement of two electron-rich and bulky phosphorous donor groups. As the most efficient and practical method towards these ruthenium complexes the direct-hydrogenation route is used, which was first published in the open literature by *Leitner* and co-workers.[35] In an one pot procedure [Ru(cod)(2-methylallyl)$_2$] **6** was hydrogenated (7 bar) at 55°C in pentane in the presence of the PNP-pincer ligand *dtbpmp* **15** on a mmol scale. It reacts cleanly to give the complex [Ru(*dtbpmp*)(H_2)H_2] **4** (Scheme 9).

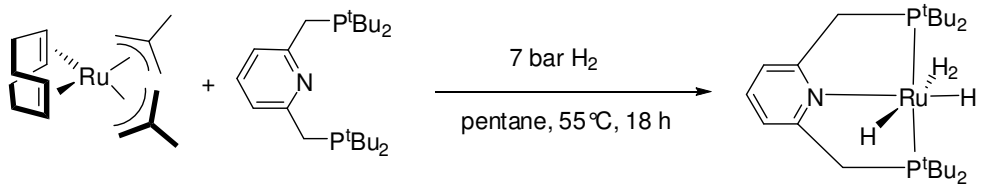

6 **15** **4**

Scheme 9: Direct hydrogenation of [Ru(cod)(metallyl)$_2$] **6** in presence of *dtbpmp* **15** to give the nonclassical ruthenium hydride complex **4**.

Complex **4** is isolated directly from the reaction mixture by cannula filtration at room temperature as a light-brown microcrystalline powder. The product was washed with pentane and dried in a hydrogen stream. Yields are typically in the range of 50-75% but reaction times strongly depend on the quality of the precursor **6**.[89] Where 18 h were sufficient in many cases, prolonged reaction time for two days were found to be necessary with certain batches. Complex **4** is surprisingly stable under argon and can be stored under argon at –20 °C for several days. Prolonged storage under argon should be avoided while hydrogen atmosphere is preferred. Nevertheless, it is recommended to produce it freshly and use it directly for further experiments.

Taniguchi´s pentahydride [Ru(*dtbpmb*)$(H_2)_2$H] **16** bears the analogue PCP-pincer but coordinates two H_2-ligands and one hydride (Figure 6).[4b] The neutral two electron donor group of the pyridine moiety in **15** results in the coordination of two classical hydrides and one molecular hydrogen ligand in [Ru(*dtbpmp*)$(H_2)H_2$] **4**.

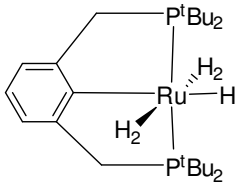

16

Figure 6: *Taniguchi´s* pentahydride [Ru(*dtbpmb*)$(H_2)_2$H] **16**.

2.1.2. Characterisation

For the structural investigation of [Ru(*dtbpmp*)(H_2)H_2] **4** we used NMR and IR methods, furthermore DFT-calculations were performed.[26] The ^{31}P-NMR shows a singlet signal indicating the equivalence of the two phosphorus atoms and the symmetric P-Ru-P *trans*-arrangement. Interestingly, complex **4** coordinates two classical hydrides and one dihydrogen which was confirmed by ^{1}H-NMR and IR spectroscopy. The hydrides are identical on the NMR scale due to fast exchange but the T_1-measurement revealed the presence of a molecular dihydrogen ligand. The IR spectra show bands characteristically for classical ruthenium hydrides at 1990, 1892 and 1700 cm^{-1} (νRu-*H*) and at 2095 cm^{-1} (νRu-*H*) for the nonclassical ruthenium dihydrogen moiety. For further details see chapter 2.1.3.2. and therein Figure 16 shows the IR spectra.

At room temperature, the ^{1}H-NMR of [Ru(*dtbpmp*)(H_2)H_2] **4** shows a signal at –7.3 ppm (t, 4 H, ^{2}J(H,P) = 13.2 Hz, Figure 7) at room temperature and by cooling the sample subsequently to –80°C the triplet changes to a broad signal. For the T_1-measurements we recorded six series with 14 spectra each between 300 and 193 K to determine the T_1(min) value which was found to be 77 ms at θ_{min} = 228 K and 400 MHz (Figure 8). This T_1(min) value fits in the predicted range (10-180ms) for a dihydrogen ligand. According to *Hamilton, Crabtree* and *Halpern*,[54, 58] we calculated the H-H distance of the H_2 moiety with equation 2 resulting in a bond length of 1.11 Å (± 0.01 Å, based on instrumental error). This value determines an upper limit for the estimated bond length due to the presence of classical hydrides which quite often results in an increase of the T_1-values and the T_1(min).

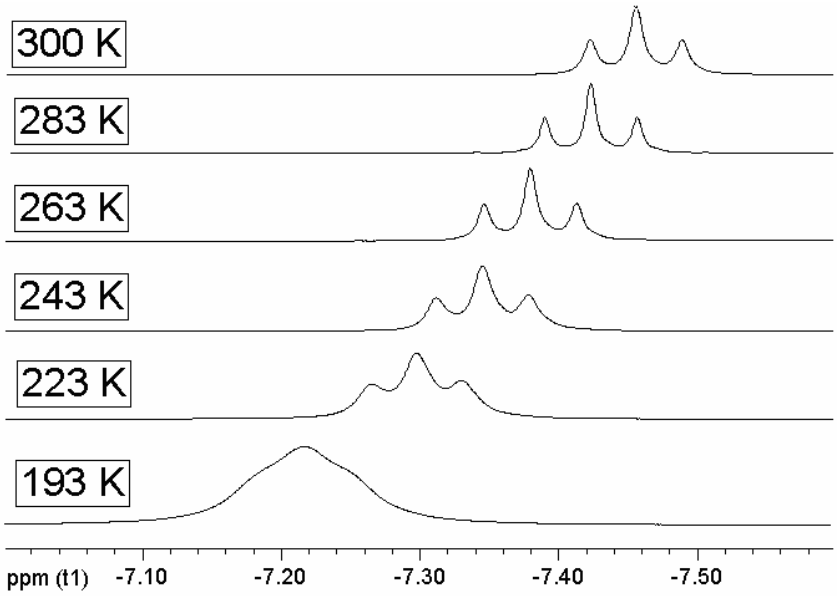

Figure 7: The ^{1}H-NMR spectra shows the hydride-signal of **4** at different temperatures.

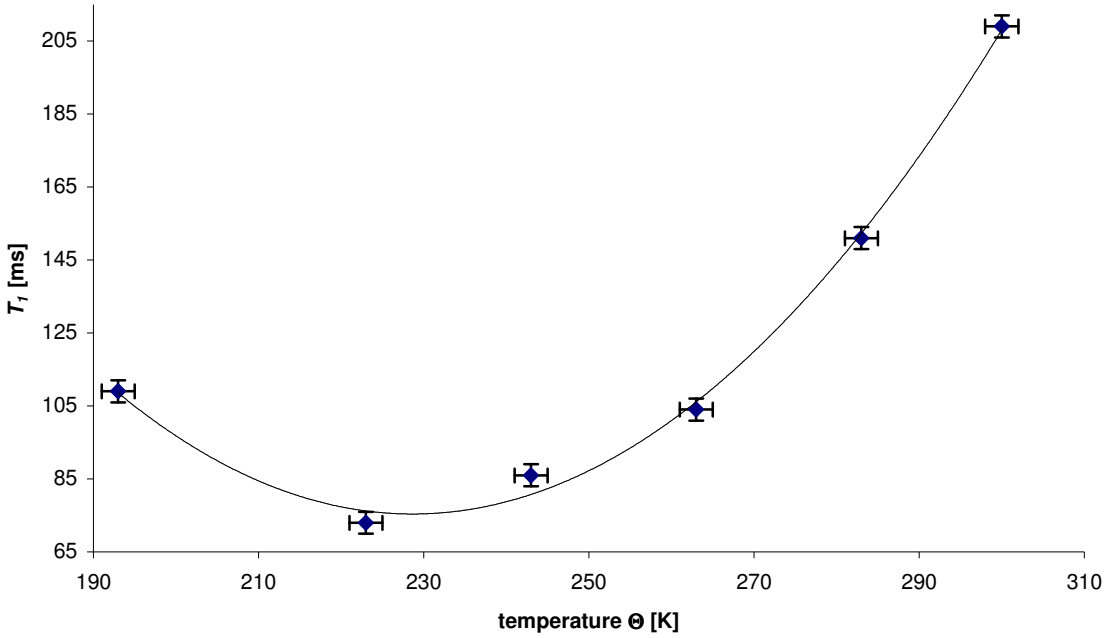

Figure 8: T_1-values as a function of temperature Θ determined for [Ru(*dtbpmp*)(H_2)H_2] **4**. T_1/ms (Δ3ms) [T/K (Δ2K)]: 209 [300], 151 [283], 104 [263], 86 [243], 73 [223], 109 [193].

Furthermore, the temperature dependences of $\ln(1/T_1)$ as a function of 1000/T in the high-temperature area results in a linear correlated slope which corresponds to the maximum activation energy of the molecular motion of the complex.*[90] The calculated apparent maximum activation energy is $E_A = 6.3$ kcal mol^{-1}.

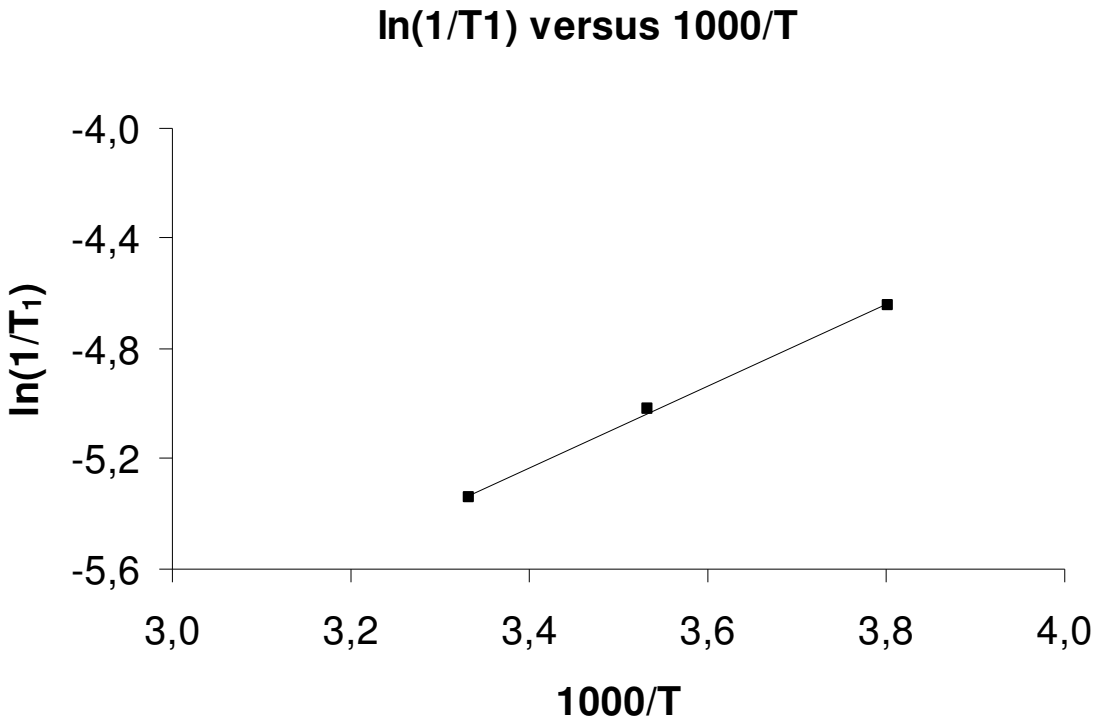

Figure 9: $\ln(1/T_1)$ as a function of 1000/T for hydride signal in the ^{1}H-NMR of [Ru(*dtbpmp*)(H_2)H_2] **4**.

To obtain further information about the coordination geometry of the ruthenium dihydrogen moiety in [Ru(*dtbpmp*)(H_2)H_2] **4** computational investigations were performed.[91] All calculations were carried out within the DFT formalism (B3LYP)[92a-d] as implemented in the Gaussian03 suite of programs.[26, 92e] As model system the *t*Bu groups at the P centres of [Ru(*dtbpmp*)(H_2)H_2] **4** were replaced by methyl substituents; [Ru(*dMepmp*)(H_2)H_2] **17** (Scheme 10).[93] The performed calculations brought clearance into the octahedral coordination-mode of ruthenium in **4**. While the *trans* arrangement of the phosphine ligands in the PNP pincer *dtbpmp* **15** could be clarified by spectroscopic methods, it is not possible to distinguish between the *cis* or *trans* arrangement of the H_2-ligand and the *N*-pyridyl unit. The DFT-calculations verified the *cis*-arrangement in **4** and a *trans*-isomer of **4** could not be localized. Instead, for the model complex **17** a classical ruthenium tetrahydride [Ru(*dMepmp*)H_4] **19** could be detected with a slightly higher energy level (3 kcal/mol) as

* The activation energy of the molecular motion of [$RuH_4(PPh_3)$] is 2.8 kcal/mol.[90]

depicted in Scheme 10.[26, 61] The transition state for the conversion of **17** into **19** is depicted in Figure 10. The *cis*-form of **4** (or **17**) regarding the H_2-ligand *cis* to the pyridine consequently results in a trans-arrangement of the dihydrogen-ligand (labile ligand) and a classical hydride (a good σ-donor). This *trans*-configuration of the H_2-ligand to a classical hydride could activate the dihydrogen unit towards H-H bond cleavage or could cause a stretched dihydrogen complex. Otherwise, the *cis*-form is much more stable with respect to H_2 loss than the *trans*-form (H_2 *trans* to pyridine) which argues for the *cis*-form as stable configuration.[7]

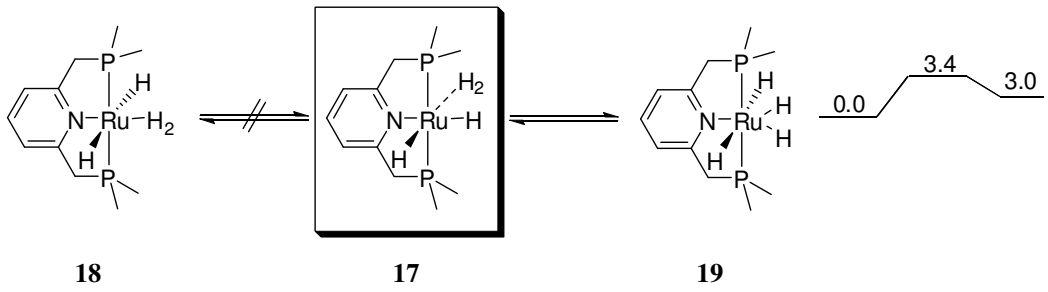

Scheme 10: Stable coordination modes of the [Ru(*dMepmp*)H_4] **19** as localized by DFT-calculations.[26, 61]

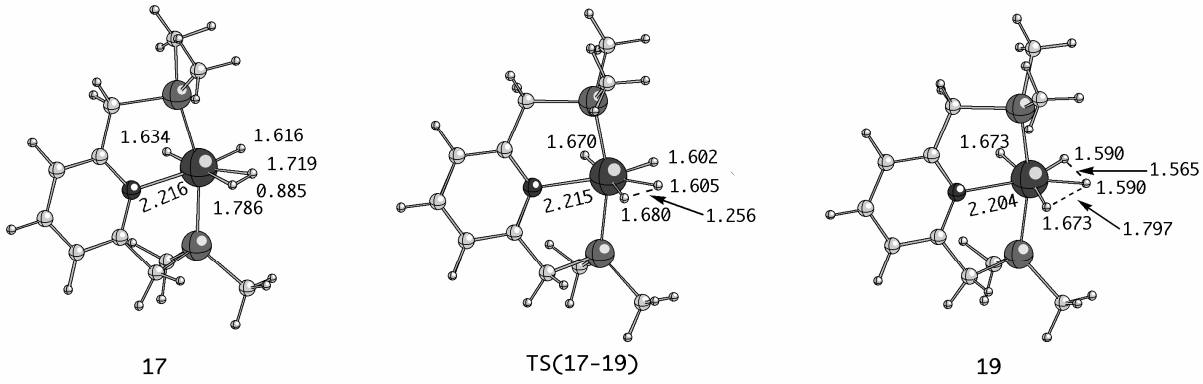

Figure 10: Ball-and-Stick models of the complexes **17**, **19** and the transition state TS(**17**-**19**). Selected bond length and H-H distances are depicted.

The existence of an analogue tetrahydride of **4** could not be verified experimentally. However, dihydrogen-dihydride equilibrium are known and such processes have activation enthalpies between 10 and 20 kcal mol^{-1}.[7] In contrast hydride formation in equilibrium in case of elongated dihydrogen complexes is even harder to be observed separately as they have an activation energy with less than 10 kcal mol^{-1}.[7] One indicator for an slightly elongated dihydrogen complex form of **4** (H-H distance: 1.1 Å) closed to the lower limit (Ct. 1.2.2., Figure 5) might be the observation that the coupling constant *J* and the chemical shift does not

show a high temperature-dependence and only small changes for δ and *J* are observed between -50°C and +27°C (δ = -7.2 to -7.4 ppm, *J* = 13.0-13.4 Hz). In contrast, a nonclassical ruthenium "trihydride" with a H_3^--ligand, [$RuH_3(Cp^*)(P^iPr_3)$], shows large temperature-dependent couplings (60 Hz at 170 K and 130 Hz at 203 K).[94] A "nonclassical trihydride" form (Scheme 11: B, C) or a tetrahydrogen intermediate of **4** is plausible due to the possible *cis*-interaction between the H_2-unit and the neighboured classical hydride in a combined associative (A-D) and dissociative (E-H) process (Scheme 11).[7] This *cis*-interaction could lead to a (nonclassical) ruthenium tetrahydride similar to **19** which can easily switch to a *cis*-formation again with involvement of all hydrogens in the ruthenium coordination sphere. In the present case, the *cis*-interaction allows the fastest exchange between the dihydrogen unit and a hydride via the associative H-H-H mechanism with a low barrier (Scheme 11: B-C). However, the dihydrogen ligand also stays *trans* to a hydride. And for this reason a dissociative process with a tetrahydride intermediate might be favoured (Scheme 11: E-H). Factors which support the dissociative pathway are flexibility of the backbone, the bulkyness of the tBu groups for the distortion of the octahedral geometry, the electron-donating phosphorus atoms and the basicity of the ruthenium core.[7] These possibilities for isomerisation between different complex forms also explain H/D-exchange of all hydride ligands e.g. under D_2 atmosphere. If just a simple H_2 / D_2-exchange at a M-H_2 moiety would occur, then one could observe just a partial deuterium incorporation in the hydride ligand sphere which usually does not occur.

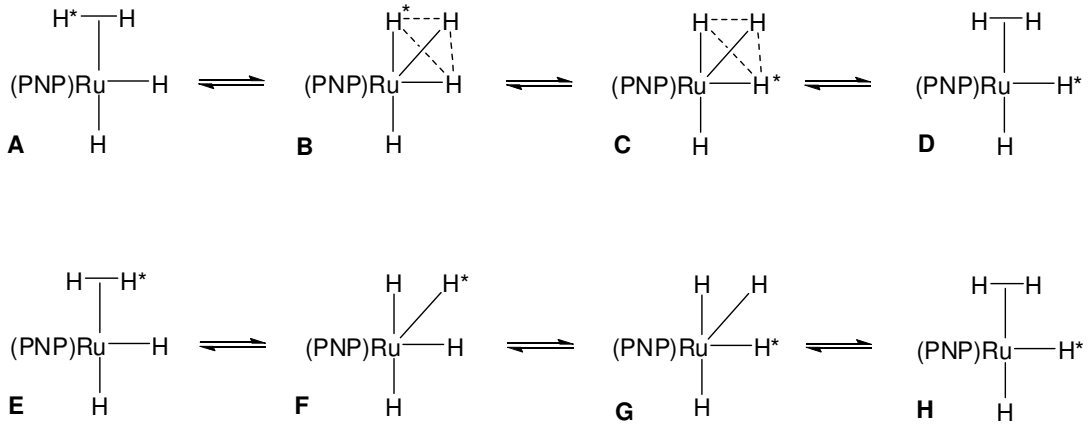

Scheme 11: Intramolecular H atom exchange: Associative process (A-D) involving a nonclassical trihydride and the dissociative process (E-H) with the classical tetrahydride.[7]

The DFT-calculations with [Ru(*dMepmp*)(H_2)H_2] **17** resulted in a H-H-distance of 0.885 Å for the ruthenium dihydrogen moiety. Further DFT-calculations with the *real* complex **4** shows that *t*Bu groups have a significant influence to the dihydrogen coordination mode resulting in a H-H-distance of 0.979 Å (Figure 12). This value is fully in line with the NMR spectroscopic value of 1.1 Å as the upper limit for the H-H distance in [Ru(*dtbpmp*)(H_2)H_2] **4**.

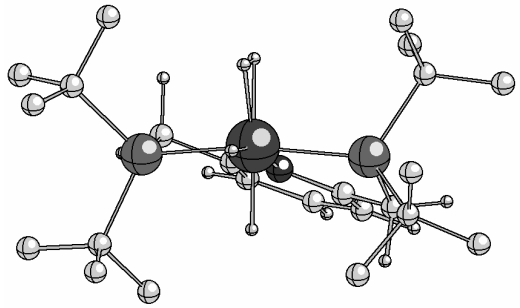

Figure 11: Ball-and-Stick-representation of the calculated structure for the complex [Ru(*dtbpmp*)(H_2)H_2] **4**. The side-view on the equatorial plane shows the twisted conformation with the CH_2 groups on different sides of the equatorial plane (PNP) resulting in a *gauche* conformation of the phosphine groups. For clearance the H-atoms in the pincer-backbone are not depicted.

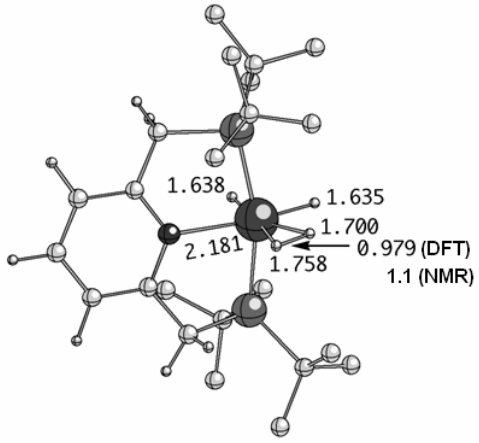

Figure 12: Ball-and-Stick-representation of the calculated structure for the complex [Ru(*dtbpmp*)(H_2)H_2] **4** with the assigned H-H distances in the RuH_2-moiety determined by NMR (1.1. Å) and DFT (0.979 Å). For the *model* complex [Ru(*dMepmp*)(H_2)H_2] **17** the assigned H-H distances in the RuH_2-moiety is 0.885 Å as determined by DFT.

Upon comparison of the two calculated structures of **4** and **17** one can see that the substitution on the phosphor atoms of the ligand sphere has significant influence on the geometric *and* electronic situation of the ruthenium atom. The Ru-P distances in complex **4** are *longer* (2.307 and 2.316 Å) and the Ru-H_2 distance is *shorter* in complex **4** (1.700 / 1.758 Å), than in the *model* complex **17** (Ru-P: 2.285 and 2.297 Å and Ru-H_2: 1.719 and 1.786 Å). The Ru-H distances of the classical hydrides are practically identical (**4**: 1.638 / 1.635 Å and **17**: 1.634 and 1.616 Å). These differences in the Ru-P and Ru-H_2 distances in **4** and **17** allow the assumption that the phosphines in **4** are bounded in a less stronger fashion to the ruthenium core than in **17**. Vice versa the dihydrogen ligand adjusts the different electronic situation and for this, it is stronger bounded in **4.** These differences might explain the longer HH-distance in the *real* [Ru(*dtbpmp*)(H_2)H_2] **4**. Furthermore, the calculated structure of **4** also shows

distortion of the octahedron. The P-Ru-P angle is 164.2° and the pincer angle is 101.0°. The CH_2 groups are rotated out of the PNP plane with a torsion angle of +19.21° and -23.15°. This twisted conformation with the CH_2 groups on different sides of the equatorial PNP plane results in a *gauche* conformation of the bulky phosphines, stays in agreement with the most complexes bearing aromatic pincer ligands.[2]

2.1.3 Reactivity

2.1.3.1. H_2 / N_2 Exchange

For further characterisation of the ruthenium dihydrogen moiety an equilibrium reaction between the weak ligands H_2 and N_2 were performed under argon and monitored by NMR spectroscopy. The Ru(*dtbpmp*)(H_2)H_2 **4** was dissolved in [D_8]toluene, to give a dark-red solution, then the solution was gently bubbled with a nitrogen stream for 90 minutes (Scheme 12).

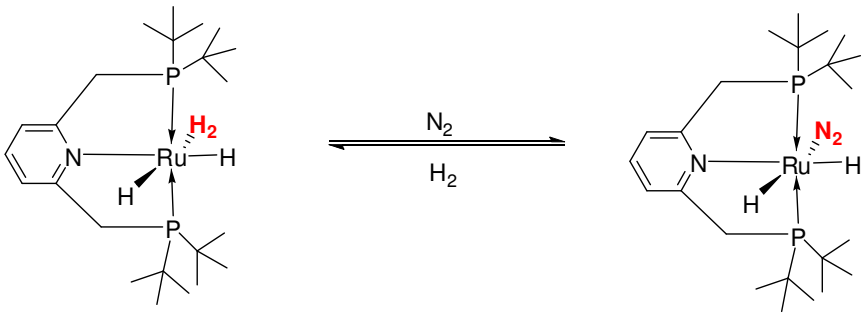

4 **20**

Scheme 12: Formation of the dinitrogen complex **20**

The dihydrogen ligand in complex **4** can be replaced by N_2, but the reactivity of **4** differs significantly from the ruthenium dihydrogen complexes **1-3** (Figure 2 and Scheme 13).[4,5] In the beginning the ligand exchange is relatively slow, reaching 66% conversion after 90 min, determined by ^{1}H NMR and ^{31}P-NMR spectroscopy. For a full conversion the NMR-tube was kept under a nitrogen stream for 20 h and spectra were recorded again. Interestingly, the colour changed from red to black and one still could not determine a full conversion to the dinitrogen complex **20** but a further decrease of the hydride signal of **4** at –7.3 ppm and a

slight increase of the signals at –4.6 and 12.8 ppm. Most notably, the ^{31}P-NMR indicated that there was still 6% of **4** left, the signal of **20** decreased from 66% to 32%. A new range of broad signals between 81 and 74 ppm (35%) as well as 70 and 65 ppm (27%) could be detected as depicted in and Figure 14. This indicates that the monomeric complex [Ru(*dtbpmp*)$H_2(N_2)$] **20** (^{31}P-NMR: +99.6 ppm; ^{1}H-NMR: –4.6 (t, ^2J(H,P) = 16.81 Hz) and –12.8 ppm) appears to be unstable and converts to a dynamic system of presumably polynuclear complexes (Scheme 13). This process is fully reversible. Complex **4** is restored quantitatively by bubbling the solution with a H_2-stream for one day as shown by NMR analyses and also the black mixture returned to a clear dark-red solution.

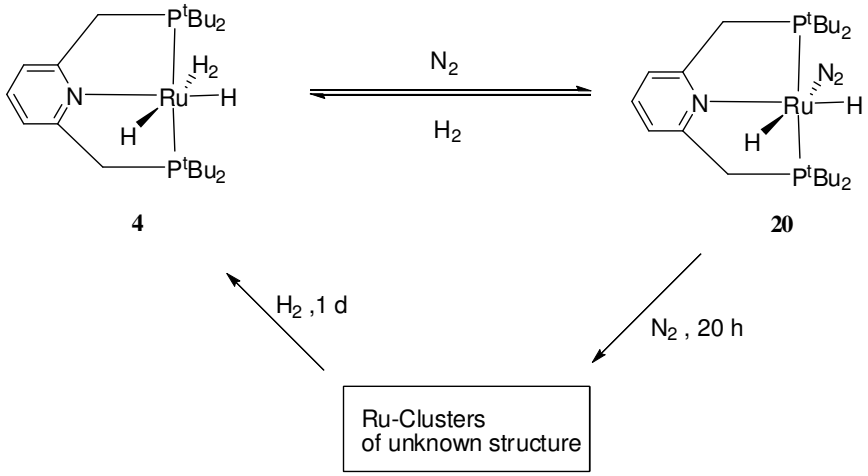

Scheme 13: Reversible formation of dinitrogen complex **20** and ruthenium clusters from **4** under N_2 and H_2 atmosphere.

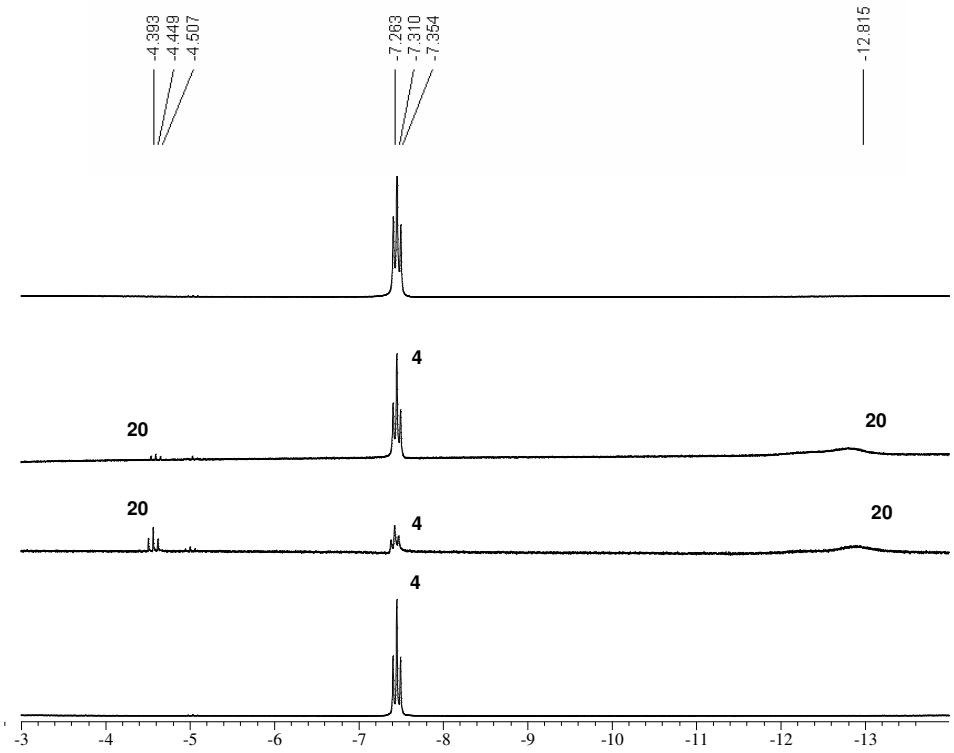

Figure 13: ^{1}H-NMR spectra (hydride area) of **4** (top: under Ar), **20** (2nd: 90 min N_2), "Ru-Cluster" (3rd: 20 h N_2) and restored **4** (bottom: 1 d H_2).

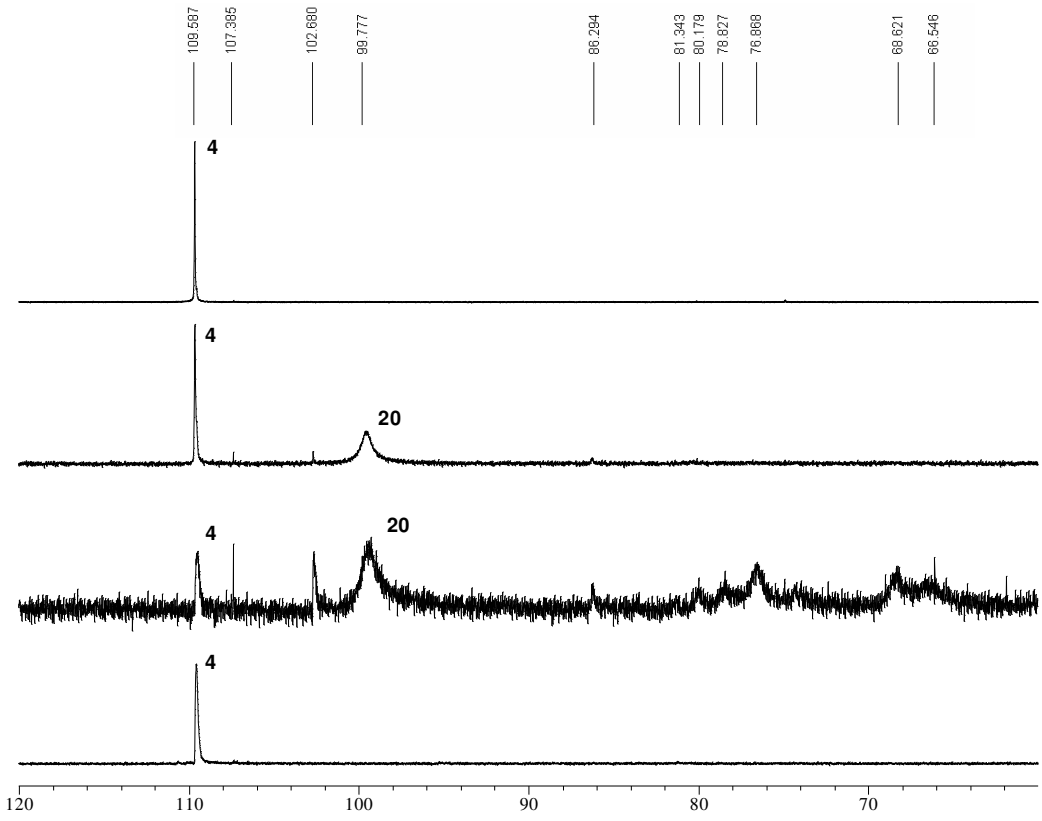

Figure 14: ^{31}P-NMR spectra of of **4** (top: under Ar), **20** (2nd: 90 min N_2), "Ru-Cluster" (3rd: 20 h N_2) and restored **4** (bottom: 1 d H_2).

Attemps to isolate either **20** or the resulting cluster(s) were unsuccessful. The treatment of Ru(*dtbpmp*)(H_2)H_2 **4** with 5 bar N_2 resulted in a brown solid which was formed in a pentane suspension. After separation of the solid material from solution that the presumed ruthenium dinitrogen complex or cluster are highly unstable under argon atmosphere which is revealed by a rapid conversion of the solid into an amorphous viscous material under gas evolution (N_2-loss). The NMR analysis of the decomposed material does not show any defined compound. This result differs from stable ruthenium dinitrogen complexes bearing the PNP pincer *dtbpmp* **15** which were recently published by *Milstein* and co-workers.[3c] A monomeric complex [Ru(*dtbpmp*)H(N_2)Cl] were obtained with the N_2-unit *trans* to the pyridine and the end-on dinitrogen-bridged dimer [(Ru(*dtbpmp*)Cl_2)$_2N_2$] which are both stable as solid and in solution. For the dimer an equilibrium with the corresponding monomer was observed depending on the N_2 and complex concentration in solution.

2.1.3.2. H / D Exchange

^{1}H-NMR studies of the long term stability of complex **4** in deuterated aromatic solvents reveal an interesting *H/D*-exchange process in [D_8]toluene or C_6D_6 whereby complex **4** incorporates deuterium from the solvents into the *PNP*-pincer backbone (**21** / [D_x]-**4**, Scheme 14). Preferably, the *C4*-position of the pyridyl-system (6.5 ppm; >95% *D*) and the benzylic positions are deuterated (3.1 ppm; ~25% *D*) within 72 h at room temperature. Interestingly, the hydride area of the ^{1}H-NMR still shows hydridic signals at this stage. This indicates that a slow H/D-exchange between **4** and the solvent is followed by a rapid exchange at the pincer backbone from the intermediate ruthenium deuteride. After three weeks, the sealed NMR sample shows a decrease of signal intensity also in the *t*-butyl resonances and a significant increase of the solvent residue H-signal is also detected. The ^{31}P-NMR spectra of this samples still shows mainly the signal of **4** at 109 ppm (>90%), with a new signal at 107 and some weak signals at 102, 99 and between 88 and 80 ppm. After 3.5 months the ^{31}P-NMR of the same sample remains identical, but the ^{1}H-NMR shows further decrease of the signal intensity in all molecular parts including the hydride moiety and an increase of the solvent residue signal. In a further experiment we performed the deuteration of **4** in C_6D_6 at 50 °C for 48 h. Analysis by ^{2}H-NMR confirmed unequivocally the incorporation of deuteration in the hydride, aliphatic and aromatic parts and ^{1}H-NMR spectroscopy revealed that > 90% of the

hydrogens in **4** are substituted by deuterium in all positions.

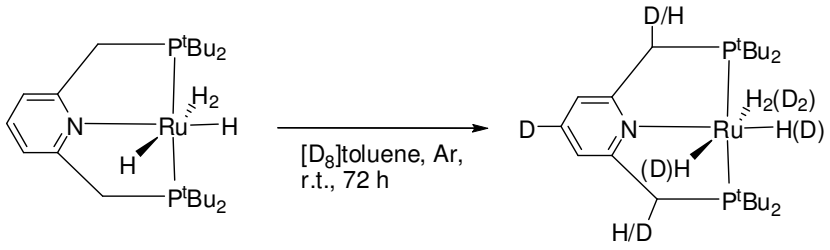

4 **21 ([D$_x$]- 4)**

Scheme 14: Formation of [D$_x$]-*Ru(dtbpmp)H$_2$(H$_2$)* **21** ([D$_x$]- **4)** starting from **4** with [D$_8$]toluene at room temperature within 72 h.

Similar results were obtained when the complex synthesis was performed using D_2-gas instead of H_2. Again the *C4*-position (>95% *D*) and the benzylic positions (~ 25% *D*) were deuterated as indicated by comparison of the NMR and IR spectra (Figure 16) of **4** and **21** (**[D$_x$]- 4**). The IR spectra of the non-deuterated complex **4** show bands characteristically for ruthenium hydrides at 1990, 1892 and 1700 cm^{-1} (ϒRu-*H*)) and at 2095 cm^{-1} (ϒRu-*H$_2$*). Moreover, the spectrum of **21** (**[D$_x$]- 4**) includes further bands at 2247, 2199 and 2151 cm^{-1} which can be assigned as (ν*CD$_{ar}$*) bands by comparison with the (ν*CH$_{ar}$*) bands according to the *Teller-Redlich-Rule*.[51] The expected bands between 1488 and 1202 cm^{-1} for ruthenium deuterides are hidden in the finger-print area. These results show that a synthesis of the ruthenium deuteride (**22** / [D$_4$]- **4,** Figure 15) seems impossible due to the rapid H/D-scrambling. As soon as deuterium is incorporated at the ruthenium core, a partly deuterated pincer-backbone is obtained whereby the expected ruthenium deuterides are exchanged to ruthenium hydrides.

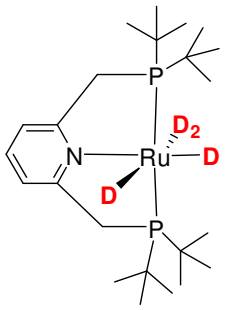

Figure 15: The nonclassical ruthenium deuteride **22** / [D$_4$]- **4**.

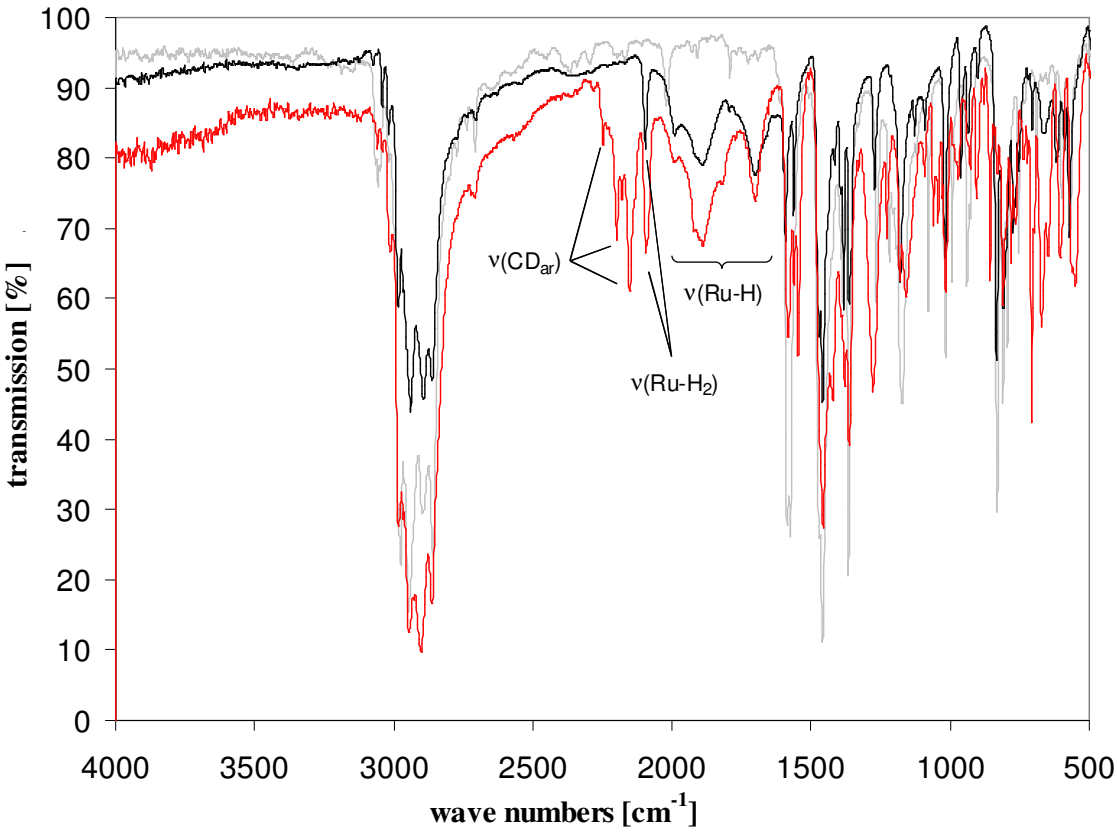

Figure 16: Comparison of the IR spectra of Ru(*dtbpmp*)$H_2(H_2)$ **4** (black), [D_x]-*Ru(dtbpmp)$H_2(H_2)$* **21** / [D_x]-**4** (red) and the free ligand *dtbpmp* **22**(light grey).

These observed results of H/D-scrambling into the pincer-backbone indicate potential catalytic activity for CH-activation. Indeed, one need to differentiate between at least two different reaction pathways: intramolecular and intermolecular. On one hand the deuteration of the para-position in the pyridyl-ring must be a reaction between two complexes, on the other hand, the deuterium incorporation into the benzylic positions and tBu groups is most likely intramolecular. Due to the propeller-like spinning of the tert-butyl groups all methyl groups in the tert-butyl groups are near enough (Ru-*H*CH_2 minimum distance = 3.2 Å) to the ruthenium centre for intramolecular CH-activation. This is in agreement with the results and the situation of the [Ru(IMes)(PCy_3)$H_2(H_2)_2$] **2**.[4b] Here the minimum distance of the methyl groups in the ortho-positions of the IMes ligand to the ruthenium core is even a little bit longer (3.5 Å), but deuteration of these positions is observed, too. The distance between the hydrogens of the benzylic positions and the ruthenium is also 3.5 Å.

Otherwise, a direct exchange seems to be possible because it is known that the benzylic positions of such a pincer-backbone in a ruthenium complex are of enhanced activity and acidity.[3c] So, one could imagine a direct exchange via σ-bond metathese. The benzylic positions also might play an important factor for the stabilization of the resulting species after slow H_2-loss of the [Ru(*dtbpmp*)(H_2)H_2] **4**: one could imagine that an unoccupied position in the trigonal bipyramidal [Ru(*dtbpmp*)H_2] **23** allows a strong agostic interaction between the ruthenium core and a benzylic hydrogen. The resulting hydride complex **24** is presumably directly converted via CH-bond cleavage into the trihydride **25** (Scheme 15) in analogy to the reactivity of literature known ruthenium hydride complexes.[3]

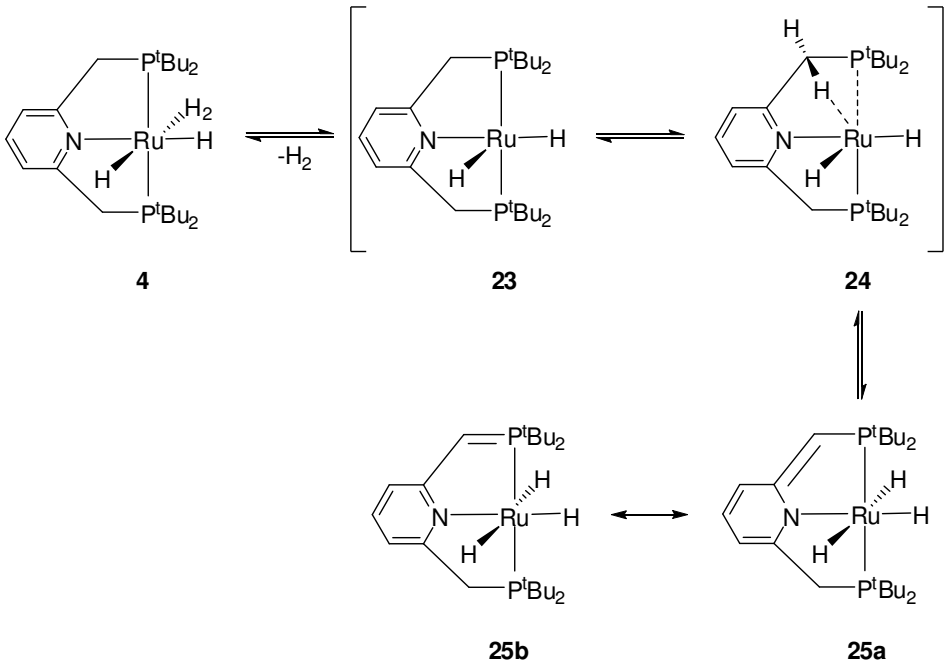

Scheme 15: Proposed dehydrogenation of **4** followed by intramolecular CH-bond cleavage via agostic interaction towards the unsaturated ruthenium trihydride **25** .

Notably, neither the trihydride **25** nor any other species could be assigned by NMR analysis, so assumable they are not formed in significant concentrations under these conditions, probably because no irreversible H_2-loss occurred. In case of the trihydride **25** especially the ^{1}H-NMR spectra should change extremely due to the unequal bond situation of the two phosphorus atoms with the benzylic positions. But neither in the ^{1}H- and ^{2}H-NMR nor in the ^{31}P-NMR new signals appeared which can be related to such a species.

To gain further experimental evidence for the enhanced reactivity of the benzylic positions in [Ru(*dtbpmp*)(H_2)H_2] **4**, the complex was dissolved in oxygen free [D_{12}]cyclohexane, followed by the addition of D_2O. The NMR-tube was shaken for a few minutes, then ^{1}H-NMR and ^{2}H-NMR spectra were measured (Scheme 16). The NMR spectra verify the unequal higher reactivity of the benzylic position. The ^{1}H-NMR shows that the benzylic positions are deuterated with 83% and the hydride-signal shows a deuterium incorporation of ca. 55% and in the *para*-position of the pyridine-ring the signal decreased only 10%. The deuterium incorporation can be qualitatively assigned in the ^{2}H-NMR for the mentioned positions, too. Noteworthy, using D_2O as deuterium source, the deuterium incorporation is likely to occur at the benzylic positions directly rather than via the ruthenium hydride core. As mentioned by *Milstein*,[3] ruthenium complexes of this pincer-ligand are highly acidic in the benzylic positions and for this, the enhanced deuterium incorporation in these positions may also come from a simple acid base exchange of protons between **4** and D_2O. Such behaviour would explain the different result in comparison with C_6D_6 or [D_8]toluene as deuterium source, where the benzylic positions were deuterated to a lower degree (~25%).

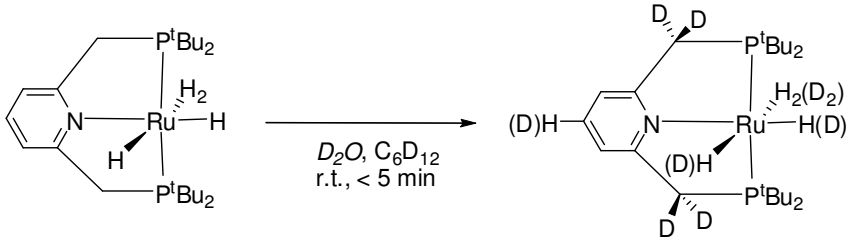

4 **26**

Scheme 16: Selective deuterium incorporation into the dihydrogen unit and the benzylic positions of **4**.

The experimental results further point at the important role of the benzylic positions in the pincer-backbone of [Ru(*dtbpmp*)(H_2)H_2] **4** towards CH-activation. Interestingly, the deuteration into these positions (83%) is even faster than the H/D-exchange of the ruthenium hydride core (55%). This result might be a hint that there are two different pathways for the deuterium incorporation depending on the deuterium source (Scheme 17). Using C_6D_6 first there is a H/D-exchange between the C_6D_6 and the ruthenium hydride core, followed by an exchange between the ruthenium deuterides and the ligand backbone, especially with the benzylic positions (25%). With D_2O, it seems most likely that the deuterium incorporation first occurs at the benzylic positions (83%), followed by an exchange between these

deuterated positions and the ruthenium hydride core (55%).

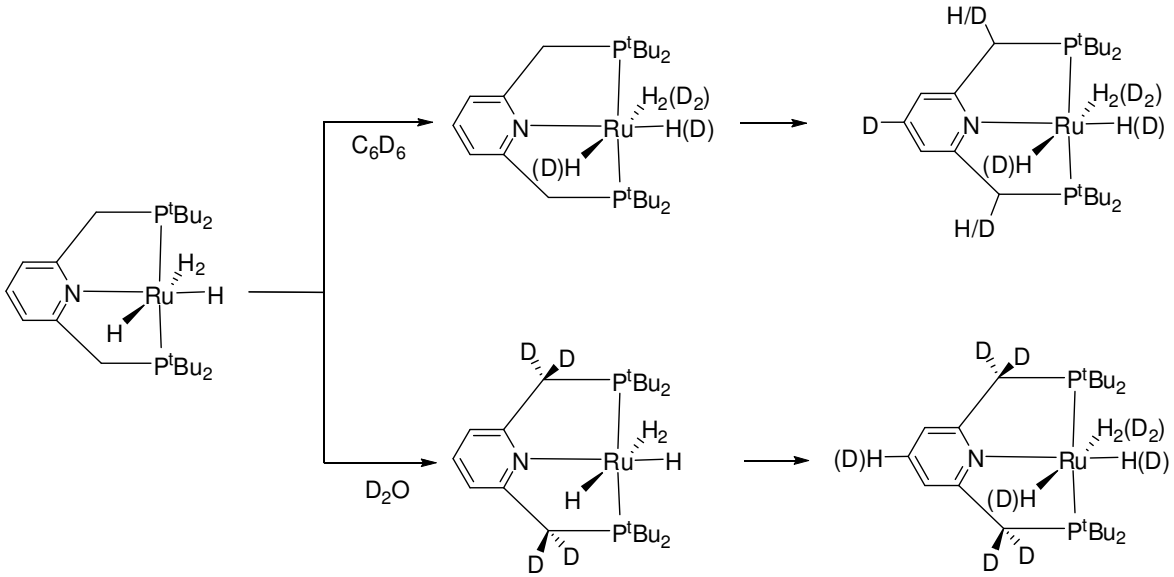

Scheme 17: Different pathways for the deuterium incorporation into complex **4** with C_6D_6 and D_2O.

2.1.3.3. Treatment with carbon monoxide

For investigations regarding the reactivity of the pincer type nonclassical hydride complexes, a solution of [Ru(*dtbpmp*)(H_2)H_2] **4** in [D_8]toluene was treated with carbon monoxide. The ^{1}H-NMR spectra shows complete disappearance of the original hydride signal. Furthermore, the doublet signal of the benzylic positions in **4** changed to a singlet in **27**. In the ^{31}P-NMR the signal of **4** at 109.6 ppm disappeared, too. Instead, there is a new principal signal at 106.5 ppm (88%) and some small signals at 90.2, 88.0 and 69.9 ppm. The main signal is assigned to a presumed 14e$^-$ species [Ru(*dtbpmp*)(CO)] **27** (Scheme 18).[95] The sample was kept under argon at room-temperature and measured again after five days. The NMR spectra changed drastically and showed approx. a 1:1 mixture of two compounds. Besides **27** a ruthenium mono-hydride **28** has been formed via transfer of a hydrogen atom from the benzylic positions (Scheme 18). By treatment of the NMR-sample with a hydrogen-stream for 20 minutes, the signal at 106.5 ppm (**27**) in the ^{31}P-NMR spectrum disappeared which indicates completed conversion and the main signal (>90%) of the ruthenium mono-hydride **28** appeared at 90.0 ppm (d, $^2J_{PP}$ = 30.3 Hz; Scheme 18). The hydride exhibits a triplet at -6.04 ppm (t, $^2J_{HP}$ = 18.2

Hz) in the ^{1}H-NMR spectra. It can be assigned as [Ru(*dtbpmp**)(CO)H] **28** comparison with *Zhang´s* [Ru(*diprpmp**)(CO)H] **29** and [RuH(PNN)CO] **30**.[3a]

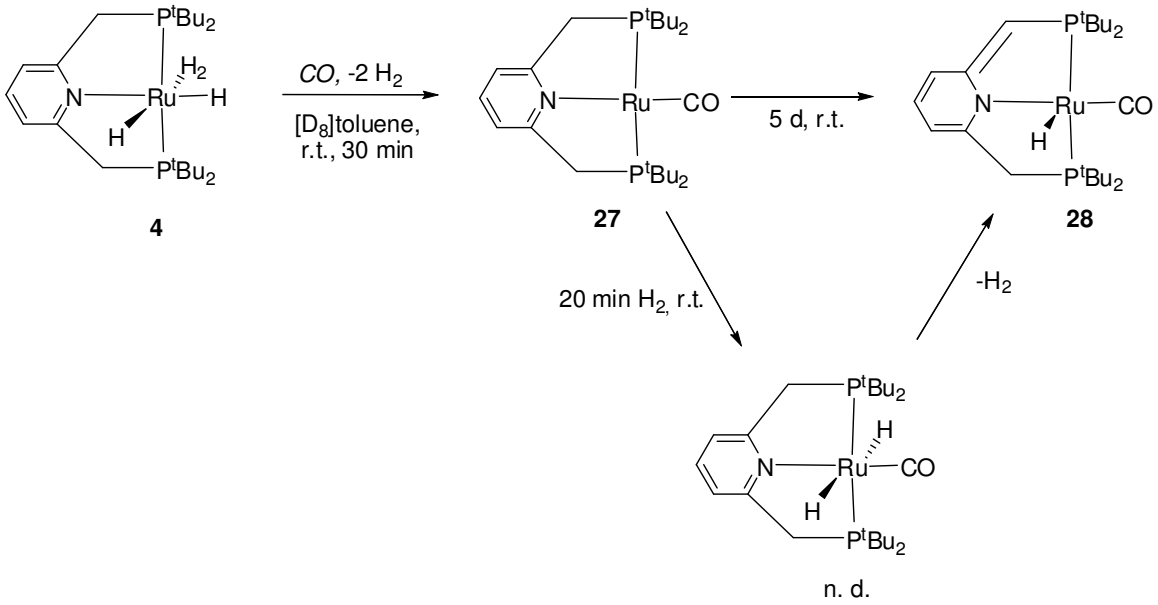

Scheme 18: Treatment of **4** with carbon monoxide and H_2 resulting in **28**.

This observation will now be discussed with respect to extensively studied ruthenium hydride complexes in the literature. The ruthenium hydride complexes $[Ru(N_2)H_2(PPh_3)_3]$ **13** and $[Ru(H_2)H_2(PPh_3)_3]$ **14** are selectively converted with carbon monoxide into *Wilkinson´s* ruthenium catalyst $[RuH_2(CO)(PPh_3)_3]$ **31** (Scheme 19).[96] It is known that **31** eliminates quickly hydrogen in solution already in presence of light resulting in the 14e$^-$ species $[Ru(CO)(PPh_3)_3]$ **32**,[95] which undergoes oxidative addition of a CH-bond resulting in a *ortho*-metalated arylphosphine of the formular $[RuH(CO)(C_6H_4PPh_2)(PPh_3)_2]$ **33** (Scheme 19).[97a]* Also, the X-ray structure of $[RuH_2(CO)(PPh_3)_3]$ **31** shows some evidence for a HH-bond between the ruthenium hydride core and an *ortho*-CH of a benzene ring,[98] which might support the tendency for the formation of a ruthenium carbon bond under H_2-loss. Presumably, the [Ru(*dtbpmp*)$(H_2)H_2$] **4** reacts in an analogous way. Due to geometrical reasons of the pincer ligand we assume that [Ru(*dtbpmp**)(CO)H] **28** has the structure

* Similar reactivity is reported for $[RuH_2(PPh_3)_4]$.[97b]

depicted in Scheme 18 also in comparable reactivity of **29** and **30** (Scheme 19).[3a]**

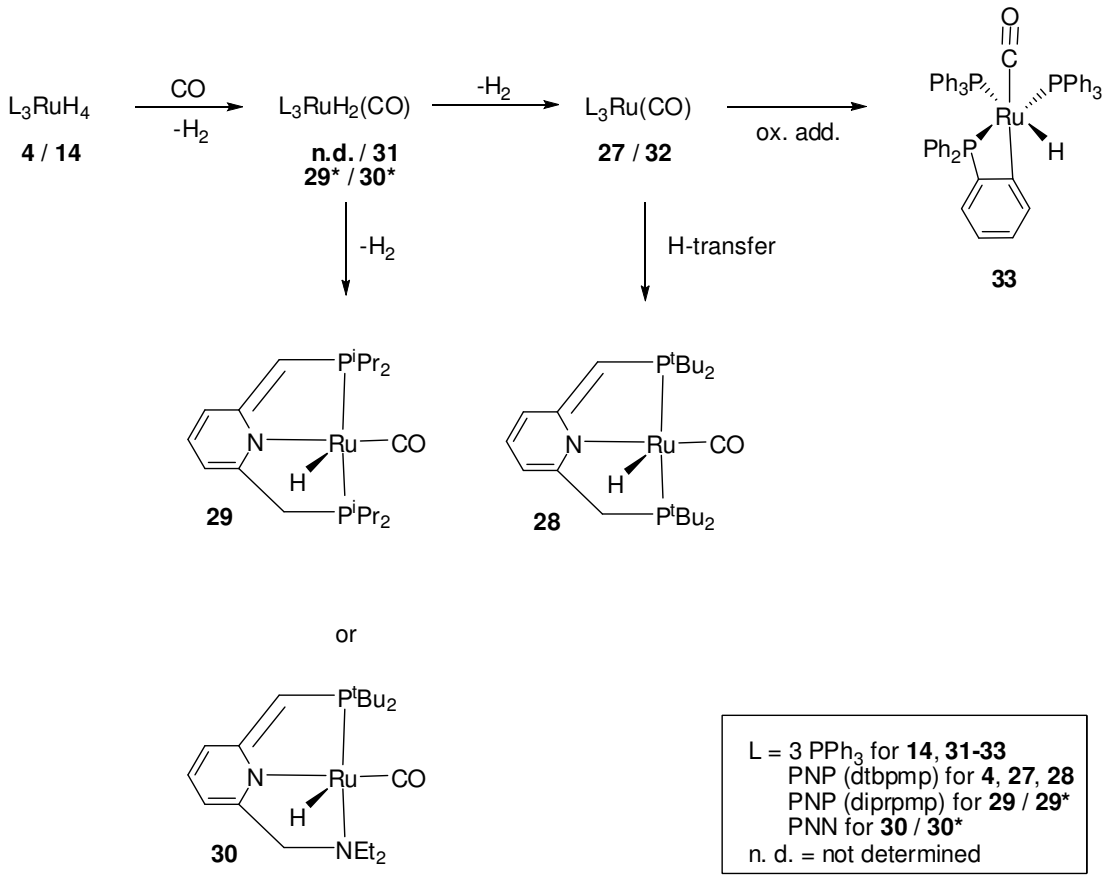

Scheme 19: Proposed mechanism for the conversion of **4** into **28** explained by the means of an analogue reactivity of $[Ru(H_2)H_2(PPh_3)_3]$ **14** into $[RuH(CO)(C_6H_4PPh_2)(PPh_3)_2]$ **33**.

Furthermore, these experiments show the different properties of the ruthenium complexes towards CH-activation. Neither complex **27** nor **28** show enhanced activity for H/D-scrambling between the $[D_8]$toluene and their pincer-backbones which is different to $[Ru(dtbpmp)(H_2)H_2]$ **4**. This behaviour supports the importance of the ruthenium dihydrogen moiety and the reactive hydrides in $[Ru(dtbpmp)(H_2)H_2]$ **4** for CH-activation and H/D-exchange reactions. This characteristic is lost by exchange of the labile/reactive ligands with a strong ligand (CO) under H_2-loss.

** The corresponding saturated *trans*-dihydrides of **29** and **30** are only stable under H_2-atmosphere.

2.1.3.4. Reaction with pinacolborane

The formation of a ruthenium borane species, might be an intermediate when [Ru(*dtbpmp*)(H_2)H_2] **4** is used as a precatalyst for hydroboration reactions with alkenes.[99] Here, the reactivity of [Ru(*dtbpmp*)(H_2)H_2] **4** with pinacolborane was studied. A NMR-sample of **4** in C_6D_6 was treated with pinacolborane **34** where gas evolution occurred due to H_2-loss (Scheme 20). [Ru(*dtbpmp*)(H_2)H_2] **4** is immediately converted into the new complex [Ru(*dtbpmp*)(H_2)H(Bpin)] **35** containing again a nonclassical Ru-H_2 moiety.

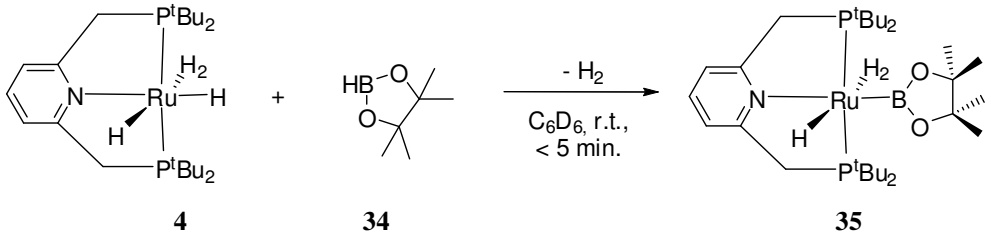

4 **34** **35**

Scheme 20: Reaction of **4** with the pinacolborane **34** under H_2-loss.

The ^{1}H-NMR-analysis allows the conclusion that the H_2-moiety is still present and a classical hydride is replaced with the borane. The ^{1}H-NMR shows two broad signals in the hydride area at -5.0 ppm (1 H) and at -11.7 ppm (2 H). Additionally the triplet of the *t*Bu groups changed to two triplets at 1.5 and 1.4 ppm. The singlet of the methyl groups in the pinacolborane are down-field shifted in comparison to the free pinacolborane **34**, which can be localized due to an unreacted excess in solution. The assumed *N-Ru-B trans*-arrangement seems plausible due to the separation of the hydride signals in **35** where two hydrogens are still identical on the NMR scale. The ^{31}P-NMR shows a singlet at +96.9 ppm and indicates 97% conversion of the [Ru(*dtbpmp*)(H_2)H_2] **4** into the [Ru(*dtbpmp*)(H_2)H(Bpin)] **35**, the ^{11}B-NMR shows the product at +22.7 ppm. Ruthenium polyhydrides of **1** with a borane ligand are usually coordinated as hydride-bridged boranes (dihydridoborate **36**) or as η^2-HBPin (hydride σ-borane **37**) as depicted in Figure 17.[100] In both coordination modes reported for complexes **36** and **37** the hydride ligands are *identical* on the NMR-scale and give one signal in the ^{1}H-NMR.[100] As already mentioned the ^{1}H-NMR of **35** gives two separated signals on the NMR-scale which supports the evidence for sterical separated (nonclassical) hydride ligands.

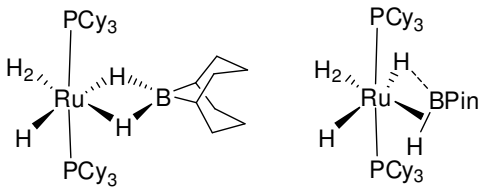

36 **37**

Figure 17: Other coordination modes of ruthenium polyhydride borane complexes: the dihydridoborate **36** and the hydride σ-borane complex **37**.

The reactivity of **4** with pinacolborane **34** prompted us to test catalytic activity for hydroboration of alkenes as previously reported by *Sabo-Etienne* using *Chaudret´s* complex **1**.[99] Noteworthy, *Sabo-Etienne et al.* reported that in absence of ruthenium hydride complex no hydroboration occurred between pinacolborane **34** and 1-octene **38**. Under catalytic conditions a solvent-free mixture of 1-octene **38** undergoes hydroboration with pinacolborane **34** at room temperature with 1 mol% catalyst loading of **4**. The reaction results in the corresponding 1-octylboronate **39** with 96% selectivity and 75% conversion accompanied with traces of 2-octylboronate **40** and alkyldiboronates (Scheme 21).

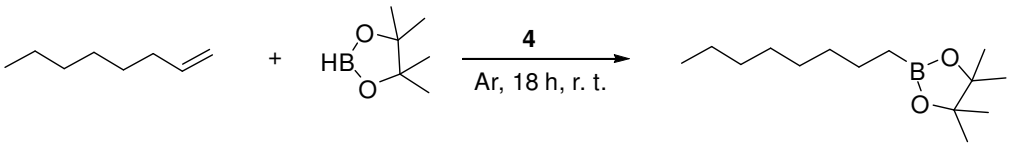

38 **34** **39**

Scheme 21: Ruthenium catalyzed hydroboration of 1-octene with pinacolborane at room temperature.

2.1.3.5. Reaction with CO_2

The crystallisation of [Ru(*dtbpmp*)(H_2)H_2] **4** to obtain suitable crystals for x-ray analysis gave an unexpected result. A solution of **4** in [D_8]toluene in a septum-sealed NMR tube was stored over dry-ice in a Dewar for several weeks. The analysis of a colourless crystal which had grown from the mother liquor revealed that some CO_2 must have entered the tube and reacted with **4** resulting in the ruthenium complex [RuH(*dtbpmp*)(HCO_2)CO] **41** (Scheme 25).

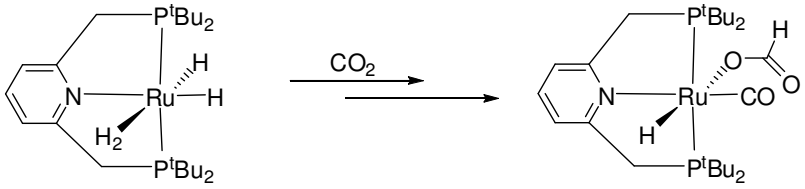

4 **41**

Scheme 22: Formation of the ruthenium hydrido formato complex **41**.

It is known for decades that ruthenium polyhydrides (**A**) such as [Ru(N_2)H_2(PPh_3)$_3$] **13**, [Ru(H_2)H_2(PPh_3)$_3$] **14** and [Ru(H_2)H_2(Cyttp)] **42** insert CO_2 into metal hydride bonds resulting in the corresponding ruthenium hydrido formates (**B**) with the formato-ligand as a bidentate *O,O*-ligand (Scheme 25).[101, 102]

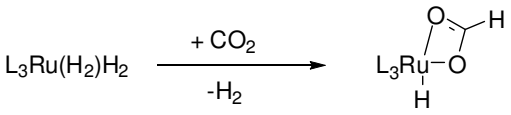

A **B**

L = 3 PPh_3
PNP (dtbpmp)

L = 3 PPh_3 (Ru)
Cyttp (Ru)

Scheme 23: CO_2-insertion into ruthenium hydride bonds resulting ruthenium hydrido formates.

A similar behaviour is also known for rhodium dihydrogen complexes bearing PCP pincer ligands like [Rh(*dtbpmb*)H_2] **43** and [Rh(*dtbppent*)H_2] **44** which form the analogue rhodium hydrido formates (**b**) as depicted in Scheme 24.[103] Interestingly, *Kaska* reported the non-catalytic reduction of CO_2 into CO and water with **43** (**b-c-d**; reverse water-gas shift reaction).[103b,c, 104] First, the reduction of CO_2 eliminates CO and a rhodium hydroxo complex

is formed and isolated (**c**). After prolongued reaction time the rhodium hydroxo complex (**c**) eliminates water and the present CO coordinates to rhodium, resulting in the isolated rhodium carbonyl complex (**d**).[103b,c] Different to this observation, *Milstein* and co-workers isolated a rhodium hydrido formate (**b**) of **44** as final product.[103c,d]

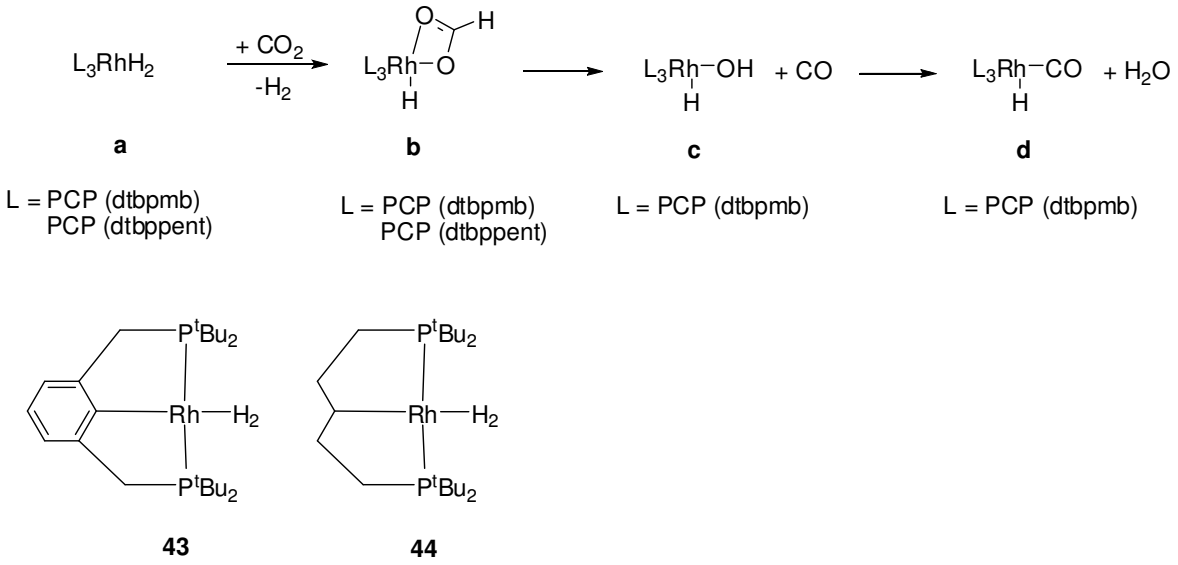

Scheme 24: Different reactivity of [Rh(*dtbpmb*)H_2] **43** and [Rh(*dtbppent*)H_2] **44**: CO_2-insertion into rhodium hydride bonds resulting in rhodium hydrido formates followed by a reverse water-gas shift reaction with *Kaska´s* rhodium dihydride complex **43**.

This different reactivity must be a result of the different ligand systems. In case of [Ru(*dtbpmp*)(H_2)H_2] **4** (**A**) the reactivity with CO_2 follows *Kaska´s* pathway in analogy the ruthenium carbonyl [Ru(*dtbpmp*)CO] **27** (**D**) is formed (Scheme 25). As discussed in chapter 2.1.3.3 [Ru(*dtbpmp*)CO] **27** reacts into [RuH(*dtbpmp**)CO] **28** (**E**) by agostic interaction* resulting in a transfer of a hydrogen atom from the benzylic position to the ruthenium core.[105] And in presence of [Ru(*dtbpmp*)(H_2)H_2] **4** as a hydrogen source the [RuH(*dtbpmp**)CO] **28** might be converted into the ruthenium dihydride (**F**) (Scheme 25).[3a] This reactivity stays in agreement with the reactivity of the reported complexes [RuH(*diprpmp*)(CO)] **29** and [RuH(PNN)CO] **30**.[3a] Alternatively, [Ru(*dtbpmp*)CO] **27** (**D**) might be directly converted into the ruthenium dihydride (**F**) in presence of hydrogen. Finally, another equivalent of CO_2 is inserted into a ruthenium hydride bond of the ruthenium dihydride (**F**) resulting in the ruthenium hydrido formato complex [RuH(*dtbpmp*)(HCO_2)CO] **41**. Different to the primarly insertion of CO_2 into a ruthenium hydride bond of

* "Agostic interaction" as originally defined by *Brookhart* and *Green* in 1983: The intramolecular interaction between a CH-bond and a transition metal center of a complex.

[Ru(*dtbpmp*)(H_2)H_2] **4**, the second insertion of CO_2 into complex (**F**) results in a mono dentate ligand because of the saturated coordination sphere of the ruthenium.

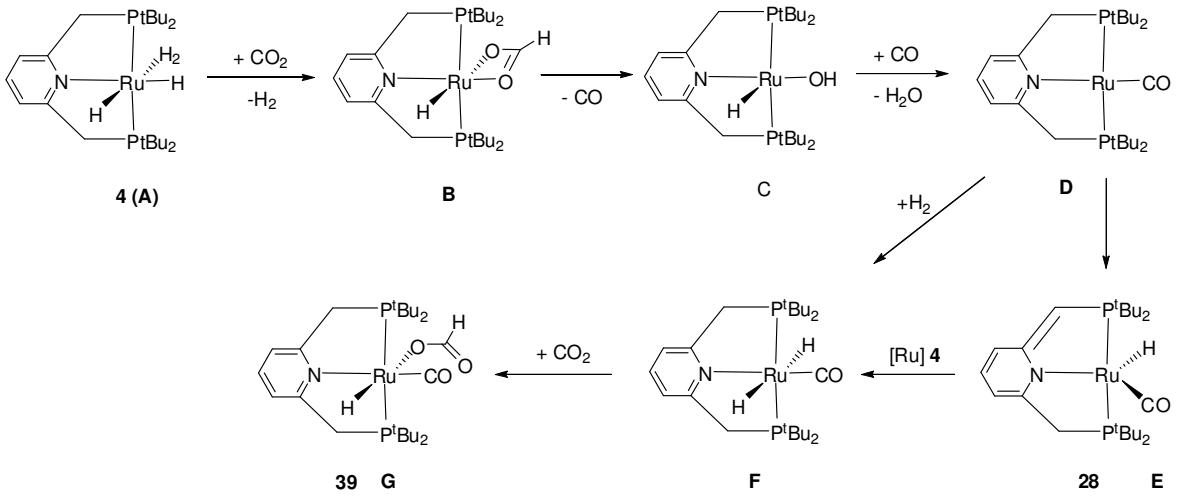

Scheme 25: Proposed formation of the ruthenium complex **41**.

The single-crystal X-ray diffraction reveals the structure of [RuH(*dtbpmp*)(HCO_2)CO] **41** (Figure 18 and Figure 19). The structure shows a distorted octahedron with a P-Ru-P angle of 158.2°, a N-Ru-CO angle of 176.0° and a pincer angle of 103.85°. The O-C-O angle of the formato ligand is 128.9°. The angles of the formato ligand over ruthenium with the other co-ligands are as followed: 173.1° ((HCO_2)-Ru-H), 103.3° ((HCO_2)-Ru-(CO)), 80.6° ((HCO_2)-Ru-N). The Ru-(OCO) bond length (2.249 Å) is shorter than the Ru-P bond lengths (2.337 / 2.333 Å). The CH_2 groups are rotated out of the PNP plane with a torsion angle of 29.57° and -23.40°. Similar to **4**, the twisted conformation with the CH_2 groups on different sides of the equatorial PNP plane results in a *gauche* conformation of the bulky phosphines. Again, the twisted conformation of the PNP pincer in **41** stays in agreement with most complexes bearing aromatic pincer ligands.[2] The distortion of the octahedral structure is also reflected in other angles over ruthenium as listed in

Table 1. The bond lengths in [RuH(*dtbpmp*)(HCO_2)CO] **41** are similar to those reported by *Milstein* for [Ru(*diprpmp*)(CO)H] **29** but the angles with ruthenium in the angular point are different (Table 1).[3a] The Ru-H bond length (1.40 Å) is remarkably short which might be due to the trans position of the formate ligand to the hydride ligand. The similar bond lengths of the PCH_2 units support the saturated structure of the pincer backbone which is different to the unsaturated situation in **29**. In **29** the corresponding P-C bond lengths are more different.[3a]

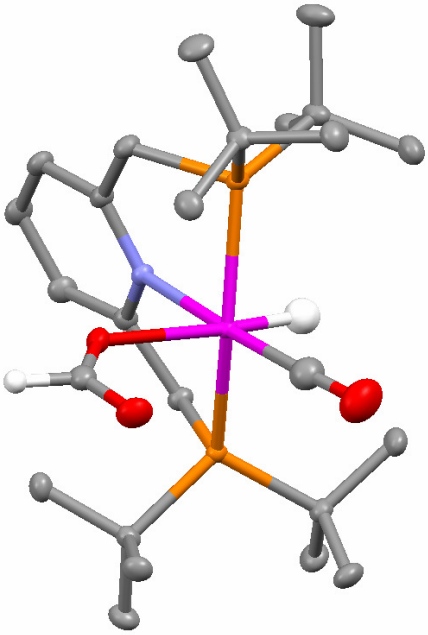

Figure 18: Single-crystal X-ray diffraction shows the structure of RuH(*dtbpmp*)(HCO_2)CO] **41**. An ORTEP model of this complex is depicted in the experimental part.

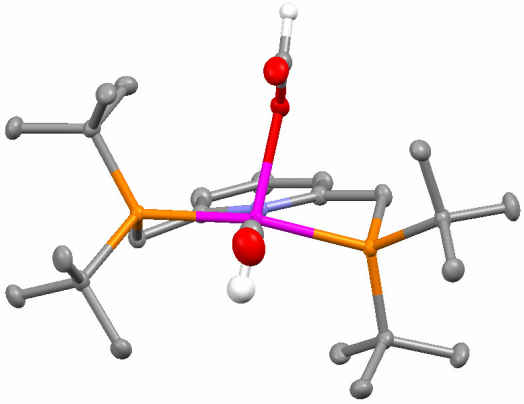

Figure 19: The side-view on the equatorial plane of [RuH(*dtbpmp*)(HCO_2)CO] **41** shows the twisted conformation with the CH_2 groups on different sides of the equatorial plane resulting in a *gauche* conformation of the phosphine groups. For clearance the H-atoms in the pincer-backbone are not depicted.

Table 1: Selected bond length and angles for the complexes **41** and **29**.

Element atom distance or angles	**[RuH(*dtbpmp*)(HCO_2)CO] 41 bond length [Å] and angle [°]**	**[Ru(*diprpmp*)(CO)H] 29 bond length [Å] and angle [°][3a]**
Ru-(CO)	1.8413(18)	1.844(7)
Ru-(OCO)	2.2487(11)	-
Ru-H	1.40(2)	1.48(11)
Ru-N	2.1286(11)	2.163(5)
Ru-P(1)	2.3366(4)	2.350(2)
Ru-P(2)	2.3334(4)	2.291(2)
P(1)-C(7) / P(1)-C(1)	1.8460(13)	1.803(6)
P(2)-C(8) / P(2)-C(7)	1.8502(14)	1.843(7)
O(1)-C(1)	1.2539(19)	-
O(2)-C(1)	1.2364(19)	-
C(1)-H(1)	1.048(19)	-
P-N-P	103.85°	
PNP(1)-CH_2	29.57°	
PNP(2)-CH_2	-23.40°	
P-Ru-P	158.197(13)°	153.1(1)
N-Ru-(CO)	176.01(7)°	171.4(2)
(HCO_2)-Ru-H	173.1(10)°	-
P(1)-Ru-N	82.24(3)°	-
P(2)-Ru-N	80.40(3)°	-
H-Ru-(CO)	83.5(10)°	-
(HCO_2)-Ru-(CO)	103.32(7)°	-
N-Ru-H	92.5(10)°	-
(HCO_2)-Ru-N	80.65(4)°	-
O-C-O	128.90(15)°	-

2.1.4. Other PNP pincer ligands for ruthenium hydride complexes

The slight variation of the PNP pincer-backbone using similar pincer ligands like *diprpmp* **45** (the isopropyl-analogue) results in a reddish-powder which could be isolated in traces (Scheme 26). The ^{1}H- and ^{31}P-NMR analyses allow the presumption that a hydride-bridged ruthenium cluster [Ru(*diprpmp*)H_x]$_y$ is formed indicated by a quartet of duplets in the ^{1}H-NMR spectra at -18.6 ppm (q, J = 13.4 Hz and 24.6 Hz) and -18.8 ppm (q, J = 13.4 Hz and 24.6 Hz) and a large coupling (d, J = 51.6 Hz). The ^{31}P-NMR spectra shows two virtual

doublets at +136.7 ppm (d, J = 27.7 Hz) and at +76.8 ppm (d, J = 22.4 Hz) in a 1:1 ratio. From the ^{1}H-NMR one could see that the hydride integrals are also in a 1:1 ratio to the signals of the pyridine-ring (e.g. PNP = 2, Hydride = 2) which can be interpreted as a further evidence for ruthenium dimer with two different type of phosphorous atoms.

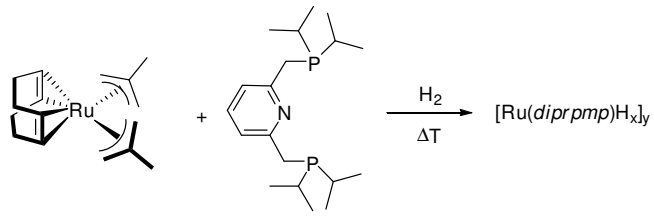

6 **45**

Scheme 26: Hydrogenation of **6** in presence of **45** forming a ruthenium cluster of unknown structure.

The cyclohexyl-analogue *dcypmp* **46** did not give any isolable product in the one pot procedure but a black precipitate is formed immediately. Maybe the [Ru(*dcypmp*)H_2(H_2)] **47** is unstable and it is not formed under these conditions due to CH-activation of the cyclohexyl-rings,[106] and followed by a ligand-cleavage under reductive conditions. However, one could see in absence of hydrogen the formation of the monomolecular complex [Ru(*dcypmp*)(2-methyl-allyl)$_2$] **48** (Scheme 27). The reaction control by ^{31}P-NMR (+76 ppm) shows just one compound. The comparison with similar ruthenium bisallyl-complexes allows the prediction for the existence of **48** which was assumed to be an appropriated precursor (Scheme 27). [35, 106, 107]

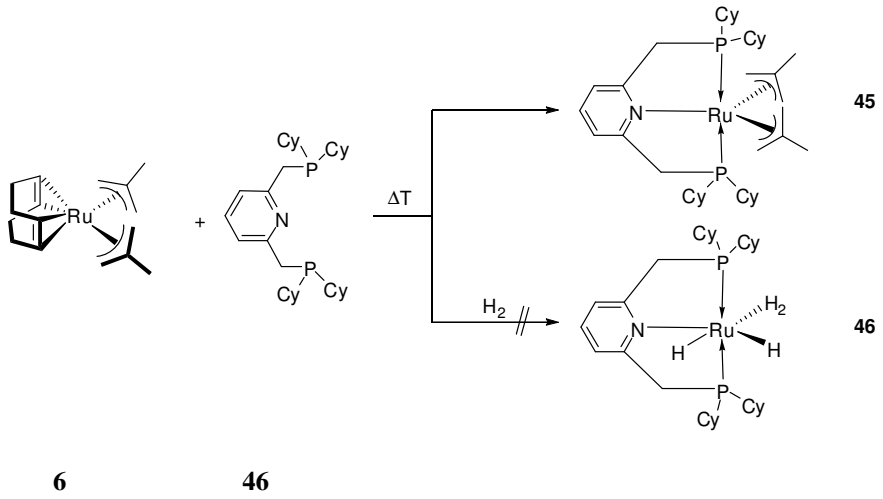

6 **46**

Scheme 27: Formation of the [Ru(*dcypmp*)(2-methyl-allyl)$_2$] **48**.

2.2. The Ruthenium Dihydrogen Complex [Ru(*dtbpoet*)(H_2)H_2]

2.2.1. Synthesis

As described in chapter 2.1.1. we found an access for monomeric nonclassical ruthenium hydride complexes bearing bulky PNP pincer ligands with a *trans* arrangement of two electron-rich and bulky phosphorous donor groups leading to [Ru(*dtbpmp*)H_2(H_2)] **4**. The investigations concerning the interesting reactivity of ruthenium nonclassical hydride complexes bearing bulky pincer ligands, motivated us for the tuning of the electronic properties of the ruthenium centre. For this, we suggested to substitute only the pyridine ring with the N-donor atom in **4** with an oxygen atom in an ether-bridge but without further modifications of the bulky tBu groups. We used the POP pincer *dbtpoet* **49**,[2] under similar conditions as for **4** in the direct hydrogenation route.[35] The hydrogenation of [Ru(cod)(2-methylallyl)$_2$] **6** in pentane under 7 bar H_2 at 55°C for two days in the presence of the POP pincer **49** leads to the ruthenium dihydrogen complex [Ru(*dtbpoet*)(H_2)H_2] **5** (Scheme 9).

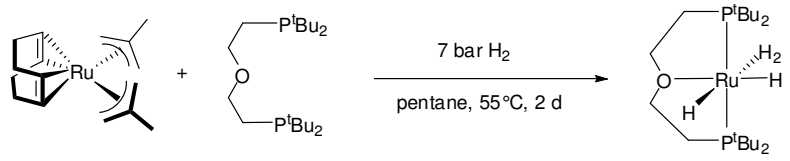

6 **49** **5**

Scheme 28: Direct hydrogenation of [Ru(cod)(metallyl)$_2$] **6** in presence of *dtbpoet* **49** leads to the nonclassical ruthenium hydride complex **5**.

Complex **5** precipitated from the mother liquor at room temperature as a greenish powder in 55% yield. After cannula filtration the product was washed with pentane and dried in a hydrogen stream. It is noticeable stable under argon and can be stored under argon at –20 °C for a prolonged time. Nevertheless, one recommends synthesizing it freshly prior to use as catalyst. Noteworthy, complex **5** is similar to *Gusev´s* dihydrogen complex [Ru(*dtbpoet*)(H_2)Cl_2] **50** but with other co-ligands and characteristics (Figure 20).[2]

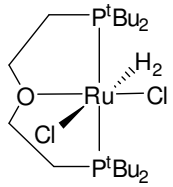

50

Figure 20: *Gusev´s* [Ru(*dtbpoet*)(H_2)Cl_2] **50**.

2.2.2. Characterisation

Structural insights of [Ru(*dtbpoet*)(H_2)H_2] **5** were again obtained from NMR- and IR-spectroscopy as well as DFT-calculations. The ^{1}H-NMR spectra shows the ^{t}Bu groups as a doublet and the ^{31}P-NMR exhibits a singulett for the phosphines. This depends on characteristic virtual coupling of the *trans* P-Ru-P bonding, indicating the *trans* arrangement of the POP pincer **49** which agrees with the NMR data of **50**.[2] As presumed, complex **5** has two classical hydrides and one dihydrogen ligand in its coordination sphere which was confirmed by IR spectroscopy and ^{1}H-NMR. The IR-analysis of **5** shows bands characteristically for ruthenium hydrides at 1994, 1905 and 1774 cm^{-1} (νRu-*H*) and at 2088 cm^{-1} for the ruthenium dihydrogen moiety (νRu-H_2). The ^{1}H-NMR spectra of [Ru(*dtbpoet*)(H_2)H_2] **5** shows a signal at –8.6 ppm (Table 2, Figure 21) at room temperature and by cooling the sample subsequently to –80°C the triplet changes to a broad signal. The T_1(min) value was determined from a curve based on six NMR series between 300 and 193 K. The T_1(min) value was found to be 38 ms (Table 2, Figure 22) which fits perfectly in the lower part of the predicted range for a H_2-moiety (10-180ms at 400 MHz or respectively 5-90ms at 200 MHz)[7]. The calculation of the H-H distance according to *equation 2* results in a H-H distance of 0.98 Å (Table 2).[54, 58] As mentioned in chapter 2.1.2. for species **4**, this value is also most likely a little over-estimated.

One can see the influence of the POP pincer to the dihydrogen moiety in comparison to [Ru(*dtbpmp*)(H_2)H_2] **4** (Table 2). For [Ru(*dtbpoet*)(H_2)H_2] **5** T_1(min) and the H-H distance are significantly smaller. In comparison with *Gusev´s* complex [Ru(*dtbpoet*)(H_2)Cl_2] **50** the NMR data also show significant differences between these complexes due to the Cl-ligands and classical hydrides. The influence of the hydride ligands results in a low field shift for all

signals in the ^{1}H-NMR spectra and the coupling constant *J* varies. The signal for the dihydrogen moiety is at -8.6 ppm for **5**, -7.3 ppm for **4** and -10.1 ppm for **50** (Table 2). The coupling constant *J* for **50** is significant smaller than those for **4** and **5** (Table 2). Also the T_1(min) with 16.1 ms and the H-H distance (1.13 Å) (Table 2)[2] **50** differ from those for complex **5**.

The comparison of the ^{31}P-NMR data exhibits that the electronic structure of **5** is more similar to **4** than to **50** (Table 2). Here we see, for the present examples, that the modification of the co-ligands has a greater influence than the exchange of the pincer-backbone but we succeeded a slightly modification of the electronic density at the ruthenium centre by changing the PNP with a POP pincer.

Table 2: Characteristic NMR-Data of the complexes **4**, **5** and **50**[2].

Complex	^{1}H-NMR	^{31}P-NMR	T_1	H-H [Å]*
4	–7.3 ppm, t, 4 H, ^{2}J(H,P) = 13.2 Hz,	+109.6 ppm, s	77ms at θ_{min} = 228 K and 400 MHz	1.1 ± 0.01
5	–8.6 ppm, t, 4 H, ^{2}J(H,P) = 14.0 Hz	+107.2 ppm, s	38 ms at θ_{min} = 221 K and 400 MHz	0.98 ± 0.01
50	-10.1 ppm, t, 2 H, ^{2}J(H,P) = 8.8 Hz	+61.4 ppm, s	16.1 ms at θ_{min} = 218 K and 300 MHz (equal to 22 ms at 400 MHz)[2, 7]	1.13 (uncorrected value)

*Error-values based on instrumental error.

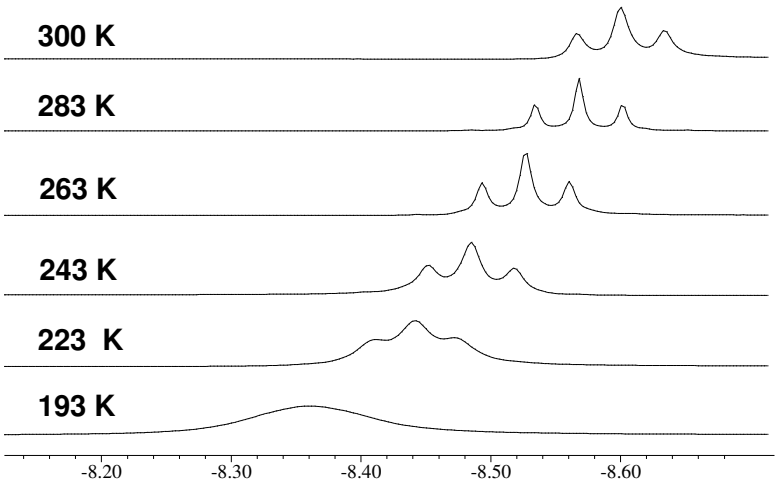

Figure 21: The hydride-area of the ^{1}H-NMR shows the hydride-signal of **5** at different temperatures.

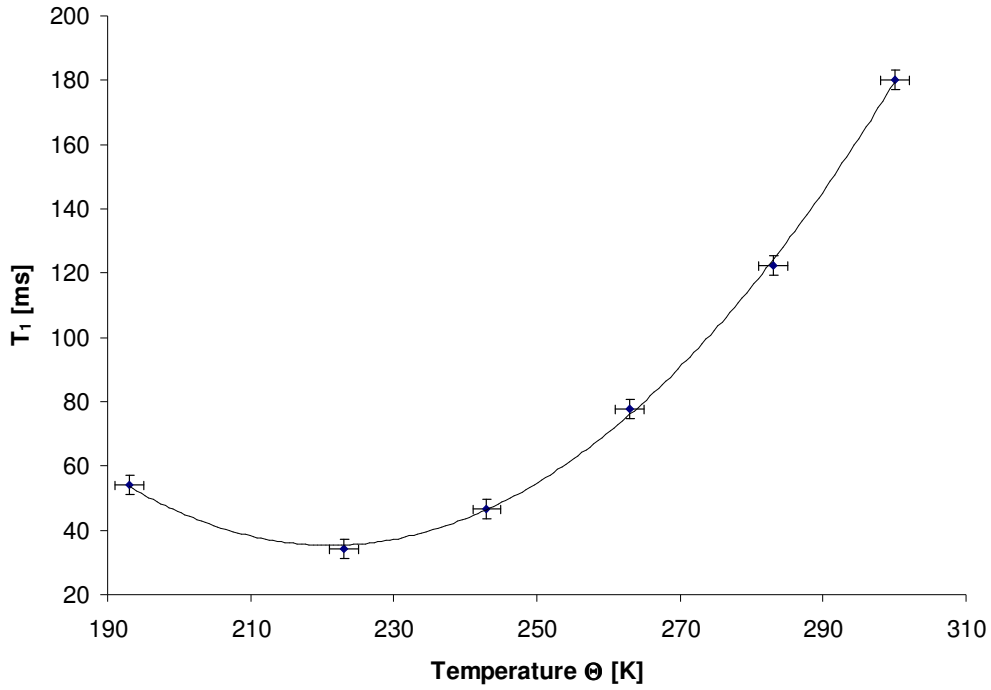

Figure 22: T_1-values as a function of temperature Θ determined for [Ru(*dtbpoet*)(H_2)H_2] **5**. T_1/ms (Δ3ms) [T/K (Δ2K)]: 180 [300], 122 [283], 78 [263], 47 [243], 34 [223], 54 [193].

The temperature dependences of the T_1 of complex [Ru(*dtbpoet*)(H_2)H_2] **5** is depicted in Figure 23 as $\ln(1/T_1)$ versus 1000/T in the high-temperature area corresponding to the maximum activation energy of the molecular motion.[90] The calculated apparent maximum activation energy is $E_A = 6.8$ kcal mol^{-1} and this energy is 0.5 kcal mol^{-1} higher than the corresponding energy of [Ru(*dtbpmp*)(H_2)H_2] **4**.

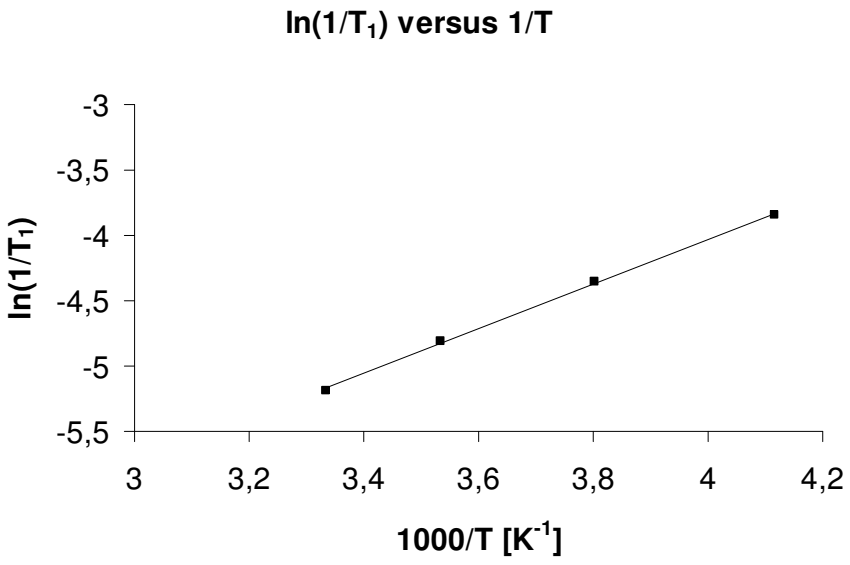

Figure 23: $\ln(1/T_1)$ as a function of 1000/T for hydride signal in the ^{1}H-NMR of [Ru(*dtbpoet*)(H_2)H_2] **5**.

For further information about the coordination geometry of the ruthenium dihydrogen moiety in [Ru(*dtbpoet*)(H_2)H_2] **5** separate computational investigations were performed equal to the methods as for **4**.[26, 91, 92a-e] As model system the *t*Bu groups at the P centres of [Ru(*dtbpoet*)(H_2)H_2] **5** (Figure 26) were replaced by methyl substituents; [Ru(*dMepoet*)(H_2)H_2] **51**.[93]

Similar to **4**, the *trans* arrangement of the phosphine ligands in the POP pincer *dbtpoet* **49** could be clarified by spectroscopic methods and by DFT. We localized the favoured *cis*-confomer of the H_2-ligand and the *O*-ether unit for [Ru(*dtbpoet*)(H_2)H_2] **5**. *Gusev* and co-workers also find that the *cis*-confomer of [Ru(*dtbpoet*)(H_2)Cl_2] **50** is 7.3 kcal/mol more stable than the *trans*-form.[2] Interestingly, in contrast to *Gusev´*s result we found again a classical ruthenium tetrahydride, and not the *trans*-form, with a slightly higher energy level.

In analogy to **4**, the *cis*-form of **5** results in a trans-arrangement of the dihydrogen-ligand (labile ligand) and a classical hydride (a good σ-donor). This situation supports the activation of the dihydrogen unit towards H-H bond cleavage or it results in a stretched dihydrogen complex. This means that the *cis*-form is much more stable with respect to H_2 loss than the *trans*-form.[7] Similar to the observation made for [Ru(*dtbpmp*)(H_2)H_2] **4**, also here the existence of an analogue tetrahydride of **5** could not be verified experimentally. However, such dihydrogen-dihydride equilibrium are known and these processes have activation enthalpies between 10 and 20 kcal mol^{-1}.[7] Interestingly, in contrast to **4** the hint for an slightly elongated dihydrogen complex **5** (temperature-*independence* of the coupling *J* and the chemical shift) is not observed. The chemical shifts for a temperature range between +27°C and –10°C varies from –8.6 to –8.5 ppm and *J* seems unchanged (J = 13.42-13.47 Hz). Instead, complex **5** shows a temperature-dependence for temperatures below -10°C. The chemical shift drifts to -8.36 ppm and the coupling *J* seems most likely to have a linear correlation with the temperature. These findings speak more for the nonclassical character of **5**, than for an elongated dihydrogen complex. Nevertheless, complex **5** does not show enhanced H/D-scrambling of all hydrides but remarkable simple partial exchange of the H_2-ligand. Therefore the assumption of a nonclassical tetrahydrogen intermediate as discussed for **4** can be excluded.

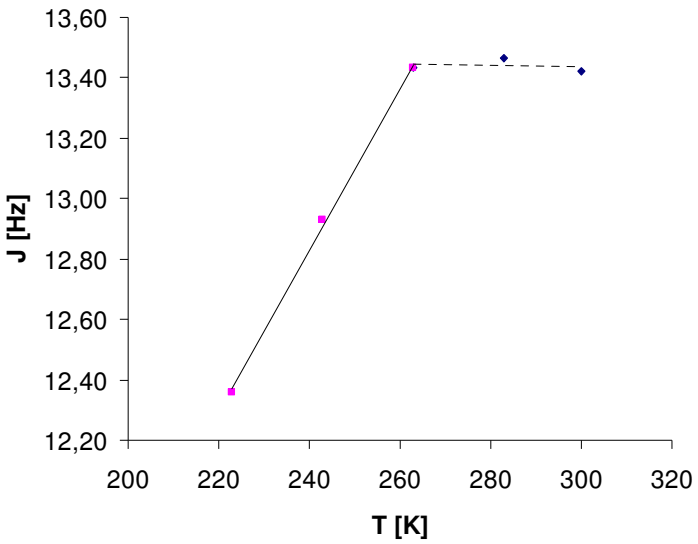

Figure 24: Variation of the coupling constant *J* of the hydride peak in the ^{1}H-NMR measurement as a function of the temperature T.

The DFT-calculations of [Ru(*dMepoet*)(H_2)H_2] **51** resulted in a H-H-distance of 0.875 Å for the ruthenium dihydrogen moiety. Again, this value differs from the one obtained by NMR-analysis due to experimental reasons but it confirms the assumption that the experimental value (0.98 Å) is over-estimated and the existence of [Ru(*dtbpoet*)(H_2)H_2] **5** in general. Similar DFT-calculation with the isolated complex **5** shows once more the significant influence of the *t*Bu groups to the dihydrogen coordination mode. A HH-distance of 0.987 Å was obtained (Figure 26). *Gusev* and co-workers calculated the HH-distance for [Ru(*dtbpoet*)(H_2)Cl_2] **50** to be 0.93 Å and determined experimentally 1.13 Å (T_1(min)). They refered the difference to methodical reasons.[2, *] Our result stays in full agreement with the experimental data and similar as for [Ru(*dtbpmp*)(H_2)H_2] **4**, one can see that also for [Ru(*dtbpoet*)(H_2)H_2] **5** the substitution on the phosphor atoms of the ligand sphere has a significant influence to the geometric and electronic situation of the ruthenium atom. As exhibited in the variation of the HH-distance of the H_2-ligand in the real complex **5** and the model **51**. The H_2-ligand adjusts the bond strength of the Ru-P bonds in the pincer-backbone which results in a longer HH-distance for **5**, as already discussed in chapter 2.1.2. for complexes **4** and **17**.

* Correspondence of the theoretical value to the electronic minimum and for the experiment they point out the influence of anharmonic vibrations on the hydrogen atoms resulting in a longer distance as for DFT.

The DFT-calculations gave the *trans* arrangement of the phosphorous atoms in the coordination sphere of the ruthenium core. And it revealed an eclipsed conformation of the phosphine groups and this stays in agreement with the discussion by *Gusev* for **50**.[2] In consequence to the eclipsed configuration, the torsion is closed to 0° (Figure 25, Table 3). These results are supported by single-crystal X-ray diffraction but we did not obtained a complete resolution of the solid structure. Only the heavy atoms of the structure fragment of [Ru(*dtbpoet*)(H_2)H_2] **5** were localized, but a localization of the H_2-moiety and the hydrides were not possible.

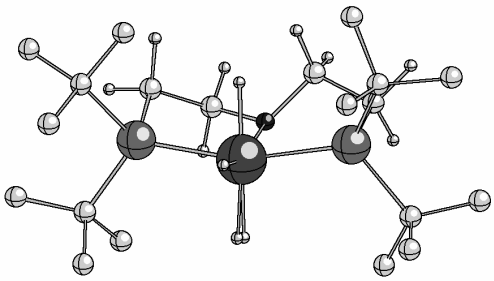

Figure 25: Ball-and-Stick-representation for the calculated [Ru(*dtbpoet*)(H_2)H_2] **5**. The side-view on the equatorial plane shows the enclipsed conformation of the phosphine groups. For clearance The H-atoms in the pincer-backbone are not depicted.

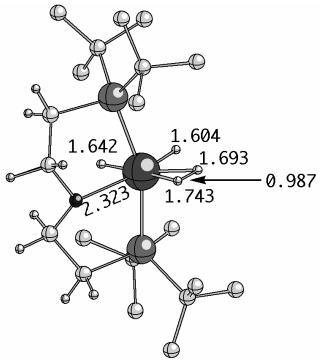

Figure 26: Ball-and-Stick-representation for the calculated [Ru(*dtbpoet*)(H_2)H_2] **5**. The assigned H-H distance in the RuH_2-moiety is determined by NMR as 0.98 Å and by DFT as 0.987 Å. For the model complex [Ru(*dMepoet*)(H_2)H_2] **51**, The assigned H-H distance in the RuH_2-moiety is determined by DFT as 0.875 Å. For clearance The H-atoms in the pincer-backbone are not depicted.

Table 3: Selected DFT data of [Ru(*dtbpoet*)(H_2)H_2] **5**.

Element	DFT
Ru-O distance	2.323 Å
Ru-P_1 distance	2.308 Å
Ru-P_2 distance	2.324 Å
P_1-Ru-P_2 angle	160.35°
P-O-P angle	96.30°
Torsion angle, plane: P_1-CH_2 and P_2-CH_2	-7.05°

2.2.3. Reactivity

Further characterisation of the ruthenium dihydrogen moiety involved the equilibrium reaction between H_2 and N_2 monitored by NMR spectroscopy. The [Ru(*dtbpoet*)(H_2)H_2] **5** gives a light green solution in [D_8]toluene which was treated with a nitrogen stream for 90 minutes resulting in a dark green solution (Scheme 29).

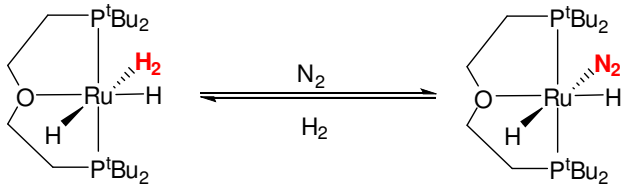

5 **52**

Scheme 29: Formation of the ruthenium dinitrogen complex **52.**

In contrast to compound **4** the dihydrogen ligand in complex **5** can be reversibly and quantitatively replaced by N_2, as were found for the ruthenium dihydrogen complexes **1-3** (Figure 2 and Scheme 13), too.[4, 5] Surprisingly the complex [Ru(*dtbpoet*)(H_2)Cl_2] **50** is not substituted with N_2 at all.[2] This allows the assumption that the classical hydride co-ligands in **5** make the substitution possible, where as in **50** the ligand exchange is suppressed due to the chlorides as co-ligands. In the ^{31}P-NMR spectra the [Ru(*dtbpoet*)H_2(N_2)] **52** can be assigned at +99.2 ppm as broad singlet signal. Furthermore, in the ^{1}H-NMR spectra the triplet at -8.4 ppm (**5**) changes to two broad signals at -12.5 ppm and -19.8 ppm (**52**).

NMR studies with [Ru(*dtbpoet*)(H_2)H_2] **5** in deuterated aromatic solvents does not show remarkable *H/D*-exchange processes in [D_8]toluene or C_6D_6. Whereby complex **4** incorporates deuterium from the solvents into the *PNP*-pincer backbone, there is fairly no incorporation into the *POP*-pincer backbone of complex **5**. By treatment with D_2-gas only the H_2-ligand is exchanged but the classical hydride co-ligands seems most likely unchanged which is assigned by ^{1}H- and ^{2}H-NMR spectroscopy.

2.3. Catalysis

The catalytic activity of the new ruthenium dihydrogen complex [Ru(*dtbpmp*)(H_2)H_2] **4** has been tested mainly in *H/D*-exchange reactions (*CH*-activation) and dehydrogenation reactions of alcohols, including domino processes.

2.3.1. Catalytic *H/D*-Exchange between Aromatic Hydrocarbons and Deuterated Solvents

2.3.1.1. D_2O as Deuterium Source

The main goal of our catalysis research challenged the target to establish a convenient green and cheap catalytic system for the deuteration of a variety of compounds with D_2O as deuterium source. Due to the limited solubility of organic molecules in deuterated water we established a biphasic system with cyclohexane (secondary solvent / internal standard) and an appropriate water-stable catalyst precursor like [Ru(*dtbpmp*)(H_2)H_2] **4**. For evaluation of the catalytic activity in general we used both [D_6]benzene and D_2O as deuterium sources and aromatic hydrocarbons as substrates. In contrast to Chaudret's hexahydride [Ru(PCy_3)$_2$(η^2-H_2)$_2$$H_2$] **1**, complexes **2**, **3** and **4** showed a much higher activity for the H/D-exchange between [D_6]benzene and other aromatic substrates. Due to the rather slow H/D-exchange between C_6D_6 and [Ru(*dtbpmp*)(H_2)H_2] **4** at room temperature, as previously discussed,[4a] we performed the catalysis at moderate temperature (50°C) under argon for three days if not other mentioned (Scheme 30).

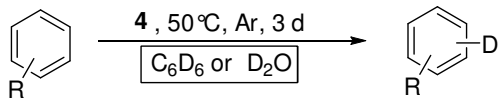

Scheme 30: Catalytic *HD*-exchange with **4** between C_6D_6 or D_2O and aromatic hydrocarbons.

For the substrate scope we have chosen some aromatic hydrocarbons and heterocycles as examples to study the deuterium incorporation and regio-selectivity. The samples were analysed by ^{1}H- and ^{2}H-NMR. In contrast to ^{1}H-NMR, the ^{13}C-NMR as well as the GC-MS spectra show a broad range of all possible isotopomeres. For this reason, MS spectra were not analysed and the ^{13}C-NMR spectra were only considered in some cases for the resolution of the regio-selectivity.

As expected, complex **4** is an active catalyst precursor for the H/D-exchange between [D_6]benzene and aromatic substrates (Scheme 31). At 50°C, deuterium is effectively transferred from C_6D_6, which is used as solvent in these experiments, into toluene with a noticeable regioselectivity for the *meta*-position.

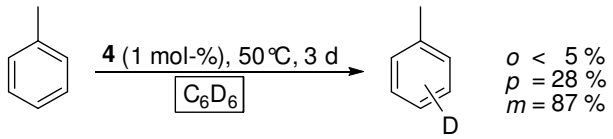

12 **[D]- 12**

Scheme 31: Deuteration of arenes with C_6D_6 and **4.**

Most intriguingly, we found that **4** is also active at the same temperature for the incorporation of deuterium into aromatic substrates from D_2O as a cheap and environmentally benign deuterium source (Scheme 32). The exchange occurs in a two phase system consisting of cyclohexane and D_2O, whereby cyclohexane served as solvent for the aromatic substrate and the catalyst. Control experiments verified that no deuterium incorporation into cyclohexane occurred under the reaction conditions. Thus, the H/D-exchange can be conveniently monitored by ^{1}H-NMR spectroscopic observation of the decrease of individual signals in the organic phase relative to the solvent signal as internal standard. Deuterium incorporation in the various positions was verified by ^{2}H-NMR and ^{13}C-NMR at the end of the reaction. Values given as "< 5%" or "> 95%" indicate that very weak signals were detected corresponding to the deuterated or non-deuterated species, respectively.

As depicted in Scheme 32, benzene **53** was deuterated quantitatively using 1 mol-% of precatalyst **4** at 50°C within three days. Other aromatic and heteroaromatic compounds were also effectively deuterated under similar mild reaction conditions, whereby a significant chemo- and regioselectivity was observed in certain cases. For toluene **12**, the incorporation occurred with preference in *meta*-position, where 84% of all protons were replaced. Additionally, 28% of the *para* protons were exchanged for deuterium, whereas no incorporation was detected in *ortho* position. The methyl group remained unreactive under the present conditions. *o*-Xylene **54** was deuterated almost exclusively in the β-positions to the methyl groups (86%) with no significant deuterium incorporation in the α-positions and the methyl groups. The treatment of naphthalene **55** under the same conditions resulted preferably in β–deuteration (62%) with a lower amount of α–deuteration (15%).

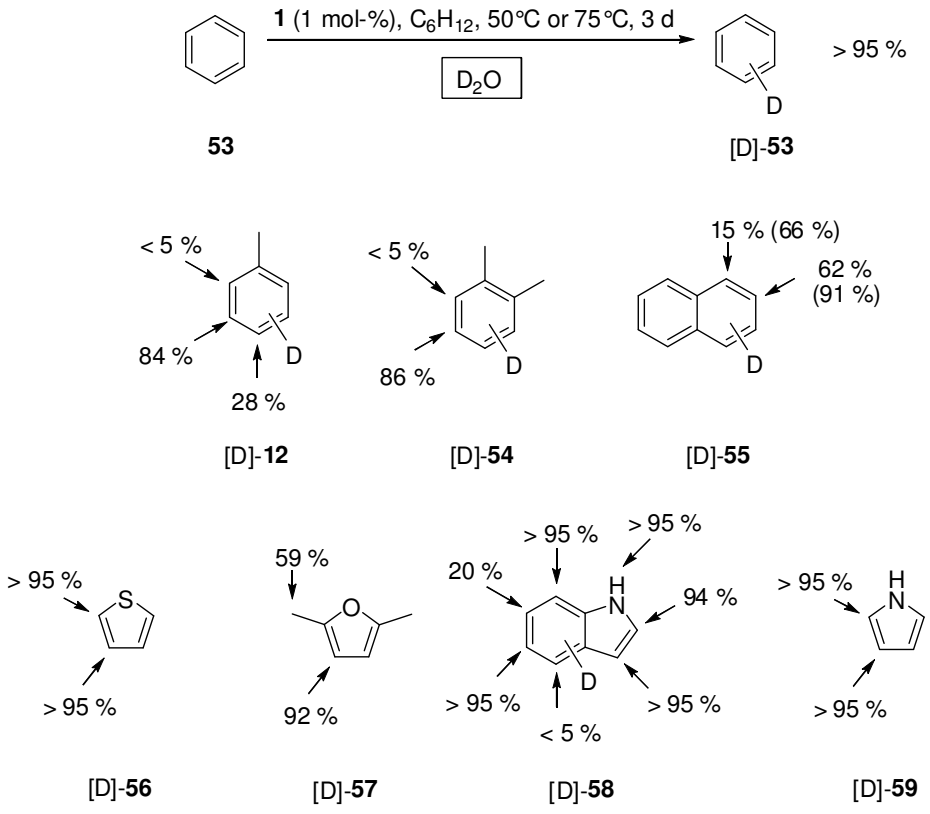

Scheme 32: Catalytic H/D exchange of aromatic and heteroaromatic compounds using D_2O as the deuterium source and complex **4** as catalyst precursor. Reaction conditions (under Argon): Substrate **12**, **53**-**59**: 1 – 1.25 mmol; Ru-cat. **4** = 1 mol-%, D_2O (1 mL), C_6H_{12} (0.7 - 1.0 mL), t = 3 days; reaction temperature: **12, 53** - **55**: T = 50 °C (75%); **56** - **59**: T = 75 °C; see experimental part for details.

The H/D exchange occurred also readily on heteroaromatic compounds even in case of potentially coordinating groups. Thiophene **56** was fully deuterated in all positions within the standard reaction time at 75°C. The treatment of 2,5-dimethylfurane **57** lead to almost quantitative deuterium incorporation at the sp^2 carbons (92%), but there was also noticeable deuteration at the methyl groups (59%). As no H/D exchange was observed in the alkyl groups of other substrates, this might indicate that in the case of **57** sp^3 C-H activation is directed by pre-coordination to the oxygen atom. Efficient H/D exchange was observed for indol **58**, whereby C-3 was found to be the least reactive position. The corresponding proton NMR signal overlapped with the NH signal and this area decreased by a total of 59%. ^{13}C-NMR analysis revealed that the incorporation at C-3 was negligible and also C-5 remained largely non-deuterated. Also in pyrrol **59** the H/D-exchange is for both positions satisfying (> 95%) where the broad NH-signal could not be localized.

The properties of the catalytic system were studied in some more detail with naphthalene **55** as benchmark substrate. The long term stability of catalytically active species at the end of the standard reaction was tested by removing the D_2O layer and replacing it with H_2O. Indeed, the amount of deuterium decreased again to 35% in β– and 5% in α-position indicating that the exchange was still going on. Increasing the reaction temperature to 75°C, **55** was deuterated within one day in the β–position to 81% accompanied by deuterium incorporation of 26% in the α–position. Again, the exchange continues over an extended period of time leading to > 95% β-[D]-**55** already after day two and reaching 77% exchange in the α-position after four days. In Figure 27 and Figure 28 the depicted ^{1}H-NMR and ^{2}H-NMR respectively, shows the monitored ongoing H/D-exchange in naphthalene **55**. Otherwise, increasing the loading of **4** to 4 mol-% and shortening the reaction time to one day lead still to high β–deuteration (60%) without significant α–deuteration at 50°C.

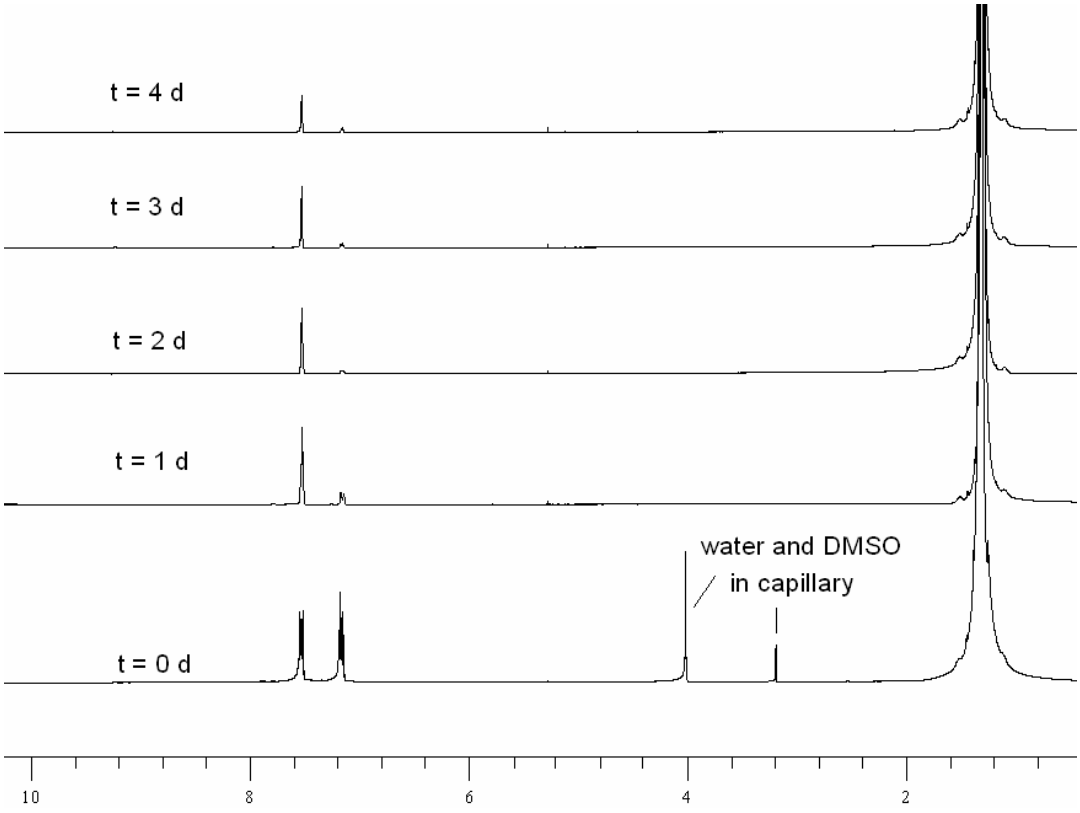

Figure 27: ^{1}H-NMR-monitoring of the deuteration of naphthalene **55**.

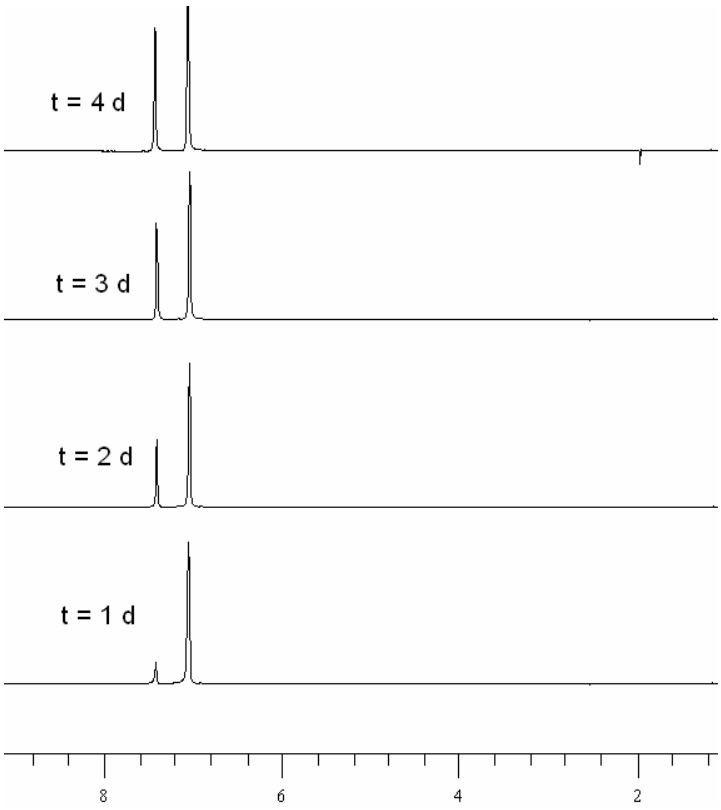

Figure 28: ^{2}H-NMR-monitoring of the deuteration of naphthalene **55**.

To investigate a possible contribution of a simple acid catalysed H/D-exchange under the present conditions, a cyclohexane solution of **12** was treated with concentrated DCl/D_2O (37%). No incorporation could be detected at 50°C over extended period time. Furthermore, the H/D-exchange in the system **55**/D_2O catalyzed by **4** was not influenced significantly by the addition of mercury (Hg/Ru = 10:1; T = 50 °C, t = 3 d, α: 15%; β: 55%), indicating, albeit not proving, that the catalytic cycle is occurring on a molecular organometallic species (T = 50 °C).[108] Finally, the choice of the ligand appears to play an important role for the catalytic properties as the use of Chaudret´s complex **1** as catalyst for the deuteration of **53** resulted only in 47% deuterium incorporation within 4.5 days as compared to quantitative incorporation after three days with **4** under otherwise identical conditions.[26]

Scheme 33 shows a plausible reaction network explaining the exchange of H and D in the coordination sphere of a pincer-ligated ruthenium with water and benzene, respectively. The corresponding intermediates and transition states were localized by DFT-calculations.[26, 91] Here model complexes were used in which the *t*Bu groups at the P centres of **4** were replaced by methyl substituents.[93] The dihydrogen molecule in precursor **17** can be replaced by a H_2O molecule yielding **60**. The aquo-complex subsequently reacts in a σ-bond metathesis to **61** containing again an H_2-ligand.[109] This reaction requires a moderate activation energy ($\Delta G^{\ddagger}$ = 12.1 kcal/mol). An alternative route (**62** to **63**) with the H_2O molecule bonded *trans* to the pyridine ring of the ligand is also possible with an activation energy of $\Delta G^{\ddagger}$ = 7.5 kcal/mol. Repeating the calculations for the corresponding D_2O-complexes of **62**, **63** and the corresponding transition states, the activation energy for the forward and for the backward reaction were found to be marginally higher by 1.0 kcal/mol ($\Delta G^{\ddagger}$ = 8.7 kcal/mol, $\Delta G^{\ddagger}$ = 9.7 kcal/mol, respectively), indicating that the incorporation of deuterium from D_2O into the metal complex is a facile process.

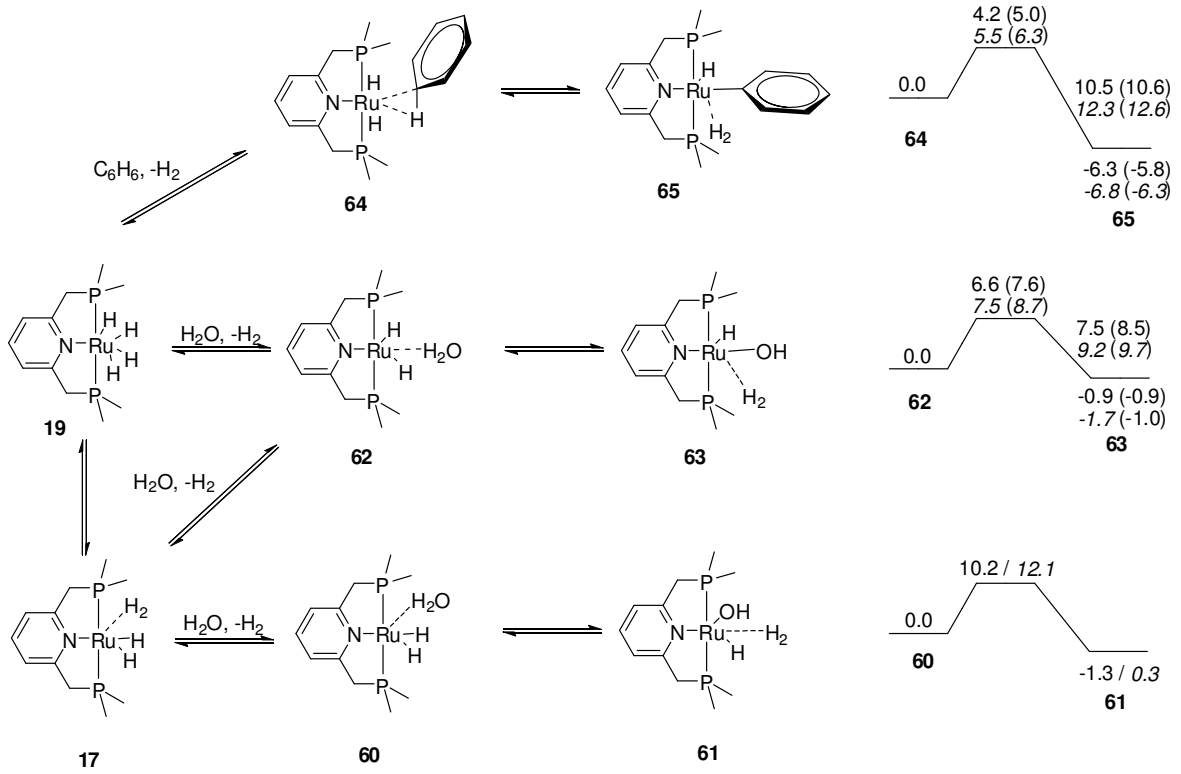

Scheme 33: Reaction steps and energy profiles (ΔH/ΔG (italics) in kcal/mol) for H/D exchange processes starting from **17** as determined by DFT calculations. Values in parenthesis denote relative energies of stationary points for the corresponding D_2O- (**62, 63**) and C_6D_6-complexes (**64**, **65**).

The stationary points for the corresponding benzene containing complexes were localised also (Scheme 33, Figure 29). In complex **64** one H_2 molecule of the parent complex **17** is replaced by benzene with the C_6H_6 molecule binding in $\eta^2_{C\text{-}H}$ mode.[109, 110] Complex **64** can react to product **65** and the activation energy for the forward reaction amounts to $\Delta G^{\ddagger}$ = 5.5 kcal/mol, while the backward reaction requires 12.3 kcal/mol. Replacement of C_6H_6 by C_6D_6 leads to a slightly higher activation energy for the forward reaction ($\Delta G^{\ddagger}$ = 6.3 kcal/mol), while the backward reaction's activation energy remains practically unchanged ($\Delta G^{\ddagger}$ = 12.6 kcal/mol).

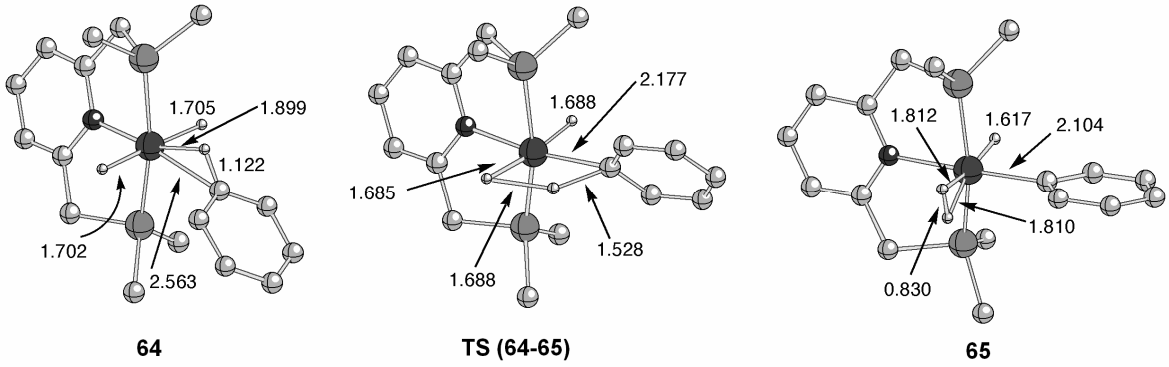

Figure 29: Ball-and-Stick-representation of some intermediates in the C-H activation of benzene. Selected bond distances are given in Å.

Scheme 34 shows the key steps of the exchange process with the real substitution pattern of catalyst precursor **4** and toluene **12** as substrate. The C-H activation step in *para*- and *meta* position were calculated to have practically the same activation energy ($\Delta G^{\ddagger}$ = 12.1 kcal/mol and $\Delta G^{\ddagger}$ = 13.2 kcal/mol, respectively). The *ortho* position, however, is clearly disfavored with a much higher activation energy of $\Delta G^{\ddagger}$ = 17.9 kcal/mol. Considering the statistic preference of the *meta* over the *para*-position, these results would predict an approximate 2:1 preference for the incorporation in *meta* over *para* in **12**, with no significant incorporation in *ortho*. Thus, the general trend of reactivity and regioselectivity is reproduced well by this calculation at the present stage of investigation, albeit additional electronic control factors clearly come into play especially for heteroaromatic substrates.

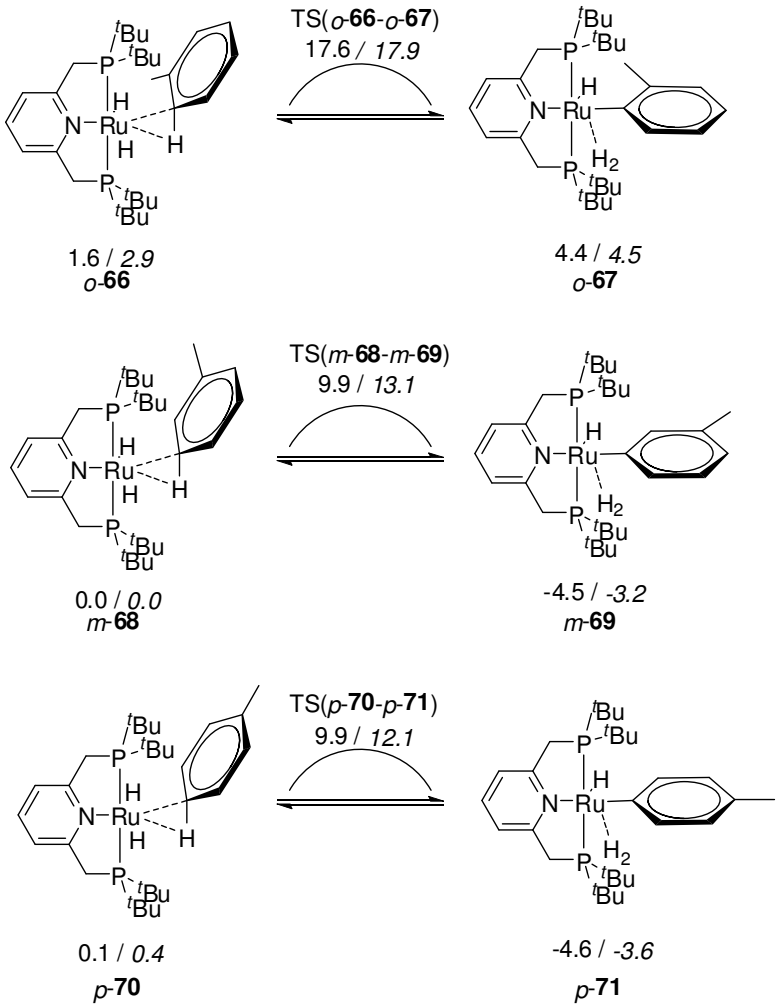

Scheme 34: Relative energies (ΔH, $\Delta H^{\ddagger}$; ΔG, $\Delta G^{\ddagger}$ [italics], kcal/mol) of reactants, products and transition states (not shown) involved in C-H exchange at toluene in ortho-, meta- and para positions (top to bottom).

2.3.1.2. C_6D_6 as Deuterium Source

Our investigations on catalytic H/D-exchange also included the experiments using C_6D_6 as deuterium source as already mentioned in chapter 2.3.1.1. Besides the substrate scope variation, we varied catalyst loadings and temperature with a benchmark substrate, too. Furthermore, we included some NMR-monitoring of the H/D-exchange where the catalyses were performed in *Young teflon capped NMR tubes*.

As depicted in Scheme 35, toluene **12** was deuterated using 1 mol-% of precatalyst **4** at 50°C within three days. For toluene **12**, the incorporation occurred with preference in *meta*-

position, where 87% of all protons were replaced. Additionally, 28% of the *para* protons were exchanged for deuterium, whereas no incorporation was detected in *ortho* position. The methyl group remained unreactive under the present conditions. Other aromatic compounds were also effectively deuterated at 50°C with 1 mol% **4**, whereby a significant chemo- and regioselectivity was observed in certain cases. *o*-Xylene **54** was deuterated exclusively in the β-positions to the methyl groups (>95%) with no significant deuterium incorporation in the α-positions and the methyl groups. In case of *m*-xylene **72** the regioselectivity is unchanged, the β-position is almost exclusively deuterated (93%) and for the α-positions the deuterium incorporation is low (15%) as well for methyl groups (6%). Unsurprisingly, there is no H/D-exchange detectable with mesitylene **73** as substrate, also with a higher catalyst load (2 mol%). The treatment of naphthalene **55** under the same conditions resulted preferably in β–deuteration (92%) with a low amount of α–deuteration (18%). Again, the H/D-exchange in the system **55/** C_6D_6 catalyzed by **4** was not influenced by the addition of mercury (Hg/Ru = 10:1; α: 18%; β: 90%), postulating that the catalytic cycle is occurring on a molecular organometallic species (Scheme 35).[108] The deuterium incorporation in the higher condensed aromatic system phenanthrene **74** is significant in just two positions (C3/C4: 94%, Scheme 35). Interestingly, isoquinoline **75** as a representative of substituted pyridines is not deuterated. This result differs totally from the tested heteroaromates thiophene **56**, 2,5-dimethylfurane **57**, indol **58** and pyrrol **59** which were highly deuterated in most positions at 75°C with D_2O.[26] This observation might be a result of the stronger coordination of the nitrogen functionality in isoquinoline **75**.

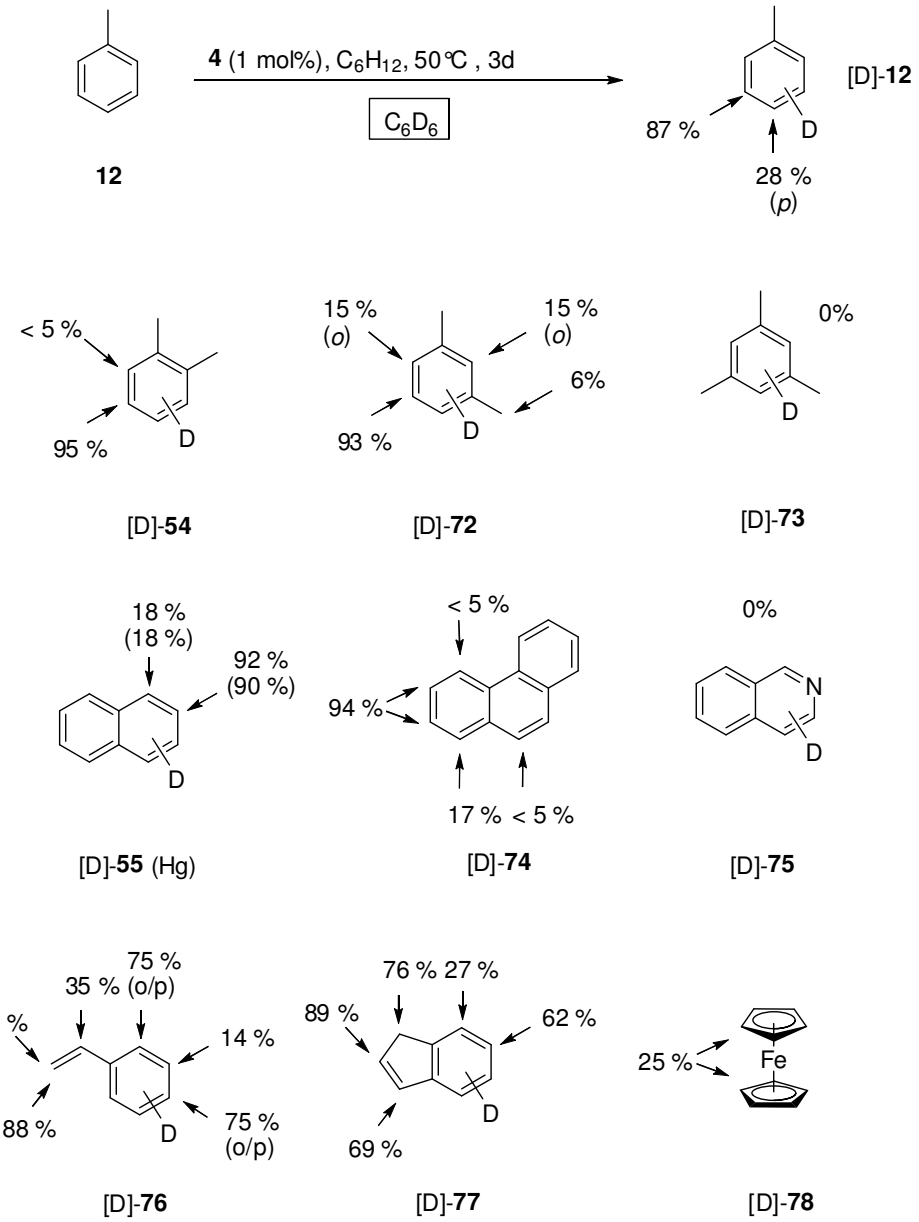

Scheme 35: Catalytic H/D exchange of aromatic compounds using C_6D_6 as the deuterium source and complex **4** as catalyst precursor. Reaction conditions (under Argon): Substrate **12**, **54**, **55**, **72**-**78**: 1.0 – 1.6 mmol; Ru-cat. **4** = 1 mol-%, C_6D_6 (0.7 mL), C_6H_{12} (0.05 mL), t = 3 days; reaction temperature: T = 50 °C; see experimental part for details.

Substrates with conjugated olefines like styrene **76** or indene **77** are also highly deuterated but with less regioselectivity. Styrene **76** shows a regioselectivity for the *ortho/para*-positions which are deuterated to 75%, whereas the *meta*-positions show low incorporation (14%). The double-bond is preferably deuterated in the β–positions (86-88%) and with a moderate α–deuteration (35%). For indene **77** (Scheme 35) the deuteration is higher in the five-membered ring (69–89%). In its benzene ring a slight preference for β–deuteration (β: 62%

vs α: 27%) was observed. The treatment of ferrocene **78** led to rather low deuterium incorporation into the Cp-rings (25%). Furthermore, we tested the deuteration of a polyfluorene which is applied as OLED (organic light-emitting diode).[111] Deuterated polyfuorene and other polymers are of enhanced interest for optical application like optical communication as deuterated light-conducting fibres. This is due to the isotopic red-shift (CH vs CD) in the infra-red which allows less distorted information transport. Unfortunately, the polymer could not be deuterated under the standard conditions. This might be due to the fact that the solubility is quite low and the obtained solution is still too viscose. For this, deuterated polymers are still limited to suitable deuterated monomers like fluorenes.

The properties of the catalytic system were studied in some more detail with the benchmark substrate naphthalene **55**. We monitored the H/D-exchange at the β–position by ^{1}H-NMR spectroscopy at different temperatures and catalyst loadings. Figure 30 shows the strong signal decrease of the β–positions, the lower decrease of the α–positions and the increase of the benzene signal both due to the H/D-exchange. As shown in Figure 31, the increase of the deuterium incorporation at the β–position with precatalyst **4** (7 mol%) at 50°C correlates with the reaction time. Of course the slope is reduced for higher conversion due to the saturation of the β–positions. After about 6.5 h the deuterium incorporation passed 79% and 90% was reached after 24 h. In a second run a deuterium incorporation of 87% (6.5 h) and 95% (one day) was obtained. The variation of the reaction temperature (40-70°C; **4** = 4 mol%) has a significant influence towards the maximum reaction rate in the initial period of the reaction (Figure 32). An *apparent* activation energy based on the reaction time between 20 and 80 minutes was determined. From the Arrhenius plot we obtained the apparent activation energy of E_A 15.8 kcal mol^{-1} (Figure 34).*

* The exclusion of the run at 45°C results in an activation energy of E_A = 16.0 kcal mol^{-1}

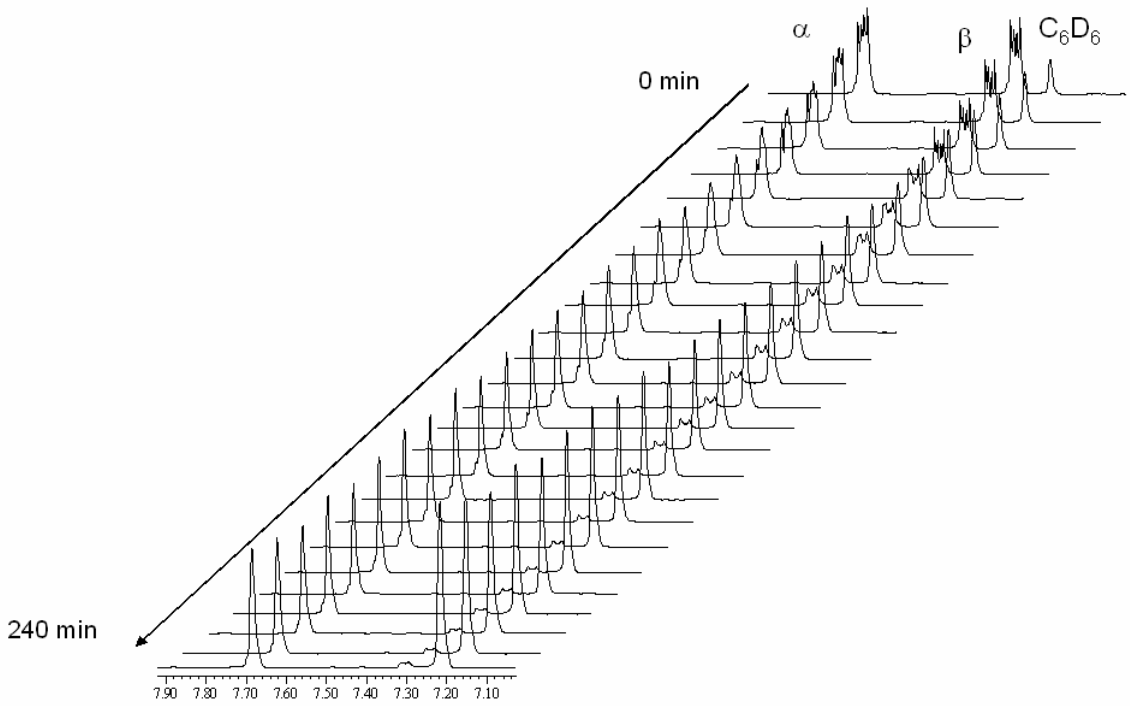

Figure 30: Time-resolved ^{1}H-NMR-monitoring of the H/D-exchange in naphthalene **55**. (Catalyst loading **4**: 4 mol%, T = 70°C, Conversion: 24% (α), 90% (β) after 240 minutes.

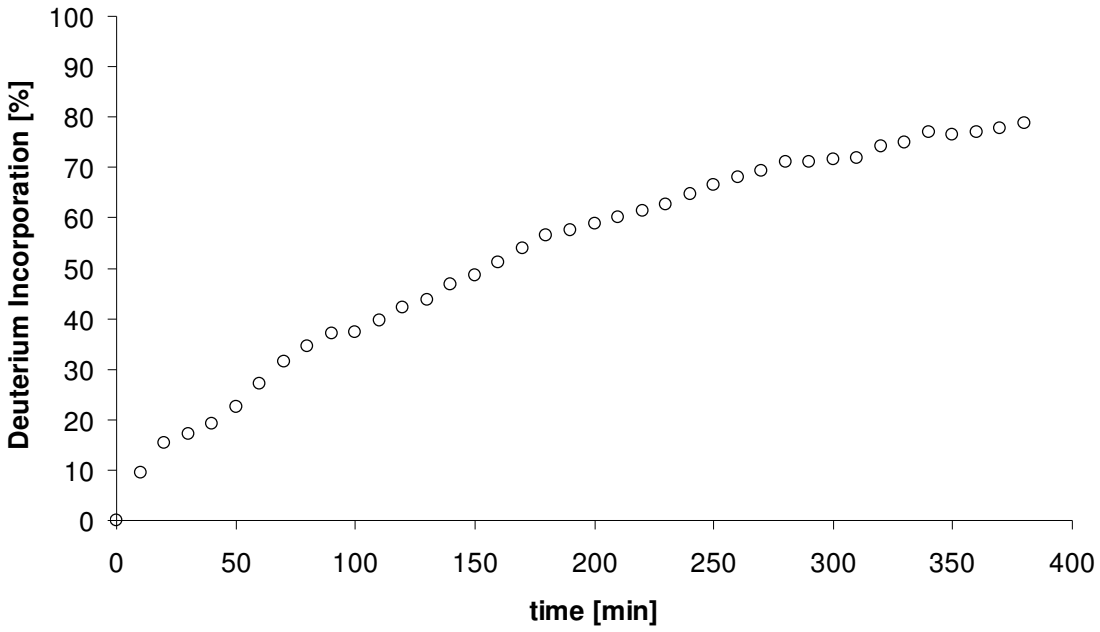

Figure 31: Slope of the [Ru(*dtbpmp*)(H_2)H_2] **4** catalysed *β*–deuteration of naphthalene **55** determined by time-resolved ^{1}H-NMR-monitoring. Catalyst loading: 7 mol%, T = 50°C, Conversion: 8% (α), 79% (β) after 380 minutes.

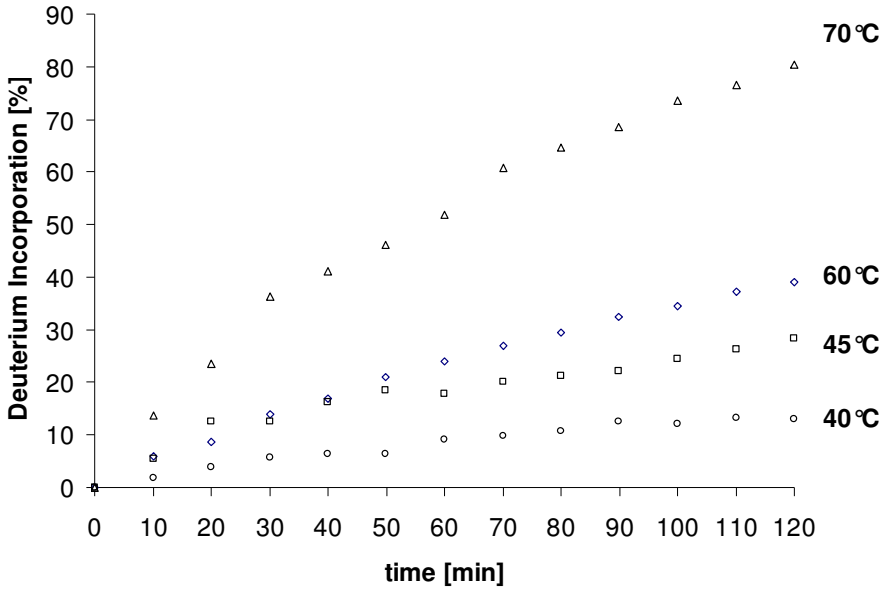

Figure 32: Slopes of the initiation period of the β–deuteration at different temperatures.

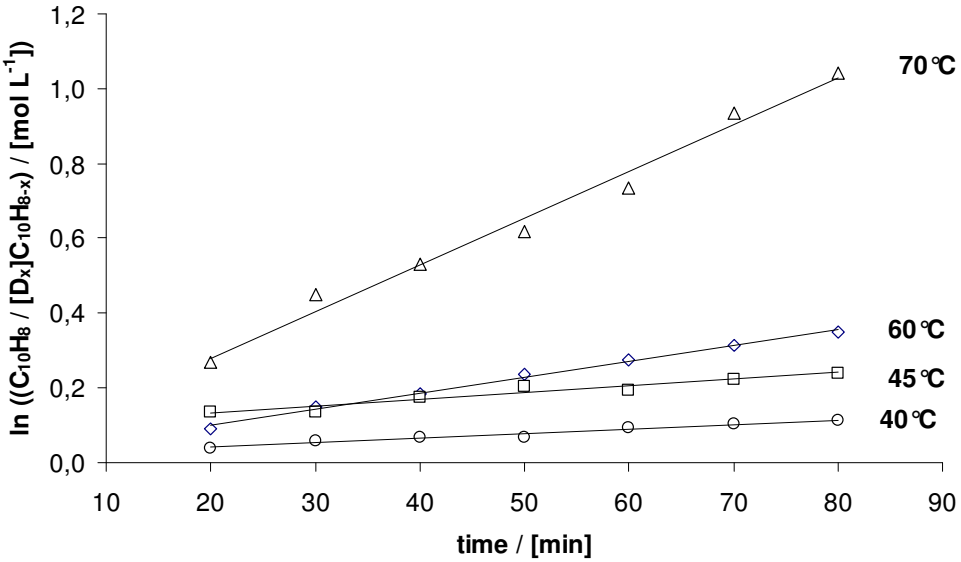

Figure 33: Logarithmic plot of the β–deuteration at different temperatures.

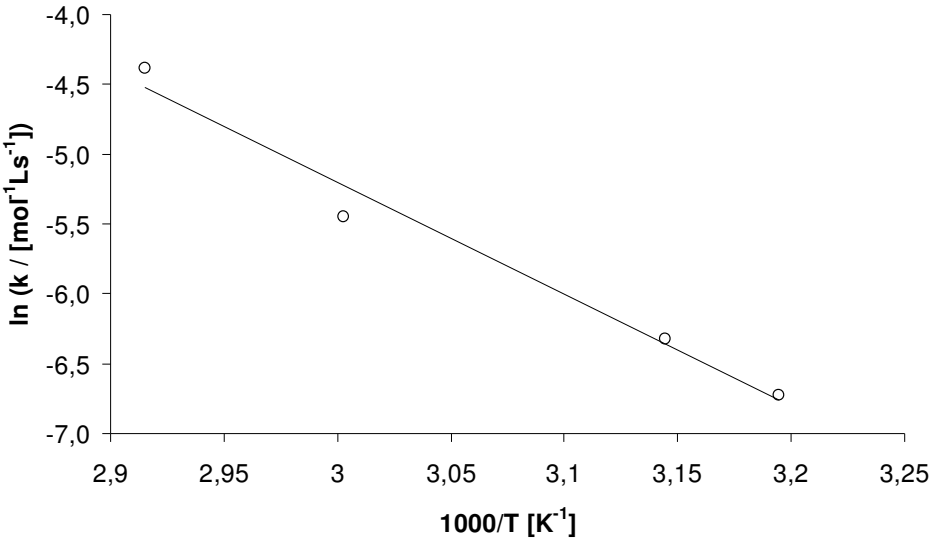

Figure 34: The Arrhenius plot for the β–deuteration in C_6D_6 catalysed by [Ru(*dtbpmp*)$(H_2)H_2$] **4**.

To determine the apparent reaction order relating to the catalyst for the initiation period, the concentration of the catalyst was varied and the substrate concentration was kept constant in a relation of the substrate/catalyst ratio (100:7, 100:4, 100:2). For the determination of the reaction rate the periods between 20 and 70 minutes were used where no conversion were higher than 32% (Figure 35).

The initial rates are $1.231*10^{-6}$ [mol L^{-1} min^{-1}] with 2 mol% catalyst, $2.769*10^{-6}$ [mol L^{-1} min^{-1}] with 4 mol% and $3.308*10^{-6}$ [mol L^{-1} min^{-1}] with 7 mol%.

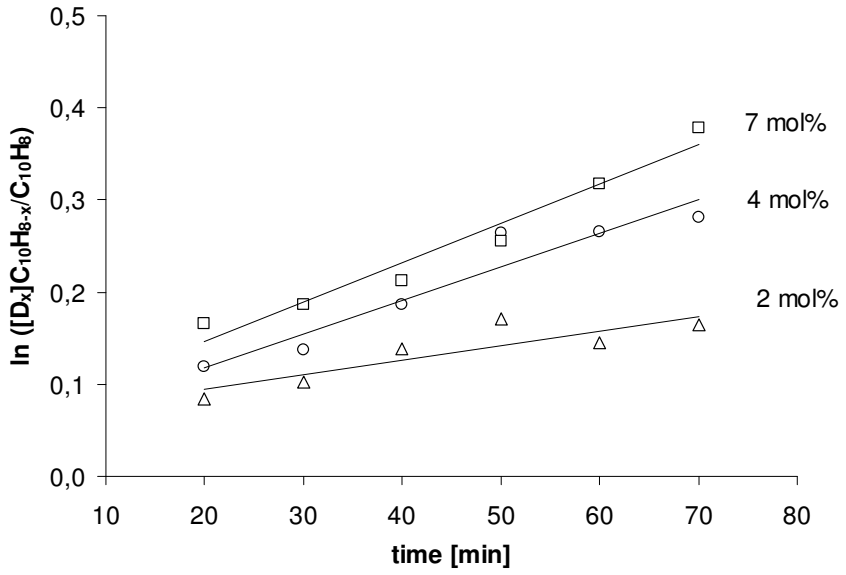

Figure 35: Logarithmic plot of the β–deuteration at different catalyst loadings.

The double logarithmic plot of the initial rate vs. catalyst concentration resulted in a broken-order reaction (0.8) for the catalyst **4** in the β–deuteration of naphthalene **55**.

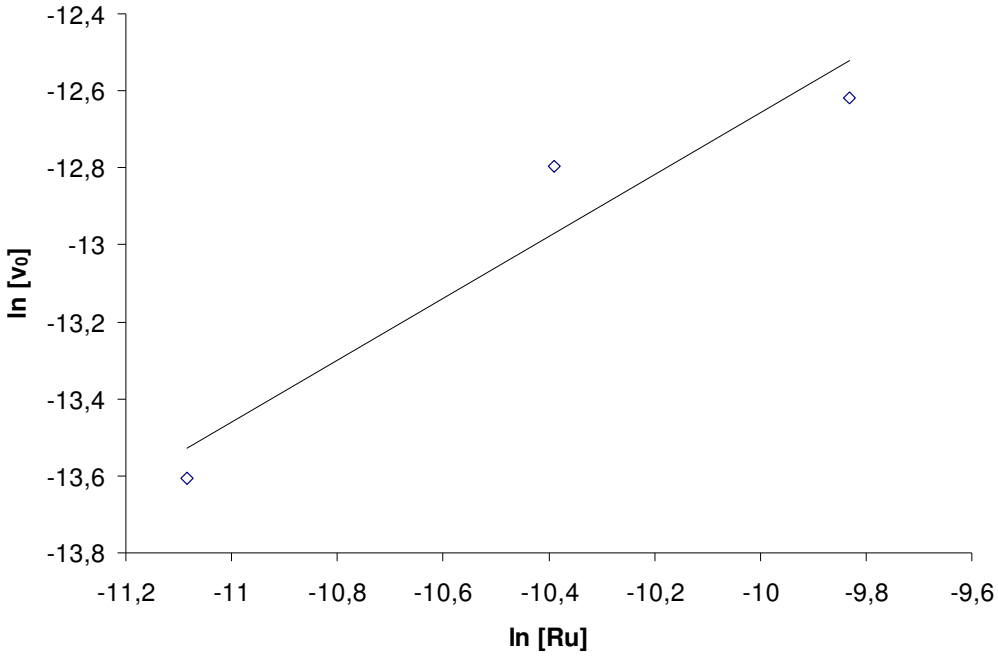

Figure 36: Logarithmic plot of the order for the catalyst.

The computational study of the β–deuteration with precatalyst **4** by means of DFT-calculations support the experimental data obtained from ^{1}H-NMR analysis. Scheme 36 shows the key steps of the exchange process of the model complex **17** and the real catalyst precursor **4** with naphthalene **55** as substrate. The C-H activation step in the $\beta-$ position were calculated to have practically a much lower activation energy than the $\alpha-$ position ($\Delta G_\beta^\ddagger$ = 5.1_{model} / 12.0_{real} kcal/mol and $\Delta G_\alpha^\ddagger$ = 9.3_{model} / 18.1_{real} kcal/mol, respectively). For this, the α–position, however, is disfavored with its higher activation energy of $\Delta G_\alpha^\ddagger$ = 18.1_{real} kcal/mol. Interestingly, one can see the influence of the bulky *t*Bu groups which lifts the activation barrier for CH-activation in comparison with the model complex. Considering the preference of the $\beta-$ position, these results would predict an exclusive incorporation in the $\beta-$ position, with no significant incorporation in the α–position. And indeed, the experiments showed that there is a regio-preference for the $\beta-$ position (up to >95%) and usually a lower $\alpha-$ deuteration (< 20%) which can be influenced by catalyst loadings, temperature and reaction time as discussed for naphthalene **55** in chapter 2.3.1.1.

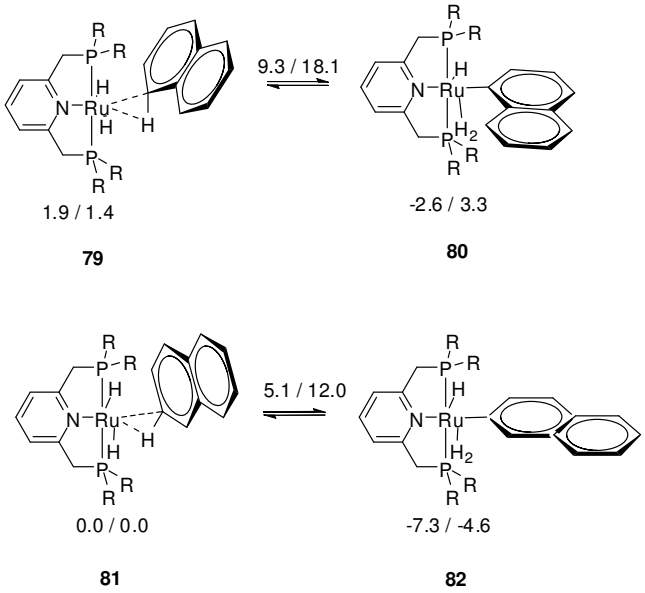

Scheme 36: Relative energies (ΔG, $\Delta G^{\ddagger}$, kcal/mol) of reactants, products and transition states (not shown) involved in C-H exchange at naphthalene in alpha- and beta- positions (top to bottom).

2.3.2. Catalytic Dehydrogenation of Alcohol and Tandem Reactions

For further evaluation of the catalytic potential of [Ru(*dtbpmp*)(η^2-H_2)H_2] **4** as precatalyst we investigated the dehydrogenation reactions of alcohols and alcohol derivatives. We discuss the catalytic conversion of primary alcohols into esters as a result of a bimolecular coupling with elimination of molecular hydrogen. In presence of phosphorylenes, primary alcohols undergo an indirect *Wittig-Reaction* and secondary alcohols are dehydrogenated into ketones or branched ketones depending on the reaction conditions (Scheme 37).

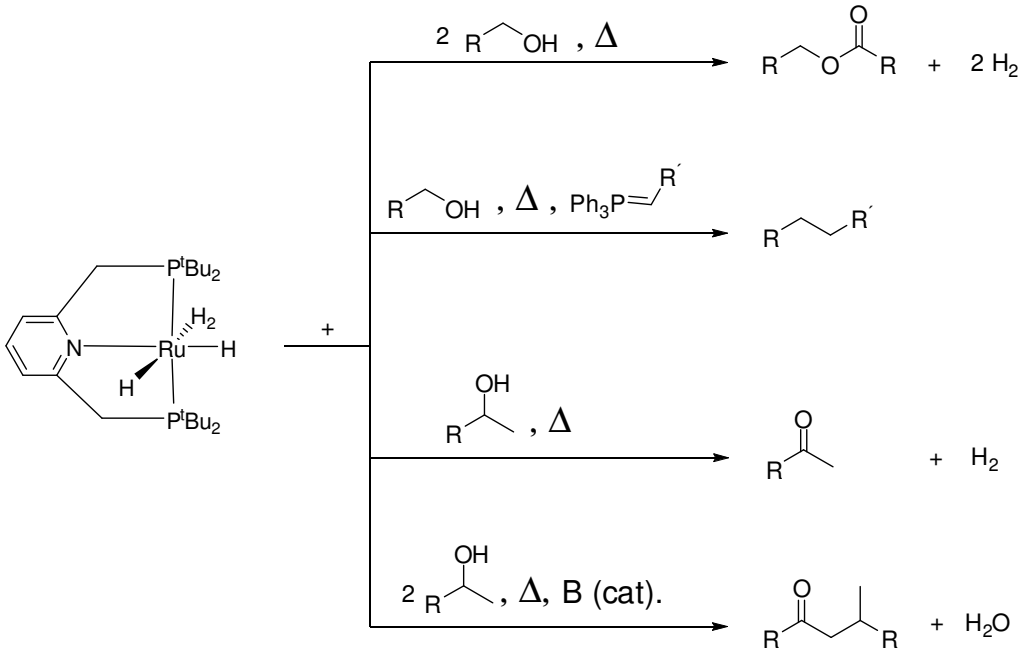

Scheme 37: Overview of the observed alcohol dehydrogenation reactions with precatalyst **4**.

2.3.2.1. Dehydrogenative Coupling of Primary Alcohols

The dehydrogenation of aliphatic as well as benzylic primary alcohols **83**-**88** under reflux in toluene using 1 mol% of **4** leads to the formation of the homoesters **89**-**93** in high conversions in between 3 and 20 hours (Scheme 38, Table 4). The conversion of 1-hexanol **83** into hexylhexanoate **89** was 85% after 3 h and >99% after 20 h by GC analysis. Here, one can see that the reaction is significantly faster at the beginning (TOF = ~28 h^{-1}) but quantitative conversion is reached within 20 h (*all-over* TOF 5 h^{-1}). The decreasing substrate

concentration is probably the main for this behaviour. The treatment of 1-butanol **84** (entry 2) gives a similar high conversion (95%). For bulky aliphatic substrates like cyclohexylmethanol **85** (entry 3) and 1-adamantylmethanol **86** (entry 4) the conversions are 88% and 86% respectively. Benzyl alcohol **87** (entry 5) is converted into benzyl benzoate **93** (90%) and some benzaldehyde could be detected, too. In contrast, the treatment of cinnamic alcohol **88** results in a mixture of saturated and unsaturated alcohols, aldehydes and esters due to transfer-hydrogenation. Further tests including the dehydrogenation of diols to generate lactones via intramolecular ring-closing esterification have not been successfully tested yet. The main problem is the lack of miscibility of the diols with toluene and the catalyst stability in other polar solvents.

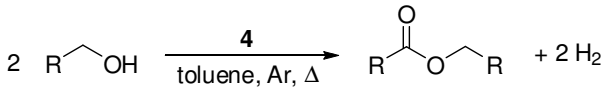

Scheme 38: Dehydrogenative conversion of primary alcohols **83-88** to the corresponding homoesters **89-93**.

Table 4: Conversion of the primary alcohols **83-88** into the corresponding esters **89-93.**

Entry	Substrate	t [h]	Conv. [%][a]	Selectivity [%] Ester (Aldehyde)
1	1-hexanol **83**	3 / 20	85 / >99	>99 / >99
2	1-butanol **84**	18	93	>99
3	cyclohexylmethanol **85**	20	88	>99
4	1-adamantylmethanol **86**	20	86	>99
5	benzyl alcohol **87**	20	>99	90 (10)

Reaction conditions (under argon): Ru-cat: **4** (1 mol%), primary alcohols **83-88** (2 mmol), toluene (5 mL), reflux. [a] Conversion determined by GC and analysed by GC-MS.

Additionally, with 1-hexanol **83** as benchmark substrate we monitored the reaction with ATR-IR online spectroscopy (Table 5).[112] We varied the temperature (50-100ºC) with constant catalyst loading (1 mol%). Another series where we varied the catalyst loading (0.5-2.0 mol%) at constant temperature was performed as well.

Table 5: IR-online study with 1-hexanol **83** as benchmark substrate**.**

Entry	Cat. [mol%]	T [°C]	t [h]	Conv [%][a]
1	1	50	18	39
2	1	70	17.5	69
3	1	85	16	87
4	1	100	6	82
5	0.5	100	12.75	68
6	1.5	100	6	87
7	2	100	4.5	88

Reaction conditions (under argon): Ru-cat: **1** (0.5-2.0 mol%), 1-hexanol **2** (4 mmol), toluene (5 mL), T = 50-100°C.
[a] Conversion determined by GC and monitored by ATR-IR operando equipment.

In Figure 37 the time-resolved ATR-IR plot of the increasing valence vibration of the CO-band at ~1740 cm^{-1} of the formed ester **89** is shown. This band correlates with the product concentration which was used to determine the temperature depending conversion rates and the activation energy of a first-order reaction. Following, the time-resolved profiles (Figure 38), the logarithmic plot (Figure 39) and the Arrhenius plot (Figure 40) are depicted. To allow temperature equilibrium after addition of the substrate, the measurements within the first three minutes after addition of the substrate (t_0) are not considered for further calculations (Figure 39).

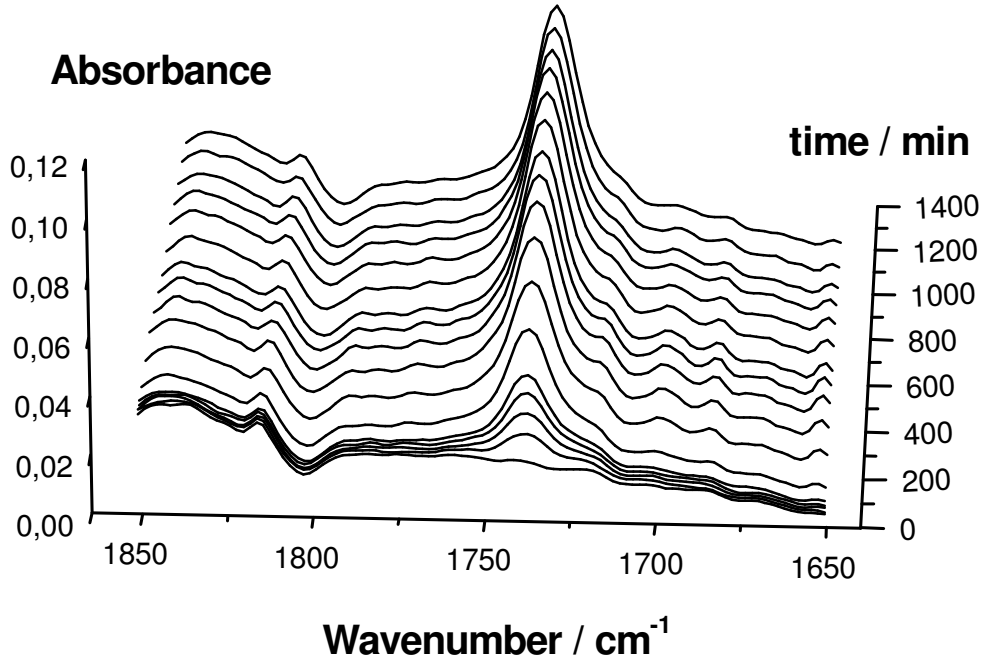

Figure 37: Time-resolved ATR-IR online spectra of the catalytic conversion of 1-hexanol **83** into hexylhexanoate **89**.

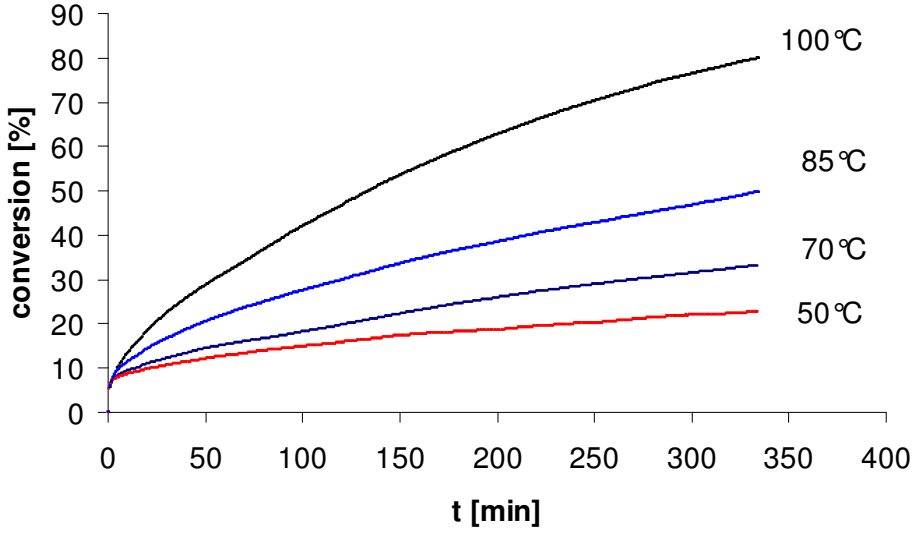

Figure 38: Time-resolved conversion plots between 50°C and 100°C.

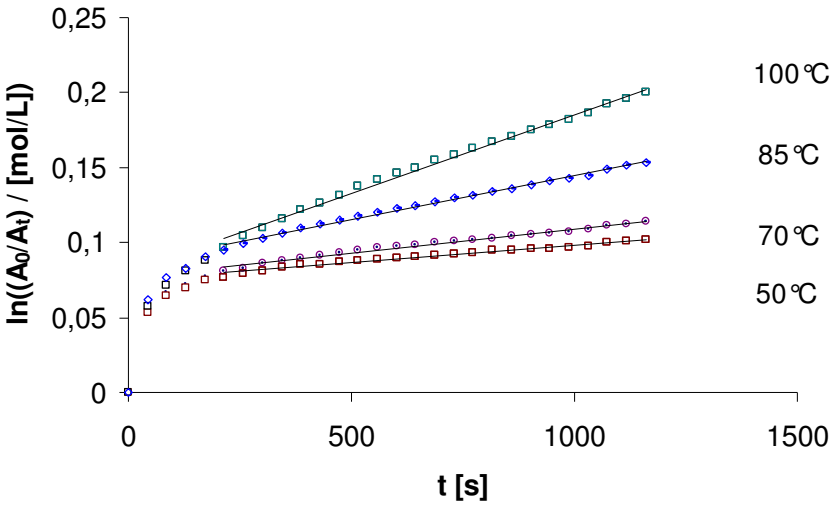

Figure 39: Logarithmic plot at different temperatures

For the reaction we tried to determine the apparent allover activation energy. With the runs between 50°C and 100°C, we found a low activation energy with E_A = 8.9 kcal mol^{-1}. But assuming that the rate-controlling step is the dehydrogenation of the alcohol,[3a, c, d] the determined activation energy for this step is not unprecedented. The literature provides in some cases dehydrogenation of alcohols with comparably low activation energies, e.g. 9.7,[113] 11.7,[114] 11.6,[115] 12.0,[116] or 13.2 kcal mol^{-1}.[113] However, we can of course not exclude under estimation of the determined activation energy.

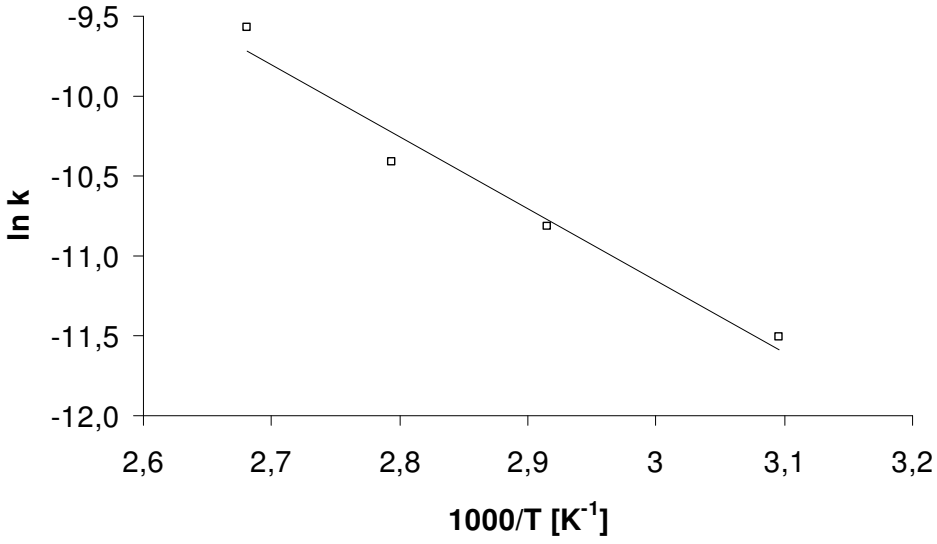

Figure 40: The Arrhenius plot for the initial period of the catalytic conversion of 1-hexanol **83** into hexylhexanoate **89** between 50°C and 100°C.

To determine the apparent reaction order relating to the catalyst for the initiation period, the concentration of the catalyst was varied and the substrate concentration was kept constant in a relation of the substrate/catalyst ratio (100:2, 100:1.5, 100:1, 100:0.5). For the determination of the reaction rate the periods between 5 and 20 minutes were used where no conversion were higher than 18%. The initial rates are $5.645*10^{-8}$ [mol L^{-1} s^{-1}] with 0.5 mol% catalyst and $8.064*10^{-8}$ [mol L^{-1} s^{-1}] with 1.0 mol%, 1.5 mol% and 2.0 mol%. The variation of the catalyst concentration did not lead to a resolution of the reaction order. But, however, one could see that the higher catalyst loadings of 1.5 and 2.0 mol% did not have significant influence on the conversion and reaction rate (Figure 41 and Figure 42). Here one could argue that this might be an evidence for a catalytically active ruthenium complex formed in rather low concentrations.

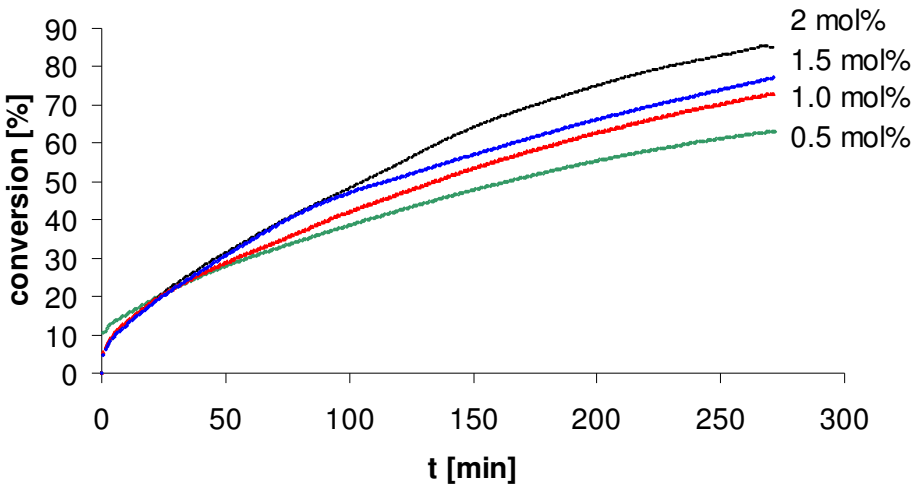

Figure 41: Variation of the substrate/catalyst ratio.

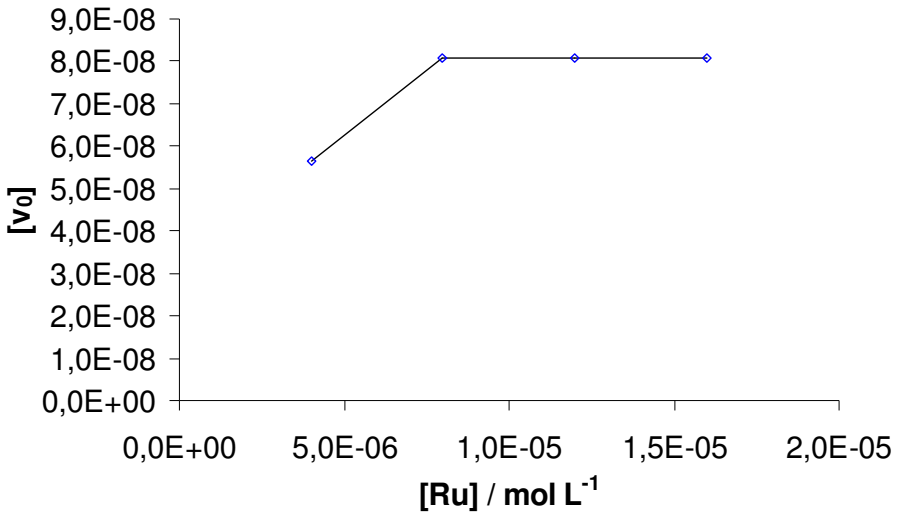

Figure 42: Reaction rate as function of the ruthenium catalyst concentration.

The dominant catalytic active species might be generated via decarbonylation of the alcohol. It is known that ruthenium hydrides catalyses the decarbonylation of primary alcohols already at room temperature.[117] This decarbonylation presumably leads to [RuH(*dtbpmp*)(CO)] **28** which is also formed by treatment of [Ru(*dtbpmp*)H_2(H_2)] **4** with carbon monoxide as described in chapter 2.1.3.3. This might explain the presence of different active species during the initiation of this reaction. First, a ruthenium dihydride [RuH_2(*dtbpmp*)] **4 (-H_2)** is formed by H_2-loss, and then the primary alcohol is decarbonylated (Scheme 39). This decarbonylation could be followed by H_2-loss resulting in another unsaturated species [Ru(*dtbpmp*)(CO)] **27**. [95] This 14e^- species is converted into [RuH(*dtbpmp**)(CO)] **28** the predominant species in the conversion of primary alcohols into esters (see also Scheme 19, p. 33).* [3a, d]

* Chapter 2.1.3.3.: The corresponding saturated *trans*-dihydrides of **29** and **30** are only stable under H_2-atmosphere.

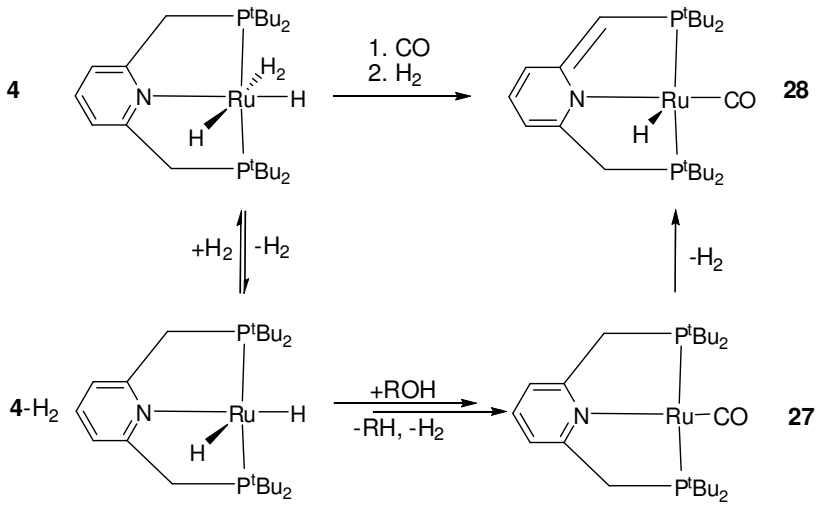

Scheme 39: Formation of the [RuH(*dtbpmp*)(CO)] **28** in presence of a primary alcohol.

To get a hint for this assumption an aliquot of a reaction mixture was analysed by ^{31}P-NMR. A weak signal could be determined at 84.7 ppm (d, $^{2}J_{PP}$ = 74.0 Hz) which might be related to a complex similar to **28**. For this reason, one could imagine that the catalytic cycle is supposed to be similar to the one described by *Milstein* using their [Ru(*diprpmp*)(CO)H] **29** and the highly active [RuH(PNN)CO] **30** catalyst (Scheme 40).[3a, d] A similar mechanism is also discussed by *Hartwig*.[77] Indeed, *Hartwig* also found a ruthenium carbonyl hydride complex ([$RuH_2(CO)(PMe_3)_3$]) as an intermediate in the lactonization of 1,4-butanediol, using a ruthenium dihydride precatalyst.[77] But one could also imagine a dehydrogenative esterification with a ruthenium dihydride species [Ru(*dtbpmp*)H_2] **4(-H_2)** as active species instead in the catalytic cycle (Scheme 40).[77] A proposed catalytic cycle with [Ru(*dtbpmp*)(CO)H] **28** is depicted in Scheme 40. Here, one could assume that the benzylic position acts as a hydrogen-donor for the ruthenium core. The precatalyst **4** reacts first with an alcohol under decarbonylation, to generate the active species **28**. Then another equivalent of an appropriated aliphatic alcohol undergoes oxidative addition (A). Followed by a hydrogen-tranfer (H*) from the benzylic position to the the ruthenium core supporting β-hydride elimination and H_2-loss in the alcohol to form a ruthenium coordinated aldehyde (B). The aldehyde is then cleaved (C) and forms in presence of alcohol the hemi-acetale (D) and **28** is reformed via reductive elimination. The hemi-acetale enters another catalytic cycle via oxidative addition (E), β-hydride elimination / reductive elimination and a ruthenium coordinated ester (F) to reform **28** and to liberate the ester as product (G).

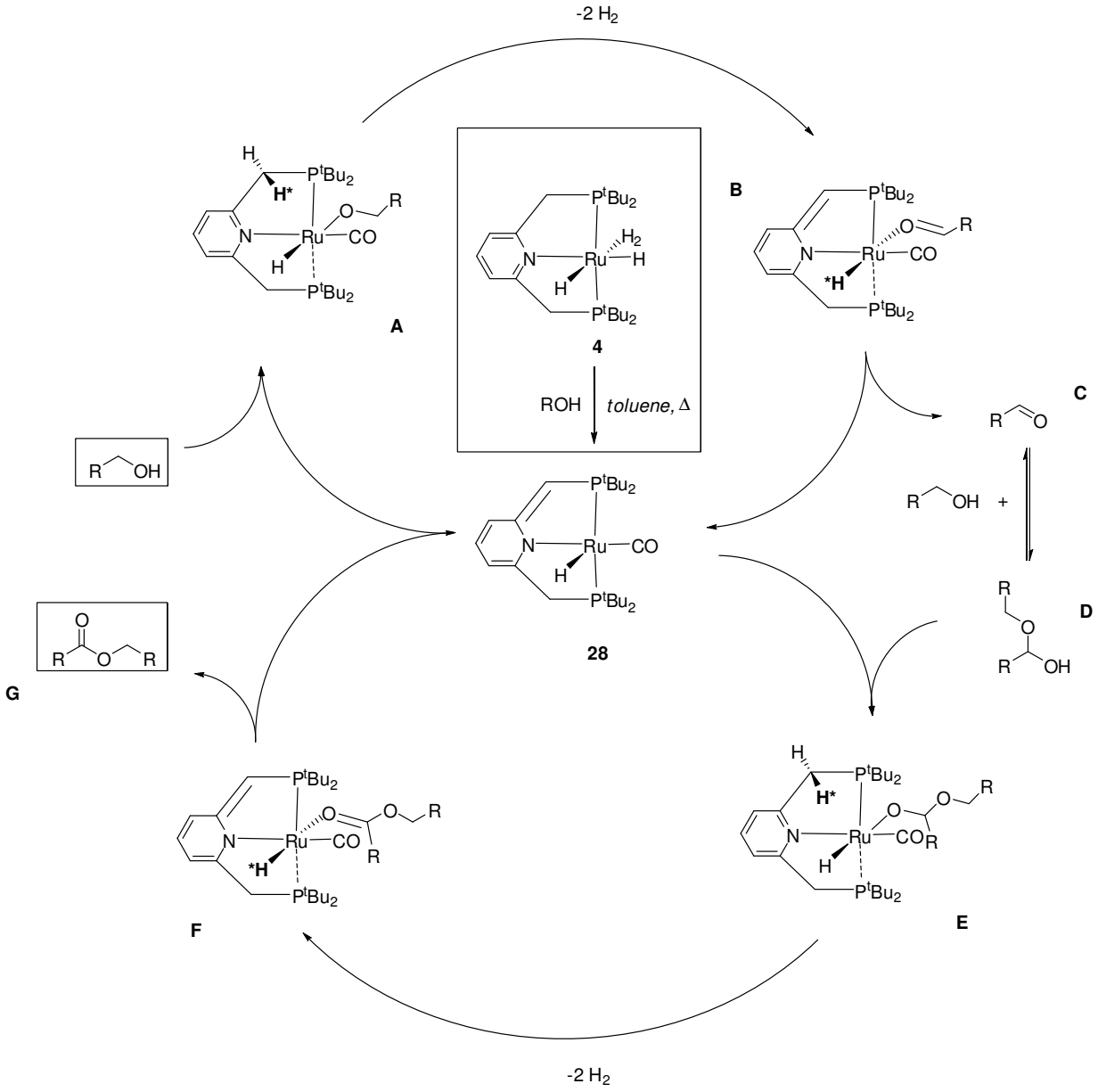

Scheme 40: Proposed catalytic dehydrogeantion cycle of primary alcohols to esters.

To support the proposed catalytic cycle which involves aldehyde and hemi-acetale as intermediates, we tried to isolate the aldehyde. For this, we tested to convert 1-hexanol **83** into 1-hexanal **94** by using coordinating additives to suppress the esterification. In case of styrene **76** one could determine some conversion into the ester **89** within 30 minutes but then after prolonged reaction time there were no further conversion detectable. We assume that the reaction stopped due to a strong coordination of styrene **76** under these conditions. In

presence of 1-octene **38** or triphenylphosphine **95**, hexylhexanoate **89** was still continuously formed.

Due to the difficulties concerning the isolation of the aldehyde in that manner, we thought about to trap the aldehyde in a different way for the verification of the aldehyde intermediate which is also assumed by *Milstein* and co-workers.[3a,d] Motivated by the results of *Williams* and co-workers,[80] who recently presented the iridium catalysed dehydrogenation of primary alcohols in presence of phosphorylenes undergoing a *Wittig*-Reaction, we added acetylmethylentriphenylphosphorane **96** to the dehydrogenation of 1-hexanol **83** (Scheme 41).

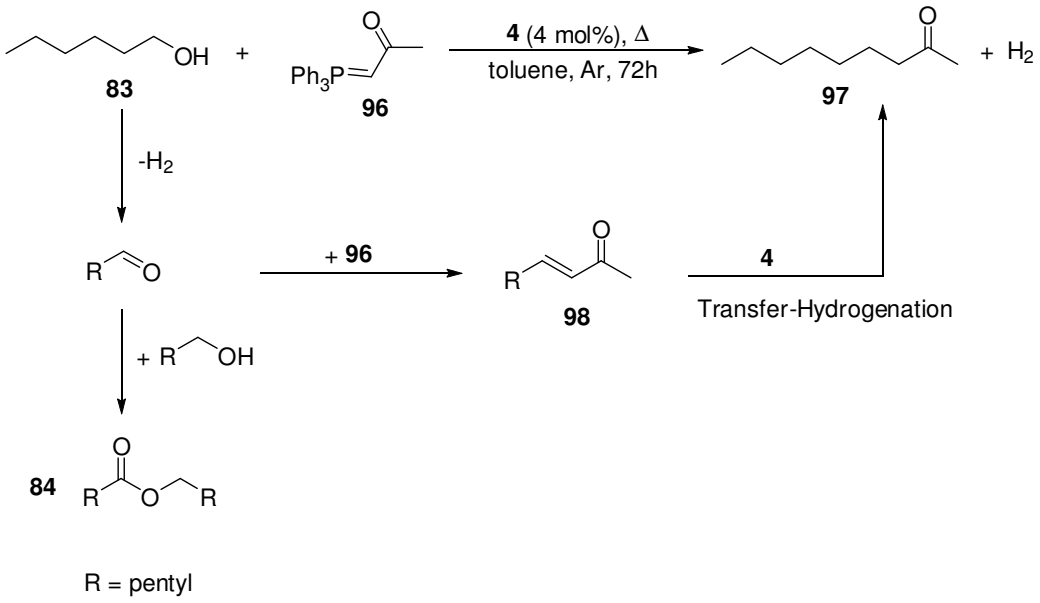

Scheme 41: Indirect Wittig-Reaction using precatalyst [Ru(*dtbpmp*)(η^2-H_2)H_2] **4**.

And indeed, the alcohol reacts with the phosphorylene to give the main product **97** (65% **97**, 9% unsaturated ketone **98**, 14% hexylhexanoate **89**). Here, the primary *Wittig*-product the unsaturated ketone **98** is transfer-hydrogenated into **97**. Interestingly, the *Wittig*-Reaction is preferred under the used reaction conditions. Noteworthy, when a lower catalyst loading (1 mol%), is used the reaction stops within one day. This might be due to a desactivation pathway of the precatalyst [Ru(*dtbpmp*)(η^2-H_2)H_2] **4** or the catalytic active species. As usual, during a *Wittig*-Reaction triphenylphosphinoxide **99** is formed but we also determined free triphenylphosphine **95** which is probably formed via a redox reaction between **99** and **4** or the catalytic active species. However, we could indentify aldehyde as a presumed intermediate for the catalytic dehydrogenation of primary alcohols. Moreover, we found another application for [Ru(*dtbpmp*)(η^2-H_2)H_2] **4** for C-C bond formation with primary alcohols as substrates.

Although the synthesis and isolation of aldehydes for a *Wittig*-Reaction is prevented, it is not yet evaluated in a sufficient manner for this transformation. Notable, *Williams* and *Whittlesey´s* catalyst systems are more evaluated and our system has no advantages for indirect *Wittig*-typed reactions.[80b, 81b] Noteworthy, as also reported by *Williams*,[80] the selectivity towards one product decreases in the presence of other functional groups which are reactive under such reaction conditions, e. g.: olefins (transfer-hydrogenation) or esters (trans-esterification). This limitation of functional groups tolerance also limits the number of appropriate substrates of interest in a synthetical approach.

2.3.2.2. Dehydrogenation of Secondary Alcohols

Under the same base-free conditions as for the esterification of the primary alcohols **83**-**88**, the precatalyst [Ru(*dtbpmp*)(η^2-H_2)H_2] **4** catalyses the acceptorless dehydrogenation of secondary alcohols 2-octanol **100** and 1-phenylethanol **101** into the ketones 2-octanone **102** and acetophenone **103** (Scheme 42, Table 6). Recently, *Milstein* presented also an acceptorless dehydrogenation of secondary alcohols using ruthenium dinitrogen complexes under *basic* conditions.[3c] With complex **4** 2-octanol **100** is dehydrogenated within three hours into 2-octanone **102** with 64%, after six hours the conversion increased to 79%. Under prolonged time (20 h) 2-octanone **102** and acetophenone **103** are formed quantitative (99%).

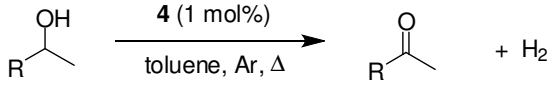

Scheme 42: Catalytic dehydrogenation of 2-ROH into ketones. R = hexyl (**100**, **102**), phenyl (**101**, **103**).

Table 6: Conversion of secondary alcohols into ketones**.**

Substrate	t [h]	Conv. [%][a]
2-octanol **100**	3	64
2-octanol **100**	6	79
2-octanol **100**	20	99
1-phenylethanol **101**	20	99

Reaction conditions (under argon): Ru-cat: **4** (1 mol%), secondary alcohols (2 mmol), toluene (5 mL), reflux. [a] Conversion determined by GC and analysed by GC-MS.

The dehydrogenation of secondary alcohols can be described as depicted in Scheme 43.[3c] In contrast to the dehydrogenation of primary alcohols, it seems most likely that the catalytic species [Ru(*dtbpmp*)H_2 **23**] (A) is already formed via H_2-Loss. Followed by oxidative addition of the secondary alcohol onto the ruthenium dihydride **23**, a ruthenium alkoxide (B) is formed. This species undergoes β-hydride elimination, liberating the ketone as product (C) under reformation of **4** or a ruthenium tetrahydride. This species is immediately converted by reductive elimination of molecular dihydrogen into the catalytic species **23** (A).

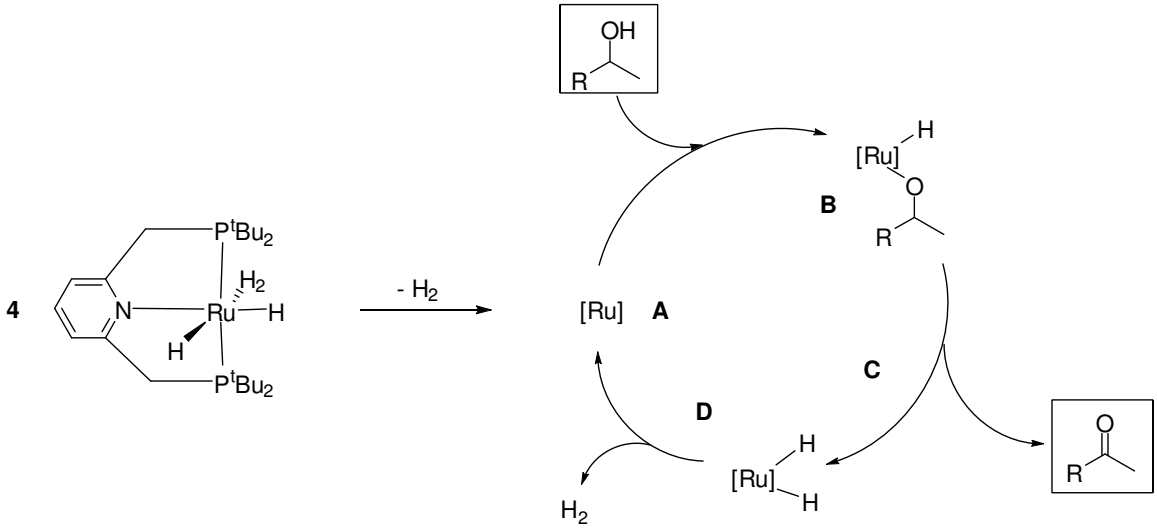

Scheme 43: Catalytic dehydrogenation of secondary alcohols. [Ru] = Ru(*dtbpmp*)H_2 **23**.

We also recognized transfer-hydrogenation as a side-effect of dehydrogenation of alcohols in presence of hydrogen-acceptors such as olefins and ketones. In a reaction performed in a *Young-capped* NMR-tube, we tested a catalytic transfer-hydrogenation reaction catalysed by [Ru(*dtbpmp*)(η^2-H_2)H_2] **4**. As hydrogen source we used an excess of isopropanol **115** for the hydrogenation of cyclohexanone **116** to cyclohexanol **117** at 50°C in C_6D_6 as reported by *Williams* (Scheme 44).[67] The conversion reached about 45% after 3.5 h and within one day the reaction is completed as determined by ^{1}H-NMR spectroscopy.

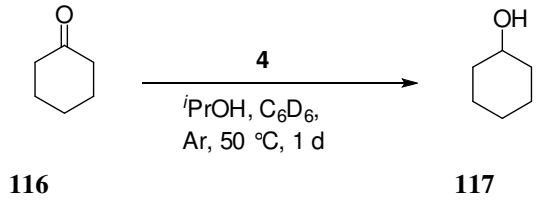

Scheme 44: Transfer-hydrogenation catalysed by **4**.

A slight modification of the dehydrogenative conditions applied on alcohols by adding a base leads to a tandem-catalysis[79] of dehydrogenation, aldol condensation and transfer-hydrogenation. Similar tandem-effects were recently also recognized by *Williams* and co-workers, using iridium or ruthenium complexes for dehydrogenation of alcohols in presence of base. Consequently they used it for *indirect* crossed-aldol, nitroaldol and *Knoevenagel* reactions.[80, 88] Indeed, this observation was originally published by *Guerbet* in 1899 (*Guerbet-Reaction*) and recently also extensively studied by *Carlini* (Combined indirect aldol / transfer-hydrogenation reaction).[86, 87] In our case, the presence of catalytic amounts of a base co-catalyst in the dehydrogenation of the alcohols **100**, **101** and 2-butanol **104** leads to branched ketones **105**-**107** (primary main compounds) via dehydrogenation of the alcohol, aldol condensation and followed by transfer-hydrogenation (Scheme 45).

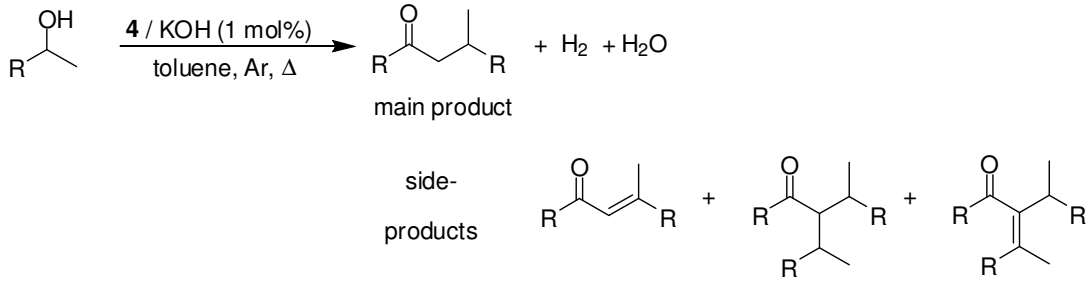

Scheme 45: Dehydrogenation of 2-ROH in presence of base into branched ketones. The primary main compounds with R = hexyl (**100**, **105**), phenyl (**101**, **106**) and ethyl (**104**, **107**).

Table 7: Conversion of secondary alcohols into branched ketones**.**

Substrate	Product ratio[a] main product	side products			
2-octanol **100**	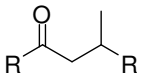 55% (**105**) R = hexyl	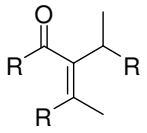 34% (**108**)	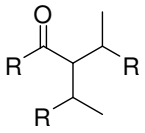 11% (**109**)		
1-phenylethanol **101**	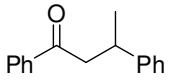 46% (**106**)	12 (**103**)	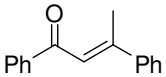 5 (**110**)	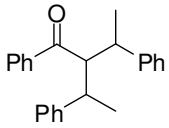 8 (**111**)	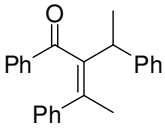 29 (**112**)
2-butanol **104**	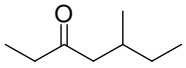 78% (**107**)				

Reaction conditions (under argon): Ru-cat: **4** (1 mol%), secondary alcohols (2 mmol), toluene (5 mL), reflux, t = 20 h, conversion: 90-98%. [a] Conversion determined by GC and analysed by GC-MS.

Within one day the substrates are converted almost quantitatively (90-98%) into branched ketones. The GC- and GC-MS analyses showed the formation 9-methylpentadecan-7-one **105**, 9-methyl-8-(octan-2-yl)pentadec-8-en-7-one **108** and 9-methyl-8-(octan-2-yl)pentadecan-7-one **109** in a ratio of 55:34:11 (**105**:**108**:**109**). The conversion of 1-phenylethanol **101** leads to 1,3-diphenylbutan-1-one **106** as primary main product accompanied with acetophenone **103**, 1,3-diphenylbut-2-en-1-one **110**, 1,3-diphenyl-2-(1-phenylethyl)butan-1-one **111** and 1,3-diphenyl-2-(1-phenylethyl)but-2-en-1-one **112** in a ratio of 12:46:5:8:29 (**103**:**106**:**110**:**111**:**112**). In a similar reaction 2-butanol **104** is converted into 5-methyl-3-heptanone **107** (78%). The by-products show the problem of this tandem-catalysis: The branched ketones **105-107** undergo additional aldol condensations. This is indicated also by means of preparative GC with a low isolated yield of 16% of **105** in contrast to high substrate consumption of **100** (98%). We have not reached a solution for this problem yet. An optimisation of this tandem-catalysis is necessary but probably the additional aldol condensations can not be suppressed.

For the formation of branched ketones we could consider two pathways. Both are based on the pre-existing dehydrogenative conversion of secondary alcohols into the corresponding ketones (Scheme 43 and Scheme 46), followed by base-catalysed aldol-condensation (Scheme 46). After these steps, the aldol condensate could enter two pathways. On one hand, transfer-

hydrogenation between an alcohol as donor and the olefin as acceptor leads directly to a branched ketone **105-107** (Scheme 46). On the other hand, the aldol condensate may be hydrogenated to the *Guerbet-Alcohol*, a branched saturated alcohol, followed by dehydrogenation of the alcohol to the corresponding branched ketone (Scheme 46). Additional aldol condensations and transfer-hydrogenation leads to the formation of the by-products.

In contrast, primary alcohols can not be converted under basic conditions into branched alcohols or aldehydes. As a test reaction with 1-butanol **84** showed that neither 2-ethylhexan-1-ol **113** nor 2-ethylhexan-1-al **114** was formed but once again the esterification is preferred and butylbutyrate **90** is formed.

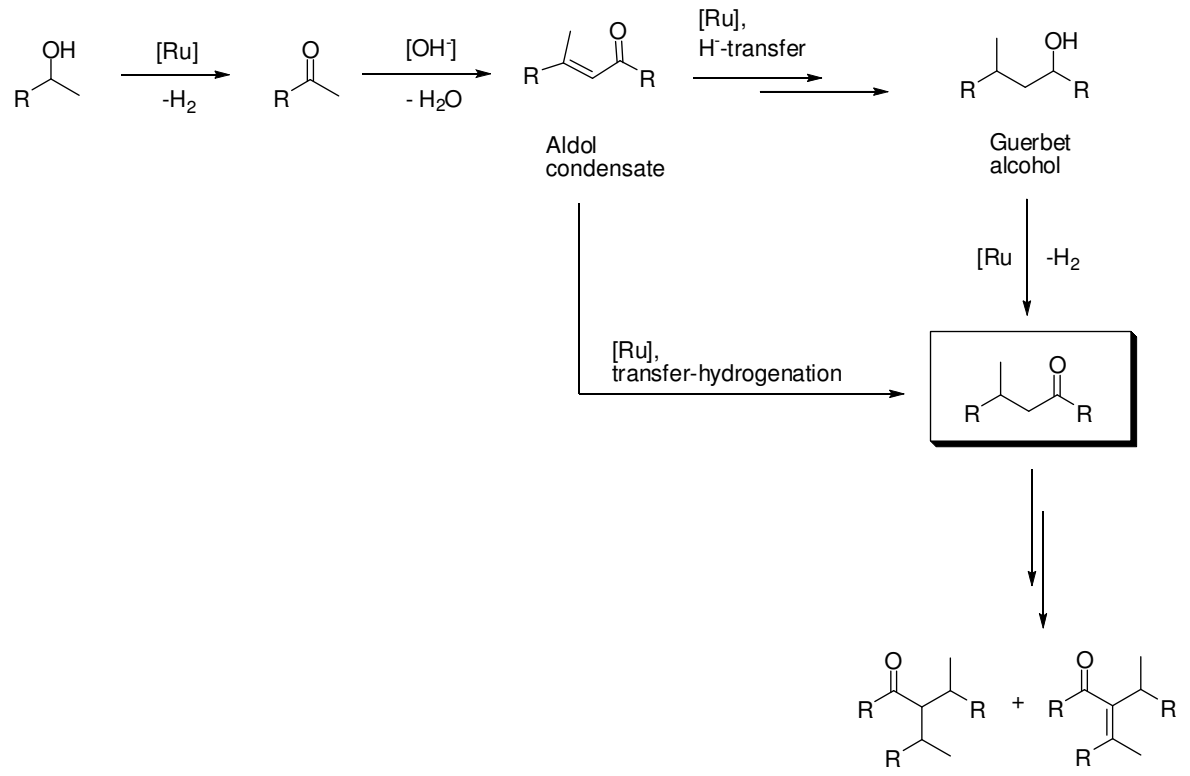

Scheme 46: Proposed mechanism for the formation of branched ketones.

3. Summary

3.1. Ruthenium Dihydrogen Complexes

In an approach to generate monomeric nonclassical ruthenium hydride complexes with a chelating ligand framework, we turned the attention toward pincer type ligands which allow a *trans* arrangement of two electron-rich and bulky phosphorous donor groups. As the most efficient and practical method towards these ruthenium complexes the direct-hydrogenation route was successfully applied using the PNP and POP pincer ligands *dtbpmp* **15** and *dtbpoet* **49** (Scheme 47).

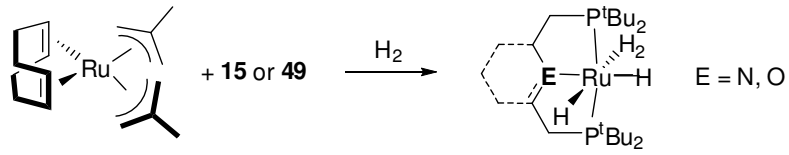

6 **4** and **5**

Scheme 47: Straight forward synthesis to the ruthenium dihydrogen complexes **4** and **5** bearing bulky PNP and POP pincer ligands.

The complex **4** [Ru(*dtbpmp*)H_2(H_2)] was isolated as light-brown microcrystalline solid in yields up to 75% and it is remarkable stable under argon. For structural investigation of complex **4** [Ru(*dtbpmp*)H_2(H_2)] we determined the T_1(min) (77 ms; θ_{min} = 228 K at 400 MHz; δ = -7.3 ppm) and the H-H distance (1.1 Å) of the side-on bonded H_2 moiety by ^{1}H-NMR spectroscopy which stays in agreement with DFT-calculations (H-H distance: 0.979 Å). Additionally, we detected the characteristic bands for ν(Ru-*H*) at 1990, 1892 and 1700 cm^{-1} and for ν(Ru-H_2) at 2095 cm^{-1} by IR spectroscopy.

Complex **4** [Ru(*dtbpmp*)H_2(H_2)] (Figure 43) exhibits interesting properties for CH-activation indicated by H/D-scrambling in the NMR- and IR-spectra using [D_6]benzene, [D_8]toluene, D_2O and D_2-gas as deuterium sources.

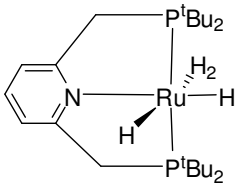

Figure 43: The unique Ru(*dtbpmp*)$H_2(H_2)$ **4** containing a PNP pincer ligand.

Furthermore, the unusual reaction behaviour with molecular nitrogen illustrated by the reversible formation of the dinitrogen complex [Ru(*dtbpmp*)$H_2(N_2)$] **20** and the formation of the ruthenium clusters most likely confirms the high reactivity and gives further evidence for a dihydrogen complex indicated by NMR-monitoring of the H_2-/N_2-equilibrium experiment.[4c] The benzylic position might play an important role for the reactivity of [Ru(*dtbpmp*)$H_2(H_2)$] **4** as indicated by very fast deuteration with D_2O and also by the reaction with CO into the assumed ruthenium monohydride [Ru(*dtbpmp*)(CO)H] **28**. The reactivity of **4** is also reflected with the CO_2 insertion into a ruthenium hydride bond and the reduction of CO_2 to CO resulting in the complex [RuH(*dtbpmp*)(HCO_2)CO] **41**. Furthermore, complex **4** also reacts with pinacolborane **34** resulting in [Ru(*dtbpmp*)(H_2)H(Bpin)] **35**.

We successfully tuned the electronic properties of the ruthenium core by the incorporation of the POP pincer *dtbpoet* **49** into the ligand sphere of the ruthenium hydride fragment. Via the direct-hydrogenation route we found an access to the new ruthenium dihydrogen complex [Ru(*dtbpoet*)(H_2)H_2] **5** bearing the bulky POP pincer ligand *dtbpoet* **49** (Figure 44). It was isolated as greenish solid in a yield of 55%. For structural investigation we determined the T_1(min) (38 ms; θ_{min} = 221 K at 400 MHz; δ = -8.6 ppm) and the H-H distance (0.98 Å) of the side-on bonded H_2 moiety by ^{1}H-NMR spectroscopy which stays in agreement with DFT-calculations (H-H distance: 0.987 Å). Additionally, we detected the characteristic bands for ν(Ru-*H*) at 1994, 1905, 1774 cm^{-1} and for ν(Ru-*H_2*) at 2088 cm^{-1} by IR spectroscopy.

It shows no remarkable activity for H/D-exchange. Furthermore, it shows the usual reversible reaction behaviour in the N_2/H_2 ligand exchange experiment forming [Ru(*dtbpoet*)$H_2(N_2)$] **52**.

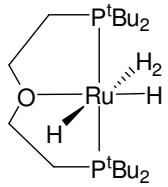

Figure 44: The [Ru(*dtbpoet*)(H_2)H_2] **5** containing a POP pincer ligand.

The application of other bulky PNP pincers did not lead to [Ru(PNP)(H_2)H_2] complexes. A satisfactory approach for future experiments might use PNP- or POP- pincer analogue with adamantyl or cyclopentyl groups or a PNP pincer with mixed chiral phosphines which would be of interest for asymmetric catalysis. It should be pointed out that the potential for catalytic activity of this complex class bearing bulky POP pincers seems to be lower as the catalyst precursor [Ru(*dtbpmp*)(H_2)H_2] **4** has shown much higher activity for C/H-activation and H/D-scrambling.[4c, 26]

3.2. Catalysis

In summary, we have shown that the nonclassical ruthenium hydride complex **4** is an effective catalyst precursor for the H/D exchange between aromatic substrates and D_2O at unprecedented mild conditions (Scheme 48). The incorporation occurs with aromatic and heteroaromatic substrates showing significant chemo- and regioselectively in certain cases. DFT calculations support a catalytic cycle comprising σ-bond metathesis as key step for the exchange processes with a strong steric component in the directing effect. Furthermore, the nonclassical ruthenium hydride complex **4** is an effective catalyst precursor for the H/D exchange between aromatic substrates and C_6D_6 at mild conditions (Scheme 48). The incorporation occurs with aromatic substrates and conjugated olefines showing significant chemo- and regioselectively in certain cases.

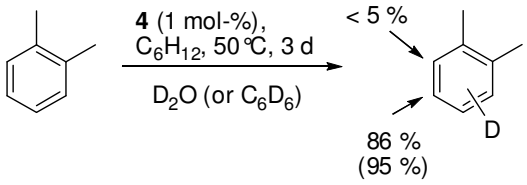

Scheme 48: Ruthenium catalyzed selecetive H/D-exchange between arenes and D_2O (or C_6D_6).

^{1}H-NMR monitoring gives some insights of the reaction showing that the reaction follows a *pseudo-first* order rate law for the *β*–deuteration of naphthalene **55** with an *apparent* activation energy of 15.8 kcal/mol. The DFT calculations support the experiments and a catalytic cycle comprising *σ*-bond metathesis as key step for the exchange processes with a strong steric component in the directing effect.

Other applications showed the potential of the nonclassical ruthenium hydride complex **4** as an effective catalyst precursor for the dehydrogenation of aliphatic and bulky primary alcohols resulting in the corresponding homoesters (Scheme 49). The assumed intermediate aldehyde could be verified by the indirect conversion of an alcohol with a phosphorylene resulting in a *Wittig*-product (Scheme 49). Complex **4** is also active for the acceptorless dehydrogenation of secondary alcohols into the corresponding ketones (Scheme 49). It seems most likely that the catalytic species is the ruthenium dihydride [Ru(*dtbpmp*)H_2 **23**]. The addition of a base co-catalyst to **4** leads to a tandem-catalysis (dehydrogenation, aldol condensation, transfer-hydrogenation, Scheme 49). We did not find conditions for a branched ketone as a single main product because the resulting branched ketone undergoes further aldol condensations. Furthermore, complex **4** catalyzed hydroboration of olefins with pinacolborane **34**.

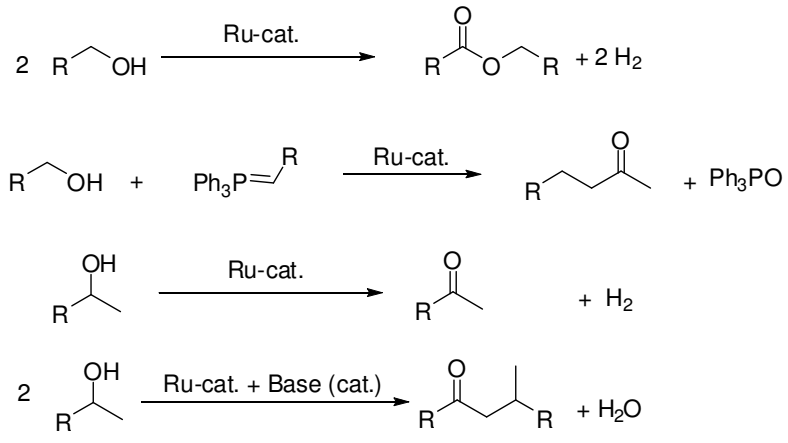

Scheme 49: Catalytic dehydrogenation of alcohols and their indirect conversions in coupling reactions.

4 Experimental Section

4.1. General

Reactions were performed under argon or hydrogen atmospheres using schlenk, canula or glove box techniques. Glassware and autoclaves were dried, evacuated and flushed with argon prior to use. Non-deuterated and deuterated solvents and substrates were purchased from Acros, Aldrich, ChemPur, Fluka, Strem or were in stock in the institute. Commercial reagents were used as received if not mentioned otherwise. Solid reagents were dried in vacuo (10^{-2} – 10^{-3}mbar), liquids were degassed and solvents were dried and purified according to standard procedures.[118] Solvents, reagents and complexes were stored under argon or hydrogen atmospheres if necessary. The gases hydrogen (Messer 5.0) deuterium (Messer 2.7), argon (Messer 4.8) and nitrogen (Messer 4.0) were used as received.

4.2. Analytic Methods

The analyses were measured in the analytical departments of the Max-Planck-Institut für Kohlenforschung in Mülheim/Ruhr if not mentioned otherwise.

4.2.1. Nuclear Magnetic Resonance Spectroscopy (NMR)

^{1}H-NMR, ^{13}C-NMR, ^{31}P-NMR and ^{11}B-NMR spectra were recorded in deuterated solvents using 5 mm NMR tubes on Bruker DPX 300 and AV 400 automatically. The same nucleus were measured on the Bruker AMX 300 spectrometer manually if *Young-Teflon-Capped NMR tubes* were used or [D_6]DMSO capillaries were used in non-deuterated solvents. The ^{1}H-NMR spectra for T_1(min) experiments were measured on a Bruker AMX 400 in deuterated solvents in sealed NMR tubes. The NMR-monitoring experiments were performed on the same spectrometer using *Young-Teflon-Capped NMR tubes*. ^{2}H-NMR and selected ^{13}C-NMR spectra were performed on a Bruker DMX 600 spectrometer. Chemical shifts δ are given in ppm and coupling constants J in Hz.

^{1}H-NMR-Spectroscopy:	BRUKER DPX 300	300.1 MHz
	BRUKER AMX-300	300.1 MHz
	BRUKER AV-400	400.1 MHz
	BRUKER AMX-400	400.1 MHz

Chemical shifts δ are relative to the solvent signal.

^{2}H-NMR-Spectroscopy:	BRUKER DMX 600	600.2 MHz

^{13}C-NMR-Spectroscopy:	BRUKER DPX-300	75.5 MHz
	BRUKER AMX-300	75.5 MHz
	BRUKER AV-400	100.6 MHz
	BRUKER DMX-600	150.9 MHz

Chemical shifts δ are relative to the solvent signal. The spectra are ^{1}H-decoupled.

^{31}P-NMR-Spectroscopy:	BRUKER DPX-300	121.5 MHz
	BRUKER AMX-300	121.5 MHz
	BRUKER AV-400	162.0 MHz

Chemical shifts δ are relative to H_3PO_4 in H_2O (85%) as external Standard. The spectra are ^{1}H-decoupled.

^{11}B-NMR-Spectroscopy:	BRUKER DPX-300	96.3 MHz
	BRUKER AV-400	128.4 MHz

Chemical shifts δ are relative to BF_3-Et_2O as external standard. The spectra are ^{1}H-decoupled.

4.2.2. Infrared Spectroscopy (IR)

IR spectra were measured in KBr or in Nujol on a NICOLET MAGNA IR 750 spektrometer.

4.2.3. Mass Spectrometry

Mass spectra were recorded on following machines:

BRUKER APEX III (FTICR-MS) ;	ESI, MALDI, CI
FINNIGAN MAT 95	ESI, EI, CI
FINNIGAN SSQ 7000 (GC-MS)	EI, CI
BRUKER ESQUIRE 3000	Ion Trap, ESI
FINNIGAN MAT 8200	EI
FINNIGAN 8400	EI
HP MS ENGINE	LC/ESI-MS

4.2.4. X-Ray

The single-crystal X-ray diffraction analyses were measured at the department for *Chemical Crystallography* at the MPI for Coal Research.

4.2.5. Microanalysis

The microanalyses were measured in the *Mikroanalytisches Laboratorium Kolbe*, Mülheim/Ruhr.

4.2.6. Autoclaves for High-Pressure Experiments

The used stainless steel autoclaves were developed and manufactured in the mechanical departments of the Max-Planck-Institutes Mülheim/Ruhr if not other mentioned.

Safety warning: The use of pressurized gases can be hazardous and must only be carried out with suitable equipment and under appropriate safety precautions!

4.2.6.1. Typ I (glass autoclave, 50 mL)

This commercial available autoclave (BÜCHI MiniClave) contains a thick-walled 50 mL glass flask surrounded by a stainless steel net container. It is topped with a screw-type cap in which a teflon cap inlet is placed containing a manometer, a security valve, a gas-inlet valve and an opening inlet. The screw-type cap is connected to a glass flask in the safety container. The maximum operating pressure is 6 bar (150 °C) and 10 bar (100 °C). For heating and stirring a conventional magnet stirring plate and an oil bath is used.

4.2.6.2. Typ II (autoclave, 36 mL)

This 36 mL high pressure stainless steel autoclave is cylindric. The autoclave is equipped with manometer, a valve gas-inlet and an opening inlet, it contains a glass insert and a thin teflon cap to prevent contact between the steel and the reaction mixture. For heating and stirring a conventional magnet heating agitator is used, the thermocouple of the heating agitator is connected with a metal block, where the autoclave is inserted for heating. For *Typ II* the maximum operating pressure is 200 bar (120 °C).

4.3. Synthetic Procedures

4.3.1. Literature Compounds

The following substances are literature known and were synthesised and purified according to literature procedures and the analyses are in agreement to published data.

Phosphine Ligands and precursors:

2,6-Bis-[(di-tert-butyl-phosphanyl)-methyl]-pyridine (*dtbpmp*) **15** [41]
$C_{23}H_{43}NP_2$. Mol. Wt.: 395.54 g mol^{-1}. Colourless solid. Yield: 3 g (60%)

2,2´-Bis-(Di-tert-butyl-phosphanyl)-diethylether (*dtbpoet*) **49** [119]
$C_{20}H_{44}OP_2$. Mol. Wt.: 362.51 g mol^{-1}. Colourless waxy-solid. Yield: 1.7 g (40%)

Di(tert.-butyl)chlorophosphine **118** [120]
$C_8H_{18}ClP$. Mol. Wt.: 180.66 g mol^{-1}. Colourless liquid. Yield: 12.55 g (85%).

Dicyclohexyl-phosphane borane complex **119** [121]
$C_{12}H_{26}BP$. Mol. Wt.: 212.12 g mol^{-1}. Colourless solid. Yield: 1.9 g (90%).

Metal Complexes:

[Bis-(2-methylallyl)cycloocta-1,5-diene]ruthenium(II) **6** [122]
$C_{16}H_{26}Ru$. Mol. Wt.: 319.45 g mol^{-1}. Brown solid. Yield: 2.97 g (65%)

Dichloro(cycloocta-1,5-dienyl)ruthenium(II) polymer **120** [123]
$C_8H_{12}Cl_2Ru$. (monomer). Mol. Wt.: 280.16 g mol^{-1}. Brown solid. Yield: 29.0g (98%)

4.3.2. Chelating Diphosphine Nitrogen Ligands (PNP-pincer)

{2,6-Bis-[(dicyclohexylphosphanyl)-methyl]-pyridine} bis-borane complex 121[121] (BH$_3$-*dcypmp*) BH$_3$-46

Dicyclohexylphosphine-BH$_3$ **119** (1.5 g; 7 mmol) was placed into a Schlenk flask, then 25 mL THF was added. The solution was cooled to −78 °C, and *n*-butyllithium (4.51 mL of a 1.6 M solution in hexane; 7.2 mmol; 1.03 eq.) was added dropwise *via* a syringe over a period of 10 min. The colourless reaction mixture was stirred for 2 h and the solution was warmed to room temperature. After the solution had been cooled to −78 °C again, bis(chloromethyl)pyridine (0.616 g; 3.5 mmol) in THF (5 mL) was slowly added *via* a syringe. The reaction mixture was kept for 2 h at −78 °C and then stirred at room temperature overnight. Evaporation of the solvent gave a white solid which was washed with pentane (5 mL) and filtered off. The filter cake was extracted with benzene (12 mL) and the benzene extract was evaporated to yield the product as a colourless solid.

$C_{31}H_{57}B_2NP_2$. Mol. Wt.: 527.36 g mol^{-1}. Colourless solid. Yield: 1.6 g (87%).
^{1}H-NMR (300.1 MHz, d$_6$-benzene): δ = 0.7-1.7 (m, 44 H, Cy), 2.8 (d, 4 H, $^2J_{PH}$ = 11.1 Hz, PCH$_2$), 6.8 (m, 3 H, py).

^{13}C-{^{1}H}-NMR (75.2 MHz, d$_6$-benzene): δ = 26.5 (C4 of Cy), 27.0-27.6 (m, C2,6 and C3,5 of Cy), 31.0 (d, $^1J_{PC}$ = 25.6 Hz, C1 of Cy), 32.4 (d, $^1J_{PC}$ = 30.2 Hz, PCH$_2$), 123.4 (C3,5 of py), 136.8 (C4 of py), 155.2 (d, $^1J_{PC}$ = 6 Hz, C2,6 of py).

^{31}P-NMR (121.5 MHz, d$_6$-benzene): δ = 30 (ψ-d, $^1J_{PB}$ = 42.6 Hz), ^{11}B-NMR (96.3 MHz, d$_6$-benzene): δ = −42 (br-s).

EI-MS [%]: 527 (2) [M$^+$], 512 (18) [M$^+$-BH$_3$], 315 (100), 302 (18), 233 (30), 150 (36).
HR-ESI(+)-MS [%]: *BH$_3$*-46-Na-adduct = 550.4041 (found), 550.4045 (calcd).

Note: The single-crystal X-ray diffraction structure data of this new compound will be published separately soon.

2,6-Bis-[(dicyclohexylphosphanyl)-methyl]-pyridine (*dcypmp*) 46

The *dcypmp*-BH_3 **121** (209 mg; 0.4 mmol) and an excess of DABCO (267 mg; 2.38 mmol) was placed into a Schlenk flask and followed by the addition of 2 mL toluene was added. The reaction mixture was stirred for 3 h at 80 °C and then cooled to room temperature. Evaporation of the solvent gave a residue which was extracted with 5 mL *n*-pentane and filtered. Then the extract was evaporated to dryness and the residue was washed with methanol (3x 1.5 mL) and dried in vacuo.

$C_{31}H_{51}NP_2$. Mol. Wt.: 499.69 g mol^{-1}. Colourless solid. Yield: 0.14 g (70%).

^{1}H-NMR (300.1 MHz, d_6-benzene): δ = 0.9-1.7 (m, 44 H, Cy), 2.8 (d, 4 H, $^2J_{PH}$ = 1.1 Hz, PCH_2), 6.8 (m, 3 H, py).

^{31}P-NMR (121.5 MHz, d_6-benzene): δ [ppm] = 3.3 (s), The analytical data comply with the data published by Katayama et. al.[124]

4.3.3. Ruthenium Dihydrogen Complexes

4.3.3.1. Preparation of [Ru(*dtbpmp*)H_2(H_2)] 4

Dihydrogendihydrido{2,6-bis-[(di-tert-butyl-phosphanyl)-methyl]-pyridine}ruthenium(II)

An argon flushed *Büchi glass-autoclave*, equipped with a stirring bar, was filled with [Ru(cod)(metallyl)$_2$] **6** (281 mg, 0.88 mmol; 1 eq.), *dtbpmp* **15** (364 mg, 0.92 mmol; 1.05 eq.) and 12 mL degassed *n*-pentane. The autoclave was flushed with 2 bar hydrogen gas at room temperature, then the temperature was increased to 55 °C (oil bath) and the H_2-pressure was stabilised at 7 bar. The reaction was stirred for 18 h (or two days), cooled down to room temperature and the H_2-pressure was decreased to 1 bar. The red solution was filtered through canula under an H_2-stream and the remaining solid was washed under a H_2-stream with *n*-

pentane to give a yellow-brown solid.* The product was transferred into a dry schlenk-tube using a glove box and further dried under a H_2-stream. Finally it was stored under argon or 1 bar hydrogen in a sealed schlenk-tube at −20 °C.

Yield: 323 mg (74%)

^{1}H-NMR (300 MHz, C_6D_6, 25 °C): δ = 6.8 (t, 1 H, ^3J(H,H) = 7.7 Hz, pyridine-H4), 6.6 (d, 2 H, ^3J(H,H) = 7.9 Hz, pyridine-H3,5), 3.1 (vt, 4 H, ^2J(H,P) = 3.2 Hz, CH_2P), 1.3 (vt, 36 H, ^3J(H,P) = 6.1 Hz, PC(CH_3)$_3$), −7.3 (t, 4 H, ^2J(H,P) = 13.2 Hz, Ru-*H*, Ru-H_2).

^{13}C-NMR (75 MHz, C_6D_6, 25 °C): δ = 164 (dvt, ^2J(C,P) = 4.8 Hz, pyridine-C2,6), 133 (s, pyridine-C4), 118 (m, pyridine-C3,5), 41 (dvt, ^1J(C,P) = 4.9 Hz, P*C*(CH$_3$)$_3$), 34 (dvt, ^1J(C,P) = 6.7 Hz, *C*H$_2$P), 30 (vt, ^2J(C,P) = 3.4 Hz, PC(*C*H$_3$)$_3$).

^{31}P-NMR (122 MHz, C_6D_6, 25°C): δ = 109.5 (s).

IR (KBr) $\tilde{\upsilon}$ = 3074 (w, ν CH$_{ar}$), 3041 (w, ν CH$_{ar}$), 3018 (w, ν CH$_{ar}$), 2983 (w, ν CH$_2$), 2940 (s, ν CH$_2$), 2893 (s, ν CH$_2$), 2862 (s, ν CH$_2$), 2095 (w, ν Ru-H$_2$), 1990-1700 (m, ν Ru-H), 1592 (m, ν C=N), 1562 (m, ν C=C), 1459 (s, δ CH$_2$), 1382 (s, δ t-Bu), 1363 (s, δ t-Bu), 1180 (m, ν C-P), 833 cm^{-1} (s, δ, CH$_{ar}$).

Detection of T_1(min) of the hydride signal: (400 MHz, [D$_8$]toluene, 25 °C): δ = −7.3 (t, 4 H, ^2J(H,P) = 13.2 Hz). T_1(min) = 77 ms (θ_{min} = 228 K), r(H-H) = 111 pm.

Elemental analysis calcd (%) for $C_{23}H_{47}NP_2Ru$ (500.7): C 55.18; H 9.46; N 2.80; P 12.37; Ru 20.19. Exp.: C 54.11; H 9.22; N 2.64; P 11.81; Ru 19.82. Found atom ratio number by *CHN:* $C_{23}H_{46.7}N_{1.0}P_{2.0}Ru_{1.0}$.

A sealed NMR-sample was used for long term-stability test and it was measured after three days, three weeks and 3.5 months. The NMR-data are comparable to **4** and **[D$_x$]-4** respectively due to H/D-scrambling.

* Alternatively the mixture can be filtered in the glovebox with a glass filter and a syringe.

Table 8: Detection of T_1(min) of the hydride signal (δ = –7.3 ppm, 400.1 MHz, [D_8]toluene).

T [K] (Δ2K)	T_1 [ms] (Δ3ms)
300	209
283	151
263	104
243	86
223	73
193	109

T_1(min) = 77 ms;

θ_{min}: 228±2 K (≈ –45 °C)

r_{HH} = 111 pm

4.3.3.2. Preparation of the complex [D_x]-[Ru(*dtbpmp*)H_2(H_2)] [D_x]-4

Prepared as **4** by the use of deuterium gas. Yellow-brown solid. Yield: 118 mg (54%).

^{1}H-NMR (300 MHz, C_6D_6, 25 °C): δ = 6.8 (t, 0.1 H, ^3J(H,H) = 7.7 Hz, pyridine-H4), 6.6 (d, 2 H, ^3J(H,H) = 7.9 Hz, pyridine-H3,5), 3.1 (vt, 3 H, ^2J(P,H) = 3.2 Hz, CH_2P), 1.3 (vt, 36 H, ^3J(P,H) = 6.1 Hz, PC(CH_3)$_3$), –7.3 (t, 4 H, ^3J(H,H) = 13.2 Hz, Ru-*H*, Ru-H_2).

^{2}H-NMR (600 MHz, C_6D_6, 25 °C): δ = 6.8 (s, weak, pyridine-D4), 6.6 (s, weak, pyridine-D3,5), 3.1 (s, CD_2P), 1.3 (s, PC(CD_3)$_3$), –7.3 (s, Ru-*D*, Ru-D_2).

^{13}C-NMR (75 MHz, C_6D_6, 25 °C): δ = 133 (s, pyridine-C4), 164 (pyridine-C2,6), 118 (m, pyridine-C3,5), 41 (P*C*(CH$_3$)$_3$), 33 (*C*H$_2$P), 30 (PC(*C*H$_3$)$_3$).

^{31}P-NMR (122 MHz, C_6D_6, 25 °C): δ = 109.1 (s).

IR (KBr) $\tilde{\upsilon}$ = 3012 (w, ν CH_{ar}), 2983 (s, ν CH_2), 2946 (s, ν CH_2), 2900 (s, ν CH_2), 2863 (s, ν CH_2), 2247 (w, ν CD_{ar}), 2199 (w, ν CD_{ar}), 2151 (w, ν CD_{ar}), 2094 (w, ν Ru-H_2), 2000-1700 (m, ν Ru-H), 1582 (m, ν C=N), 1546 (m, ν C=C), 1458 (s, δ CH_2), 1362 (s, δ t-Bu), 707 (s, δ CH_{ar}).

4.3.3.3. Reaction of [Ru(*dtbpmp*)H_2(H_2)] 4 with C_6D_6 to highly deuterated [D_x]-4

A *Young Teflon capped NMR tube* was filled with ruthenium complex **4** (20 mg, 39.9 µmol) and 0.5 mL C_6D_6 was added. The red solution was stirred at 50 °C for 2 days, cooled to r. t. and the ^{1}H-NMR, ^{31}P-NMR and ^{2}H-NMR spectra were measured manually locked on C_6D_6. Deuteration-degree: >90%.

^{1}H-NMR (300 MHz, C_6D_6, 25 °C): δ = 6.8 (residue, pyridine-H4), 6.6 (residue, pyridine-H3,5), 3.1 (residue, C*H*$_2$P), 1.3 (residue, PC(C*H*$_3$)$_3$), -7.3 (residue, Ru-*H*, Ru-*H*$_2$).

^{2}H-NMR (600 MHz, C_6D_6, 25 °C): δ = 6.8 (s, pyridine-D4), 6.6 (s, pyridine-D3,5), 3.1 (s, C*D*$_2$P), 1.3 (s, PC(C*D*$_3$)$_3$), −7.3 (s, Ru-*D*, Ru-*D*$_2$).

^{31}P-NMR (122 MHz, C_6D_6, 25 °C): δ = 108.1(s).

4.3.3.4. Reaction of [Ru(*dtbpmp*)H_2(H_2)] 4 with D_2O in C_6D_{12} to [D_6]-4 / 26

A *Young Teflon capped NMR tube* was filled with ruthenium complex 4 (10 mg, 20.0 µmol), 0.6 mL C_6D_{12} and 0.05 mL D_2O were added. The sample was shaken for a few minutes, and then ^{1}H-NMR and ^{2}H-NMR were measured immediately.

^{1}H-NMR (600 MHz, C_6D_{12}, 25 °C): δ = 6.8 (vt, 0.9 H, 10% D, pyridine-H4), 6.6 (d, 2 H, pyridine-H3,5), 3.1 (0.7 H, 83% D, C*H*$_2$P), 1.3 (36 H, PC(C*H*$_3$)$_3$), -7.3 (1.8 H, 55% D, Ru-*H*, Ru-*H*$_2$).

^{2}H-NMR (600 MHz, C_6D_{12}, 25 °C): δ = 7.3 (s, 0.4 D, pyridine-D4), 3.3 (s, 3.2 D, 80D[%], C*D*$_2$P), −7.7 (s, 2.2 D, 55D[%],Ru-*D*, Ru-*D*$_2$).

^{31}P-NMR (122 MHz, C_6D_{12}, 25 °C): δ = 111.9 (s).

4.3.3.5. Reaction of [Ru(*dtbpmp*)H_2(H_2)] 4 with N_2 to [Ru(*dtbpmp*)H_2(N_2)] 20

Dinitrogendihydrido{2,6-bis-[(di-tert-butyl-phosphanyl)-methyl]-pyridine}ruthenium(II)

A *Young-Teflon-Capped NMR-tube* containing a dark red [D_8]toluene (0.6 mL) solution of **4** (20 mg, 39.9 µmol) was slowly bubbled with N_2 at room temperature. ^{1}H- and ^{31}P-NMR were measured after 90 min (red solution) and 20 h (black mixture). Then the black mixture was bubbled with H_2 for one day and it returned to a red solution anew. ^{1}H- and ^{31}P-NMR were recorded again. Additionally, after two weeks ^{2}H-NMR were recorded. Conversion: 66% (^{31}P-NMR after 90 min).

^{1}H-NMR (300 MHz, [D_8]toluene, 25 °C): δ = −4.6 (t, ^2J(H,P) = 16.8 Hz), −12.8 (weak, broad);

^{31}P-NMR (122 MHz, [D_8]toluene, 25°C): δ = 99.6 (s, broad).

^{2}H-NMR (600.2 MHz, [D_8]toluene, 25 °C): δ = -7.4 (s, Ru-*D*, Ru-D_2), 1.3 (s, PC(CD_3)$_3$), 3.1 (s, CD_2P), 6.6 (no detection, pyridine-D3,5), 6.9 (s, weak, pyridine-D4). For further details see chapter 2.1.3.

Table 9: NMR-data of the equilibrium between **4** and **20**.

	t_0 (exclusive presence of 4)	**90 min in N_2-atmosphere (Formation of 20)**	**20 h in N_2-atmosphere (Formation of Ru-clusters)**	**1 d in H_2-atmosphere (Reformation of 4)**
^{1}H-NMR (300 MHz, [D_8]toluene, 25°C): δ =	−7.3	−7.3. −4.6 (weak, t, ^2J(H,P) = 16.81 Hz) −12.8 (weak, broad)	−7.3 (residue) −4.6 (increased, t, ^2J(H,P) = 16.81 Hz)) −12.8 (weak, broad)	−7.3
^{31}P-NMR (122 MHz, [D_8]toluene, 25°C): δ =	109.6	109.6 (33%), 99.6 (66%)	109.6 (6%) 99.6 (32%) 81-74 (35%) 70-65 (27%)	109.6

4.3.3.6. Reaction of [Ru(*dtbpmp*)$H_2(H_2)$] 4 with carbon monoxide and hydrogen gas to [Ru(*dtbpmp*)(CO)H] 28

An autoclave with glass-inlet containing a dark red [D_8]toluene (1.0 mL) solution of **4** (17 mg, 34.0 µmol) was flushed with carbon monoxide and stirred for 30 minutes. The yellow solution was transferred via syringe into a septum capped NMR tube and analysed immediately by NMR and again after five days. After a treatment with a hydrogen-stream for 20 minutes, the sample was analysed again by NMR.

Data of [Ru(*dtbpmp*)(CO)] **27**: Conversion: 88% of **27** is formed (^{31}P-NMR).

^{1}H-NMR (400 MHz, [D_8]toluene, 25 °C): δ = 6.6 (t, 1 H, ^3J(H,H) = 7.1 Hz, pyridine-H4), 6.6 (d, 2 H, ^3J(H,H) = 7.8 Hz, pyridine-H3,5), 3.0 (vs, 4 H, CH_2P), 1.3 (vt, 36 H, ^3J(H,P) = 5.7 Hz, PC(CH_3)$_3$).

^{31}P-NMR (161 MHz, [D_8]toluene, 25°C): δ = 99.6 (s, 88%), 90 (5%), 88 (4%), 70 (3%).

Data of [Ru(*dtbpmp*)(CO)H] **28**: Conversion: > 90% of **28** is formed (^{31}P-NMR).

^{1}H-NMR (400 MHz, [D_8]toluene, 25 °C): δ = 6.4 (vt, 1 H, ^3J(H,H) = 7.8 Hz, pyridine-H4), 6.2 (vd, 1 H, ^3J(H,H) = 7.7 Hz, pyridine-H3/5), 5.4 (vd, 1 H, ^3J(H,H) = 5.7 Hz, pyridine-H3/5), 3.6 (vs, 1 H, *H*C=P), 2.8 (vd, 2 H, ^3J(H,H) = 4.7 Hz, CH_2P), 1.4 (vt, 18 H, ^3J(H,P) = 10.8 Hz, PC(CH_3)$_3$), 1.1 (vt, 18 H, ^3J(H,P) = 9.5 Hz, PC(CH_3)$_3$), -6.0 (t, 1 H, ^2J(P,H) = 18.2 Hz, Ru-*H*),

^{31}P-NMR (161 MHz, [D_8]toluene, 25°C): δ = 90.0 (d, ^2J(P,P) = 30.3 Hz) 88 (6%), 70 (2%).

4.3.3.7. Reaction of [Ru(*dtbpmp*)$H_2(H_2)$] 4 with pinacolborane

To a septum capped NMR tube containing a dark red [D_6]benzene (0.7 mL) solution of **4** (10 mg, 20.0 µmol) pinacolborane **34** (9 µL, 3 eq.) was added via syringe. After the addition the colour changed to yellow and gas evolution was observed. The sample was analysed immediately by NMR and after one day again.

Data of [Ru(*dtbpmp*)H_3(BPin)] **35**: Conversion: 94% of **4** is converted into **35** (^{31}P-NMR); After a few minutes:

^{1}H-NMR (400 MHz, C_6D_6, 25 °C): δ = 6.7 (vt, 1 H, ^{3}J(H,H) = 7.5 Hz, pyridine-H4), 6.5 (vd, 2 H, ^{3}J(H,H) = 7.3 Hz, pyridine-H3,5), 3.2 (vq, 4 H, ^{3}J(H,H) = 10.9 Hz, ^{3}J(H,H) = 16.3 Hz, CH_2P), 1.5 (vt, 18 H, ^{3}J(H,P) = 6.0 Hz, PC(CH_3)$_3$), 1.4 (vt, 18 H, ^{3}J(H,P) = 6.1 Hz, PC(CH_3)$_3$), 1.27 (s, 12 H, OC(CH_3)$_2$), -5.0 (br s, 1 H, Ru-*H*), -11.7 (s, 2 H, Ru-H_2). Free boranes: 1.0-0.95 ((BPin)$_2$ / HBPin).

^{13}C-NMR (100 MHz, C_6D_6, 25 °C): δ = 164.4 (pyridine-C2,6), 133.3 (pyridine-C4), 118.2 (pyridine-C3,5), 81.2 (*C*O, BPin), 40.8 (P*C*(CH$_3$)$_3$), 34.5 (*C*H$_2$P), 30.5 (PC(*C*H$_3$)$_3$), 24.9 (CH$_3$, BPin); ^{31}P-NMR (161 MHz, C_6D_6, 25°C): δ = 96.9 (s, 94%).

^{11}B-NMR (128 MHz, C_6D_6, 25 °C): δ = 22.7 (s). Other compounds: ^{1}H-NMR (400 MHz, C_6D_6, 25 °C): δ = 1.0 (s, (BPin)$_2$), 0.97 (s, HBPin).

^{31}P-NMR (161 MHz, C_6D_6, 25°C): δ = 110 (3%), 96 (3%), (unidentified compounds). ^{11}B-NMR (128 MHz, C_6D_6, 25 °C): Free boranes: δ = 38.7 (s, (BPin)$_2$), 29.3 (d, ^{1}J(B,H) = 174.4 Hz, HBPin).

Procedure for the catalytic hydroboration with olefins and pinacolborane 34

To a schlenk-flask with [Ru(dtbpmp)H_2(H_2)] **4** (0.05 mmol, 1 mol%) the substrates 1-octene **38** (4.9 mmol) and pinacolborane **34** (5.0 mmol) were added via syringe. The red mixture was stirred for 18 h at room temperature. An aliquot was analyzed by GC and GC-MS. Conversion: 75%. Selectivity: 96% 1-octylboronate **39** and traces of 2-octylboronate **40** and alkyldiboronates).

GC-MS (70 eV, EI): m/z [%] = 240 (1) [M$^+$], 225 (71), 183 (7), 154 (14), 140 (14), 129 (100), 111 (20), 97 (55), 85 (98), 69 (45), 57 (52), 43 (71).

4.3.3.8. Solid State Structure: Reaction with CO_2

A suitable crystal of [RuH(*dtbpmp*)(HCO_2)CO] **41** for single-crystal x-ray diffraction was obtained by storage under argon of a [D_8]toluene solution of [Ru(*dtbpmp*)H_2(H_2)] **4** in a septum-sealed NMR-tube over dry-ice for several weeks. [RuH(*dtbpmp*)(HCO_2)CO] **41** was formed by diffusion of CO_2 into the solution.

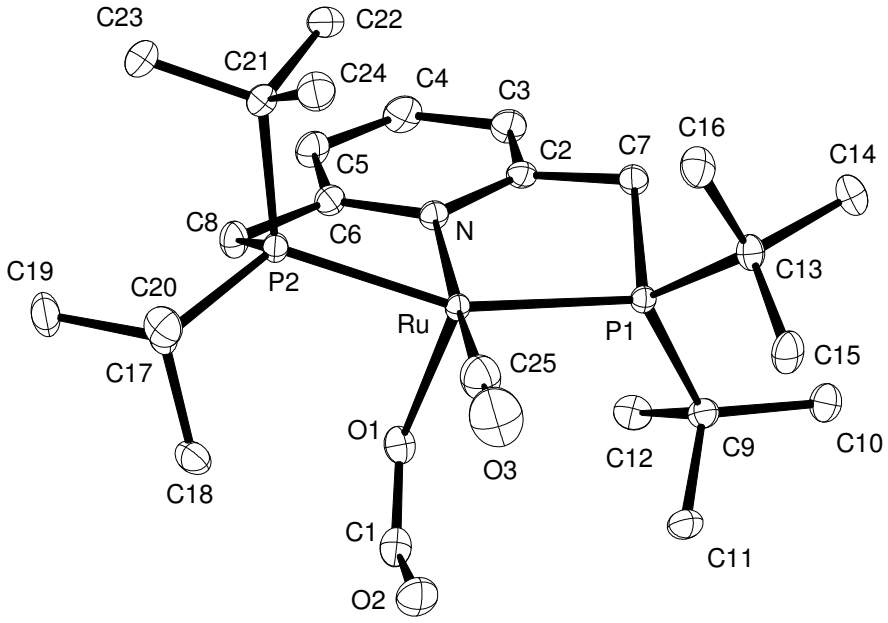

Figure 45: ORTEP diagram of [RuH(*dtbpmp*)(HCO_2)CO] **41** with thermal ellipsoids set at 50% probability.

Table 10: Crystal data and structure refinement.

Identification code	5753	
Empirical formula	$C_{25}H_{45}NO_3P_2Ru$	
Color	colourless	
Formula weight	570.63 g · mol^{-1}	
Temperature	100 K	
Wavelength	0.71073 Å	
Crystal system	Monoclinic	
Space group	**$P2_1/c$, (no. 14)**	
Unit cell dimensions	a = 14.3177(3) Å	α= 90.0°
	b = 12.0309(2) Å	β= 91.817(1)°
	c = 16.1548(3) Å	γ = 90.0°

Volume	2781.34(9) $Å^3$	
Z	4	
Density (calculated)	1.363 $Mg \cdot m^{-3}$	
Absorption coefficient	0.704 mm^{-1}	
F(000)	1200 e	
Crystal size	0.12 x 0.10 x 0.016 mm^3	
θ range for data collection	2.94 to 31.52°.	
Index ranges	$-21 \le h \le 21$, $-17 \le k \le 17$, $-23 \le l \le 23$	
Reflections collected	60938	
Independent reflections	9262 [R_{int} = 0.0357]	
Reflections with I>2σ(I)	8403	
Completeness to θ = 31.52°	99.9%	
Absorption correction	Gaussian	
Max. and min. transmission	0.98905 and 0.91786	
Refinement method	Full-matrix least-squares on F^2	
Data / restraints / parameters	9262 / 0 / 297	
Goodness-of-fit on F^2	1.070	
Final R indices [I>2σ(I)]	R_1 = 0.0248	wR^2 = 0.0630
R indices (all data)	R_1 = 0.0301	wR^2 = 0.0653
Largest diff. peak and hole	1.062 and -0.941 e $\cdot Å^{-3}$	

Table 11: Atomic coordinates and equivalent isotropic displacement parameters ($Å^2$).

U_{eq} is defined as one third of the trace of the orthogonalized U_{ij} tensor.

	x	y	z	U_{eq}
C(1)	0.0676(1)	0.6287(1)	0.2251(1)	0.020(1)
C(2)	0.1776(1)	0.6205(1)	0.5175(1)	0.013(1)
C(3)	0.1265(1)	0.5876(1)	0.5852(1)	0.018(1)
C(4)	0.0882(1)	0.4817(1)	0.5864(1)	0.019(1)
C(5)	0.1034(1)	0.4108(1)	0.5207(1)	0.018(1)
C(6)	0.1523(1)	0.4485(1)	0.4533(1)	0.014(1)
C(7)	0.2278(1)	0.7304(1)	0.5170(1)	0.014(1)
C(8)	0.1699(1)	0.3740(1)	0.3807(1)	0.016(1)
C(9)	0.1330(1)	0.8732(1)	0.3932(1)	0.014(1)
C(10)	0.1294(1)	0.9836(1)	0.4408(1)	0.021(1)
C(11)	0.1208(1)	0.8950(1)	0.2997(1)	0.019(1)
C(12)	0.0505(1)	0.8017(1)	0.4213(1)	0.018(1)
C(13)	0.3472(1)	0.8733(1)	0.4192(1)	0.015(1)
C(14)	0.3500(1)	0.9478(1)	0.4969(1)	0.021(1)
C(15)	0.3538(1)	0.9443(1)	0.3407(1)	0.021(1)
C(16)	0.4345(1)	0.7989(1)	0.4250(1)	0.021(1)
C(17)	0.2603(1)	0.3479(1)	0.2225(1)	0.016(1)
C(18)	0.1887(1)	0.4145(1)	0.1703(1)	0.020(1)
C(19)	0.2243(1)	0.2275(1)	0.2281(1)	0.025(1)
C(20)	0.3528(1)	0.3501(1)	0.1769(1)	0.022(1)
C(21)	0.3774(1)	0.3631(1)	0.3863(1)	0.018(1)
C(22)	0.3674(1)	0.3941(1)	0.4782(1)	0.022(1)
C(23)	0.3853(1)	0.2360(1)	0.3814(1)	0.026(1)
C(24)	0.4683(1)	0.4164(1)	0.3565(1)	0.023(1)
C(25)	0.3131(1)	0.6629(2)	0.2515(1)	0.028(1)
N	0.1871(1)	0.5533(1)	0.4509(1)	0.012(1)
O(1)	0.1018(1)	0.5981(1)	0.2938(1)	0.017(1)
O(2)	0.1077(1)	0.6688(1)	0.1653(1)	0.026(1)
O(3)	0.3571(1)	0.6945(1)	0.1963(1)	0.044(1)
P(1)	0.2396(1)	0.7828(1)	0.4104(1)	0.011(1)
P(2)	0.2736(1)	0.4219(1)	0.3252(1)	0.012(1)
Ru	0.2504(1)	0.6125(1)	0.3419(1)	0.010(1)

Table 12: Bond lengths [Å] and angles [°].

C(1)-O(2)	1.2364(19)	C(1)-O(1)	1.2539(19)
C(1)-H(1)	1.048(19)	C(2)-N	1.3554(17)
C(2)-C(3)	1.3926(19)	C(2)-C(7)	1.5046(19)
C(3)-C(4)	1.387(2)	C(4)-C(5)	1.384(2)
C(5)-C(6)	1.3893(19)	C(6)-N	1.3571(17)
C(6)-C(8)	1.5049(19)	C(7)-P(1)	1.8460(13)
C(8)-P(2)	1.8502(14)	C(9)-C(10)	1.535(2)
C(9)-C(11)	1.538(2)	C(9)-C(12)	1.542(2)
C(9)-P(1)	1.8874(14)	C(13)-C(15)	1.534(2)
C(13)-C(16)	1.538(2)	C(13)-C(14)	1.542(2)
C(13)-P(1)	1.8886(14)	C(17)-C(18)	1.533(2)
C(17)-C(20)	1.536(2)	C(17)-C(19)	1.541(2)
C(17)-P(2)	1.8868(14)	C(21)-C(23)	1.536(2)
C(21)-C(24)	1.540(2)	C(21)-C(22)	1.542(2)
C(21)-P(2)	1.8950(15)	C(25)-O(3)	1.171(2)
C(25)-Ru	1.8413(18)	N-Ru	2.1286(11)
O(1)-Ru	2.2487(11)	P(1)-Ru	2.3366(4)
P(2)-Ru	2.3334(4)	Ru-H	1.40(2)

O(2)-C(1)-O(1)	128.90(15)	O(2)-C(1)-H(1)	117.4(11)
O(1)-C(1)-H(1)	113.6(11)	N-C(2)-C(3)	121.45(13)
N-C(2)-C(7)	117.35(12)	C(3)-C(2)-C(7)	121.15(12)
C(4)-C(3)-C(2)	119.36(13)	C(5)-C(4)-C(3)	118.88(13)
C(4)-C(5)-C(6)	119.68(13)	N-C(6)-C(5)	121.36(13)
N-C(6)-C(8)	117.42(12)	C(5)-C(6)-C(8)	121.21(13)
C(2)-C(7)-P(1)	111.31(9)	C(6)-C(8)-P(2)	110.43(10)
C(10)-C(9)-C(11)	109.87(12)	C(10)-C(9)-C(12)	107.31(12)
C(11)-C(9)-C(12)	108.67(12)	C(10)-C(9)-P(1)	117.67(10)
C(11)-C(9)-P(1)	107.97(9)	C(12)-C(9)-P(1)	104.97(9)
C(15)-C(13)-C(16)	107.63(12)	C(15)-C(13)-C(14)	110.41(12)
C(16)-C(13)-C(14)	106.76(12)	C(15)-C(13)-P(1)	109.28(10)
C(16)-C(13)-P(1)	109.21(10)	C(14)-C(13)-P(1)	113.37(10)
C(18)-C(17)-C(20)	107.41(12)	C(18)-C(17)-C(19)	107.73(13)
C(20)-C(17)-C(19)	109.82(13)	C(18)-C(17)-P(2)	106.53(10)
C(20)-C(17)-P(2)	110.41(10)	C(19)-C(17)-P(2)	114.61(10)
C(23)-C(21)-C(24)	109.49(13)	C(23)-C(21)-C(22)	107.48(13)
C(24)-C(21)-C(22)	107.75(13)	C(23)-C(21)-P(2)	113.74(11)

C(24)-C(21)-P(2)	109.77(10)	C(22)-C(21)-P(2)	108.43(10)
O(3)-C(25)-Ru	176.56(18)	C(2)-N-C(6)	119.04(11)
C(2)-N-Ru	120.87(9)	C(6)-N-Ru	120.05(9)
C(1)-O(1)-Ru	128.44(10)	C(7)-P(1)-C(9)	103.72(6)
C(7)-P(1)-C(13)	103.03(6)	C(9)-P(1)-C(13)	109.44(6)
C(7)-P(1)-Ru	98.70(4)	C(9)-P(1)-Ru	120.09(5)
C(13)-P(1)-Ru	118.35(5)	C(8)-P(2)-C(17)	102.62(6)
C(8)-P(2)-C(21)	105.02(7)	C(17)-P(2)-C(21)	109.74(7)
C(8)-P(2)-Ru	97.52(5)	C(17)-P(2)-Ru	123.69(5)
C(21)-P(2)-Ru	114.74(5)	C(25)-Ru-N	176.01(7)
C(25)-Ru-O(1)	103.32(7)	N-Ru-O(1)	80.65(4)
C(25)-Ru-P(2)	99.05(6)	N-Ru-P(2)	80.40(3)
O(1)-Ru-P(2)	91.18(3)	C(25)-Ru-P(1)	97.35(6)
N-Ru-P(1)	82.24(3)	O(1)-Ru-P(1)	98.92(3)
P(2)-Ru-P(1)	158.197(13)	C(25)-Ru-H	83.5(10)
N-Ru-H	92.5(10)	O(1)-Ru-H	173.1(10)
P(2)-Ru-H	87.1(9)	P(1)-Ru-H	80.6(9)

Table 13: Anisotropic displacement parameters ($Å^2$)**.**

The anisotropic displacement factor exponent takes the form:

$-2\pi^2[h^2 a^{*2}U_{11} + ... + 2 h k a^* b^* U_{12}]$.

	U_{11}	U_{22}	U_{33}	U_{23}	U_{13}	U_{12}
C(1)	0.021(1)	0.015(1)	0.023(1)	-0.002(1)	0.002(1)	-0.001(1)
C(2)	0.016(1)	0.014(1)	0.010(1)	0.001(1)	0.000(1)	0.001(1)
C(3)	0.023(1)	0.019(1)	0.011(1)	0.002(1)	0.004(1)	0.000(1)
C(4)	0.023(1)	0.021(1)	0.015(1)	0.005(1)	0.006(1)	-0.002(1)
C(5)	0.020(1)	0.015(1)	0.017(1)	0.004(1)	0.004(1)	-0.003(1)
C(6)	0.016(1)	0.013(1)	0.013(1)	0.002(1)	0.001(1)	-0.002(1)
C(7)	0.018(1)	0.013(1)	0.010(1)	0.000(1)	0.001(1)	-0.002(1)
C(8)	0.020(1)	0.013(1)	0.016(1)	0.000(1)	0.004(1)	-0.004(1)
C(9)	0.015(1)	0.015(1)	0.013(1)	0.000(1)	0.001(1)	0.002(1)
C(10)	0.023(1)	0.016(1)	0.022(1)	-0.005(1)	0.001(1)	0.005(1)
C(11)	0.023(1)	0.018(1)	0.014(1)	0.003(1)	-0.002(1)	0.003(1)
C(12)	0.014(1)	0.023(1)	0.018(1)	0.000(1)	0.002(1)	0.001(1)
C(13)	0.016(1)	0.013(1)	0.017(1)	-0.002(1)	0.003(1)	-0.003(1)
C(14)	0.022(1)	0.020(1)	0.021(1)	-0.005(1)	0.000(1)	-0.005(1)
C(15)	0.026(1)	0.015(1)	0.021(1)	0.001(1)	0.007(1)	-0.005(1)
C(16)	0.015(1)	0.020(1)	0.029(1)	-0.002(1)	0.001(1)	-0.002(1)

C(17)	0.018(1)	0.014(1)	0.015(1)	-0.003(1)	0.001(1)	-0.001(1)
C(18)	0.021(1)	0.023(1)	0.015(1)	-0.004(1)	-0.002(1)	0.001(1)
C(19)	0.035(1)	0.016(1)	0.023(1)	-0.005(1)	0.000(1)	-0.006(1)
C(20)	0.022(1)	0.024(1)	0.019(1)	-0.004(1)	0.005(1)	0.002(1)
C(21)	0.020(1)	0.014(1)	0.020(1)	-0.001(1)	-0.003(1)	0.003(1)
C(22)	0.026(1)	0.020(1)	0.018(1)	0.000(1)	-0.006(1)	0.004(1)
C(23)	0.034(1)	0.015(1)	0.028(1)	0.000(1)	-0.007(1)	0.005(1)
C(24)	0.017(1)	0.023(1)	0.029(1)	-0.003(1)	-0.002(1)	0.003(1)
C(25)	0.032(1)	0.026(1)	0.026(1)	-0.002(1)	0.003(1)	-0.002(1)
N	0.014(1)	0.012(1)	0.011(1)	0.001(1)	0.002(1)	-0.001(1)
O(1)	0.015(1)	0.016(1)	0.019(1)	-0.002(1)	0.004(1)	-0.002(1)
O(2)	0.035(1)	0.024(1)	0.018(1)	0.005(1)	0.002(1)	-0.001(1)
O(3)	0.053(1)	0.047(1)	0.034(1)	0.001(1)	0.014(1)	-0.011(1)
P(1)	0.013(1)	0.010(1)	0.010(1)	0.000(1)	0.001(1)	0.000(1)
P(2)	0.014(1)	0.010(1)	0.012(1)	-0.001(1)	0.001(1)	-0.001(1)
Ru	0.012(1)	0.009(1)	0.009(1)	0.000(1)	0.002(1)	-0.001(1)

4.3.3.9. Preparation of [Ru(*dtbpoet*)H_2(H_2)] 5

Dihydrogendihydrido[2,2´-bis-(di-tert-butyl-phosphanyl)-diethylether]ruthenium(II)

An argon flushed *Büchi glass-autoclave*, equipped with a stirring bar, was filled with [Ru(cod)(metallyl)$_2$] **6** (100 mg, 0.31 mmol; 1 eq.), *dtbpoet* **49** (116 mg, 0.32 mmol; 1.02 eq.) and 4 mL degassed *n*-pentane. The autoclave was flushed with 2 bar hydrogen gas (or deuterium gas) at room temperature, then the temperature was increased to 55 °C (oil bath) and the H_2-pressure was stabilized at 7 bar. The reaction was stirred for two days, cooled down to room temperature and the H_2-pressure was decreased to 1 bar. The red solution was filtered through canula under an H_2-stream and the remaining solid was washed under a H_2-stream with *n*-pentane to give a greenish solid.[*] The product was transferred into a dry schlenk-tube using a glove box and further dried under a H_2-stream. Finally it was stored under argon or 1 bar hydrogen in a sealed schlenk-tube at −20 °C. Yield: 80 mg (55%).

[*] Alternatively the mixture can be filtered in the glovebox with a glass filter and syringe.

^{1}H-NMR (400 MHz, [D$_8$]toluene, 25 °C): δ = 2.9 (vquint, 4 H, ^{3}J(H,H) = 7.2 Hz, ^{3}J(H,H) = 6.3 Hz, OCH_2), 1.3 (m, 4 H, PCH_2), 3.1 (vt, 4 H, ^{2}J(H,P) = 3.2 Hz, CH_2P), 1.2 (vt, 36 H, ^{3}J(H,P) = 6.0 Hz, PC(CH_3)$_3$), −8.8 (t, 4 H, ^{2}J(H,H) = 13.5 Hz, Ru-*H*, Ru-H_2).

^{13}C-NMR (100 MHz, [D$_8$]toluene, 25 °C): δ = 76.6 (vt, ^{2}J(C,P) = 2.5 Hz, O*C*H$_2$), 33.7 (vt, ^{1}J(C,P) = 6.6 Hz, P*C*(CH$_3$)$_3$), 30.9 (vt, ^{2}J(C,P) = 3.5 Hz, PC(*C*H$_3$)$_3$), 26.6 (vt, ^{1}J(C,P) = 3.4 Hz, P*C*H$_2$); ^{31}P-NMR (161 MHz, [D$_8$]toluene, 25°C): δ = 107.7 (s).

IR (KBr) $\tilde{\upsilon}$ = 2952 (s, ν; CH$_2$), 2894 (s, ν; CH$_2$), 2863 (s, ν; CH$_2$), 2088 (w, ν; Ru-H$_2$), 1994-1700 (m, ν; Ru-H), 1475 (s, δ; CH$_2$), 1384 (s, δ; t-Bu), 1361 (s, δ; t-Bu), 1178 (m, ν; C-P), 1061 (s, ν; CO), 805 cm^{-1} (s).

Detection of T_1(min) of the hydride signal: (400 MHz, [D$_8$]toluene, 25 °C): δ = −8.6 (t, 4 H, ^{2}J(H,P) = 14.0 Hz). T_1(min) = 38 ms (θ_{min} = 221 K), r(H-H) = 98 pm.

Elemental analysis calcd (%) for C$_{20}$H$_{48}$OP$_2$Ru (467,6): C 51.37; H 10.35; O 3.42; P 13.25; Ru 21.61. Exp.: C 51.15; H 10.18; P 13.18; Ru 21.42. Found atom ratio number by *CHN:* C$_{20}$H$_{47.4}$O$_{1.2}$P$_{2.0}$Ru$_{1.0}$

Table 14: Determination of T_1(min) of the hydride signal (δ = −8.6 ppm, 400.1 MHz, [D$_8$]toluene).

T [K] (Δ2K)	T$_1$ [ms] (Δ3ms)
300	180
283	122
263	78
243	47
223	34
193	54

T_1(min) = 38 ms

θ_{min}: 221±2 K (≈ –52 °C)

r_{HH} = 98 pm

4.3.3.10. Reaction of [Ru(*dtbpoet*)H_2(H_2)] 5 with N_2 to [Ru(*dtbpoet*)H_2(N_2)] 52

Dinitrogendihydrido[2,2´-bis-(di-tert-butyl-phosphanyl)-diethylether]ruthenium(II)

A *Young-Teflon-Capped NMR-tube* containing a [D_8]toluene (0.6 mL) solution of **5** (15 mg, 32.1 µmol) was slowly bubbled with N_2 at room temperature. ^{1}H- and ^{31}P-NMR were measured after 90 min and 20 h. Then the solution was bubbled with H_2 for one day. ^{1}H- and ^{31}P-NMR were recorded again.

After 20 h N_2-stream:

^{1}H-NMR (300 MHz, [D_8]toluene, 25 °C): δ = −12.5 (s, broad), −19.8 (s, broad);

^{31}P-NMR (122 MHz, [D_8]toluene, 25°C): δ = 99.2 (s, broad).

After 90 min, H_2-stream:

^{1}H-NMR (300 MHz, [D_8]toluene, 25 °C): δ = -8.4 (t, ^2J(H,P) = 13.5 Hz); ^{31}P-NMR (122 MHz, [D_8]toluene, 25°C): δ = 106.7 (s).

4.3.3.11. Reaction of [Ru(*dtbpoet*)H_2(H_2)] 5 with D_2 to [D_x]-[Ru(*dtbpoet*)H_2(H_2)] [D_x]-5

A *Young-Teflon-Capped NMR-tube* containing a [D_8]toluene (0.6 mL) solution of **5** (20 mg, 42.8 µmol) was slowly bubbled with D_2 at room temperature for a few minutes and ^{1}H-NMR and ^{2}H-NMR were recorded right after. After 2.5 months the sample was analysed again by ^{1}H-NMR and ^{31}P-NMR.

^{1}H-NMR (600 MHz, [D_8]toluene, 25 °C): δ = −8.6 (broad signal, 2 H). ^{2}H-NMR (600 MHz, [D_8]toluene, 25 °C): δ = 1.3 (weak signal, PC(CD_3)$_3$), −8.6 (s, Ru-*D*, Ru-D_2).

After 2.5 months: ^{1}H-NMR (300 MHz, [D_8]toluene, 25 °C): δ = −8.6 (t, 4 H, ^2J(H,H) = 13.5 Hz, Ru-*H*, Ru-H_2). ^{31}P-NMR (122 MHz, [D_8]toluene, 25 °C): δ = 106.4 (s).

4.3.4. Catalysis

The H/D-exchange catalyses were analysed by ^{1}H-NMR and the conversions were quantified by integration of the substrate / product signals in ratio to cyclohexane (100.0) as internal standard. The substrate-cyclohexane solutions were measured by the use of a [D_6]DMSO capillary. The product-cyclohexane solutions were measured with the lock-signal on the deuterated product or [D_6]DMSO-capillary. The deuterium incorporation was verified by ^{2}H-NMR. In case of signal overlaps of different protons in the ^{1}H-NMR spectra the deuterium incorporation was clarified with ^{13}C-NMR for toluene **12** (D_2O), *o*-xylene **54** (C_6D_6) and indol **57** (D_2O). The NMR-spectra were recorded on a BRUKER AMX-300 and BRUKER DMX 600 (^{2}H-NMR).

4.3.4.1. Catalytic *H/D*-exchange with D_2O as Deuterium Source

Procedure for catalytic H/D-exchange with [Ru(*dtbpmp*)(η^2-H_2)H_2] 4 as catalyst, here described for toluene 12:

The sample was prepared under argon atmosphere. The substrate **12** (2.5 mmol) was mixed with cyclohexane (here 1.4 mL). [Ru(*dtbpmp*)(η^2-H_2)H_2] **4** (1 mol%) was introduced in a *Young-teflon-capped* Schlenk-tube containing a teflon-coated stirring bar and one half of the substrate solution (1.25 mmol) was added to it. Under a flow of argon degassed deuterium oxide (1 mL) was added via syringe to the sample. The mixture was stirred at the indicated temperature (here 50°C) under argon for three days. Afterwards the organic layer was transferred via syringe into a *Young-teflon-capped NMR-tube* and the NMR was measured with the lock-signal on a [D_6]DMSO-capillary.

From the other half of the substrate-cyclohexane solution containing the substrate **12** (1.25 mmol) a ^{1}H-NMR was measured for the determination of the substrate-cylohexane ratio as starting point of the reaction. The substrate-cyclohexane solution was locked on [D_6]DMSO-capillary.

Conversion: 84% (*meta*), 28% (*ortho/para*), 0% (Me).

^{1}H-NMR (300 MHz, C_6H_{12}/[D_6]DMSO, 25 °C, before H/D-exchange): δ = 7.0 (1.88, *meta*-H), 6.9 (2.8, *ortho/para*-H), 2.1 (4.1, Me), 1.3 (100.0, C_6H_{12}, internal standard).

^{1}H-NMR (300 MHz, C_6H_{12}/[D_6]DMSO, 25 °C, after H/D-exchange): δ = 7.0 (0.3, *meta*-H),

6.9 (2.0, *ortho/para*-H), 2.1 (4.1, Me), 1.3 (100.0, C_6H_{12}, internal standard).

^{2}H-NMR (600 MHz, C_6H_{12}/[D_x]toluene, 25 °C, after H/D-exchange): δ = 7.3 (*meta*-H), 7.2 (*ortho/para*-H), 2.4 (residue, Me).

^{13}C-NMR (150 MHz, C_6H_{12}/[D_x]toluene, 25 °C): δ = 137.1 (*C*Me), 128.6 (*o*-*C*H, meta-H_2-isotopomer, H_8-Tol), 128.5 (*o*-*C*H, *m*-D_2-isotopomer, overlap with *o*-*C*H, *m*-H_1/D_1-isotopomer), 127.8 (*m*-*C*H, *m*-H_2, H_8-Tol), 127.7 (*m*-*C*H, *m*-D_1-isotopomer), 127.4 (*m*-*C*D, *m*-D_2 main isotopomer, t, ^1J(C,D) = 24.1 Hz), 127.35 (*m*-*C*D, *m*-D_1 isotopomer, *t*, ^1J(C,D) = 23.5 Hz), 125.0 (*p*-H, H_8-Tol), 124.9 (*p*-*C*H, *m*-D_1 isotopomer), 124.8 (*p*-*C*H, *m*-D_2 isotopomer), 124.6 (*m*-*C*D, *m*-D_1 isotopomer) 124.5 (*p*-*C*D, *m*-D2 main isotopomer, *t*, ^1J(C,D) = 24.7 Hz, D_3-Tol), 124.4 (*p*-D, D_1-Tol), 20.9 (Me).

^{31}P-NMR (122 MHz, C_6H_{12}/[D_6]DMSO, 25 °C, after H/D-exchange): δ = 108.4 (main signal).

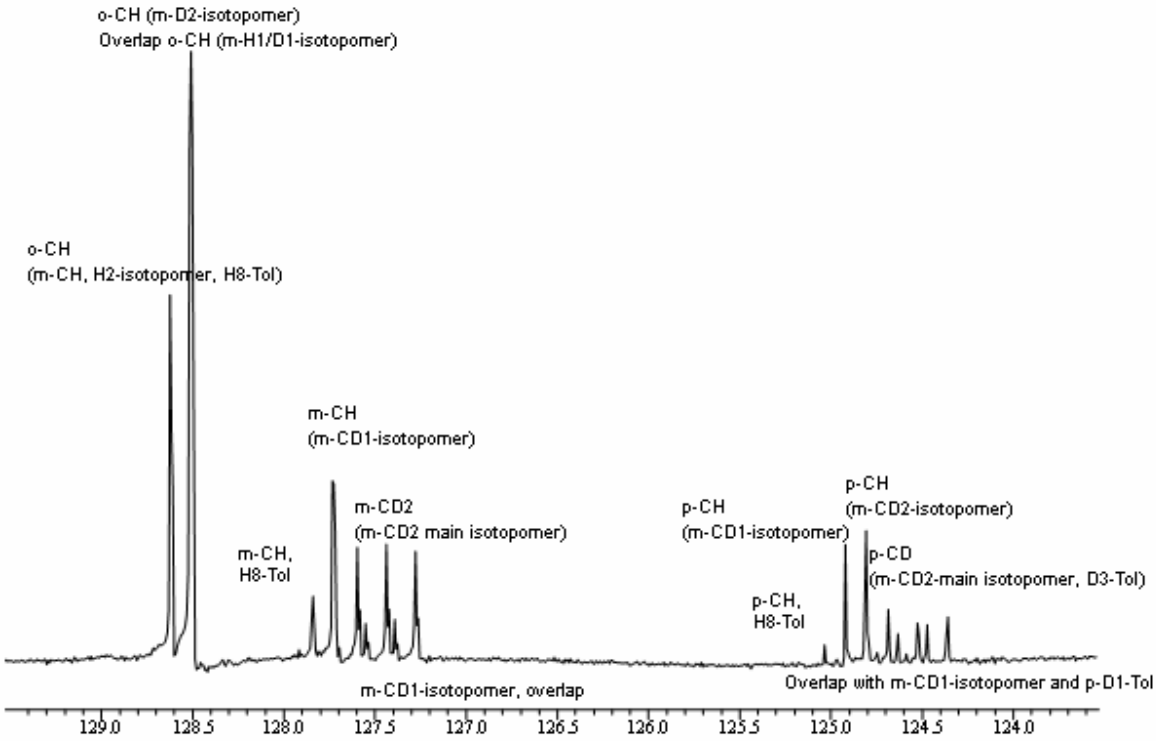

Figure 46: ^{13}C-NMR of [D_x]toluene **12** – Chemical shifts of the different *meta*- / *para*- / *ortho* isotopomeres.

Benzene **53**: Ru-cat **4**: 1 mol%, T = 50°C, Substrate: 1.1 mmol, 1 mL D_2O, 0.7 mL C_6H_{12}, t = 3 days. Conversion: 96%.

^{1}H-NMR (300 MHz, C_6H_{12}/[D_6]DMSO, 25 °C, before H/D-exchange): δ = 7.0 (8.2, CH), 1.3 (100.0, C_6H_{12}, internal standard).

^{1}H-NMR (300 MHz, C_6H_{12}/[D_x]benzene, 25 °C, after H/D-exchange): δ = 7.0 (0.3), 1.3

(100.0, C_6H_{12}, internal standard).

^{2}H-NMR (600 MHz, C_6H_{12}/[D_x]benzene, 25 °C, after H/D-exchange): δ = 7.16 (*CD*),

^{31}P-NMR (122 MHz, C_6H_{12}/[D_x]benzene, 25 °C, after H/D-exchange): δ = 108.4 (main signal).

o-Xylene **54**: Ru-cat **4**: 1 mol%, T = 50°C, Substrate: 1.2 mmol, 1 mL D_2O, 0.7 mL C_6H_{12}, t = 3 days. Conversion: 86% (β), < 5% (α).

^{1}H-NMR (300 MHz, C_6H_{12}/[D_6]DMSO, 25 °C, before H/D-exchange): δ = 6.8 (3.7, (α/β), 2.0 (6.3, Me), 1.3 (100.0, C_6H_{12}, internal standard).

^{1}H-NMR (300 MHz, C_6H_{12}/[D_6]DMSO, 25 °C, after H/D-exchange): δ = 6.8 (2.2 α/β), 2.0 (6.3, Me), 1.3 (100.0, C_6H_{12}, internal standard).

^{2}H-NMR (600 MHz, C_6H_{12}/[D_x]xylene, 25 °C, after H/D-exchange): δ = 6.9 (β-*CD*),

^{31}P-NMR (122 MHz, C_6H_{12}/[D_x]xylene, 25 °C, after H/D-exchange): δ = 108.3 (main signal).

Napthalene **55**:

Table 15: Benchmark-tests with **55**.

Exp.-No	Ru-cat 4 [mol-%]	T [°C]	55 [mmol]	D_2O [mL]	C_6H_{12} [mL]	t [d]	D-[%] (α), (β)
1	1	50	1.0	1.0	0.7	3	15%, 62%
2	1	75	1.0	1.0	1.0	3	66%, 91%
3	1	50	1.0	1.0 (H_2O)	0.7	3	5%, 35%
4	1 + 10 Hg*	50	1.0	1.0	0.7	3	15%, 55%
5	4	50	1.0	1.0	1.0	1	0%, 60%
6	1	75	4.0	4.0 (2x)	4.0	4	1st d: 26%, 81% 2nd d: 49%, 94% 3rd d: 63%, 95% 4th d: 77%, 96%

*Whitesides-Test: 10 mol% mercury (Hg) was added to the reaction with a 100µL *Hamilton Micro Syringe* without a canula.

Exp. No 6.:

Start:

^{1}H-NMR (300 MHz, C_6H_{12}/[D_6]DMSO, 25 °C, before H/D-exchange): δ = 7.5 (3.5, α), 7.1 (3.6, β), 1.3 (100.0, C_6H_{12}, internal standard).

1st day:

^{1}H-NMR (300 MHz, C_6H_{12}/[D_x]naphthalene, 25 °C, after H/D-exchange): δ = 7.5 (2.5, α), 7.2 (0.8, β), 1.3 (100.0, C_6H_{12}, internal standard). ^{2}H-NMR (600 MHz, C_6H_{12}/[D_x]naphthalene, 25 °C, after H/D-exchange): δ = 7.4 (α), 7.1 (β).

2nd day:

^{1}H-NMR (300 MHz, C_6H_{12}/[D_x]naphthalene, 25 °C, after H/D-exchange): δ = 7.5 (1.8, α), 7.2 (0.2, β), 1.3 (100.0, C_6H_{12}, internal standard). ^{2}H-NMR (600 MHz, C_6H_{12}/[D_x]naphthalene, 25 °C, after H/D-exchange): δ = 7.4 (α), 7.1 (β).

3rd day:

^{1}H-NMR (300 MHz, C_6H_{12}/[D_x]naphthalene, 25 °C, after H/D-exchange): δ = 7.5 (1.3, α), 7.2 (<0.2, β), 1.3 (100.0, C_6H_{12}, internal standard). ^{2}H-NMR (600 MHz, C_6H_{12}/[D_x]naphthalene,

25 °C, after H/D-exchange): δ = 7.4 (*α*), 7.1 (*β*).

4th day:

^{1}H-NMR (300 MHz, C_6H_{12}/[D_x]naphthalene, 25 °C, after H/D-exchange): δ = 7.5 (0.8, α), 7.2 (<0.2, β), 1.3 (100.0, C_6H_{12}, internal standard). ^{2}H-NMR (600 MHz, C_6H_{12}/[D_x]naphthalene, 25 °C, after H/D-exchange): δ = 7.4 (*α*), 7.1 (*β*).

Thiophene **55**: Ru-cat **4**: 1 mol%, T = 75°C, Substrate: 1.1 mmol, 1 mL D_2O, 1.0 mL C_6H_{12}, t = 3 days. Conversion: 99% (*β*), 99% (*α*).

^{1}H-NMR (300 MHz, C_6H_{12} / [D_6]DMSO, 25 °C, before H/D-exchange): δ = 7.1 (1.5, *α*), 6.9 (1.5, *β*), 1.3 (100.0, C_6H_{12}, internal standard).

^{1}H-NMR (300 MHz, C_6H_{12}/[D_6]DMSO, 25 °C, after H/D-exchange): δ = 7.1 (0.05, *α*), 6.9 (0.05, *β*), 1.3 (100.0, C_6H_{12}, internal standard).

^{2}H-NMR (600 MHz, C_6H_{12}/[D_6]DMSO, 25 °C, after H/D-exchange): δ = 7.0 (*α*), 6.8 (*β*).

2,5-Dimethylfurane **56**: Ru-cat **4**: 1 mol%, T = 75°C, Substrate: 0.94 mmol, 1 mL D_2O, 1.0 mL C_6H_{12}, t = 3 days. Conversion: 92% (CH), 59% (Me).

^{1}H-NMR (300 MHz, C_6H_{12} / [D_6]DMSO, 25 °C, before H/D-exchange): δ = 5.6 (1.5, CH), 2.0 (5.1, Me), 1.3 (100.0, C_6H_{12}, internal standard).

^{1}H-NMR (300 MHz, C_6H_{12}/[D_6]DMSO, 25 °C, after H/D-exchange): δ = 5.6 (0.1, CH), 2.0 (2.1, Me), 1.3 (100.0, C_6H_{12}, internal standard). ^{2}H-NMR (600 MHz, C_6H_{12}/[D_6]DMSO, 25 °C, after H/D-exchange): δ = 5.6 (CD), 2.0 (Me).

Indol **57**: Ru-cat **4**: 1 mol%, T = 75°C, Substrate: 1.0 mmol, 1 mL D_2O, 1.0 mL C_6H_{12}, t = 3 days. Conversion: see Figure 47.

^{1}H-NMR (300 MHz, C_6H_{12}/[D_6]DMSO, 25 °C, before H/D-exchange): δ = 7.4-7.3 (0.9, NH, C3), 7.0-6.8 (1.8, C5, C6), 6.6 (1.6, C4), 6.3 (0.9, NC*H*), 6.2 (0.9, NC=C*H*), 1.3 (100.0, C_6H_{12}, internal standard).

^{1}H-NMR (300 MHz, C_6H_{12}/[D_6]DMSO, 25 °C, after H/D-exchange): δ = 7.4-7.3 (0.37, NH, C3), 6.9-6.7 (0.39, C5, C6), 6.5 (0.04, C4), 6.4 (0.04, NC*H*), 6.2 (0.04, NC=C*H*), 1.3 (100.0, C_6H_{12}, internal standard).

^{2}H-NMR (600 MHz, C_6H_{12}/[D_6]DMSO, 25 °C, after H/D-exchange): δ = 7.2 (ND), 6.8 (C6), 6.6 (C5), 6.4 (C4), 6.3 (NC*D*), 6.1 (NC=C*D*).

^{13}C-NMR (150 MHz, C_6H_{12}/[D_6]DMSO, 25 °C, after H/D-Exchange): δ = 135.1 (C2a), 127.3 (C6a), 127.2 (C6a, D-C6), 123.0 (C1), 122.8 (D-C1, *t*, ^{1}J(C,D) = 28.7 Hz), 120.8 (C4), 120.6-120.3 (D-C4), 119.7 (C3), 118.8 (C5), 110.2 (C6), 110.0 (D-C1, *t*, ^{1}J(C,D) = 24.5 Hz), 101.1 (C2), 100.9 ((D-C1, *t*, ^{1}J(C,D) = 26.5 Hz).

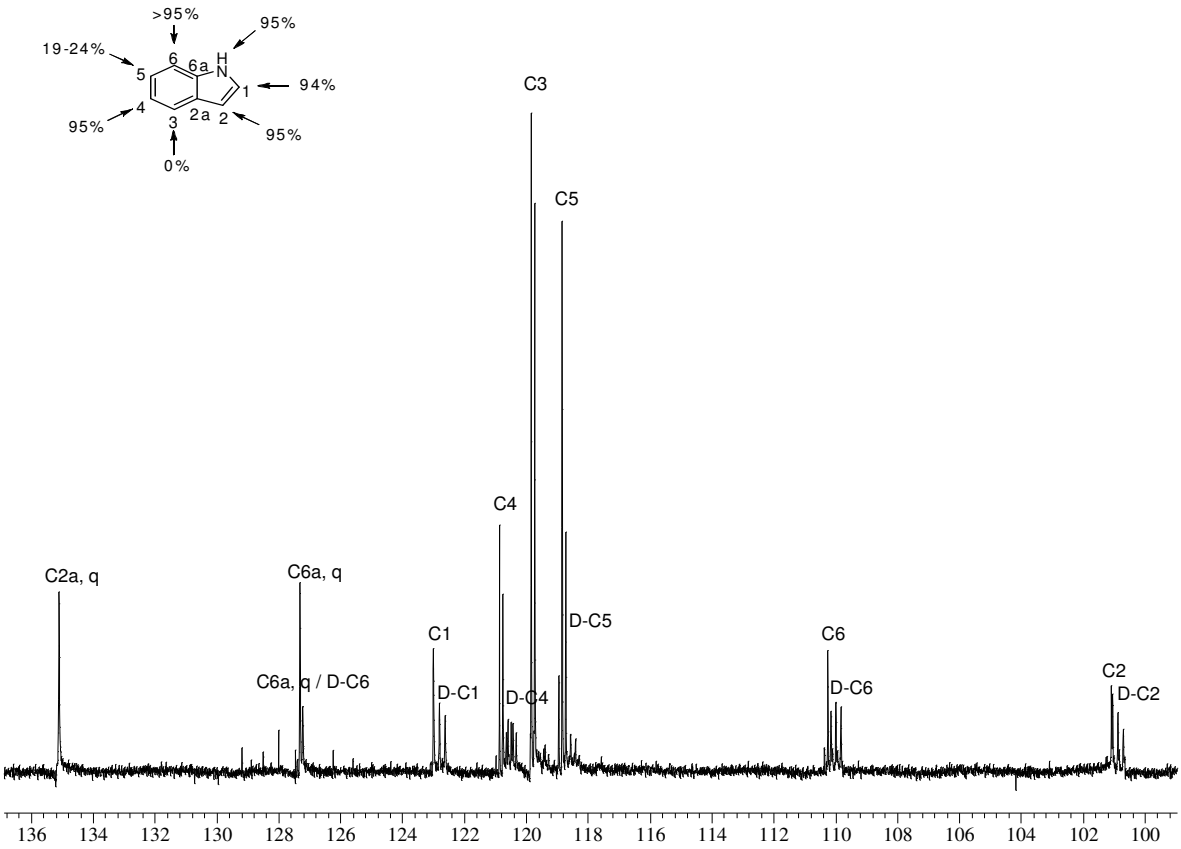

Figure 47: ^{13}C-NMR of [D_x]indol **57**.

Pyrrol **58**: Ru-cat **4**: 1 mol%, T = 75°C, Substrate: 1.0 mmol, 1 mL D_2O, 1.0 mL C_6H_{12}, t = 3 days. Conversion: 98% (*β*), 95% (*α*), n. d. (NH).

^{1}H-NMR (300 MHz, C_6H_{12}/[D_6]DMSO, 25 °C, before H/D-exchange): δ = 6.3 (1.2, *α*), 6.0 (1.2, *β*), 1.3 (100.0, C_6H_{12}, internal standard).

^{1}H-NMR (300 MHz, C_6H_{12}/[D_6]DMSO, 25 °C, after H/D-exchange): 6.3 (0.02, *α*), 6.0 (0.06, *β*), 1.3 (100.0, C_6H_{12}, internal standard). ^{2}H-NMR (600 MHz, C_6H_{12}/[D_6]DMSO, 25 °C, after H/D-exchange): δ = 6.4 (*α*), 5.9 (*β*).

Blank-test: Toluene **12**: DCl (37% in D_2O) and 10 mol% DCl in 1 mL D_2O, T = 50°C, Substrate: 1.0 mmol, 1 mL D_2O, 1.0 mL C_6H_{12}, t = 3 days. Conversion: 0%.

^{1}H-NMR (300 MHz, C_6H_{12} / [D_6]DMSO, 25 °C, before H/D-exchange): δ = 7.0 (1.6, *meta*-H), 6.9 (2.3, *ortho/para*-H), 2.1 ((2.7, Me), 1.3 (100.0, C_6H_{12}, internal standard).

^{1}H-NMR (300 MHz, C_6H_{12} / [D_6]DMSO, 25 °C, after H/D-exchange): δ = 7.0 (1.6, *meta*-H), 6.9 (2.3, *ortho/para*-H), 2.1 (2.7, Me), 1.3 (100.0, C_6H_{12}, internal standard).

^{2}H-NMR (600 MHz, C_6H_{12} / [D_x]toluene, 25 °C, after H/D-exchange): no significant signal.

4.3.4.2. Catalytic *H/D*-exchange with [D_6]benzene as Deuterium Source

Procedure for catalytic H/D-exchange with [Ru(*dtbpmp*)(η^2-H_2)H_2] 4 as catalyst, here described for toluene 12:

A *Young Teflon capped NMR tube* was filled with the catalyst **4** (1 mol%) followed by the addition of 0.6 mL C_6D_6. Then the substrate **12** (1.0 mmol) and 0.05 mL cyclohexane (internal standard) were added. Immediately, ^{1}H-NMR was measured to determine the substrate/internal standard ratio as starting point of the reaction. The mixture is kept for three days at 50 °C, afterwards it was cooled to r.t. and the ^{1}H- / ^{2}H-NMR spectra were measured manually locked on [D_6]benzene. Conversion: 87% (*meta*), 28% (*para*), < 5% (*ortho*), 1% (Me).

^{1}H-NMR (300 MHz, C_6H_{12}/[D_6]benzene, 25 °C, before H/D-exchange): δ = 7.1 (23.5, *meta*-H), 7.0 (32.5, *ortho/para*-H), 2.1 ((48.4, Me), 1.3 (100.0, C_6H_{12}, internal standard), -7.5 (Ru-H).

^{1}H-NMR (300 MHz, C_6H_{12}/[D_6]benzene, 25 °C, after H/D-exchange): δ = 7.07 (3.0, *meta*-H), 6.8 (23.4, *ortho/para*-H), 2.1 (47.8, Me), 1.3 (100.0, C_6H_{12}, internal standard).

^{2}H-NMR (600 MHz, C_6H_{12}/[D_6]benzene, 25 °C, after H/D-exchange): δ = 7.3 (*meta*-D), 7.2 (*ortho/para*-D), 2.4 (weak, Me).

^{31}P-NMR (122 MHz, C_6H_{12}/[D_6]benzene, 25 °C, after H/D-exchange): δ = 108.2 (main signal).

o-Xylene **54**: Ru-cat **4**: 1 mol%, T = 50°C, Substrate: 1.6 mmol, 0.5 mL C_6D_6, 0.1 mL C_6H_{12}, t = 3 days. Conversion: 95% (β), < 5% (α), < 5% (Me).

^{1}H-NMR (300 MHz, C_6H_{12}/[D_6]benzene, 25 °C, before H/D-exchange): δ = 7.0 (48.6, α/β), 2.0 (120, Me), 1.3 (100.0, C_6H_{12}, internal standard).

^{1}H-NMR (300 MHz, C_6H_{12}/[D_6]benzene, 25 °C, after H/D-exchange): δ = 7.0 (25.9 α/β), 2.0 (117.7, Me), 1.3 (100.0, C_6H_{12}, internal standard).

^{2}H-NMR (600 MHz, C_6H_{12}/[D_6]benzene, 25 °C, after H/D-exchange): δ = 6.9 (β-*CD*), 2.0 (residue, Me).

^{13}C-NMR (75 MHz, C_6H_{12}/[D_6]benzene, 25 °C): δ = 136.5 (*C*Me), 130.1 (α-*C*H, β-D_1-isotopomer), 130.1 (α-*C*H, meta-D_2-isotopomer), 126.3 (β-*C*H, β-D_1-isotopomer), 126.0 (β-*C*D, β-D_2-isotopomer, *t*, ^{1}J(C,D) = 24.2 Hz).

^{31}P-NMR (122 MHz, C_6H_{12}/[D_6]benzene, 25 °C, after H/D-exchange): δ = 108.2 (main signal).

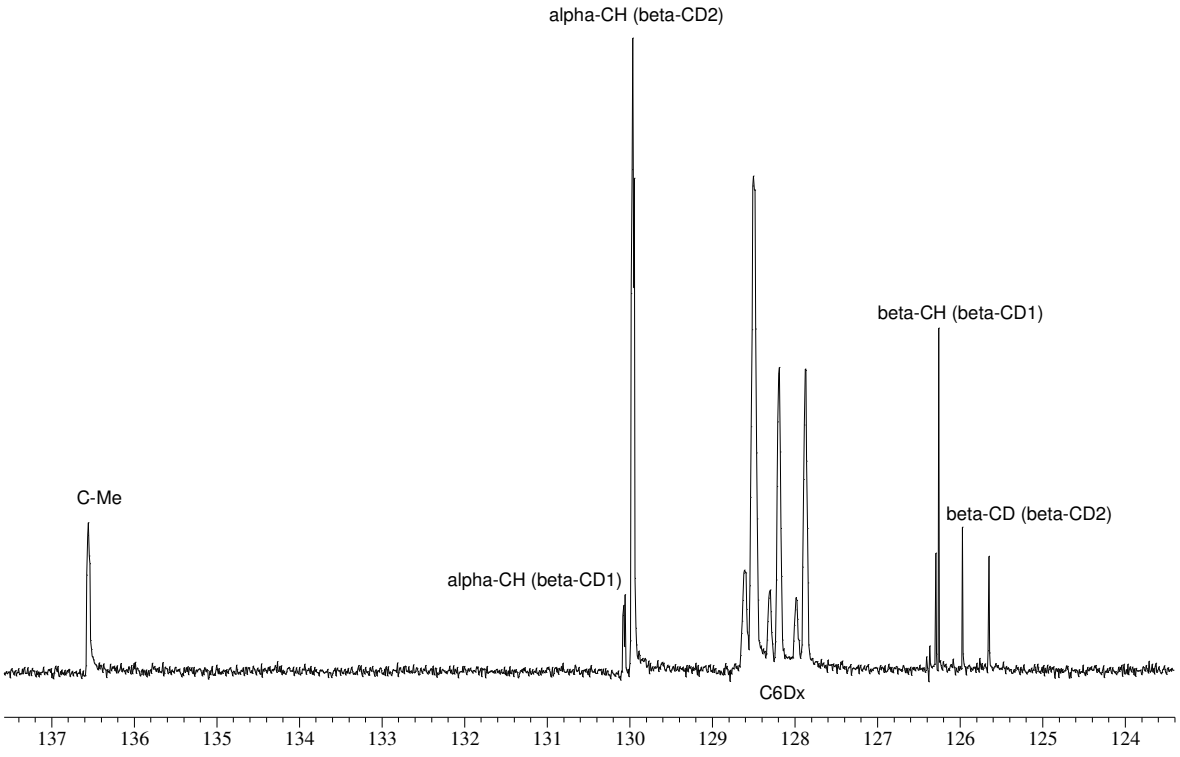

Figure 48: ^{13}C-NMR of [D_x]*o*-xylene **54** – chemical shifts of deuterated and non-deuterated aromatic carbons.

m-xylene **72**: Ru-cat **4**: 1 mol%, T = 50°C, Substrate: 1.6 mmol, 0.5 mL C_6D_6, 0.1 mL C_6H_{12}, t = 3 days. Conversion: 93% (β), 15% (α), 6% (Me).

^{1}H-NMR (300 MHz, C_6H_{12}/[D_6]benzene, 25 °C, before H/D-exchange): δ = 7.1 (10.8, β), 6.9 (31.2, α), 2.1 (90.0, Me), 1.3 (100.0, C_6H_{12}, internal standard).

^{1}H-NMR (300 MHz, C_6H_{12}/[D_6]benzene, 25 °C, after H/D-exchange): δ = 7.1 (0.75, β), 6.9 (26.4, α), 2.1 (84.7, Me), 1.3 (100.0, C_6H_{12}, internal standard).

^{2}H-NMR (600 MHz, C_6H_{12}/[D_6]benzene, 25 °C, after H/D-exchange): δ = 7.1 (s, β-*CD*), 7.0 (residue, α-*CD*), 2.1 (residue, Me).

^{31}P-NMR (122 MHz, C_6H_{12}/[D_6]benzene, 25 °C, after H/D-exchange): δ = 108.2 (main signal).

Mesitylene **73**: Ru-cat **4**: 1 mol%, T = 50°C, Substrate: 1.6 mmol, 0.5 mL C_6D_6, 0.1 mL C_6H_{12}, t = 3 days. No conversion detectable.

Napthalene **55:**

Table 16: Benchmark-tests with **55**. (Whitesides-Test and NMR-monitoring)

Exp.-No	Ru-cat 4 [mol-%]	T [°C]	55 [mmol]	C_6D_6 [mL]	C_6H_{12} [mL]	t [h]	D-[%] (α) / (β)
1	1	50	1.0	0.6	0.05	68	18 (α), 90 (β)
2	1 + 10 Hg	50	1.0	0.6	0.05	68	18 (α), 92 (β)
3	7	50	0.28	0.6	0.05	6.5 / 24	79 (β), 90 (β)
4	7	50	0.28	0.6	0.05	6.5 / 24	87 (β), 95 (β)
5	4	70	0.5	0.6	0.05	1.3 / 4	65 (β), 90 (β)
6	4	60	0.5	0.6	0.05	1.3 / 4	30 (β), 64 (β)
7	4	45	0.5	0.6	0.05	1.3 / 4	21 (β), 48 (β)
8	4	40	0.5	0.6	0.05	1.3 / 4	11 (β), 22 (β)
9	2	50	0.25	0.6	0.05	1.2	15 (β)
10	4	50	0.5	0.6	0.05	1.3 / 4	28 (β), 54 (β)

The Exp.-No 3-9 were analysed by ^{1}H-NMR every ten minutes. Further details see in chapter 2.3.1.2.

Exp. No 2. (Whitesides-Test: 10 mol% mercury (Hg) was added to the reaction with a 100µL *Hamilton Micro Syringe* without a canula):

^{1}H-NMR (300 MHz, C_6H_{12}/[D_6]benzene, 25 °C, before H/D-exchange): δ = 7.6 (17.1, α), 7.2 (16.3, β), 1.4 (100.0, C_6H_{12}, internal standard).

^{1}H-NMR (300 MHz, C_6H_{12}/[D_6]benzene, 25 °C, after H/D-exchange): δ = 7.6 (14.1, α), 7.1 (1.6, β), 1.4 (100.0, C_6H_{12}, internal standard).

^{2}H-NMR (600 MHz, C_6H_{12}/[D_6]benzene, 25 °C, after H/D-exchange): δ = 7.7 (residue, α), 7.3 (β). ^{31}P-NMR (122 MHz, C_6H_{12}/[D_6]benzene, 25 °C, after H/D-exchange): δ = 108.0 (s, main signal).

Phenanthrene **74**:

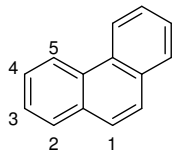

Ru-cat **4**: 1 mol%, T = 50°C, Substrate: 1.0 mmol, 0.5 mL C_6D_6, 0.05 mL C_6H_{12}, t = 3 days. Conversion: < 5% (C1), 7% (C2), 40% (C3, C4), < 5% (C5).

^{1}H-NMR (300 MHz, C_6H_{12}/[D_6]benzene, 25 °C, before H/D-exchange): δ = 8.4 (17.6, C5), 7.6 (15.9, C2), 7.4 (16.4, C1), 7.3 (31.5, C3/C4), 1.4 (100.0, C_6H_{12}, internal standard).

^{1}H-NMR (300 MHz, C_6H_{12}/[D_6]benzene, 25 °C, after H/D-exchange): δ = 8.4 (16.9, C5), 7.6 (13.2, C2), 7.4 (15.7, C1), 7.2 (1.9, C3/C4), 1.4 (100.0, C_6H_{12}, internal standard).

^{2}H-NMR (600 MHz, C_6H_{12}/[D_6]benzene, 25 °C, after H/D-exchange): δ = 7.3 (C3/C4).

^{31}P-NMR (122 MHz, C_6H_{12}/[D_6]benzene, 25 °C, after H/D-exchange): δ = 108.2 (main signal).

Isoquinoline **75**: Ru-cat **4**: 1 mol%, T = 50°C, Substrate: 1.0 mmol, 0.5 mL C_6D_6, 0.05 mL C_6H_{12}, t = 3 days. No conversion detectable.

Styrene **76**:

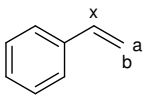

Ru-cat **4**: 1 mol%, T = 50°C, Substrate: 1.0 mmol, 0.5 mL C_6D_6, 0.05 mL C_6H_{12}, t = 3 days. Conversion: 14% (*m*), 74% (*o/p*), 35% (x), 86% (a), 88% (b).

^{1}H-NMR (300 MHz, C_6H_{12}/[D_6]benzene, 25 °C, before H/D-exchange): δ = 7.0 (33.7, *m*), 6.8 (50.3, *o/p*), 6.3 (15.9, x), 5.3 (18.1, a), 4.8 (17.1, b), 1.2 (100.0, C_6H_{12}, internal standard).

^{1}H-NMR (300 MHz, C_6H_{12}/[D_6]benzene, 25 °C, after H/D-exchange): δ = 7.0 (29.0, *m*), 6.8 (12.8, *o/p*), 6.3 (10.4, x), 5.3 (2.5, a), 4.8 (2.0, b), 1.3 (100.0, C_6H_{12}, internal standard).

^{2}H-NMR (600 MHz, C_6H_{12}/[D_6]benzene, 25 °C, after H/D-exchange): δ = 7.3 (*m*), 7.1 (*o/p*), 6.6 (x), 5.6 (a), 5.1 (b).

Indene **77**:

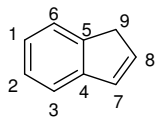

Ru-cat **4**: 1 mol%, T = 50°C, Substrate: 1.0 mmol, 0.5 mL C_6D_6, 0.05 mL C_6H_{12}, t = 3 days. Conversion: 62% (C1, C2), 27% (C3, C6), 69% (C7), 89% (C8), 76% (C9).

^{1}H-NMR (300 MHz, C_6H_{12}/[D_6]benzene, 25 °C, before H/D-exchange): δ = 7.3 (31.6, C1, C2), 7.3-7.1 (33.2, C3, C6), 6.7 (17.1, C7), 6.2 (14.9, C8), 3.0 (42.0, C9), 1.4 (100.0, C_6H_{12}, internal standard).

^{1}H-NMR (300 MHz, C_6H_{12}/[D_6]benzene, 25 °C, after H/D-exchange): δ = 7.3 (23.1, C1, C2), 7.3-7.1 (12.7, C3, C6), 6.7 (5.3, C7), 6.2 (1.6, C8), 3.0 (10.0, C9), 1.4 (100.0, C_6H_{12}, internal standard).

^{2}H-NMR (600 MHz, C_6H_{12}/[D_6]benzene, 25 °C, after H/D-exchange): δ = 7.3 (C1, C2), 7.1-7.0 (C3, C6), 6.7 (C7), 6.2 (C8), 3.0 (C9).

Ferrocene **78**: Ru-cat **4**: 1 mol%, T = 50°C, Substrate: 1.0 mmol, 0.6 mL C_6D_6, 0.05 mL C_6H_{12}, t = 3 days. Conversion: 25%.

^{1}H-NMR (300 MHz, C_6H_{12}/[D_6]benzene, 25 °C, before H/D-exchange): δ = 4.0 (35.2, Cp-H), 1.4 (100.0, C_6H_{12}, internal standard).

^{1}H-NMR (300 MHz, C_6H_{12}/[D_6]benzene, 25 °C, after H/D-exchange): δ = 3.7 (26.5, Cp-H), 1.4 (100.0, C_6H_{12}, internal standard).

^{2}H-NMR (600 MHz, C_6H_{12}/[D_6]benzene, 25 °C, after H/D-exchange): δ = 4.0 (Cp-D). ^{31}P-NMR (122 MHz, C_6H_{12}/[D_6]benzene, 25 °C, after H/D-exchange): δ = 108.1 (main signal).

4.3.4.3. Catalytic Dehydrogenation of Alcohols

The dehydrogenation products were characterised by GC and GC-MS and NMR through comparison with authentical samples. The conversions were quantified by the substrate / product ratio with GC. The comparison of GC runs with and without internal standard have shown that the results are similar (Δ 0.5%). For this reason the given conversions are based on the substrate / product ratio considering the reaction stoichometry. The GC analyses were performed at the chromatography department or on a HP 6890 with a RTX-1 column (30m). The GC-MS were performed at the MS department (GC-MS/GC-EI SSQ7000) or on a HP 6890 GC System/ HP Mass Selective Detector 5973.

The IR-online monitoring were performed with a *Bruker IR-Cube spectrometer* equipped with an ATR-IR fibre sensor.[112] The IR used the following parameters: optical resolution 4 cm^{-1}, data resolution 1929 cm^{-1}, 100 scans per spectra, mirror velocity 20 kHz and one spectra per 43 seconds. The IR data were processed with *Opus 6.0* and *DIAdem 9.0* Software.[112] For the quantification the carbonyl band (1755-1710 cm^{-1}) of each spectra was integrated with a linear baseline. The resulting slope was straightened with a moving average and then normalized to the calculated conversions of the GC analyses (measured at the chromatography department).

Procedure for catalytic dehydrogenation of primary alcohols into esters with [Ru(*dtbpmp*)(η^2-H_2)H_2] 4 as catalyst, here described for 1-adamantyl methanol 86 → 1-adamantylmethyl adamantylcarboxylate 92:

The experiment was performed under argon and absence of water in a 20 mL two-neck round-bottom flask with a reflux condenser equipped with an argon inlet and a bubbler. The second neck of the flask is equipped with a quick-fit and a double-septum inlet (teflon/silicon). The flask is filled with the catalyst **4** (1 mol%), 5 mL toluene and 1-adamantyl methanol **86** (2 mmol). The solution is magnetically stirred and refluxed for 20 h afterwards an aliquot was analysed by GC and GC-MS. Conversion: 86%. GC: method 50°C (1 min), 20°C/min until 270°C (hold 5 min). t_R: 20.88 min (**92**).

GC-MS (70eV, EI): m/z [%] = 328 (1) [M^+], 193 (38) [M-Ad], 148 (80), 135 (100), 93 (24), 79 (25).

Cyclohexyl methanol **85** → cyclohexylmethyl cyclohexanecarboxylate **91**: Ru-cat **4**: 1 mol%, reflux, substrate: 2.0 mmol, 5 mL toluene, t = 20 h. Conversion: 88%. GC: method 50°C (1 min), 20°C/min until 220°C (hold 5 min). t_R: 12.31 min (**91**).

GC-MS (70eV, EI): m/z [%] = 225 (1) [M^++H], 111 (20), 97 (20), 96 (100), 83 (60), 81 (70), 67 (33), 55 (79).

1-Butanol **84** → butyl butyrate **90**: Ru-cat **4**: 1 mol%, reflux, substrate: 2.0 mmol, 5 mL toluene, t = 20 h. Conversion: 96%. GC: method 50°C (1 min), 20°C/min until 220°C (hold 5 min). t_R: 7.21 min (**90**).

GC-MS (70eV, EI): m/z [%] = 101 (14), 89 (92), 71 (100), 56 (65).

Benzyl alcohol **87** → benzyl benzoate **93**: Ru-cat **4**: 1 mol%, reflux, substrate: 2.0 mmol, 5 mL toluene, t = 20 h. Conversion: 94% (GC). GC: method 50°C (1 min), 20°C/min until 220°C (hold 5 min). t_R: 13.51 min (**93**).

GC-MS (70eV, EI): m/z [%] = 212 (48) [M^+], 194 (24), 105 (100), 91 (66), 77 (54).

1-hexanol **83** → hexyl hexanoate **89**:

For further information see Table 5 in Ct. 2.3.2.1.

Ru-cat **4**: 1 mol%, reflux, substrate: 2.0 mmol, 5 mL toluene. Conversion: 85% (t = 3h), >99% (t = 20 h).

GC: method 50°C (1 min), 20°C/min until 220°C (hold 5 min). t_R: 10.13 min (**89**).

GC-MS (70eV, EI): m/z [%] = 200 (1) [M^+], 117 (100), 99 (90), 84 (75) 69 (45), 56 (65). IR (toluene) $\bar{\upsilon}$ = 1755-1710 (ν; CO).

Procedure for the catalytic dehydrogenative *indirect Wittig Reaction* of primary alcohols with [Ru(*dtbpmp*)(η^2-H_2)H_2] 4 as catalyst:

The experiment was performed in a 20 mL two-neck round-bottom flask with a reflux condenser equipped with an argon inlet and a bubbler. The second neck of the flask is equipped with a quick-fit and a double-septum inlet (teflon/silicon). The flask is filled with the catalyst **4** (4 mol%), 5 mL toluene, 1-hexanol **83** (1 mmol) and acetylmethylentriphenylphosphorane 96 (1 mmol). The solution is magnetically stirred and refluxed for three days. Afterwards an aliquot was analysed by GC and GC-MS. Conversion: 65% 2-nonanone **97**, 9% non-3-en-2-one **98**, 14% hexylhexanoate **89**. (GC) GC: method 50°C (hold 1 min), 20°C/min until 270°C (hold 5 min). t_R: 7.1 min (**98**), 7.87 min (**97**), 10.04 min (**89**).

Compound (**97**): GC-MS (70eV, EI): m/z [%] = 142 (21) [M^+], 127 (10), 71 (34), 58 (100), 54 (14).

Compound (**98**): GC-MS (70eV, EI): m/z [%] = 140 (1) [M^+], 125 (48), 97 (32), 71 (20), 55 (100).

Compound (**89**): GC-MS (70eV, EI): m/z [%] = 200 (1) [M^+], 117 (100), 99 (69), 84 (53) 69 (25), 56 (44).

Procedure for catalytic dehydrogenation of secondary alcohols into ketones with [Ru(*dtbpmp*)(η^2-H_2)H_2] 4 as catalyst, here described for 2-octanol 100 → 2-octanone 102:

The experiment was performed under argon and absence of water in a 20 mL two-neck round-bottom flask with a reflux condenser equipped with an argon inlet and a bubbler. The second neck of the flask is equipped with a quick-fit and a double-septum inlet (teflon/silicon). The flask is filled with the catalyst **4** (1 mol%), 5 mL toluene and 2-octanol **100** (2 mmol). The solution is magnetically stirred and refluxed for 20 h. Afterwards an aliquot was analysed by GC and GC-MS.

Conversion: 99%. GC: method 50°C (1 min), 20°C/min until 220°C (hold 5 min). t_R: 7.1 min (**102**). GC-MS (70eV, EI): m/z [%] = 128 (28) [M^+], 113 (20), 85 (24), 71 (44), 58 (100).

1-Phenyl ethanol **101** → acetophenone **103**: Ru-cat **4**: 1 mol%, reflux, substrate: 2.0 mmol, 5 mL toluene, t = 20 h. Conversion: 99%. GC : method 50°C (1 min), 20°C/min until 220°C (hold 5 min). t_R: 7.54 min (**103**). GC-MS (70eV, EI): m/z [%] = 120 (29) [M^+], 105 (100), 77 (88), 51 (43).

Procedure for catalytic dehydrogenation of secondary alcohols into branched ketones with [Ru(*dtbpmp*)(η^2-H_2)H_2] 4 as catalyst, here described for 2-octanol 100 → 9-methylpentadecan-7-one 105:

The experiment was performed under argon and absence of water in a 20 mL two-neck round-bottom flask with a reflux condenser equipped with an argon inlet and a bubbler. The second neck of the flask is equipped with a quick-fit and a double-septum inlet (teflon/silicon). The flask is filled with the catalyst **4** (1 mol%), dried KOH (1 mol%), 5 mL toluene and 2-octanol **100** (2 mmol). The solution is magnetically stirred and refluxed for 20 h. Afterwards an aliquot was analysed by GC and GC-MS.

Conversion: 55% (**105**), 34% (**108**), 11% (**109**), isolated yield of **105**: 16% (preparative GC).

GC: method 50°C (1 min), 20°C/min until 270°C (hold 5 min). t_R: 14.26 min (**105**), 19.57 min (**108**), 20.15 min (**109**).

Compound (**105**)**:**

GC-MS (70eV, EI): m/z [%] = 240 (2) [M^+], 211 (11), 155 (100), 129 (64), 113 (44), 85 (79), 71 (64), 57 (43).

^{1}H-NMR (300 MHz, [D_6]acetone, 25 °C): δ = 2.6-1.9 (m, 4 H, C6H_2 / C8H_2), 1.7 (m, 1 H, C9H), 1.3 (m, 2 H, C5H_2), 1.2-0.9 (m, 16 H, CH_2), 0.7-0.6 (m, 9 H, 3x CH_3).

^{13}C-NMR (75 MHz, [D_6]acetone, 25 °C): δ = 206.5 (CO), 50.9 (C8), 43.9 (C7), 38.0 (C10), 33.0 (C3 / C13), 32.8 (C3 / 13), 30.6 (CH_2), 30.1 (H*C*Me), 30.0 (CH_2), 28.0 (CH_2), 24.8 (CH_2), 23.7 (CH_2), 23.6 (CH_2), 20.6 (Me), 14.8 (Me), 14.7 (Me).

Compound (**108**): GC-MS (70eV, EI): m/z [%] = 348 (19) [M^+], 291 (64), 263 (100), 235 (8), 193 (8), 121 (13).

Compound: (**109**) GC-MS (70eV, EI): m/z [%] = 350 (1) [M^+], 348 (1) [M^+-2H], 278 (10), 263 (30), 193 (100), 109 (12).

1-Phenyl ethanol **101** → 1,3-diphenyl-butan-1-one **106**:

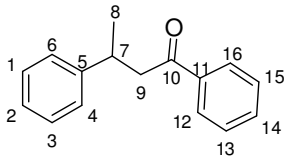

Ru-cat **4**: 1 mol% and 1 mol% KOH, reflux, substrate: 2.0 mmol, 5 mL toluene, t = 20 h. Conversion: 12% (**103**), 46% (**106**), 5% (**110**), 8% (**111**), 29% (**112**).

GC: method 50°C (1 min), 20°C/min until 270°C (hold 5 min). t_R: 13.10 min (**106**). Compound: (**106**): GC-MS (70eV, EI): m/z [%] = 224 (37) [M^+], 209 (63), 120 (27), 105 (100), 91 (17), 77 (53).

^{1}H-NMR (300 MHz, [D_6]acetone, 25 °C): δ = 7.8 (m, 2 H, C12-H, C16-H), 7.5 (vt, 1 H, ^3J(H,H) = 7.3 Hz, C14-H), 7.4 (vt, 2 H, ^3J(H,H) = 7.4 Hz, C13-H, C15-H), 7.3-7.1 (m, 4 H, C1-H, C3-H, C4-H, C6-H), 7.0 (vt, 1 H, ^3J(H,H) = 7.3 Hz, C2-H), 3.4-3.28 (m, 1 H, C7-H), 3.26-3.1 (m, 1 H, C9-H), 1.2 (d, 3 H, ^3J(H,H) = 6.7 Hz, CH_3).

^{13}C-NMR (75 MHz, [D_6]acetone, 25 °C): δ = 206.5 (CO), 134 (C_{ar}), 129.8 (C_{ar}), 129.6 (C_{ar}),

129.2 (C_{ar}), 128.2 (C_{ar}), 127.3 (C_{ar}), 47.5 (C9), 36.8 (C7), 22.9 (C8).

Compound: (**110**): GC-MS (70eV, EI): m/z [%] = 222 (67) [M^+], 221 (100) [M^+-H], 207 (11), 145 (15), 115 (33), 105 (15), 91 (11), 77 (26).

Compound: (**111**): GC-MS (70eV, EI): m/z [%] = 328 (3) [M^+], 324 (100), 247 (25), 189 (13), 105 (46), 77 (22).

Compound: (**112**): GC-MS (70eV, EI): m/z [%] = 326 (4) [M^+], 322 (100), 307 (90), 291 (16), 231 (39), 215 (33), 204 (19), 105 (20), 77 (10).

2-Butanol **104** → 5-methyl-3-heptanone **107**: Ru-cat **4**: 1 mol% and 1 mol% KOH, reflux, substrate: 2.0 mmol, 5 mL toluene, t = 20 h. Conversion: 78%. GC: method 50°C (1 min), 20°C/min until 220°C (hold 5 min). t_R: 6.74 min (**107**).

GC-MS (70eV, EI): m/z [%] = 128 (9) [M^+], 99 (43), 71 (77), 57 (93), 43 (100), 29 (57).

^{1}H-NMR (300 MHz, [D_6]acetone, 25 °C): δ = 2.5-2.1 (m, 4 H, C2H_2 / C4H_2), 1.9 (m, 1 H, C5H), 1.4-1.1 (m, 2 H, C6H_2), 1.0 (t, 3 H, ^3J(H,H) = 7.3 Hz, C1H_3), 0.9-0.8 (t, 3 H, ^3J(H,H) = 7.3 Hz, C7H_3 and d, 3 H, ^3J(H,H) = 6.7 Hz, C5H-*C8H$_3$*).

^{13}C-NMR (75 MHz, [D_6]acetone, 25 °C): δ = 204.4 (CO), 48.0 (C4), 34.8 (C2), 29.8 (C5), 28.4 (C6) 18.0 (C8), 9.9 (C7), 6.3 (C1).

Procedure for catalytic transfer-hydrogenation of ketones into secondary alcohols with [Ru(*dtbpmp*)(η^2-H_2)H_2] 4 as catalyst, here described for cyclohexanone 116 → cyclohexanol 117:

The substrate (0.3 mmol) was added in a *Young Teflon capped NMR tube* to Ru(*dtbpmp*)H_2(H_2) 4 (2 mol%) dissolved in 0.6 mL C_6D_6 at room temperature, followed by addition of isopropanol (1.5 mmol). The reaction mixture was heated to 50 °C. ^{1}H-NMR spectra were recorded at regular intervals and products were confirmed by comparison with spectral data of authentic samples. The conversion of starting material to product was determined by integration of the product resonances relative to substrate resonances in the ^{1}H-NMR spectrum. Conversion: 45% (3.5 h). >99% (24 h).

^{1}H-NMR (300 MHz, 25°C, [D_6]benzene): δ = 1.0-1.2 (m, 4 H), 1.35-1.45 (m, 5 H), 1.6-1.7 (m, 2 H), 3.3 (sept., 1 H).

5 Figure Index

Figure 1: Schematic bonding model between molecular hydrogen and a metal. 2
Figure 2: $Ru(H_2)_2(H)_2(PCy_3)_2$ 1a, $Ru(H_2)_2(H)_2(PCy_3)(IMes)$ 2, $Ru(H_2)_2(H)_2(IMes)_2$ 3. 3
Figure 3: Complexes with pincer ligands. 4
Figure 4: New pincer-type mononuclear complexes [Ru(*dtbpmp*)$(H_2)H_2$] 4 and [Ru(*dtbpoet*)$(H_2)H_2$] 5 6
Figure 5: Different metal hydride forms. 7
Figure 6: *Taniguchi´s* pentahydride [Ru(*dtbpmb*)$(H_2)_2H$] 16. 16
Figure 7: The ^{1}H-NMR spectra shows the hydride-signal of 4 at different temperatures. . 18
Figure 8: T_1-values as a function of temperature Θ determined for [Ru(*dtbpmp*)$(H_2)H_2$] 4. T_1/ms (Δ3ms) [T/K (Δ2K)]: 209 [300], 151 [283], 104 [263], 86 [243], 73 [223], 109 [193]. 18
Figure 9: $\ln(1/T_1)$ as a function of 1000/T for hydride signal in the ^{1}H-NMR of [Ru(*dtbpmp*)$(H_2)H_2$] 4. 19
Figure 10: Ball-and-Stick models of the complexes 17, 19 and the transition state TS(17-19). Selected bond length and H-H distances are depicted. 20
Figure 11: Ball-and-Stick-representation of the calculated structure for the complex [Ru(*dtbpmp*)$(H_2)H_2$] 4. The side-view on the equatorial plane. 22
Figure 12: Ball-and-Stick-representation of the calculated structure for the complex [Ru(*dtbpmp*)$(H_2)H_2$] 4 with the assigned H-H distances in the RuH_2-moiety determined by NMR (1.1. Å) and DFT (0.979 Å). 22
Figure 13: ^{1}H-NMR spectra (hydride area) of 4 (top: under Ar), 20 (2^{nd}: 90 min N_2), "Ru-Cluster" (3^{rd}: 20 h N_2) and restored 4 (bottom: 1 d H_2). 25
Figure 14: ^{31}P-NMR spectra of of 4 (top: under Ar), 20 (2^{nd}: 90 min N_2), "Ru-Cluster" (3^{rd}: 20 h N_2) and restored 4 (bottom: 1 d H_2). 25
Figure 15: The nonclassical ruthenium deuteride 22 / $[D_4]$- 4. 27
Figure 16: Comparison of the IR spectra of Ru(*dtbpmp*)$H_2(H_2)$ 4, $[D_x]$-*Ru(dtbpmp)H₂(H₂)* 21 / $[D_x]$-4 and the free ligand *dtbpmp* 22. 28
Figure 17: Other coordination modes for the reaction of 4 with pinacolborane 34: the dihydridoborate 36 and the hydride σ-borane complex 37. 35
Figure 18: X-ray structure of RuH(*dtbpmp*)$(HCO_2)CO$] 41. An ORTEP model of this complex is depicted in the experimental part. 39

Figure 19: The side-view on the equatorial plane of [RuH(*dtbpmp*)(HCO_2)CO] 41 39
Figure 20: *Gusev´s* [Ru(*dtbpoet*)(H_2)Cl_2] 50. 43
Figure 21: The hydride-area of the ^{1}H-NMR shows the hydride-signal of 5 at different temperatures. 44
Figure 22: T_1-values as a function of temperature Θ determined for [Ru(*dtbpoet*)(H_2)H_2] 5. T_1/ms (Δ3ms) [T/K (Δ2K)]: 180 [300], 122 [283], 78 [263], 47 [243], 34 [223], 54 [193]. 45
Figure 23: ln($1/T_1$) as a function of 1000/T for hydride signal in the ^{1}H-NMR of [Ru(*dtbpoet*)(H_2)H_2] 5. 45
Figure 24: Variation of the coupling constant *J* of the hydride peak in the ^{1}H-NMR measurement as a function of the temperature T. 47
Figure 25: Ball-and-Stick-representation for the calculated [Ru(*dtbpoet*)(H_2)H_2] 5. The side-view on the equatorial plane shows the enclipsed conformation of the phosphine groups. For clearance The H-atoms in the pincer-backbone are not depicted. 48
Figure 26: Ball-and-Stick-representation for the calculated [Ru(*dtbpoet*)(H_2)H_2] 5. The assigned H-H distance in the RuH_2-moiety is determined by NMR as 0.98 Å and by DFT as 0.987 Å. For the model complex [Ru(*dMepoet*)(H_2)H_2] 51, The assigned H-H distance in the RuH_2-moiety is determined by DFT as 0.875 Å. The H-atoms in the pincer-backbone are not depicted. 48
Figure 27: ^{1}H-NMR-monitoring of the deuteration of naphthalene 55. 54
Figure 28: ^{2}H-NMR-monitoring of the deuteration of naphthalene 55. 54
Figure 29: Ball-and-Stick-representation of some intermediates in the C-H activation of benzene. Selected bond distances are given in Å. 57
Figure 30: Time-resolved ^{1}H-NMR-monitoring of the H/D-exchange in naphthalene 62
Figure 31: Slope of the [Ru(*dtbpmp*)(H_2)H_2] 4 catalysed *β*–deuteration of napthalene 62
Figure 32: Slopes of the initiation period of the *β*–deuteration at different temperatures. . 63
Figure 33: Logarithmic plot of the *β*–deuteration at different temperatures. 63
Figure 34: The Arrhenius plot for the *β*–deuteration in C_6D_6 catalysed by [Ru(*dtbpmp*)(H_2)H_2] 4. 64
Figure 35: Logarithmic plot of the *β*–deuteration at different catalyst loadings. 64
Figure 36: Logarithmic plot of the order for the catalyst. 65
Figure 37: Time-resolved ATR-IR online spectra of the catalytic conversion of

1-hexanol 83 into hexylhexanoate 89. 70
Figure 38: Time-resolved conversion plots between 50°C and 100°C. 70
Figure 39: Logarithmic plot at different temperatures 71
Figure 40: The Arrhenius plot for the initial period of the catalytic conversion of 1-hexanol 83 into hexylhexanoate 89 between 50°C and 100°C. 71
Figure 41: Variation of the substrate/catalyst ratio. 72
Figure 42: Reaction rate as function of the ruthenium catalyst concentration. 73
Figure 43: The unique Ru(*dtbpmp*)H_2(H_2) 4 containing a PNP pincer ligand. 83
Figure 44: The [Ru(*dtbpoet*)(H_2)H_2] 5 containing a POP pincer ligand. 84
Figure 45: ORTEP diagram of [RuH(*dtbpmp*)(HCO_2)CO] **41** with thermal ellipsoids set at 50% probability. 99
Figure 46: ^{13}C-NMR of [D_x]toluene 12 – Chemical shifts of the different *meta-* / *para-* / *ortho* isotopomeres. 108
Figure 47: ^{13}C-NMR of [D_x]indol 57. 112
Figure 48: ^{13}C-NMR of [D_x]*o*-xylene 54 – chemical shifts of deuterated and non-deuterated aromatic carbons. 114

6 Scheme Index

Scheme 1: Synthesis of the *Chaudret*-complex 1 according to *Leitner* and co-workers. 5
Scheme 2: Synthesis of ruthenium dihydrogen complexes. [35] 5
Scheme 3: *Murai-reaction* 9
Scheme 4: Deuteration of toluene 12 using 2 as catalyst and C_6D_6 as deuterium source... 10
Scheme 5: Iridium catalyzed deuteration of toluene 12 with deuterium oxide as deuterium source. 10
Scheme 6: Ruthenium hydride catalyzed conversion of primary alcohols into esters. 12
Scheme 7: Ruthenium hydride catalyzed conversion of primary alcohols with phosphorylenes in an *indirect Wittig Reaction*. 13
Scheme 8: Catalysis test reactions for dehydrogenation of secondary alcohols and Guerbet-type coupling. 14
Scheme 9: Direct hydrogenation of [Ru(cod)(metallyl)$_2$] 6 in presence of *dtbpmp* 15 to give the nonclassical ruthenium hydride complex 4. 15
Scheme 10: Stable coordination modes of the [Ru(*dMepmp*)H_4] 19 as localized by DFT-calculations.[26, 61] 20
Scheme 11: Intramolecular H atom exchange: Associative process (A-D) involving a nonclassical trihydride and the dissociative process (E-H) with the classical tetrahydride.[7] 21
Scheme 12: Formation of the dinitrogen complex 20 23
Scheme 13: Reversible formation of dinitrogen complex 20 and ruthenium clusters from 4 under N_2 and H_2 atmosphere. 24
Scheme 14: Formation of [D_x]-*Ru(dtbpmp)H_2(H_2)* 21 ([D_x]- 4) starting from 4 with [D_8]toluene at room temperature within 72 h. 27
Scheme 15: Proposed dehydrogenation of 4 followed by intramolecular CH-bond cleavage via agostic interaction towards the unsaturated ruthenium trihydride 25 29
Scheme 16: Selective deuterium incorporation into the dihydrogen unit and the benzylic positions of 4. 30
Scheme 17: Different pathways for the deuterium incorporation into complex 4 with C_6D_6 and D_2O. 31
Scheme 18: Treatment of 4 with carbon monoxide and H_2 resulting in 28. 32

Scheme 19: Proposed mechanism for the conversion of 4 into 28 explained by the means of an analogue reactivity of [Ru(H_2)H_2(PPh_3)$_3$] 14 into [RuH(CO)($C_6H_4PPh_2$)(PPh_3)$_2$] 33. 33
Scheme 20: Reaction of 4 with the pinacolborane 34 under H_2-loss. 34
Scheme 21: Ruthenium catalyzed hydroboration of 1-octene with pinacolborane at room temperature. 35
Scheme 22: Formation of the ruthenium hydrido formato complex 41. 36
Scheme 23: CO_2-insertion into ruthenium hydride bonds resulting ruthenium hydrido formates. 36
Scheme 24: Different reactivity of [Rh(*dtbpmb*)H_2] 43 and [Rh(*dtbppent*)H_2] 44: CO_2-insertion into rhodium hydride bonds resulting in rhodium hydrido formates followed by a reverse water-gas shift reaction with *Kaska´s* rhodium dihydride complex 43. 37
Scheme 25: Proposed formation of the ruthenium complex 41. 38
Scheme 26: Hydrogenation of 6 in presence of 45 forming a ruthenium cluster of unknown structure. 41
Scheme 27: Formation of the [Ru(*dcypmp*)(2-methyl-allyl)$_2$] 48. 41
Scheme 28: Direct hydrogenation of [Ru(cod)(metallyl)$_2$] 6 in presence of *dtbpoet* 49 leads to the nonclassical ruthenium hydride complex 5. 42
Scheme 29: Formation of the ruthenium dinitrogen complex 52. 49
Scheme 30: Catalytic *HD*-exchange with 4 between C_6D_6 or D_2O and aromatic hydrocarbons. 50
Scheme 31: Deuteration of arenes with C_6D_6 and 4. 51
Scheme 32: Catalytic H/D exchange of aromatic and heteroaromatic compounds using D_2O as the deuterium source and complex 4 as catalyst precursor. 52
Scheme 33: Reaction steps and energy profiles (ΔH/ΔG (italics) in kcal/mol) for H/D exchange processes starting from 17 as determined by DFT calculations. Values in parenthesis denote relative energies of stationary points for the corresponding D_2O- (62, 63) and C_6D_6-complexes (64, 65). 56
Scheme 34: Relative energies (ΔH, $\Delta H^{\ddagger}$; ΔG, $\Delta G^{\ddagger}$ [italics], kcal/mol) of reactants, products and transition states (not shown) involved in C-H exchange at toluene in ortho-, meta- and para positions (top to bottom). 58

Scheme 35: Catalytic H/D exchange of aromatic compounds using C_6D_6 as the deuterium source and complex 4 as catalyst precursor.. 60
Scheme 36: Relative energies (ΔG, $\Delta G^{\ddagger}$, kcal/mol) of reactants, products and transition states (not shown) involved in C-H exchange at naphthalene in alpha- and beta- positions (top to bottom)..... 66
Scheme 37: Overview of the observed alcohol dehydrogenation reactions with precatalyst 4..... 67
Scheme 38: Dehydrogenative conversion of primary alcohols 83-88 to the corresponding homoesters 89-93..... 68
Scheme 39: Formation of the [RuH(*dtbpmp*)(CO)] 28 in presence of a primary alcohol. . 74
Scheme 40: Proposed catalytic dehydrogeantion cycle of primary alcohols to esters..... 75
Scheme 41: Indirect Wittig-Reaction using precatalyst [Ru(*dtbpmp*)(η^2-H_2)H_2] 4. 76
Scheme 42: Catalytic dehydrogenation of 2-ROH into ketones. R = hexyl (100, 102), phenyl (101, 103). 77
Scheme 43: Catalytic dehydrogenation of secondary alcohols. [Ru] = Ru(*dtbpmp*)H_2 78
Scheme 44: Transfer-hydrogenation catalysed by 4. 79
Scheme 45: Dehydrogenation of 2-ROH in presence of base into branched ketones. The primary main compounds with R = hexyl (100, 105), phenyl (101, 106) and ethyl (104, 107). 79
Scheme 46: Proposed mechanism for the formation of branched ketones. 81
Scheme 47: Straight forward synthesis to the ruthenium dihydrogen complexes 4 and 5 bearing bulky PNP and POP pincer ligands. 82
Scheme 48: Ruthenium catalyzed selecetive H/D-exchange between arenes and D_2O (or C_6D_6). 84
Scheme 49: Catalytic dehydrogenation of alcohols and their indirect conversions in coupling reactions. 85

7 Table Index

Table 1: Selected bond length and angles for the complexes 41 and 29..... 40
Table 2: Characteristic NMR-Data of the complexes 4, 5 and 50[2]. 44
Table 3: Selected DFT data of [Ru(*dtbpoet*)(H_2)H_2] 5. 48
Table 4: Conversion of the primary alcohols 83-88 into the corresponding esters 89-93. . 68
Table 5: IR-online study with 1-hexanol 83 as benchmark substrate. 69
Table 6: Conversion of secondary alcohols into ketones. 78
Table 7: Conversion of secondary alcohols into branched ketones. 80
Table 8: Detection of T_1(min) of the hydride signal
(δ = −7.3 ppm, 400.1 MHz, [D_8]toluene)..... 94
Table 9: NMR-data of the equilibrium between 4 and 20..... 96
Table 10: Crystal data and structure refinement. 99
Table 11: Atomic coordinates and equivalent isotropic displacement parameters ($Å^2$)... 101
Table 12: Bond lengths [Å] and angles [°]..... 102
Table 13: Anisotropic displacement parameters ($Å^2$). 103
Table 14: Determination of T_1(min) of the hydride signal
(δ = −8.6 ppm, 400.1 MHz, [D_8]toluene)..... 105
Table 15: Benchmark-tests with 55..... 110
Table 16: Benchmark-tests with 55. (Whitesides-Test and NMR-monitoring)..... 116

8 Abbreviation Index

Ad	adamantyl	EI	electron impact (MS)
Å	Ångstrøm	ESI	electron spray ionization (MS)
ATR	Attenuated Total Reflection (IR)	Et	ethyl
bn	benzyl	Et_2O	diethylether
BPin	pinacolborane	FT	Fourier-transformation
br	broad (NMR, IR)	GC	gas chromatography
Bu	butyl	h	hour
cat	catalyst	H/D-exchange	hydrogen / deuterium exchange
CI	chemical ionization (MS)	Hz	Hertz
cod	cyclooctadiene	IR	infrared spectroscopy
cy	cyclohexyl	*J*	coupling constant
cyp	cyclopentyl	L	ligand
δ	- deformation oscillation (IR)	M	metal
	- chemical shift (NMR)	M	mega
d	day	*m*	meta
	- doublet (NMR)	m	medium (IR)
dd	doublet of doublet (NMR)	m	multiplet (NMR)
DFT	density functional theory	Mol. Wt.	molecular weight
dt	doublet of triplet (NMR)	[m/z]	mass-charge relation (MS)
$[D_x]$	deuterium degree (NMR)	Me	methyl
dcypmp	2,6-bis-[(di-cyclohexyl-phosphanyl)-methyl]-pyridine	MS	mass spectroscopy
diprpmp	2,6-bis-[(di-isopropyl-phosphanyl)-methyl]-pyridine	n	normal
dMepmp	2,6-bis-[(dimethyl-phosphanyl)-methyl]-pyridine	n. d.	not determined
dMepoet	2,2´-bis-(dimethyl-phosphanyl)-diethylether	NEt_3	triethylamine
DMSO	dimethylsulphoxide	NMR	nuclear magnetic resonance
dtbpmb	2,6-bis-[(di-tert-butyl-phosphanyl)-methyl]-benzene	ν	valence oscillation (IR)
dtbpmp	2,6-bis-[(di-tert-butyl-phosphanyl)-methyl]-pyridine	$\tilde{\upsilon}$	wave number (IR)
dtbpoet	2,2´-Bis-(Di-tert-butyl-phosphanyl)-diethylether	*o*	ortho
dtbppent	2,6-bis-(di-tert-butyl-phosphanyl)pentane	OLED	organic light-emitting diode
η^n	coordination mode	*p*	para

P_2	bidentate phosphane ligand	sext	sextet (NMR)
PNP	phosphor nitrogen phosphor; pincer ligand	t	triplet (NMR)
POP	phosphor oxygen phosphor; pincer ligand	t	time
Ph	phenyl	t_R	retention time (GC)
py	pyridine	THF	tetrahydrofurane
q	quartet (NMR)	TON	turn over number
quint	quintet (NMR)	TOF	turn over frequency
R	organic substitute	TS	transition state
ROH	alcohol	T_1	spin-lattice relaxation time [ms] (NMR)
RT	room temperature	T_1(min)	minimum T_1 (NMR)
r_{HH}	hydrogen-hydrogen atom distance	θ(min)	temperature of T_1(min) (NMR)
s	strong (IR)	v	virtual (NMR)
s	singulet (NMR)	w	weak (IR)
sept	septet (NMR)		

9 Compound Name Index

1 bis(dihydrogen)dihydridoobis(tricyclohexylphosphin)ruthenium(II)

2 bis(dihydrogen)dihydridoo(tricyclohexylphosphin)[1,3-bis(2,4,6-trimethylphenyl)imidazol-2-ylidene]ruthenium(II)

3 bis(dihydrogen)dihydridoobis[1,3-bis(2,4,6-trimethylphenyl)imidazol-2-ylidene]ruthenium(II)

4 dihydrogendihydrido{2,6-bis-[(di-tert-butyl-phosphanyl)-methyl]-pyridine}ruthenium(II)

5 dihydrogendihydrido[2,2´-bis-(di-tert-butyl-phosphanyl)-diethylether]ruthenium(II)

6 [bis-(2-methylallyl)cycloocta-1,5-diene]ruthenium(II)

7 tricyclohexylphosphine

8 acetophenone

9 ethene

10 1-(2-ethylphenyl)ethanone

11 1-(2,6-diethylphenyl)ethanone

12 toluene

13 dihydrido(dinitrogen)tris(triphenylphosphine)ruthenium(II)

14 tetrahydridotris(triphenylphosphine)ruthenium(II)

15 2,6-bis-[(di-tert-butyl-phosphanyl)-methyl]-pyridine (*dtbpmp*)

16 bis(dihydrogen)hydrido{2,6-bis-[(di-tert-butyl-phosphanyl)-methyl]-benzene}ruthenium(II)

17 cis-dihydrogendihydrido{2,6-bis-[(di-methyl-phosphanyl)-methyl]-pyridine}ruthenium(II)

18 trans-dihydrogendihydrido{2,6-bis-[(di-methyl-phosphanyl)-methyl]-pyridine}ruthenium(II)

19 tetrahydrido{2,6-bis-[(di-methyl-phosphanyl)-methyl]-pyridine}ruthenium(II)

20 dinitrogendihydrido{2,6-bis-[(di-tert-butyl-phosphanyl)-methyl]-pyridine}ruthenium(II)

21 [D_x]-Dihydrogendihydrido{2,6-bis-[(di-tert-butyl-phosphanyl)-methyl]-pyridine}ruthenium(II)

22 dideuteriumdideuterido{2,6-bis-[(di-tert-butyl-phosphanyl)-methyl]-pyridine}ruthenium(II)

23 dihydrido{2,6-bis-[(di-tert-butyl-phosphanyl)-methyl]-pyridine}ruthenium(II)

26 dideuteriumdihydrido{2,6-bis-[(di-tert-butyl-phosphanyl)-[D_2]-methyl]-pyridine}ruthenium(II)

27 {2,6-bis-[(di-tert-butyl-phosphanyl)-methyl]-pyridine}ruthenium(II)monocarbonyl

28 - 30 no names defined

31 dihydridotris(triphenylphosphine)ruthenium(II)carbonyl

32 tris(triphenylphosphine)ruthenium(II)carbonyl

33 no name defined

34 pinacolborane

35 dihydrogenhydrido(pinacol boryl) {2,6-bis-[(di-tert-butyl-phosphanyl)-methyl]-pyridine}ruthenium(II)

36 - 37 no names defiend

38 1-octene

39 1-octylboronate

40 2-octylboronate

41 hydridoformato{2,6-bis-[(di-tert-butyl-phosphanyl)-methyl]-pyridine}ruthenium(II)carbonyl

42 no name defined

43 dihydrogen{2,6-bis-[(di-tert-butyl-phosphanyl)-methyl]-benzene}rhodium

44 dihydrogen{1,5-bis-(di-tert-butyl-phosphanyl)-pentane}rhodium

45 2,6-bis-[(di-isopropyl-phosphanyl)-methyl]-pyridine (*diprpmp*)

46 2,6-bis((dicyclohexylphosphino)methyl)pyridine (*dcypmp*)

47 dihydrogendihydrido{2,6-bis-[(di-cyclohexyl-phosphanyl)-methyl]-pyridine}ruthenium(II)

48 bis(2-methylallyl){2,6-bis-[(di-cyclohexyl-phosphanyl)-methyl]-pyridine}ruthenium(II)

49 2,2´-Bis-(Di-tert-butyl-phosphanyl)-diethylether (*dtbpoet*)

50 dihydrogendichloro[2,2´-bis-(di-tert-butyl-phosphanyl)-diethylether]ruthenium(II)

51 dihydrogendihydrido[2,2´-bis-(di-methyl-phosphanyl)-diethylether]ruthenium(II)

52 dinitrogendihydrido[2,2´-bis-(di-tert-butyl-phosphanyl)-diethylether]ruthenium(II)

53 benzene

54 *o*-xylene

55 napthalene

56 thiophene

57 2,5-dimethylfurane

58 indol

59 pyrrol

60 - 71 no names defined

72 *m*-xylene

73 mesitylene

74 phenanthrene

75 isoquinoline

76 styrene

77 indene

78 ferrocene

79 - 82 no names defined

83 1-hexanol

84 1-butanol

85 cyclohexyl methanol

86 1-adamantyl methanol

87 benzyl alcohol

88 cinammic alcohol

89 hexyl hexanoate

90 butyl butyrate

91 cyclohexylmethyl cyclohexanecarboxylate

92 1-adamantylmethyl adamantylcarboxylate

93 benzyl benzoate

94 1-hexanal

95 triphenylphosphine

96 acetylmethylentriphenylphosphorane

97 2-nonanone

98 non-3en-2one

99 triphenylphosphinoxide

100 2-octanol

101 1-phenylethanol

102 2-octanone

103 acetophenone

104 2-butanol

105 9-methylpentadecan-7-one

106 1,3-diphenyl-butan-1-one

107 5-methyl-3-heptanone

108 9-methyl-8-(octan-2-yl)pentadec-8-en-7-one

109 9-methyl-8-(octan-2-yl)pentadecan-7-one

110 1,3-diphenylbut-2-en-1-one

111 1,3-diphenyl-2-(1-phenylethyl)butan-1-one

112 1,3-diphenyl-2-(1-phenylethyl)but-2-en-1-one

113 ethyl-2-hexanol

114 ethyl-2-hexanal

115 isopropanol

116 cyclohexanone

117 cyclohexanol

118 Di(tert.-butyl)chlorophosphine

119 Dicyclohexyl-phosphane borane complex

120 Dichloro(cycloocta-1,5-dienyl)ruthenium(II) polymer

121 2,6-bis((dicyclohexylphosphino)methyl)pyridine bisborane complex

10 Compound Structure Index

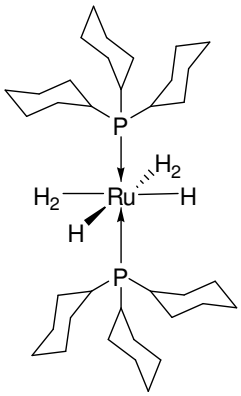

1

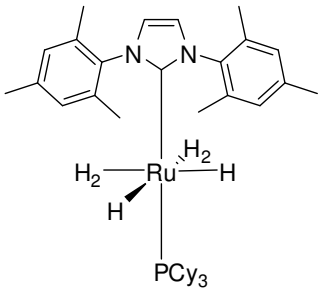

2

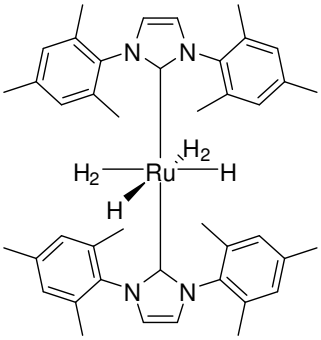

3

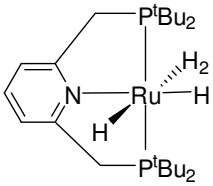

4

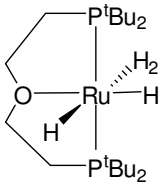

5

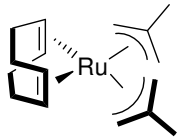

6

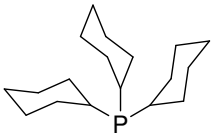

7

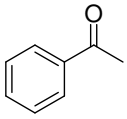

8

9

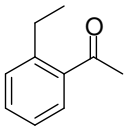

10

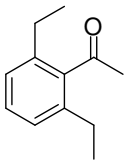

11

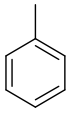

12

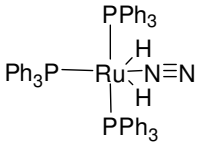

13

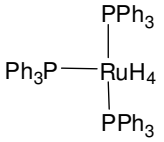

14

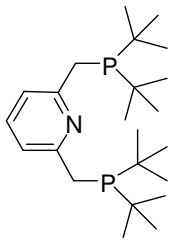

15

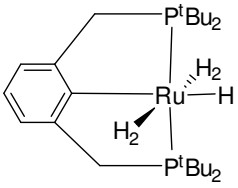

16

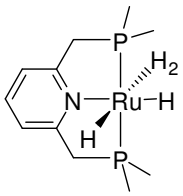

17

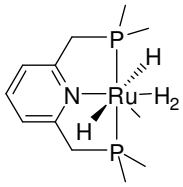

18

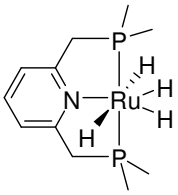

19

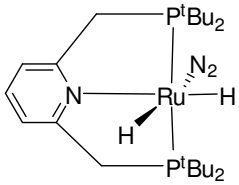

20

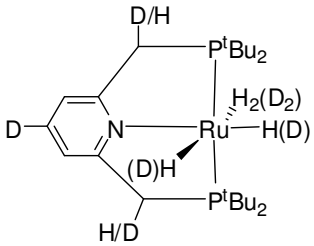

21

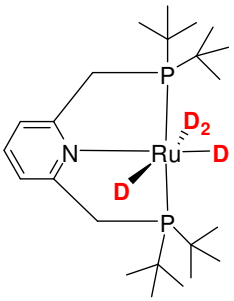

22

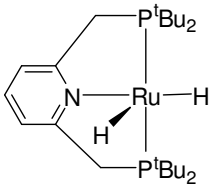

23

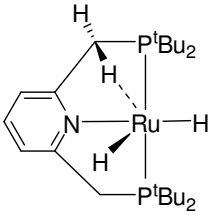

24

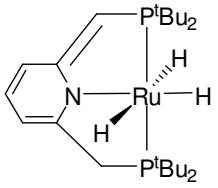

25

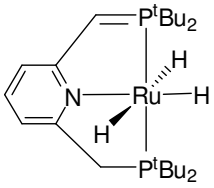

25

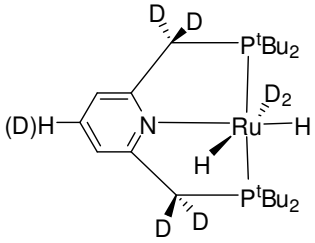

26

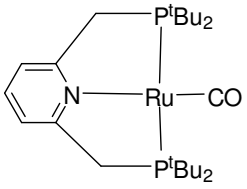

27

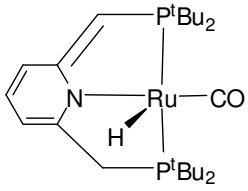

28

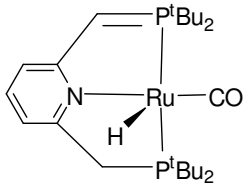

28

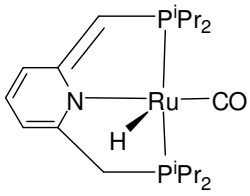

29

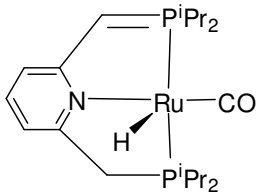

29

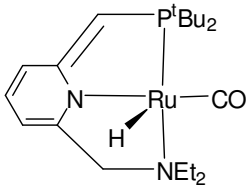

30

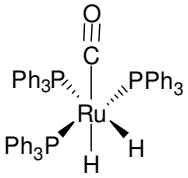

31

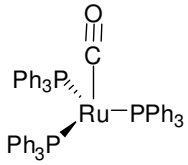

32

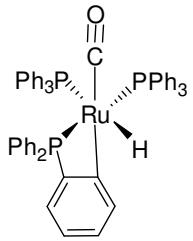

33

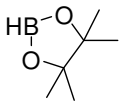

34

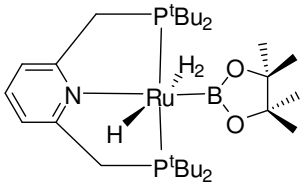

35

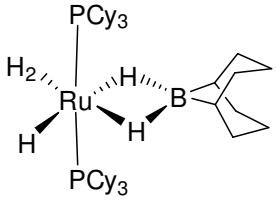

36

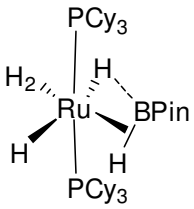

37

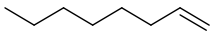

38

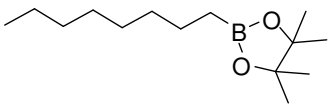

39

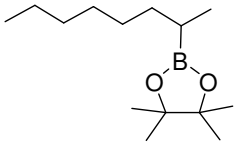

40

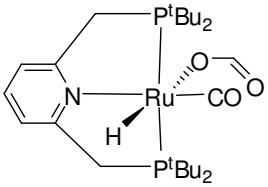

41

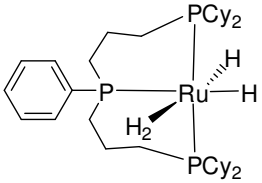

42

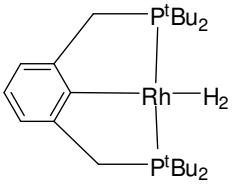

43

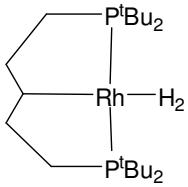

44

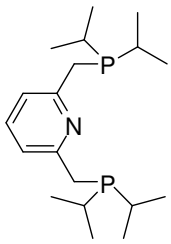

45

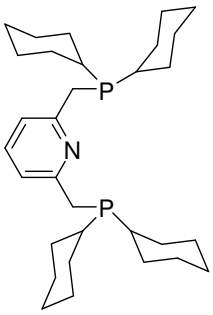

46

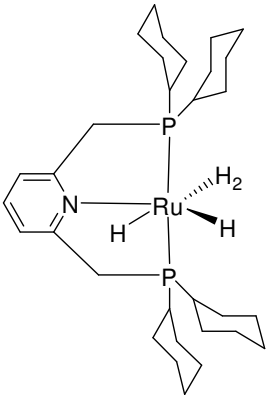

47

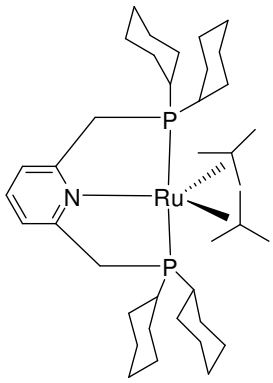

48

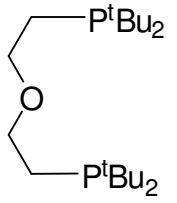

49

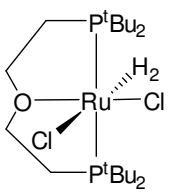

50

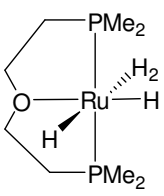

51

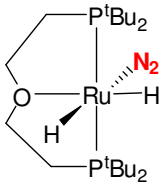

52

53

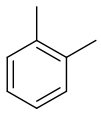

54

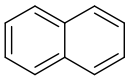

55

56

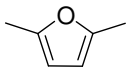

57

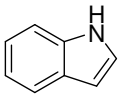

58

59

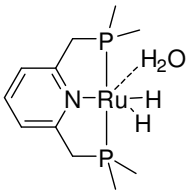

60

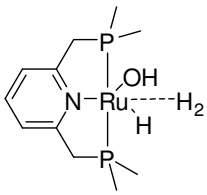

61

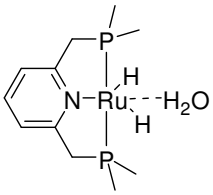

62

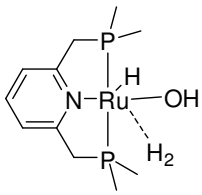

63

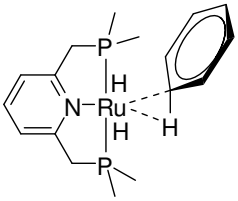

64

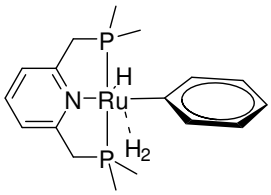

65

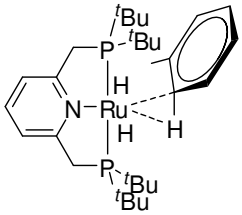

66

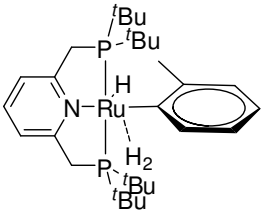

67

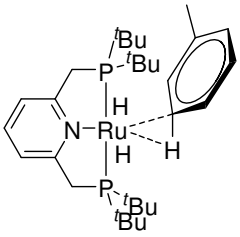

68

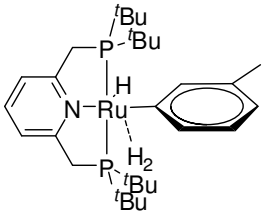

69

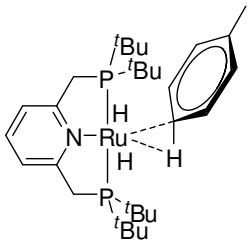

70

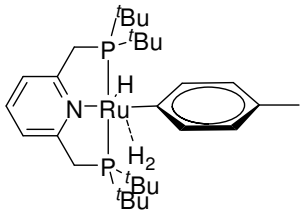

71

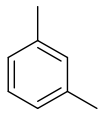

72

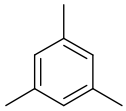

73

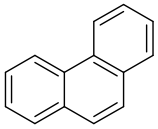

74

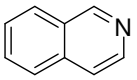

75

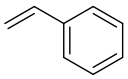

76

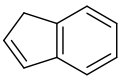

77

78

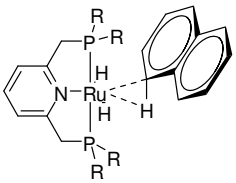

79

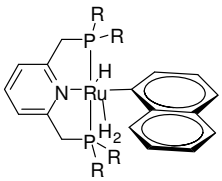

80

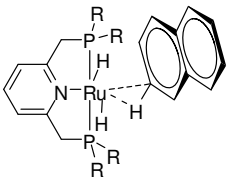

81

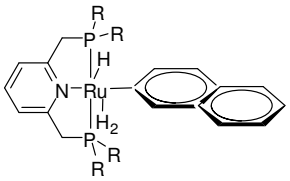

82

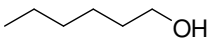

83

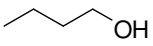

84

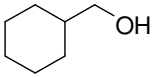

85

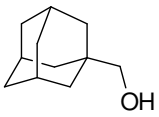

86

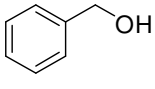

87

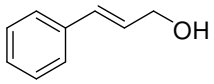

88

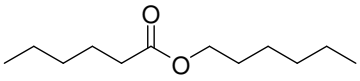

89

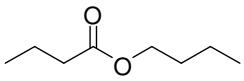

90

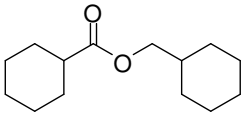

91

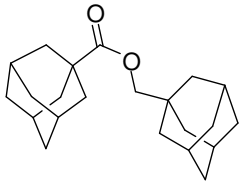

92

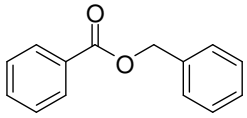

93

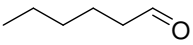

94

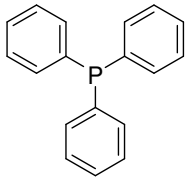

95

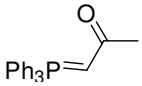

96

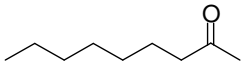

97

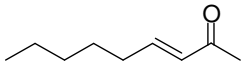

98

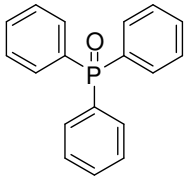

99

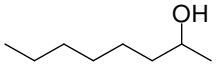

100

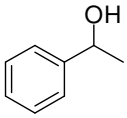

101

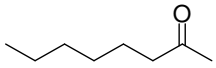

102

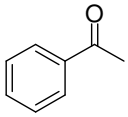

103

104

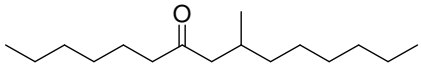

105

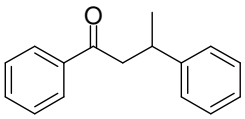

106

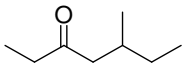

107

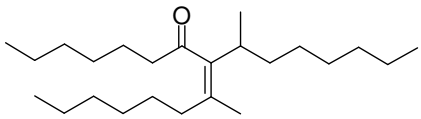

108

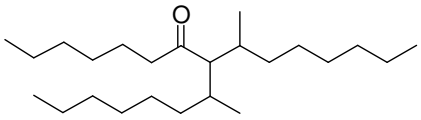

109

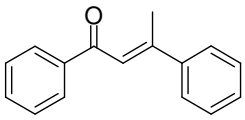

110

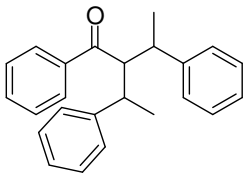

111

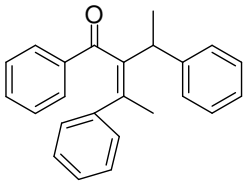

112

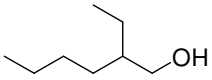

113

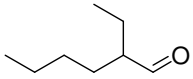

114

115

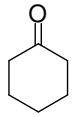

116

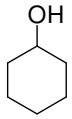

117

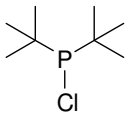

118

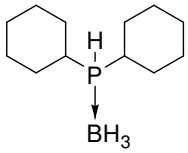

119

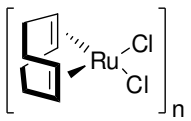

120

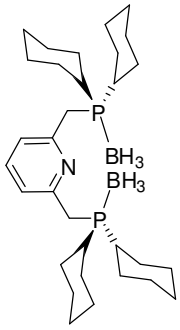

121

11 Literature

[1] a) B. Chaudret, R. Poilblanc., *Organometallics* **1985**, *4*, 1722-1726. b) T. Arliguie, B. Chaudret, R. H. Morris, A. Sella, *Inorg. Chem.* **1988**, *27*, 598-599. c) A. F. Borowski, B. Donnadieu, J.-C. Daran, S. Sabo-Etienne, B. Chaudret, *Chem. Commun.* **2000**, 543-544. d) M. Grellier, L. Vendier, B. Chaudret, A. Albinati, S. Rizzato, S. Mason, S. Sabo-Etienne, *J. Am. Chem. Soc.* **2005**, *127*, 17592-17593.

[2] Q. Major, A. J. Lough, D. G. Gusev, *Organometallics* **2005**, *24*, 2492-2501.

[3] a) J. Zhang, G. Leitus, Y. Ben-David, D. Milstein, *J. Am. Chem. Soc.* **2005**, *127*, 10840-10841. b) D. Hermann, M. Gandelman, H. Rozenberg, L. J. W. Shimon, D. Milstein, *Organometallics* **2002,** *21,* 812-818. c) J. Zhang, M. Gandelman, L. J. W. Shimon, H. Rozenberg, D. Milstein, *Organometallics* **2004**, *23*, 4026-4033. d) J. Zhang, G. Leitus, Y. Ben-David, D. Milstein, *Angew. Chem. Int. Ed.* **2006**, 45, 1113 –1115.

[4] a) D. Giunta D, *Dissertation* **2004**, RWTH Aachen. (b) D. Giunta, M. Hölscher, C. W. Lehmann, R. Mynott, C. Wirtz, W. Leitner, *Adv. Synth. Catal.* **2003**, *345*, 1139-1145. c) M. H. G. Prechtl, Y. Ben-David, D. Giunta, S. Busch, Y. Taniguchi, W. Wisniewski, H. Görls, R. J. Mynott, N. Theyssen, D. Milstein, W. Leitner, *Chem. Eur. J.* **2007***, 13*, 1539-1546.

[5] S. Busch, W. Leitner, *Adv. Synth. Catal.* **2001**, *343*, 192-195.

[6] a) P. Buskens, D. Giunta, W. Leitner, *Inorganica Chimica Acta* **2004**, *357*, 1969-1974. b) P. Buskens, *Diplomarbeit* **2003**, RWTH Aachen.

[7] P. J. Jessop, R. H. Morris, *Coord. Chem. Rev.* **1992**, *121*, 155-284.

[8] S. Sabo-Etienne, B. Chaudret, *Coord. Chem. Rev.* **1998**, *178-180*, 381-407.

[9] a) J. T. Golden, R. A. Andersen, R. G. Bergman, *J. Am. Chem. Soc.* **2001**, *123*, 5837-5838. b) S. R. Klei, J. T. Golden, T. D. Tilley, R. G. Bergman, *J. Am. Chem. Soc.* **2002**, *124*, 2092-2093. c) S. R. Klei, T. D. Tilley, R. G. Bergman, *Organometallics* **2002**, *21*, 4905-4911. d) M. R. Skaddan, C. M. Yung, R. G. Bergman, *Org. Lett.* **2004**, Vol 6, No 1, 11-13. e) C. M. Yung, M. R. Skaddan, R. G. Bergman, *J. Am. Chem. Soc.* **2004**, *126*, 13033-13043.

[10] A. F. Thomas, *Deuterium Labelling in Organic Chemistry* **1971**, Meridith Cooperation, New York.

[11] T. H. Lowry, K. S. Richardson, *Mechanism and Theory in Organic Chemistry* **1987**, Harper and Row, New York.

[12] M. Yamamoto, Y. Yokota, K. Oshima, S. Matsubara, *Chem. Commun.* **2004**, 1714-1715.

[13] a) S. Murai, F. Kakiuchi, S. Sekine, Y. Tanaka, A. Kamatani, M. Sonoda, N. Chatani, *Nature* **1993**, *366*, 529-531. b) Y. Guari, A. Castellanos, S. Sabo-Etienne, B. Chaudret, *J. Mol. Catal. A: Chemical* **2004**, *212,* 77–82.

[14] a) R. P. Beatty, R. A. Paciello R. A., *US Patent Wo 96/23802*, **1996**. b) R. P. Beatty, R. A. Paciello, *US Patent 5,559,262*, **1996**.

[15] a) M. Mc Coy, *Chem. Eng. News*, **2000**, *78*, 32. b) D. Tichit, R. Durand, A. Rolland, B. Coq, J. Lopez, P. Marion, *J. Catal.* **2002**, *211*, 511.

[16] a) M. D. Fryzuk, J. B. Love, S. J. Rettig, V. G. Young, *Science* **1997**, *275*, 1445-1447. b) M. D. Fryzuk, *Nature* **2004**, *427*, 498-499. c) E. A. MacLachlan, M. D. Fryzuk, *Organometallics* **2006**, *25*, 1530-1543. d) R. R. Schrock, *Science* **2003**, *301*, 76-78. e) J. A. Pool, E. Lobkovsky, P. J. Chirik, *Nature* **2004,** *427*,

527-530. f) F. Studt, F. Tuczek, *Angew. Chem. Int. Ed.* **2005**, *44*, 5639-5642. g) M. Hölscher, W. Leitner, *Eur. J. Inorg. Chem.* **2006**, 4407-4417.

[17] G. J. Kubas, R. R. Ryan, B. I. Swanson, P. J. Vergamini, H. J. Wasserman, *J. Am. Chem. Soc.*, **1984**, *106*, 451ff.

[18] a) G. J. Kubas, *Acc. Chem. Res.* **1988**, *21*, 120-128. b) G. J. Kubas, *Metal Dihydrogen and σ-Bond Complexes*, Kluwer Academic/Plenum Press, New York, **2001**. c) G. J. Kubas, *J. Organomet. Chem.* **2001**, *635*, 37-68.

[19] a) A. M. Kjoshi, K. S. MacFarlane, B. R. James, *J. Organomet. Chem.* **1995**, *488*, 161-167 ; b) G. Jia, W. S. Ng, C. P. Lau, *Organometallics* **1998**, *17*, 4538-4540.

[20] A. Dedieu, *Transition Metal Hydrides* **1990**, VCH Weinheim

[21] M. Y. Darensburg, E. J. Lyon, J. J. Smee, *Coord. Chem. Rev.* **2000**, *206-207*, 533-561.

[22] a) D. M. Heinekey, W. R. Oldham, *Chem. Rev.* **1993**, *93*, 913-926. (b) D. M. Heinekey, A. Lledós, J. M. Lluch, *Chem. Soc. Rev.* **2004**, *33*, 175-182.

[23] G. J. Kubas, *Catalysis Letters* **2005**, *104, 1-2,* 79-101.

[24] G. J. Kubas, C. J. Burns, J. Eckert, S. Johnson, A. C. Larson, P. J. Vergamini, C. J. Unkefer, G. R. K. Khalsa, S. A. Jackson, O. Eisenstein, *J. Am. Chem. Soc.* **1993**, *115*, 569-581.

[25] K. Almeida Leñero, M. Kranenburg, Y. Guari, P. C. J. Kamer, P. W. N. M. van Leeuwen, S. Sabo-Etienne, B. Chaudret, *Inorg. Chem.* **2003**, *42*, 2859-2866.

[26] M. H. G. Prechtl, M. Hölscher, Y. Ben-David, N. Theyssen, R. Loschen, D. Milstein, W. Leitner, *Angew. Chem.* **2007**, *119*, 2319-2322. *Angew. Chem. Int. Ed.* **2007**, *46*, 2269-2272. This publication and its supporting information also contains further details and literature references about the DFT-calculations which were performed with the program suite GAUSSIAN03.

[27] L. A. Oro, M. A. Esteruelas, *Chem. Rev.* **1998**, *98*, 577-588.

[28] a) S. Schlaf, A. J. Lough, R. H. Morris, *Organometallics* **1997**, *16*, 1253-1259. b) K. Abdur-Rashid, D. G. Gusev, A. J. Lough, R. H. Morris, *Organometallics* **2000**, *19*, 1652-1660. c) K. Abdur-Rashid, M. Faatz, A. J. Lough, R. H. Morris, *J. Am. Chem. Soc.* **2001**, *123*, 7473-7474.

[29] a) M. L. Christ, S. Sabo-Etienne, B. Chaudret, *Organometallics* **1995**, *14*, 1082-1084. b) M. Kranenburg, P. J. C. Kamer, P. W. N. M. van Leeuwen, B. Chaudret, *Chem. Comm.* **1997**, 373-374. c) A. F. Borowski, S. Sabo-Etienne, M. L. Christ, B. Donnadieu, B. Chaudret, *Organometallics* **1996**, *15*, 1427-1434. d) C. Vicente, G. B. Shul´pin, B. Moreno, S. Sabo-Etienne, B. Chaudret, *J. Mol.Cat. A: Chem.* **1995**, *98*, L5-L8.

[30] a) B. Chaudret, G. Chung, O. Eisenstein, S. A. Jackson, F. J. Lahoz, J. A. Lopez, *J. Am. Chem. Soc.* **1991**, *113*, 2314-2316; b) G. Chung, T. Arliguie, B. Chaudret, *New J. Chem.* **1992**, *16*, 369-374; c) M. L. Christ, S. Sabo-Etienne, B. Chaudret, *Organometallics* **1994**, *13*, 3800-3804.

[31] Y. Guari, S. Sabo-Etienne, B. Chaudret, *J. Am. Chem. Soc.* **1998**, *120*, 4228-4229.

[32] F. Delpech, S. Sabo-Etienne, B. Donnadieu, B. Chaudret, *Organometallics* **1998**, *17*, 4926-4928.

[33] S. Murai, F. Kakiuchi, S. Sekine, Y. Tanaka, A. Kamatani, M. Sonoda, N. Chatani, *Nature* **1993**, *366*, 529-531.

[34] T. R. Balderrain, R. H. Grubbs, *Organometallics* **1997**, *16*, 4001-4003.

[35] S. Busch, W. Leitner, *Chem. Commun.* **1999**, 2305-2306.

[36] a) M. E. van der Boom, D. Milstein, *Chem. Rev.* **2003**, *103*, 1759-1792. b) M. E. van der Boom, L. Hassner, Y. Ben-David, D. Milstein, *Organometallics* **1999**, *18*, 3873-3884. c) M. E. van der Boom, M. A. Iron, O. Atasoylu, L. J. W. Shimon, H. Rozenberg, Y. Ben-David, L. Konstantinovski, J. M. L. Martin, D. Milstein, *Inorg. Chim. Acta* **2004**, *357/6*, 1854-1864

[37] D. Milstein, *Pure Appl. Chem.* **2003**, 445–460.

[38] a) E. Peris, R. H. Crabtree*, Coordination Chemistry Reviews* **2004**, *248*, 2239–2246. b) R. H. Crabtree, *Pure Appl. Chem.* **2003**, 435–443.

[39] a) B. Rybtchinski and D. Milstein, *Angew. Chem. Int. Ed.* **1999**, *38*, 870-883. b) E. Ben-Ari, M. Gandelman, H. Rozenberg., L. J. W. Shimon, D. Milstein, *J. Am. Chem. Soc.* **2003**, *125*, 4714-4715.

[40] a) E. Peris, J. A. Loch, J. A. Mata, R. H. Crabtree, *Chem. Commun.* **2001**, 201–202. b) S. Gründemann, M. Albrecht, J. A. Loch, J. W. Faller, R. H. Crabtree, *Organometallics* **2001**, *20,* 5485-5488. c) M. Poyatos, J. A. Mata, E. Falomir, R. H. Crabtree, E. Peris, *Organometallics* **2003**, *22,* 1110-1114.

[41] a) D. G. Gusev, M. Madott, F. M. Dolgushin, K. A. Lyssenko, M. Y. Antipin, *Organometallics* **2000**, *19*, 1734-1739; b) D. G. Gusev, F. M. Dolgushin, M. Y. Antipin, *Organometallics* **2000**, *19*, 3429-3434; c) D. G. Gusev, T. Maxwell, F. M. Dolgushin, K. A. Lyssenko, A. J. Lough, *Organometallics* **2002**, *21*, 1095-1100; d) E. J. Farrington, E. M. Viviente, B. S. Williams, G. van Koten, J. M. Brown, *Chem. Commun.* **2002**, 308-309.

[42] M. Kawatsura, J. F. Hartwig, *Organometallics* **2001,** *20,* 1960-1964.

[43] A. A. D. Tulloch, A. A. Danopoulos, G. J. Tizzard, S. J. Coles, M. B. Hursthouse, R. S. Hay-Motherwell, W. B. Motherwell, *Chem. Commun.* **2001**, 1270–1271. b) A. A. Danopoulos, S. Winston, W. B. Motherwell, *Chem. Commun.* **2002**, 1376–1377. c) A. A. Danopoulos, J. A. Wright, W. B. Motherwell, Chem. Commun. **2005**, 784–786.

[44] R. Sablong, C. Newton, P. Dierkes, J. A. Osborn, *Tetrahedron Letters* **1996**, 4933-4936.

[45] Belderrain T.R., Grubbs R.H., *Organometallics* **1997**, *16*, 4001-4003.

[46] R. Gelabert, M. Moreno, J. M. Lluch, *Chem. Eur. J.* **2005**, 6315-6325.

[47] M. Yousufuddin, T. B. Wen, S. A. Mason, G. J. McIntyre, G. Jia, R. Bau, *Angew. Chem. Int. Ed.* **2005**, *44*, 7227-7230.

[48] C. Bianchini, C. Mealli M. Peruzzini, F. Zanobini, *J. Am. Chem. Soc*. **1992**, *114*, 5905-5906.

[49] G. J. Kubas, *J. Less Com. Met*. **1991**, *173*, 475-484.

[50] B. R. Bender, G. J. Kubas, L. H. Jones, B. I. Swanson, J. Eckert, K. B. Capps, C. D. Hoff, *J. Am. Chem. Soc*. **1997**, *119*, 9179-9190.

[51] L. A. Woodward, Introduction to the Theory of Molecular Vibrations and Vibrational Spectroscopy **1972**, Oxford Univ. Press, London, p 207-214.

[52] P. E. Bloyce, A. J. Rest, I. Whitwell, W. A. G. Graham, R. Holmes-Smith, *Chem. Comm.* **1988**, 846-848.

[53] R. H. Crabtree, M. Lavin, *Chem. Commun*. **1985**, 1661-1662.

[54] D. G. Hamilton, R. H. Crabtree, *J. Am. Chem. Soc.* **1988**, *110*, 4126-4133.

[55] K. A. Earl, G. Jia, P. A. Maltby, R. H. Morris, *J. Am. Chem. Soc.* **1991**, *113*, 3027-3039.

[56] S. Antoniutti, G. Albertin, P. Amendola, E. Bordignon, *Chem. Commun.* **1989**, 229-230.

[57] a) D. G. Gusev, A. B. Vymentis, V. I. Bakhmutov, *Inorg. Chem.* **1991**, *30*, 3116-3118. b) X. L. Luo, J. A. K. Howard, R. H. Crabtree, *Magn. Reson. Chem.* **1991**, *29*, S89-S93.

[58] P. J. Desrosiers, L. Cai, Z. Lin, R. Richards, J. Halpern, *J. Am. Chem. Soc*. **1991**, *113*, 4173-4184.

[59] a) K. W. Zilm, R. A. Merill, M. W. Kummer, G. J. Kubas, *J. Am. Chem. Soc*. **1986**, *108*, 7837-7839. b) K. W. Zilm, J. M. Millar, *Adv. Magn. Opt. Reson*. **1990**, *15*, 163-200.

[60] a) H. J. Wassermann, G. J. Kubas, R. R. Ryan, *J. Am. Chem. Soc.* **1986**, *108*, 2294-2301. b) G. J. Kubas, C. J. Unkefer, B. I. Swanson, E. Fukushima, *J. Am. Chem. Soc.* **1986**, *108*, 7000-7009.

[61] M. H. G Prechtl, M. Hölscher, W. Leitner, *Chem. Eur. J.* **2007**, accepted for publication.

[62] B. Rybtchinski, R. Cohen, Y. Ben-David, J. M. L.Martin, D. Milstein, *J. Am. Chem. Soc.* **2003**, *125*, 11041-11050.

[63] a) C. P. Lenges, P. S. White, M. Brookhart, *J. Am. Chem. Soc.* **1999**, *121*, 4385-4396. b) B. McAuley, M. J. Hockey, L. P. Kingston, J. R. Jones, W. J. S. Lockley, A. N. Mather, E. Spink , S. P. Thompson, D. J. Wilkinson, *J. Label. Compd. Radiopharm.* **2003**, *46*, 1191-1204. c) J. Krüger, B. Manmontri, G. Fels, *Eur. J. Org. Chem.* **2005**, 1402-1408. d) Q.-X. Guo, B.-J. Shen, H.-Q. Guo, T. Takahashi, *Chin. J. Chem.* **2005**, *23*, 341-344.

[64] a) A. G. Wong-Foy, G. Bhalla, X. Y. Liu, R. A. Periana, *J. Am. Chem. Soc.* **2003**, *125*, 14292-14293. b) G. Bhalla, X. Y. Liu, J. Oxgaard, W. A. Goddard III, R. A. Periana, *J. Am. Chem. Soc.* **2005**, *127*, 11372-11389. c) W. J. Tenn III, K. J. H. Young, G. Bhalla, J. Oxgaard, W. A. Goddard III, R. A. Periana, *J. Am. Chem. Soc.* **2005**, *127*, 14172-14174. d) W. J. Tenn III, K. J. J. Young, J. Oxgaard, R. J. Nielsen, W. A. Goddard III, R. A. Periana, *Organometallics* **2006**, *25*, 5173-5175.

[65] Hermann W.A., Kohlpaintner C.W., *Angew. Chem.* **1993**, *105*, 1588-1609.

[66] a) K. W Kottsieper, O. Stelzer, P. Wasserscheid, *J. Mol.Cat. A: Chem.* **2001**, *175*, 285-288. b) D. J. Brauer, M. Hingst, K. W. Kottsieper, C. Liek, T. Nickel, M. Tepper, O. Stelzer, W. S. Sheldrick, *J. Organomet. Chem.* **2002**, *645*, 14-26. c) K. Kottsieper, *Dissertation* **2004**, RWTH Aachen. d) B. Mohr, D. M. Lynn, R. H. Grubbs, *Organometallics* **1996**, 4317-4325.

[67] a) Y. Lin, Y. Zhou, *J. Organomet. Chem.* **1990**, *381*, 135-138. b) S. Burling, M. K. Whittlesey, J. M. J. Williams, *Adv. Synth. Catal.* **2005**, *347*, 591-594

[68] a) C. P. Lau, L. Cheng, *J. Mol. Cat. A: Chem.*, **1993**, *84*, 39-50. b) W. K. Fung, X. Huang, M. L. Man, S. M. Ng, M. Y. Hung, Z. Lin, C. P. Lau, *J. Am. Chem. Soc.* **2003**, *125*, 11539-11544.

[69] C. W. Jung, P. E. Garrou, *Organometallics* **1982**, *1*, 658-666.

[70] R. H. Crabtree, D. G. Hamilton, *J. Am. Chem. Soc.* **1986**, *108*, 3124-3125.

[71] a) D. Morton, D. J. Cole-Hamilton, I. D. Utuk, M. Paneque-Sosa, M. Lopez-Poveda, *J. Chem. Soc. Dalton. Trans* **1989**, 489-495. b) D. Morton, D. J. Cole-Hamilton, *J. Chem. Soc Chem. Commun.* **1988**, 1154-1156.

[72] a) D. Morton, D. J. Cole-Hamilton, *J. Chem. Soc. Chem. Commun.* **1987**, 248-249. b) D. Morton, D. J. Cole-Hamilton, *Polyhedron* **1987**, *6*, 12, 2187-2189.

[73] a) H. Junge, M. Beller, *Tetrahedron Letters* **2005**, 1031-1034. b) H. Junge, B. Loges, M. Beller, *Chem. Commun.* **2007**, 522-524.

[74] a) Y. Blum, D. Reshef, Y. Shivo, *Tetrahedron Lett.* **1981**, *22*, 1541-1544; b) Y. Blum, Y. Shivo, *J. Organomet. Chem.* **1985**, *282*, C7-C10.

[75] a) S.-I. Murahashi, T. Naota, K. Ito, Y. Maeda, H. Taki, *Tetrahedron Lett.* **1981**, *22*, 5327-5330; b) S.-I. Murahashi, K. Ito, T. Naota, Y. Maeda, *J. Org. Chem.* **1987**, *52*, 4319-4327.

[76] J. Zhang, M. Gandelman, L. J. W. Shimon, D. Milstein, *Dalton. Trans.*, **2007**, 107-113.

[77] J. Zhao, J. F. Hartwig, *Organometallics* **2005**, *24*, 2441-2446.

[78] Y. Lin, X. Zhu, Y. Zhou, *J. Organomet. Chem.* **1992**, 269-274.

[79] a) D. E. Fogg, E. N. dos Santos, *Coord. Chem. Rev.* **2004**, *248*, 2365-2379. b) J.-C. Wasilke, S. J. Obrey, R. T. Baker, G. C. Bazan, *Chem. Rev.* **2005**, *105*, 1001-1020.

[80] a) M. G. Edwards, J. M. J. Williams, *Angew. Chem. Int. Ed.* **2002**, *41*, 4740-4743. b) M. G. Edwards, R. F. R. Jazzar, B. M. Paine, D. J. Shermer, M. K. Whittlesey, J. M. J. Williams, D. D. Edney, *Chem. Commun.* **2004**, 90-91. c) P. J. Black, M. G. Edwards, J. M. J. Williams, *Eur. J. Org. Chem.* **2006**, 4367-4378. d) G. Cami-Kobeci, J. M. J. Williams, *Chem. Commun.* **2004**, 1072-1073. e) P. J. Black, G. Cami-Kobeci, M. G. Edwards, P. A. Slatford, M. K. Whittlesey, J. M. J. Williams, *Org. Biomol. Chem.* **2006**, *4*, 116-125.

[81] a) R. F. R. Jazzar, S. A. Macgregor, M. F. Mahon, S. P. Richards, M. K. Whittlesey, *J. Am. Chem. Soc.* **2002**, *124*, 4944-4945. b) S. Burling, B. M. Paine, D. Nama, V. S. Brown, M. F. Mahon, T. J. Prior, P. S. Pregosin, M. K. Whittlesey, J. M. J. Williams, *J. Am. Chem. Soc* **2007**, *129*, 1987-1995.

[82] Y. Lin, X. Zhu, M. Xiang, *J. Organomet. Chem.* **1993**, *448*, 215-218.

[83] A. Dobson, S. Robinson, *J. Organomet. Chem.* **1975**, 87, C52-C53.

[84] Y. Lin, D. Ma, X. Liu, *Tetrahdron Lett.* **1987**, *28*, No 27, 3115-3118.

[85] G. B. W. L. Ligthart, R. H. Meijer, M. P. J. Donners, J. Meuldijk, J. A. J. M. Vekemans, L. A. Hulshof, *Tetrahedron Lett.* **2003**, *44*, 1507-1509.

[86] a) M. Guebert, C. R. H. Acad. Sci **1899**, *128*, 511; b) H. Machemer, Angew. Chem 1952, 64, 213-220;

[87] A whole series of related papers by C. Carlini can be found in *J. Mol. Catal. A: Chem.* between 2002 and 2004. The only paper describing Ruthenium-catalysts is given here: C. Carlini, A. Maciani, M. Marchionna, M. Noviello, A. M. R. Galletti, G. Sbrana, *J. Mol. Catal. A: Chem.* **2003**, *206*, 409-418.

[88] G. R. A. Adair, J. M. J. Williams, *Tetrahedron Lett.* **2005**, *46*, 8233-8235.

[89] Similar observations were made by S. Busch. S. Busch, *PhD-thesis* **2001**, University of Jena, Jena / Max-Planck-Institut für Kohlenforschung, Mülheim.

[90] D. G. Gusev, A. B. Vymenits, V. I. Bakhmutov, *Inorganica Chimica Acta* **1991**, *179*, 195-201.

[91] The DFT calculations were performed by M. Hölscher, ITMC, RWTH Aachen.

[92] a) A. D. Becke, *J. Chem. Phys.* **1993**, *98*, 5648. b) C. Lee, W. Yang, R. G. Parr, *Phys. Rev.* **1988**, *37*, 785. (c) S. H. Vosko, L. Wilk, M. Nusair, *Can. J. Phys.* **1980**, *58*, 1200. (d) P. J. Stephens, F. J. Delvin, C. F. Chabalowski, M. J. Frisch, *J. Phys. Chem.* **1994**, *98*, 11623. e) Gaussian 03, Revision B.03, M. J. Frisch, G. W. Trucks, H. B. Schlegel, G. E. Scuseria, M. A. Robb, J. R. Cheeseman, J. A. Montgomery, Jr., T. Vreven, K. N. Kudin, J. C. Burant, J. M. Millam, S. S. Iyengar, J. Tomasi, V. Barone, B. Mennucci, M. Cossi, G. Scalmani, N. Rega, G. A. Petersson, H. Nakatsuji, M. Hada, M. Ehara, K. Toyota, R. Fukuda, J. Hasegawa, M. Ishida, T. Nakajima, Y. Honda, O. Kitao, H. Nakai, M. Klene, X. Li, J. E. Knox, H. P. Hratchian, J. B. Cross, C. Adamo, J. Jaramillo, R. Gomperts, R. E. Stratmann, O. Yazyev, A. J. Austin, R. Cammi, C. Pomelli, J. W. Ochterski, P. Y. Ayala, K. Morokuma, G. A. Voth, P. Salvador, J. J. Dannenberg, V. G. Zakrzewski, S. Dapprich, A. D. Daniels, M. C. Strain, O. Farkas, D. K. Malick, A. D. Rabuck, K. Raghavachari, J. B. Foresman, J. V. Ortiz, Q. Cui, A. G. Baboul, S. Clifford, J. Cioslowski, B. B. Stefanov, G. Liu, A. Liashenko, P. Piskorz, I. Komaromi, R. L. Martin, D. J. Fox, T. Keith, M. A. Al-Laham, C. Y. Peng, A. Nanayakkara, M. Challacombe, P. M. W. Gill, B. Johnson, W. Chen, M. W.

Wong, C. Gonzalez, and J. A. Pople, Gaussian, Inc., Pittsburgh PA, **2003**. f) A. Schäfer, C. Huber, R. Ahlrichs, *J. Chem. Phys.* **1994**, *100*, 5829; g) D. Andrae, U. Haeussermann, M. Dolg, H. Stoll, H. Preuss, *Theor. Chim. Acta* **1990**, *77*, 123. h) R. Ditchfield, W. J. Hehre, J. A. Pople, *J. Chem. Phys.* **1971**, 54, 724; i) W. J Hehre, R. Ditchfield, J. A. Pople, *J. Chem. Phys.* **1972**, *56*, 2257; j) P. C. Hariharan, J. A. Pople, *Mol. Phys.* **1974**, *27*, 209; k) M. S. Gordon, *Chem. Phys. Lett.* **1980**, *76*, 163; l) P. C. Hariharan, J. A. Pople, *Theor. Chim. Acta* **1973**, *28*, 213; m) G. Frenking, I. Antes, M. Böhne, S. Dapprich, A. W. Ehlers, V. Jonas, A. Neuhaus, M. Otto, R. Stegmann, A. Veldkamp, S. F. Vyboishchikov, in *Reviews in Computational Chemistry*; K. B. Lipkowitz, D. B. Boyd, Eds.; VCH: New York, **1996**, *Vol. 8*, pp 63-144; n) P. J. Hay, W. R. Wadt, *J. Chem. Phys.* **1985**, *82*, 299.

[93] H-X bond activation (X=O, S, N, C, F) were studied computationally and experimentally: S. L. Chatwin, M. G. Davidson, C. Doherty, S. M. Donald, R. F. R. Jazzar, S. A. Macgregor, G. J. McIntyre, M. F. Mahon, M. K. Whittlesey, *Organometallics* **2006**, *25*, 99.

[94] A, Antinol, B. Chaudret, G. Commenges, M. Fajardo, F. Jalon, R. H. Morris, A. Otero, C. T. Schweltzer, *J. Chem. Soc. Chem. Commun.* **1988**, 1210-1212-

[95] M. Colomb, M. W. George, J. N. Moore, D. L. Pattison, R. N. Perutz, I. G. Virrels, T. Q. Ye, *J. Chem. Soc. Dalton Trans.* **1997**, 2857-2859.

[96] a) P. S. Hallmann, B. R. McGarvaey, G. Wilkinson, *J. Chem. Soc (A) Inorg. Phys. Theor.* **1968**, 3143-3150. b) W. H. Knoth, *J. Am. Chem. Soc.* **1972**, *94*, 104-109.

[97] W. R. Roper, L. J. Wright, *J. Organomet. Chem.* **1982**, *234*, C5-C8.

[98] P. C. Junk, J, W, Seed, *J. Organomet. Chem.* **1999**, *587*, 191-194.

[99] A. Caballero, S. Sabo-Etienne, *Organometallics* **2007**, *26*, 1191-1195.

[100] S. Lachaize, K. Essalah, V. Montiel-Palma, L. Vendier, B. Chaudret, J. Barthelat, S. Sabo-Etienne, *Organometallics* **2005**, *24*, 2935-2943.

[101] a) S. Komiya, A. Yamamoto, *J. Organomet. Chem.* **1972**, *46*, C58-C60. b) S. Komiya, A. Yamamoto, *Bull. Chem. Soc. Jap.* **1976**, *49* (3), 784-787. c) I. S. Kolomnikov, A. I. Gusev, G. G. Aleksandrov, T. S. Lobeeva, Yu. T. Struchkov, M. E. Vol´Pin, *J. Organomet. Chem.* **1973**, *59*, 349-351. d) G. Jia, D. W. Meek, *J. Am. Chem. Soc.* **1989**, *111*, 757-758. e) G. Jia, D. W. Meek, *Inorg. Chem.* **1991**, *30*, 1953-1955.

[102] a) W. Leitner, *Coord. Chem. Rev.* **1996**, *153*, 257-284. b) P. G. Jessop, F. Joó, C.-C. Tai, *Coord. Chem. Rev.* **2004**, *248*, 2424-2442. c) E. Dinjus, W. Leitner, *Carbon Dioxide Chemistry: Environmental Issues, J. Paul, C.-M. Pradier, (eds.), Royal Society of Chemistry* **1994**, 82-92. d) W. Leitner, E. Dinjus, F. Gaßner, *J. Organomet. Chem.* **1994**, *475*, 257-266. e) R. Fornika, H. Görls, B. Seemann, W. Leitner, *J. Chem. Soc. Chem. Commun.* **1995**, 1479-1481. e) W. Leitner, *Angew. Chem.* **1995**, *107*, 2391-2405. *Angew. Chem. Int. Ed. Engl.* **1995**, *34*, 2207-2221.

[103] a) S. Nemeh, C. Jensen, E. Binamira,-Soriaga, W. C. Kaska, *Organometallics* **1983**, *2*, 1442-1447. b) W. C. Kaska, S. Nemeh, A. Shirazi, S. Potuznik, *Organometallics* **1988**, *7*, 13-15. c) K.-W. Hunag, J. H. Han, C. B. Musgrave, E. Fujita, *Organometallics* **2007**, *26*, 508-513. d) A. Vigalok, Y. Ben-David, D. Milstein, **1996**, *15*, 1839-1844.

[104] K.-I. Tominaga, Y. Sasaki, K. Hagihara, T. Watanabe, M. Saito, *Chem. Lett.* **1994**, 1391-1394.

[105] M. Brookhart, M. L. H. Green, *J. Organomet. Chem.* **1983**, *250*, 395.

[106] C. Six, B. Gabor, H. Görls, R. Mynott, P.Philipps, W. Leitner, *Organometallics* **1999**, *18*, 3316-3326.

[107] J. P. Genêt, C. Pinel, V. Ratovelomanana-Vidal, S. Mallart, X. Pfister, M. C. Caño de Andrade,

J. A. Laffitte, *Tetrahedron Asymmetry* **1994**, *5*, 665-674.

[108] a) P. Foley, R. DiCosimo, G. M. Whitesides, *J. Am. Chem. Soc.* **1980**, *102*, 6713-6725; b) G. M. Whitesides, M. Hackett, R. L. Brainard, J.-P. P. M. Lavalleye, A. F. Sowinski, A. N. Izumi, S. S. Moore, D. W. Brown, E. M. Staudt, *Organometallics* **1985**, *4*, 1819-1830; c) C. Paal, W. Hartmann, *Chem. Ber.* **1918**, *51*, 711-737.

[109] Related C-H activation mechanisms were described for Rh and Ir-complexes: E. Ben-Ari, R. Cohen, M. Gandelman, L. J. W. Shimon, J. M. L. Martin, D. Milstein, *Organometallics* **2006**, *25*, 3190.

[110] Arene C-H activation with subsequent H-transfer to olefins was described for Ru complexes: a) M. Lail, C. M. Bell, D. Conner, T. R. Cundari, T. B. Gunnoe, J. L. Petersen, *Organometallics* **2004**, *23*, 5007; b) H. Weissman, X.-P. Song, D. Milstein, *J. Am. Chem. Soc.* **2001**, *123*, 337.

[111] a) M. Gross, D. C. Müller, H.-G. Nothofer, U. Scherf, D. Neher, C. Bräuchle, K. Meerholz, *Nature* **2000**, 661-665. b) F. Galbrecht, X. H. Yang, B. S. Nehls, D. Neher, T. Farrell, U. Scherf, *Chem. Commun.* **2005**, 2378–2380. c) K.-H. Weinfurtner, H. Fujikawa, S. Tokito, Y. Taga, *Appl. Phys. Lett.* **2000**, 2502-2504.

[112] The IR studies and the IR data were measured, processed, analysed and interpreted in collaboration with C. Minnich at the ITMC, RWTH Aachen. For further details about IR Reaction Monitoring with the used IR setup see: C. B. Minnich, P. Buskens, H. C. Steffens, P. S. Baeuerlein, L. N. Butvina, L. Kuepper, W. Leitner, M. A. Liauw, L. Greiner, "Highly Flexible Fibre-Optic ATR-IR Probe for Inline Reaction Monitoring.", *Organic Process Research & Development* **2007**, *11*(1), 94-97.

[113] F. M. T. Mendes, M. Schmal, *Appl. Catal. A* **1997**, *163*, 153-164.

[114] R. M. Rioux, M. A. Vannice, *J. Catal.* **2003**, *216*, 362-376, and the references therein.

[115] H. Idriss, E. G. Seebauer, *J. Mol. Catal. A* **2000**, *152*, 201-212, and the references therein.

[116] Y.-J. Tu, C. Li, Y.-W. Chen, *J. Chem. Tech. Biotechnol.* **1994**, *59*, 141.

[117] L. S. Van Der Sluys, G. J. Kubas, K. G. Caulton, *Organometallics* **1991**, *10*, 1033-1038.

[118] (a) D. D. Perrin, W. L. F. Armarego, *Purification of Laboratory Chemicals* **1988** (Pergamon Press), Oxford, 3rd Ed. (b) K. Schwetlick et al., *Organikum* **1981**, 15th Ed., VEB-DVW Berlin.

[119] K. Timmer, D. H. M. W. Thewissen, J. W. Marsman, *Rec. Trav. Chim. Pays-Bas* **1988**, *107/3*, 248-255.

[120] A. A. Naiini, Y. Han, M. Akinc, J. G. Verkade, *Inorg. Chem.* **1993**, *32*, 5394-5395.

[121] B. Mohr, D. M. Lynn, R. H. Grubbs, *Organometallics* **1996**, 4317-4325.

[122] J. E. Rauhaus, *Diploma-thesis* **2004**, BU Wuppertal / MPI Mülheim.

[123] T. Doi, H. Nagamiya, M. Kokubo, K. Hirabayashi, T. Takahashi, *Tetrahedron* **2002**, 2957-2963.

[124] H. Katayama, C. Wada, K. Taniguchi, F. Ozawa, *Organometallics* **2002**, *21*, 3285-3291.

Academic Curriculum Vitae

Name:	Martin H. G. Prechtl	Profession:	Diplom-Chemiker

Birthday: 1st of June 1977 in Offenbach am Main, Germany
Nationality: German

Academic Education

June 28th 2007	*RWTH Aachen:* Oral defence of the PhD-thesis.
09 / 2004 – 06 / 2007	*Max-Planck-Institute for Coal Research*, Mülheim an der Ruhr, and *RWTH Aachen - University of Technology*, Aachen, Germany: PhD-Studies in Organometallic Chemistry.
March 31st 2004	Graduation: Diplom-Chemiker *Bergische University Wuppertal* (*BU Wuppertal*), Wuppertal, Germany.
10 / 1999 - 03 / 2004	Studies in Chemistry and Food Chemistry, *Bergische University Wuppertal*, Wuppertal, Germany.
10 / 2003 - 03 / 2004	*BU Wuppertal*: Diploma-Thesis in Organic Chemistry.
10 / 2002 - 06 / 2003	*University of São Paulo*, São Paulo, Brazil: Graduate studies as *DAAD-fellow* - research projects in Organic Chemistry and Physical Organic Chemistry.
08 / 2001 - 10 / 2001	*University of West Indies - Cave Hill Campus*, St. Michael, Barbados: Granted research project in Organic Chemistry.
07 / 2001	*BU Wuppertal: Vordiplom* („diploma pre-degree“) in Chemistry.
1984 – 1997	*Otto-Hahn-Schule* (1984-1988), *Adolf-Reichwein-Schule* (1988-1990), *Adolf-Reichwein-Gymnasium* (1990-1997), Heusenstamm, Germany.

Foundation-Awards

Alexander-Von-Humboldt-Foundation (“Feodor-Lynen”-Postdoctoral Fellowship, 2007/2008)
DAAD (research fellowship and extra-ordinary extended grant, 2002/2003)